Cancer and Genetics
School of Medicine
Cardiff University

A Genotypic, Phenotypic and Functional Exploration of Multiple Myeloma Sub-Clones

A thesis submitted to the School of Medicine, Cardiff University in partial fulfilment for the degree of Doctor of Philosophy

James William Murray

December 2019

Acknowledgements

I would like to give a huge thanks to my supervisors, Professor Chris Pepper and Professor Chris Fegan for not only giving me the opportunity to undertake this PhD, but also for all their support, guidance and mentorship over the past five years. Also, I would like to thank Leukaemia Research Appeal of Wales who funded this PhD project.

This has been an incredible experience and a huge challenge for me, I was completely out of my comfort zone from the start, I could barely use a pipette. So, a massive thanks for all those in the Research Group who took the time to explain the most mundane of lab tasks right from the start. Despite being one the oldest students, I really was a novice!

A huge thank you goes to all of you on the first floor of the CG building. I made some great friends and couldn't have asked to work in a friendlier environment. I will truly miss actually having time for lunch, cups of tea and actually not getting to the end of the day feeling dehydrated! Research couldn't have been more chalk and cheese to clinical life, but the skills and thought processes I developed along the way will have lasting effect on me and the way I practice medicine and all for the better.

From the bench to the bedside, thanks also to those over at UHW, especially Dr Raz Alikhan. Both yours and Chris F's guidance and mentorship you have shown over the last 8 years has really been appreciated. Starting life as a new consultant, I will very much use the basis of our chats as how to mentor my own trainees in the future.

Lastly, a thank you to my family. My parents have been brilliant, helping with childcare and all too willing 'nudges of encouragement', I'm sure GH Murray would have very proud. But the biggest thanks to my long-suffering wife Catherine. You had a pretty awful time during the research and write up period, so the least I can do is dedicate it to you. I hope it will make a good door stop. You often said this was the third child in our lives and am sure you will be the happiest of everyone when I can finally put it to bed. All I can say is thank you for putting up with it and me!

Summary

The concept of genetic clonal tiding is well established in Multiple myeloma. Immunophenotypic analysis as a means of sub-clone distinction is less well recognised. In this thesis, a 10-colour panel was designed that showed examples of distinct CD38, CD138, CXCR4, MMP-9, IL-6 and CD49d sub-populations in both primary MM samples and cell lines. The huge variation in CD38 expression amongst the samples and its positive correlation with Ki-67, CXCR4 and CD56 expression was of particular interest, culminating in the previously undescribed discovery of a bimodal CD38 expression in the well-known cell line, MM.1S. In terms of function, I showed that CD38 expression was a predictor of myeloma cell migration; high expression was associated with increased cell migration. Furthermore, I developed a novel migratory model in MM, that had been previously used in our research group for CLL. In this dynamic circulatory model, I showed that pharmacological inhibition of CXCR4 and CD49d inhibited MM migration.

To further explore the functional difference in CD38 expressing sub-populations, the MM.1S CD38 populations were cell sorted and the distinct subsets were examined in terms of phenotype, function and genotype. The weakly expressing CD38 population, termed MM.1S^{dim}, was shown to contain a mutation in the gene *MKI67*, providing a rationale for the observed decrease in cell growth. Through further genetic analysis, sub-clonality between the 3 populations were proven, ultimately showing that both of the MM.1S CD38 sub-clones were manifest in the MM.1R cell line. The exome analysis also identified that the CD38 sub-clones harboured distinct genetic mutations, which conferred differential sensitivity to molecular targeted inhibitors such as PI3K.

This, combined with my migratory work, showed the potential for developing bespoke treatment plans based on the identification of cell signalling pathway mutations via genomic sequencing and immunophenotypic analysis. By selective targeting of these genetic lesions it may be possible to remove multiple sub-clones thereby diminishing the potential for clonal tiding and the development of drug resistance.

Presentations and Publications

Conference abstract publications:

Murray JW, Ashelford K, Fegan C, Pepper C
Genetic Analysis of Distinct Phenotypic Subsets within MM1.S Multiple Myeloma Cell Line Reveals the Pre-Existence of MM.1R-like Glucocorticoid Resistance and a Sub-Clone with an Activating PI3-Kinase Delta Mutation That Is Preferentially Sensitive to the Selective PI3-Kinase Inhibitor, Idelalisib. *Blood* (2016) 128 (22): 4449.
https://doi.org/10.1182/blood.V128.22.4449.4449

Murray JW, Fegan C, Pepper C
Analysis of the MM.1S multiple myeloma cell line reveals a distinct phenotypic and genetic architecture including a pre-existing MM.1R-like glucocorticoid resistant sub-clonal population. *British Journal of Haematology* (2016) 178 (S1): 183

List of Abbreviations

#	Number
1D	1-Dimensional
1KGP	1000 Genomes project
Akt	Protein B kinase
ANOVA	Analysis of Variance
APC	Allophycocyanin
ASO-qPCR	Allele-Specific Oligonucleotide qPCR
B2M	β2 microglobulin
Bcl-2	B-cell lymphoma protein-2
BCR	B-cell receptor
BGI	Beijing Genomics Institute
BM(SC)	bone marrow (stromal cells)
BSA	Bovine serum albumin
CAM-DR	cell adhesion-mediated drug resistance
CD	Cluster differentiation
cDNA	Complementary DNA
CLL	Chronic lymphocytic leukaemia
CNV	Copy-number variation
Conc.	Concentration
CSR	class switch recombination
dd	Double deionised
DMEM	Dulbecco's Modified Eagle's Medium
DMSO	Dimethyl sulfoxide
DNA	Deoxyribonucleic acid
ds	Double stranded
ECM	Extra cellular matrix
EDTA	Ethylene diamine tetra-acetic acid
ELISA	Enzyme linked immunosorbent assay
EVS	Extra-vascular space
FACS	Flow cytometry-based cell sorting
FCS	Foetal calf serum
FGFR	Fibroblast growth factor receptor
FISH	Fluorescent in situ hybridization
FITC	Fluorescein isothiocyanate
GFP	Green fluorescent protein

GR	Glucocorticoid receptor
GWAS	Genome wide association studies
H+L	Heavy and light chains
HDAC	Histone deacetylase
HRP	Horseradish peroxidase
HUVEC	Human vein endothelial cell
IC_{50}	Inhibitory concentration for 50% of the cells
ICAM-1	Intracellular adhesion molecule 1
Ig	Immunoglobulin
IL	Interleukin
IMWG	International Myeloma Working Group
InDel	**In**sertion or **del**etion of bases
ISS	International Staging System
LD_{50}	Lethal dose for 50% of the cells
LDH	Lactate Dehydrogenase
MAPK	Mitogen-activated protein kinase
Mcl-1	Myeloid cell leukaemia sequence 1
MEK	MAPK-ERK kinase
MFC	Multiparameter Flow Cytometry
MFI	Median Fluorescence intensity (unless otherwise specified, mean)
MGUS	Monoclonal Gammopathy of Undetermined Significance
MHC	Major histocompatibility complex
MM	Multiple Myeloma
MRD	Minimal Residual Disease
mTOR	Mammalian target of rapamycin
MZ	Marginal zone
NF-κB	nuclear factor-κB
NGS	Next Generation Sequencing
NICE	National Institute for Health and Care Excellence
NK	Natural killer
OS	Overall survival
PBMC	Peripheral Blood mononuclear cells
PBS	Phosphate buffered saline
P-gp	P-glycoprotein
PCR	Polymerase chain reaction
PCs	Plasma cells
PCL	Plasma cell Leukaemia

PE	Phycoerythrin
PFA	Paraformaldehyde
PFS	Progression free survival
PI	Propidium iodide
PI3K	Phosphoinositide 3-kinase
PKC	protein kinase C
PMSF	Phenylmethosulfonylfuoride
PTK2	Protein tyrosine kinase 2 (also known as Focal Adhesion Kinase)
PVDF	Polyvinylidene difluoride
qPCR	quantitative Polymerase Chain Reaction
RANKL	Receptor activator of nuclear factor kappa-B ligand
Rb	Retinoblastoma
RNA	Ribonucleic acid
ROS	Reactive Oxygen Species
RPM	Revolutions per minute
RPMI	Roswell Park Memorial Institute culture media
RRMM	Relapsed refractory multiple myeloma
RT	Reverse Transcriptase
SD	Standard Deviation
SDF-1	Stromal cell derived factor -1 (also known as CXCL12)
SDS-PAGE	Sodium dodecyl sulphate-polyacrylamide gel electrophoresis
SEM	Standard error of the mean
SFLC	Serum free light chains
SHM	somatic hypermutation
SMM	Smouldering Multiple Myeloma
SNP	Single nucleotide polymorphism
SNV (NS-)	Single nucleotide variant (non-synonymous)
TCR	T cell receptor
TERT	Telomerase Reverse Transcriptase
TGF	Transforming growth factor
TNF	Tumour necrosis factor
VCAM-1	vascular adhesion molecule 1
V(D)J	Variable (diversity) joining
VEGF	Vascular endothelial growth factor
VLA-4	Very late antigen-4 (integrin $\alpha 4\beta 1$)
WES	Whole Exome Sequencing

Table of Contents

CHAPTER 1:

Introduction

1.1 Multiple Myeloma

Multiple myeloma (MM) is an incurable cancer of plasma cells that is usually fatal. Over 5,000 new cases are reported yearly in the UK, accounting for 2% of all new cancer cases and 13% of haematological malignancies. Its incidence is increasing, current rates are 9 cases per 100,000, which represents a 32% increase since the early 1990's (Altekruse et al. 2010; Cancer Research UK 2015). MM is part of a spectrum of disorders termed plasma cell dyscrasias, that encompasses Monoclonal Gammopathy of Undetermined Significance (MGUS), asymptomatic MM (also known as smouldering myeloma (SMM)), single and multiple plasmacytomas, symptomatic MM and plasma cell leukaemia (Rajkumar 2016).

The treatment of MM has remained challenging due to predominantly being a disease of the elderly and of its natural disease course, one of repeated relapses/remissions through numerous lines of therapy. Despite the challenges, overall survival has greatly increased over the last two decades. Before the introduction of '*novel agents*' such as the immunomodulatory drugs thalidomide and lenalidomide and the proteasome inhibitor bortezomib in the mid 2000's, the 10-year overall survival for myeloma was 17.4% (Brenner et al. 2008). Since their introduction, the 10-year overall survival has doubled to 33% (Cancer Research UK 2014).

1.1.1 Normal plasma cell development

Plasma cells are terminally differentiated B lymphocytes that have the capacity to produce and secrete large amounts of antibodies. These antibodies, also known as immunoglobulins, target specific foreign antigens that once bound, initiate destruction of the antigen or antigen-expressing cell. This process forms a key component of the adaptive immune system.

The immature B-cell arises from a haematopoietic stem cell within the bone marrow. The early part of B-cell formation is characterised by immunoglobulin gene loci rearrangement through a process known as V(D)J recombination. The V(D)J region of the immunoglobulin gene encodes for the region of the protein that recognises antigen. The

alternative splicing of different V, (D) and J segments provides a multitude of possible combinations of both light and heavy chain immunoglobulins that form distinct antibodies. B-cells that auto-react to the host are deleted by a process called negative selection or *"clonal deletion"* (Halverson et al. 2004; Shapiro-Shelef and Calame 2005), whilst those remaining are allowed to migrate out of the marrow and traffic to the lymphoid tissues.

B-cells can also act as antigen presenting cells (APCs), thus allowing the internalisation of foreign antigens, whereupon the antigen is broken up into peptides and presented, in the context of MHC molecules, on the cell's surface, usually within the lymphoid tissue. The immature B-cell can then be activated by either T-cells or a subset of B-cells termed marginal zone (MZ) B-cells, resulting in further maturation into plasmablasts. This phase of maturation into an immature plasma cells signals the cell's ability to secrete large amounts of antibodies but still have the capacity to class switch antibody production termed class switch recombination (CSR), which is regulated by the PI3-Kinase pathway. In this process, the constant region of the immunoglobulin switches from IgM and IgD to either IgA, IgG or IgE (Lopes-Carvalho and Kearney 2004; Stavnezer and Amemiya 2004; Shapiro-Shelef and Calame 2005; Omori et al. 2006).

The plasmablast either becomes a short-lived antibody-secreting cell or undergoes additional activation and proliferation following entry into the germinal centre within lymphoid tissue. It is within the germinal centre that enhanced affinity of the B-cell's immunoglobulin to the antigen occurs through somatic hypermutation (SHM) of the variable (V) region of the gene. The germinal centre reaction gives rise to both memory B-cells, and high-affinity antibody-producing plasma cells upon exposure to the original antigen/pathogen (Jacob et al. 1991; Allen et al. 2007; Shlomchik and Weisel 2012).

The key enzyme in antibody diversification is Activation-induced Cytidine Deaminase (AID) and is fundamental in the regulation of SHM and CSR. AID results in Double strand DNA breaks (DSB) leading to variation in antibodies and a functionally active immune system (Morgan et al. 2012b). However, DSBs, although repaired locally, can potentially join to DSBs elsewhere in the genome and in the case of a different chromosome, result in chromosomal translocation. This is why the IgH loci is a hotbed of chromosome translocations (Gonzalez et al. 2007). Although DSB rearrangements occur normally in heathy immune systems, it remains a key origin of the formation of B-cell malignancies including MGUS and MM.

1.1.2 Genetic architecture of MM

Figure 1.1 outlines the genetic changes that occur in the development of MM; a multi-stage transformational process. Initiating genetic events that characterise the disease occur during B-cell development and are predominately chromosome abnormalities such as trisomies (chromosomes 3, 5, 7, 9, 11, 15, 19 and 21) and IgH rearrangement (14q32). IgH translocations result in proximal relocation of IgH enhancers such as Eμ, Eα1 and Eα2 leading to the increased transcription of oncogenes such as:

i. *CCND1* (11q13 coding for cyclin-D1 protein)
ii. *CCND3* (6p21 coding for cyclin-D3 protein)
iii. *MAF* (16q23 coding for c-maf protein)
iv. *FGFR3/MMSET* (4p16 coding for fibroblast growth factor receptor 3 protein)
v. *MAFB* (20q12 coding for Transcription factor MafB protein)

Cyclins drive cells through the G1/S phase of the cell cycle, by activating cyclin dependent kinases (CDK). This in turn is able to phosphorylate and inactivate the tumour suppressor protein retinoblastoma (Rb), which leads to cell cycle progression. Cyclin translocations, as well trisomy 21 and 1q gain, are regarded as poor prognostic factors in MM, whereas other trisomies are deemed more favourable (Lundberg and Weinberg 1998; Bergsagel and Kuehl 2001; Smadja et al. 2001; Chretien et al. 2015).

1.1.2.1 Secondary Genetic events

Almost half of MGUS patients have an IgH translocation, however such events are insufficient to cause the malignant transformation to MM. Secondary genetic abnormalities, either from somatic 'driver' mutations, epigenetic changes or further chromosomal changes are required for disease progression (Morgan et al. 2012b).

The advent of more widely available and efficient next generation sequencing (NGS) has provided the tools to identify frequent and potential driver mutations, i.e. mutations essential for disease progression and clonal evolution. Early results in relatively small cohorts of patients indicated that MM was a very heterogeneous disease, with multiple sub-clonal structure at diagnosis, but with only a few recurrently mutated genes of likely pathogenetic significance (Bolli et al. 2014). These included *KRAS, NRAS, TP53, BRAF* and *FAM46C* (Chapman et al. 2011; Egan et al. 2012; Walker et al. 2014).

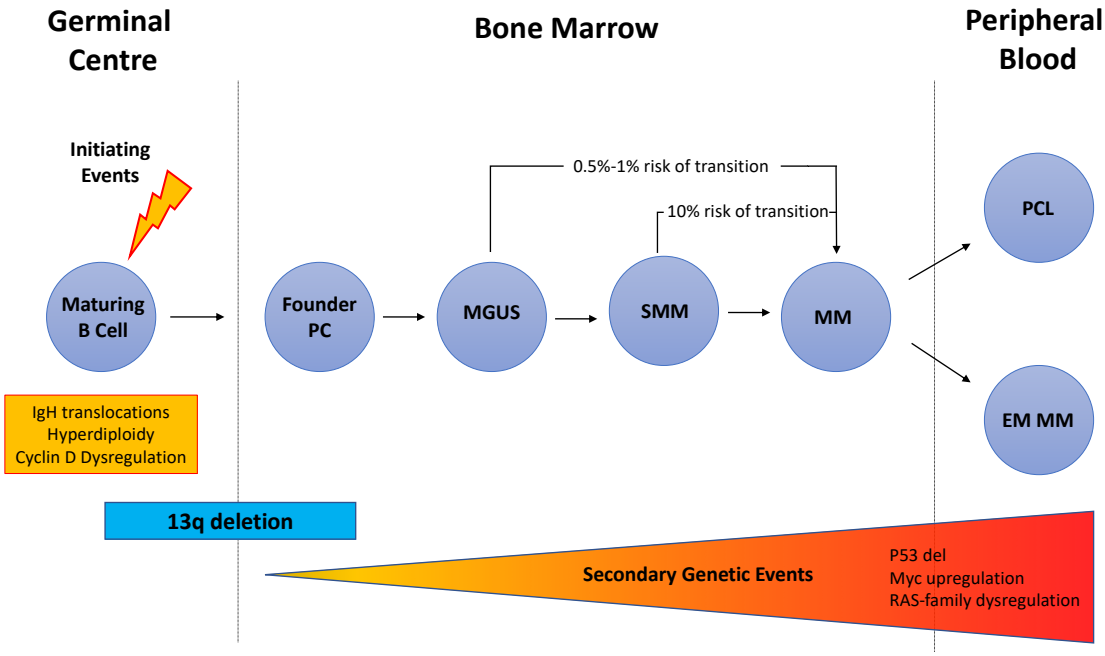

Figure 1.1. The development and genetic events of Multiple Myeloma (MM). *Initiating genetic events occur during normal B-cell development, resulting in Monoclonal Gammopathy of Undetermined Significance (MGUS). In addition to 13q deletion, these mutations are believed to be the cause of cancer. Further mutations labelled as secondary genetic events have to occur before Smouldering Multiple Myeloma (SMM) occurs that leads onto the final transformation to symptomatic MM. Eventually the MM clone will lose its bone marrow microenvironment dependency through additional mutations to form either Plasma Cell Leukaemia (PCL) or Extramedullary Myeloma (EM). Adapted from (Dutta et al. 2017).*

TP53 gene mutations or deletion of the short arm of chromosome 17 are seen in approximately 11% of patients. The tumour suppressor protein p53 has multiple functions in preventing oncogenesis, including invoking G1/S cell cycle arrest, activating DNA repair and initiating apoptotic pathways. Deletion or loss of the gene confers a poor prognosis and is regarded as a high-risk cytogenetic abnormality in the revised ISS prognostic scoring system (Avet-Loiseau et al. 2007; Palumbo et al. 2015).

The RAS family of genes (*HRAS*, *KRAS* and *NRAS*) are the most commonly mutated genes in MM, with an incidence of 25% in newly diagnosed patients, increasing to 45% at relapse (Chng et al. 2008). The RAS/MAPK pathway is frequently deregulated in the disease, with its function primarily in the regulation of cell proliferation (Bolli et al. 2014). Although *RAS* mutations are regarded as one of the key driver mutations for disease progression/sub-clonal evolution and associated with higher tumour burden (Chng et al. 2008), data from the UK Myeloma XI trial, showed it did not have a prognostic implication (Walker et al. 2015). The Myc family of proto-oncogenes (including c-Myc) is frequently upregulated in MM, they function as transcription factors that result in many genes related to cell survival and proliferation being upregulated. The c-Myc locus is on chromosome 8

and in 15% of symptomatic MM patients is translocated with the IgH locus - t(8:14) (Avet-Loiseau et al. 2001). 13q deletions or monosomy 13 can occur in up to half of MM patients. Deletion can be regarded as both an initiating event and a driver of disease, i.e. secondary genetic event. Located within the 13q arm is the *RB* gene; loss of expression or mutation is correlated with a reduced overall survival (Chiecchio et al. 2006).

Additional genetic events that are not deemed essential for disease progression but nevertheless result in the biological sequelae of MM include secondary translocations, mutations causing increased RANKL/OPG expression resulting in osteoclast activation, mutations that cause increased immune evasion and mutations that result in cytokine and growth factor changes.

1.1.2.2 NGS in MM patients

One of the first published collections of MM next generation sequencing (NGS) was in 2011 (Chapman et al. 2011). 38 samples were sequenced in an attempt to identify mutations of high frequency. Chapman concluded that there were no common recurrent mutations, with a median number of mutations per genome around 60 (21-488). Subsequent NGS analysis of larger cohorts has revised the number upwards to approximately 200 (Corre et al. 2015), which when compared to other cancers is roughly average, but higher than many other haematological cancers (Bolli et al. 2014).

Figure 1.2 combines the gene mutation incidence of the 3 largest NGS cohorts published to date, showing that only a few mutations are recurrent, with less than 10 genes having a mutation incidence of 5% or more (Corre et al. 2015). Furthermore, many of the listed genes in Figure 1.2 (notably *NRAS*, *KRAS* and *BRAF*) can be clone specific within the same patient, inferring a single driver mutation is sufficient to form a new sub-clone (Lohr et al. 2014). To add to the complexity, there is huge spatial genomic heterogeneity within MM, i.e. different clones existing at different sites of the body/bone marrow. Indeed, one study suggested that more than 75% of patients had evidence of spatial heterogeneity, including clones with inactivating mutations of *CDKN2C*, *TP53* and mutations affecting mitogen-activated protein kinase genes (Rasche et al. 2017).

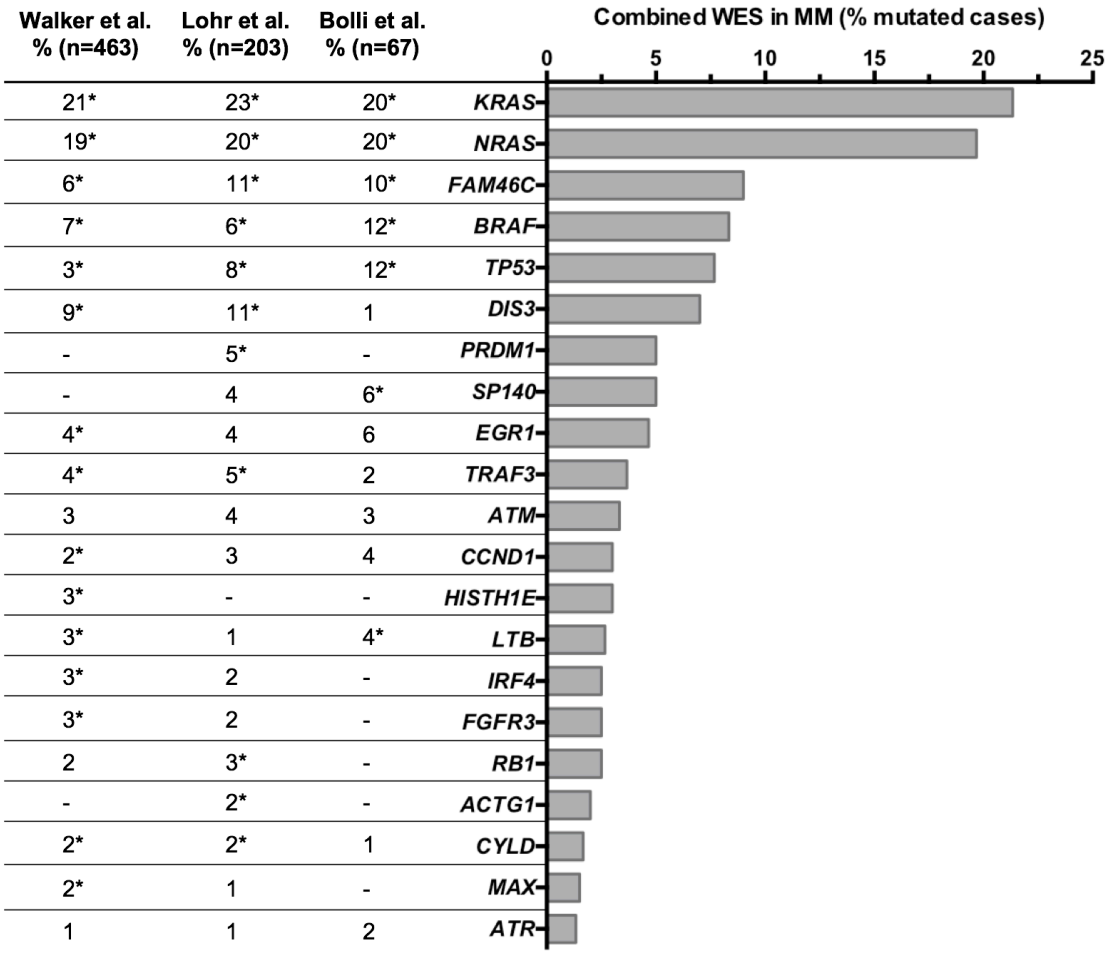

Figure 1.2. Most frequent somatic mutations in patients with MM*. Mutation frequencies are average of data from three whole-exome sequencing studies, totalling 733 patients (Bolli et al. 2014; Lohr et al. 2014; Walker et al. 2015). MM - multiple myeloma; WES – whole exome sequencing; * - Mutations reaching significance. Figure modified from (Manier et al. 2017).*

1.1.3 Clinical classification of Myeloma

1.1.3.1 MGUS/Asymptomatic myeloma:

The International Myeloma Working Group 2014 (IMWG) definition of MGUS and asymptomatic myeloma, state that both conditions present in the absence of a myeloma defining event or amyloidosis. Myeloma defining events are regarded as either bone marrow plasma cell population >10% with end-organ damage (CRAB features see Table 1.2), or in the absence of CRAB features bone marrow plasma cells have to be >60% or a serum-free light chain (SFLC) ratio of >100.

MGUS differs from SMM in that paraprotein levels are less than 30g/L (>30g/L for SMM) and bone marrow plasma cells percentage is less than 10% (between 10-60% for SMM) (Rajkumar 2016). MGUS is primarily a condition of the elderly, with incidence increasing

with age. It is estimated 3% of the general population over 60 have it (Kyle et al. 2007). MGUS shares a number of cytogenetic and molecular abnormalities with MM such as heavy chain translocations, trisomies and increased expression of cyclin D1 (Palumbo and Anderson 2011). This strong molecular association is suggestive that MGUS consistently precedes MM (Landgren et al. 2009).

As is the case with many other cancers, genome-wide association studies (GWAS) have identified common genetic variations associated with the development of myeloma (Law et al. 2017; Went et al. 2018). It is already accepted that inherited factors contribute to the development of MM or MGUS, with a 4.25-fold increase of developing it, if a first-degree relative has either condition (Altieri et al. 2006). MGUS has a 1% annual rate of progression to MM, whereas with SMM the annual rate of progression increases to 10% (Kyle et al. 2002; Kyle et al. 2007). This relatively low rate of progression combined with toxic side effects of treatment options and the lack of clinical trials for these patients, is why the current IMWG guidelines do not advise treatment for either condition (Rajkumar 2016). Controversially, this stance currently precludes treatment of the so called 'high-risk' SMM whose risk of transforming to MM can be as high as 72% in the first 5 years (Pérez-Persona et al. 2007).

1.1.3.2 Defining high-risk SMM

The categorisation of 'high-risk' patients allows for the early identification of those likely to progress to MM. Debate surrounds whether such patients should be treated, as although not technically classified as MM, studies have shown improved OS and PFS with early intervention (Mateos et al. 2013). Such studies aim is to halt clonal progression of the more aggressive clones, that are more likely to become drug resistant. The two most widely used models (Table 1.1), are the 3-factor Mayo Clinic and the 2-factor Spanish PETHEMA. The reliability of these models has been questionable, with large discrepancies (71.4% discordance) observed between them (Cherry et al. 2013). The newer Penn prognostic models (based on the Mayo clinic model) addressed these discrepancies and has a calculated 2-year transformation rate within the high-risk group of 81% (Waxman et al. 2014).

Model	Median TTP	Risk Factors
Mayo Clinic (Dispenzieri et al. 2008)	8.4 months (3 factors)	Bone marrow plasma cells ≥ 10% Paraprotein ≥ 30 g/L SFLC ratio < 0.125 or > 8
PETHEMA (Pérez-Persona et al. 2007)	23 months (3 factors)	≥ 95% aberrant plasma cells Immunoparesis DNA aneuploidy
Penn (Waxman et al. 2014)	4.2 months (3 factors)	Bone marrow plasma cells ≥ 40% Serum free light chain ratio ≥ 50 Albumin ≤ 30 g/L
Updated Mayo Clinic, incorporating revised 2014 IMWG diagnostic criteria. (Lakshman et al. 2018)	29 months (2 ≥ factors)	Bone marrow plasma cells ≥20% SFLC ratio ≥20 Paraprotein ≥ 20 g/L

Table 1.1. The differing models for determining MGUS or SMM patients who have a high-risk of MM transformation*. TTP – Time to progression; IMWG – International Myeloma working group; SFLC - Serum free light chain*

1.1.3.3 Symptomatic MM

The clonal expansion of malignant plasma cells in the bone marrow, leading to an excess of myeloma cells, ultimately results in marrow failure and organ damage through various protein secretions and inhibition of bone marrow stromal cells. The end organ damage or CRAB features are the defining events that are required for disease diagnosis (Table 1.2). The cause of anaemia is multifactorial and includes; reduction of normal haematopoiesis caused by plasma cell overexpansion in the bone marrow, inhibition of stromal cells and the increase in hepcidin expression (Mittelman 2003). Renal failure occurs predominantly through secretion of SFLC (known as Bence Jones protein when detected in the urine), which aggregate in the nephrons resulting in damage. Lytic bone lesions that lead to hypercalcaemia and bone fractures occur through osteoclast activation and osteoblast inhibition by secretion of receptor activator of nuclear factor kappa-B ligand (RANKL) and osteoprotegerin (Tai et al. 2007).

End organ damage criteria/CRAB features	Biomarkers of malignancy criteria:
Hyper**c**alcaemia: serum calcium >2·75 mmol/L	Clonal bone marrow plasma cell percentage ≥60%
Renal insufficiency: creatinine clearance <40 ml/min or serum creatinine >177 µmol/L	Involved: uninvolved serum free light chain ratio ≥100
Anaemia: haemoglobin value of <100 g/L or >20g/L below the lower limit of normal	>1 focal lesion on MRI studies
Bone lesions: one or more osteolytic lesions on skeletal radiography, CT, MRI or PET-CT	

Table 1.2. List of the myeloma defining events *required to make a diagnosis of MM from the IMWG 2014 (Rajkumar 2016) classification of MM. Diagnosis of MM being a clonal bone marrow plasma cells ≥10% or biopsy-proven bony or extramedullary plasmacytoma and any one or more of the above myeloma defining events. Criteria divided into end organ damage or biomarker.*

1.1.4 Prognostic factors in MM

The huge clinical heterogeneity of MM is reflected in the diverse survival outcomes amongst patients, ranging from a couple of months to over 10 years. Certain prognostic factors have allowed clinicians to predict survival outcome (e.g. tumour burden and disease complications) and, in some circumstances, these can also help determine treatment strategies.

1.1.4.1 Tumour burden, disease complications and cytogenetic factors

Calculation of bone marrow infiltration of plasma cells and disease complications by paraprotein levels, anaemia, renal involvement and lytic lesions can offer limited prognostic information and formed the basis of the Durie-Salmon classifications (Durie and Salmon 1975). However, this staging system has been widely replaced, first by the international staging system (ISS) and more recently by the revised-ISS, which aimed to simplify disease classification as well as incorporate advances in our understanding of the cytogenetics of the malignant clones. The ISS (Table 1.3) uses only two disease markers (β2-microglobulin and serum albumin). As well as being a better predictor of survival, it is simpler and easier to implement in the clinic compared to the Durie-Salmon classification.

Stage	Criteria	Median overall survival
I	β2-microglobulin <3.5mg/dL and Serum albumin >3.5mg/dL	62 months
II	Neither stage I or stage II	44 months
III	β2-microglobulin >5.5mg/dL	29 months

Table 1.3. ISS criteria *and median overall survival related to the stage (Greipp et al. 2005).*

Although the ISS was derived from the analysis of over 11,000 patients (Greipp et al. 2005), it pre-dates the widespread use of the so called *'novel therapies'* (proteasome inhibitors and/or immunomodulatory drugs), which have made a great impact on disease survival and therefore a revision was made in 2015 (Palumbo et al. 2015). The R-ISS reflects the advances in treatment on overall survival and further stratifies prognostic groups by including high-risk chromosomal abnormalities (del(17p), t(4;14), t(14;16)) as well as serum lactate dehydrogenase (LDH). The staging system is still divided into 3 subgroups, but survival of each group is now given as a percentage alive at 5 years (stage I-82%, stage II-62% and stage III-40%).

1.1.4.2 Other prognostic factors

Host factors such as performance status (ECOG <2) and age are well established. The response to treatment is also a key factor, with the depth of response, largely inferring longer progression-free survival (PFS) and overall survival (Martinez-Lopez et al. 2014; Munshi et al. 2017). The ideal method to measure response is debatable, the IMWG response criteria, utilising percentage of bone marrow plasma cells as well as paraprotein levels, is a relatively simple method that is applied to virtually all patients undergoing treatment.

The use of minimal residual disease (MRD) either using flow cytometry or next generation sequencing to detect low level disease, can better predict overall survival and/or time to progression, but these methodologies are not widely available (Munshi et al. 2017). Further, the best method for assessing MRD and what constitutes the critical level of response required is still debatable. Multi-parameter flow cytometry (MFC), is the most widely used MRD assessment tool with a sensitivity of around 1 in 10^5 cell detection (Rawstron et al. 2013). Molecular deep sequencing of bone marrow is regarded as more reliable and accurate method than MFC, being able to detect disease down to 1 in 10^6 cells (Rack et al. 2016). Furthermore, a strong correlation between depth of response and overall survive, most notably in the post-transplant setting, has been shown (Martinez-

Lopez et al. 2014). However, the need for the design of patient-specific primers, the technical expertise required and the associated expense, has meant that these methods are not widely available. The two most commonly used molecular deep sequencing methods are, Allele-specific oligonucleotide-quantitative polymerase chain reaction (ASO-PCR) and NGS of the patient's unique immunoglobulin region (IgH VDJ assay). In an attempt to reduce costs, commercially available pre-designed V(D)J multiplexed PCR amplification assays such as LymphoSIGHT™ are available. This method also has the advantage of being able to monitor specific sub-clones throughout the lifetime of the disease.

Gene expression profiling (Szalat et al. 2016) has also been shown to identify patients with poorer prognosis as well as CT-PET imaging, whereby 7 lesions or more corresponds to a worse outcome (Hillengass et al. 2019).

1.2 Myeloma Therapy

Standard of care for patients with newly diagnosed MM, who are eligible for high dose therapy, currently involves the combination of the so called '*novel agents*'; Proteasome Inhibitors (PI) such as bortezomib and carfilzomib, with one of the immunomodulatory drugs (IMiDs) thalidomide or lenalidomide. These drugs are usually combined with cyclophosphamide and/or dexamethasone. The synergistic effect of the novel agents has been widely documented, with response rates of around 85% for single agent treatment increasing to 98%, when PI and IMiD are combined (Richardson et al. 2009; Kumar et al. 2011; Morgan et al. 2012a). If fit, treatment should be consolidated with a high dose melphalan autologous stem cell transplant, which when combined with lenalidomide maintenance has been shown to increase PFS compared to no transplant (50 months vs 36 months), although overall survival difference is not as impressive (Attal et al. 2017).

Targeting patients with high-risk asymptomatic myeloma/SMM has remained an area of ongoing clinical research. In theory, by targeting high-risk patients for treatment, the aim is to remove clones before they accrue secondary mutations (e.g. molecular alterations of *TP53* or oncogenic activation genes) and more aggressive sub-clones arise. Although current treatment is unlikely to permanently eradicate all disease, numerous studies involving novel therapies are being developed and trialled in the high-risk SMM group. For example, treatment with lenalidomide, carfilzomib and dexamethasone, followed by 2 years of lenalidomide maintenance achieved a 100% very good partial response (VGPR – defined as >90% decrease in paraprotein) or better (Landgren et al. 2013).

1.2.1 Glucocorticoids (GC)

Steroids have been used to treat MM since the 1960's (Mass 1962) and have remained a key component of today's MM treatment regimens. Short pulses of dexamethasone are the preferred method of glucocorticoid administration and induce cell death either through cell apoptosis or necrosis (Alexanian et al. 1992).

1.2.1.1 Cellular apoptosis

Cellular apoptosis is induced through the actions of the glucocorticoid receptor (GR) and so its expression is crucial in determining glucocorticoid sensitivity (Reichardt et al. 2000). The mechanism by which cells undergo apoptosis upon activation of the GR varies dependent on the cell type and the expression of key proteins such as Bim, Bcl-2 and

Glucocorticoid-induced leucine zipper (GILZ). GR on the cell surface when activated will cause a number of changes that include: activation of RAFTK (normally deactivated by IL-6), causing apoptosis through the activity of protease enzymes and caspases; the inhibition of the proliferate pathways, MAPK (a key driver of IL-6 production, mediated by the inflammatory cytokine TNF-α) and PI3K/Akt, resulting in G1-phase growth arrest; and the block of NF-κB-mediated transcription of pro-survival/anti-apoptotic genes (Wang et al. 2003; Smith and Cidlowski 2010).

1.2.1.2 Cellular necrosis

Cellular necrosis can be an indirect consequence of gene dysregulation. Internalisation and cytoplasmic glucocorticoids can result in a rapid turnover of gene transcription, resulting in cellular distress and cell death, either triggered by calcium flux, oxygen radicals, changes in cellular volume or pH (Fernandez et al. 1995; Gomez-Angelats et al. 2000; Matsuyama and Reed 2000; Schmidt et al. 2004).

1.2.2 Proteasome Inhibitors (PI)

1.2.2.1 The Ubiquitin Proteasome System

The ubiquitin proteasome system regulates the destruction of misfolded or no longer required proteins inside cells. This occurs by the regulatory protein ubiquitin being attached to the protein by a process called ubiquitination. In this process, 3 separate ubiquitin-activating enzymes, E1, E2 and E3 are required to add ubiquitin to the protein. The enzymes are highly specific to the protein to be degraded, thus allowing the cell to only degrade specific proteins. Once 3-4 ubiquitin molecules are added onto the protein, the proteasomes recognise the complex and can degrade it. In disease, the proteasomes can be either overactive, so essential cell function proteins are destroyed, or underactive, thereby allowing the build-up of toxic, harmful proteins (Pickart and Eddins 2004). The 26S proteasome consists of a core 20S complex and one or two 19S regulatory complexes. Within the core complex are 3 sites of action (Adams 2003);

- β5 are “chymotrypsin-like” (Chym-L)
- β2 are “trypsin-like” (Tr-L)
- β1 are “caspase-like” (Casp-L)

The Chym-L site is seen as the most important for protein breakdown, knockout Chym-L mice experiments have shown retardation of growth and accumulation of proteasomes (Chen and Hochstrasser 1996; Heinemeyer et al. 1997).

Proteasome inhibition has been shown to be an attractive treatment for cancer cells, including MM (Hideshima et al. 2002b). The build-up of toxic proteins, in high protein output cells such as plasma cells that produce immunoglobulins can cause cell death as well as preventing degradation of pro-apoptotic proteins. Bortezomib, the first in class proteasome inhibitor (PI), has been shown to stop degradation of the inhibitor of NF-κB (IκB), through inhibition of the proteasome β5 and β1 subunits. A relative increase in IκB, results in NF-κB inhibition, a key signalling pathway involved in cancer survival and proliferation (Jourdan et al. 2007; Chen et al. 2011). The additional inhibition of β1 "caspase like" subunit sites are thought to sensitise the cell for additional "chymotrypsin-like" inhibition, maximising cytotoxicity, although the newer generation of PIs are not believed to inhibit β1 subunits (Britton et al. 2009).

1.2.2.2 Bortezomib, the first licensed PI and the emergence of the 2nd generation PI's

Bortezomib is currently the only PI approved for first line treatment by both the FDA and NICE. The irreversible, more selective PI, carfilzomib is more widely used in the relapsed refractory (RRMM) setting, having been approved for this use by the FDA in 2012, with use as a front-line agent limited to trials such as the now closed NCRI Myeloma XI trial. Trials of carfilzomib as a front-line agent have tended to show superior activity when compared to bortezomib, resulting in a 96% response rate with 62% achieving a near complete response (CR) with an estimated PFS of 92% at 24 months (Jakubowiak et al. 2012). Its use in the relapse refractory setting as monotherapy in heavily pre-treated patients (including bortezomib) has seen response rates up to 52% and a medium duration of response of up to 7.8 months (O'Connor et al. 2009; Siegel et al. 2012; Vij et al. 2012). Although carfilzomib has a similar side effect profile to bortezomib, which includes fatigue (55%), myelosuppression and peripheral neuropathy (13.9%), the incidence of these features is reported to be lower, potentially making it a more attractive PI, especially in those not suitable for high dose therapy or those with pre-existing neuropathy (Argyriou et al. 2008; Jain et al. 2011; Siegel et al. 2012). Although the eldest in these early trials was 88 years old, the higher cardiotoxic signal seen with carfilzomib compared to bortezomib makes it less appealing in the very elderly, especially with those with pre-existing heart conditions.

The first orally available, and third PI to be approved by the FDA is ixazomib. Results in phase II trials in combination with lenalidomide and dexamethasone for newly diagnosed patients have shown similar results to bortezomib, with a 96% response rate, 26% showing

a complete response (Kumar et al. 2012). The tolerability of the drug, favourable side effect profile and ease of use make it an attractive option in the relapsed/refractory setting where PFS is increased by 6 months when combined with lenalidomide (Moreau et al. 2016) and also as a maintenance regime (Richardson et al. 2013a). Table 1.4 outlines the comparison between proteasome inhibitors.

1.2.3 Immunomodulatory drugs (IMiD)

Table 1.4 compares the three FDA approved immunomodulatory drugs. Despite the variation in activity, they are chemically very similar. Pomalidomide and lenalidomide contain an extra amino group on the fourth carbon of the phthaloyl ring of thalidomide, with pomalidomide retaining an oxygen atom that lenalidomide losses, essentially making pomalidomide the combined chemical structure of thalidomide and lenalidomide (Quach et al. 2010). They all share similar anti-angiogenic activity, but pomalidomide has greater immunomodulatory effect than the other two, especially compared with thalidomide; it is 15,000 times more potent at inhibiting malignant B-cell proliferation and TNF-α activity (Corral et al. 1999).

Despite the potency and more tolerable side-effect profile of the next generation IMiDs, NICE currently only recommends thalidomide as front line IMiD therapy, despite being shown to be inferior to lenalidomide (Jackson et al. 2017). Upon achieving a remission, their use as maintenance therapy has been shown to increase PFS (Hicks et al. 2008; Jackson et al. 2017). However, it remains controversial whether IMiD maintenance therapy can improve OS, with some experts claiming that the side effect profile, including the incidence of secondary malignancies associated with lenalidomide treatment, outweighs any gain in PFS (Attal et al. 2012; McCarthy et al. 2012; Palumbo et al. 2012; Singh et al. 2013).

The 2014 updated BCSH Myeloma guidelines (Pratt et al. 2014), provides the option of thalidomide maintenance post autograft. However, this does not necessarily correlate to an increase in OS (Barlogie et al. 2006) with therapy strongly associated with peripheral neuropathy and the attendant reduction in the quality of life. These factors will likely mean both thalidomide and lenalidomide, will fall short of the ideal maintenance therapy, that of a single agent, that improves overall survival, with minimal toxicity.

	Proteasome Inhibitors			Immunomodulatory Drugs		
	Bortezomib	Carfilzomib	Ixazomib	Thalidomide	Lenalidomide	Pomalidomide
Activity						
Anti-angiogenic	-	-	-	++++	+++	+++
Anti-inflammatory	-	-	-	+	++++	+++++
T-cell co-stimulation	-	-	-	+	++++	+++++
T-regs suppression	-	-	-	-	+	+
NK/NKT cell activation	-	-	-	+	++++	+++++
ADCC	-	-	-	-	++++	++++
Anti-proliferative	++++++	++++++	++++++	+	+++	+++
Proteasome Features						
Active moiety	Boronate	Epoxyketone	Boronate	-	-	-
Subunits inhibited	β5, β1	β5	β5	-	-	-
Binding kinetics	Reversible	Irreversible	Reversible	-	-	-
β5/Chymotrypsin IC_{50} (nM)	2.4-7.9	6	3.4	-	-	-
β2/Tryspin IC_{50} (nM)	590-4200	3600	3500	-	-	-
β1/Caspase IC_{50} (nM)	24-74	2400	31	-	-	-
MM IC_{50} (nM)*	5.7	5.0	7.85	>400 $x10^3$	>400 $x10^3$	8 $x10^3$
Half-life (hours)	1.8	<0.5	0.3	4-9	3.1-4.5	6.2-7.9
Metabolism/excretion	Hepatic	Hepatic	Hepatic	Hepatic	Renal	Renal
Route of administration	IV/SC	IV	Oral/IV	Oral	Oral	Oral
FDA approval	2003	2012	2015	2006	2006	2013

Table 1.4. Comparison between proteasome inhibitors and immunomodulatory drugs used in MM *(Adapted from (Quach et al. 2010; Schmidt et al. 2011; Moreau et al. 2012; Guglielmelli et al. 2015; Place 2015).*against RPMI-8266 MM cell line; FDA - Food and Drug Administration; IV - intravenous; SC - subcutaneous; '+' relative potency factor of 10; Ic50 indicated half-maximal inhibitory concentration; ADCC – antibody-dependent cell-mediated cytotoxicity; NK(T) – Natural killer (T) cells.*

The 3rd generation IMiD, pomalidomide has been mainly used in the relapsed/refractory setting both as monotherapy or in combination. The potency of pomalidomide persists even in those refractory to lenalidomide and bortezomib where phase II trials have shown up to 40% response rates, double of that compared to single agent dexamethasone, with improved PFS and increased OS rates to 14.9 months even in those with poor-risk cytogenetics, notably del 17p (Shah et al. 2012; Leleu et al. 2013; San Miguel et al. 2013; Richardson et al. 2014).

Treatment of high-risk SMM patients has been predominantly with IMiDs. Initial trials showed little gain in OS when treated with thalidomide or melphalan (Barlogie et al. 2008). However, the seminal QuiRedex study (Mateos et al. 2013) was the first to specifically look at treating high-risk SMM patients with lenalidomide and dexamethasone. The treatment arm showed an increase in both PFS (77% vs 30%) and OS (94% vs 80%). This trial cemented the belief that a cure for MM lies within early treatment to remove the possibility of sub-clonal progression.

1.2.4 Histone Deacetylase Inhibitors (HDACI)

The mechanism of action of HDACI such as panobinostat and vorinostat involves preventing the inactivation of p53 and the blockade of the Unfolded Protein Response (UPR), a set of signalling pathways, which are essential for the survival of MM cells and also the site of activity for proteasome inhibitors. In the event that proteins marked for degradation build up in the cell, they form aggregates of misfolded/unfolded proteins that is termed an aggresome. The formation of aggresomes are highly organised and are a coping mechanism of the cell when proteasome function has reached full capacity or when proteasome function is inhibited (Johnston et al. 1998). Aggresome formation is dependent on histone deacetylase 6 (HDAC-6) (Ouyang et al. 2012) and has become a target of inhibition in cancers with possible synergy with PIs (Hideshima et al. 2011). Although improved depth of responses are seen when combined with bortezomib, it is unclear if this translates into improved OS and the tolerability of these agents is relatively poor (Kaufman et al. 2012; Dimopoulos et al. 2013; Richardson et al. 2013b). These factors, combined with the emergence of targeted immunotherapy, likely infers HDACI will have a very limited role in the future.

1.2.5 Monoclonal antibodies (mAb)

The anti-CD38 mAbs Daratumumab and Isatuximab, have both shown to be well tolerated with limited toxicity (Plesner et al. 2012; Martin et al. 2013). Daratumumab was the first mAb to obtain FDA approval in 2015 in the relapsed setting for MM as monotherapy, on the back of a phase I/II trial showing increased PFS of 5.6 months and a ORR of 36% (Lokhorst et al. 2015). It has been shown to have potent anti-myeloma activity both in vitro and vivo with multiple mechanisms of action that include complement-dependent cytotoxicity (CDC), antibody-dependent cell mediated cytotoxicity (ADCC), antibody-dependent cellular phagocytosis (ADCP), Fcγ*R*-mediated apoptosis and CD38 ecto-enzyme inhibition (Lee and Weber 2016; Lonial et al. 2016). The phase III trials CASTOR and POLLUX used daratumumab in combination with either bortezomib or lenalidomide in RRMM. Both trials showed promising interim data with the lenalidomide combination showing slightly better response rates (93% vs 83%) (Dimopoulos et al. 2016; Palumbo et al. 2016).

More recent trials have shown the benefit of adding Daratumumab to frontline treatment, for both transplant eligible (TEP) and non-transplant eligible patients (NTEP). The CASSIOPEA trial for TEP, combined daratumumab with bortezomib, thalidomide and dexamethasone, (Moreau et al. 2019), whereas the MAIA (Facon et al. 2019) and ALCYONE (Mateos et al. 2018) NTEP trials combined daratumumab with lenalidomide and bortezomib respectively. Each of these trials showed impressive statistically significant increases in both complete remission rates and minimal residual disease negatively. and ALCYONE trial, combined with bortezomib. Furthermore, the use in high-risk smouldering myeloma shows encouraging responses in preventing MM transformation. The Centaurus trial used single agent Daratumumab for up to 2 years, obtaining a 12-month PFS of 98% (Hofmeister et al. 2017).

The second FDA approved mAb is elotuzumab. This antibody targets the cell marker SLAM7 (previously known as CS1) and is highly specific to plasma cells. Unlike daratumumab its mechanism of action is solely through ADCC, although inhibition of adhesion to bone marrow stromal cells is observed suggesting SLAMF7 plays a role within the MM microenvironment (Lee and Weber 2016). The results of single agent use in RRMM were disappointing with no activity observed in phase I trials (Zonder et al. 2012). However, when used in combination with lenalidomide and dexamethasone in the relapse/refactory setting, the results have been more encouraging with 24-month PFS increased from 27% to 41% (Lonial et al. 2015).

1.2.6 Signal transduction pathways inhibitors

Signal transduction pathways (notably PI3K/AKT/mTOR, MEK and NF-κB) play an important role in the pathogenesis of myeloma with upregulation of these pathways often observed and usually as a result of specific gene mutations e.g. MEK upregulation due to *RAS* mutation. Therefore, not surprisingly small molecular inhibitors of these pathways have been in early phase I/II development for a number of years.

1.2.6.1 Phosphoinositide 3-kinase (PI3K) inhibitors

PI3K is a lipid kinase signal transducer involved in the regulation of various cellular functions that include growth, proliferation, differentiation, and survival. Three classes of PI3K exist, with class 1 catalytic isoforms (p110) currently the main target for drug design (Jean and Kiger 2014; Naymagon and Abdul-Hay 2016). Within myeloma, the most advanced of these are the oral AKT inhibitors perifosine and afuresertib. Inhibition of the AKT/PI3K signalling pathway has been shown to promote cell apoptosis, with additional cell death synergy when combined with bortezomib (Hideshima et al. 2007a). Perifosine despite promising phase I/II data, saw the larger phase III trial halted early as little benefit was observed (Richardson et al. 2011; El-Amm and Tabbara 2013). Meanwhile, Afuresertib in a dose escalating phase I trial was shown to have a 41% overall response rate when combined with bortezomib and dexamethasone and was reported as having a manageable safety prolife (Trudel 2016).

The most established PI3K inhibitor in haematological malignancies is currently idelalisib. This Class I p110δ PI3K inhibitor was approved in 2014 for the treatment of p53 mutated and relapsed CLL and follicular lymphoma. It has also been trialled in other B-cell malignancies, including MM (Jabbour et al. 2014), where it has been shown to have a direct effect on MM growth and cell survival. Furthermore, it seemingly can overcome the protective effects of cytokines IL-6 and IGF-I within the BM milieu (Ikeda et al. 2010). However to date, no PI3K inhibitor clinical trials in MM have been designed, partly due to the concerns over toxicity (Cheah and Fowler 2016). Despite this, numerous PI3K inhibitors have undergone preclinical investigations in MM models. The class I pan-PI3K inhibitors PIK-C98 and Buparlisib have shown potent preclinical effects on MM cell lines, with Buparlisib having a potential impact on the bone marrow microenvironment through downregulation of osteoclasts and upregulation of osteoblasts, thus potentially reducing osteolytic lesions (Martin et al. 2015; Zhu et al. 2015). Specific class I isoform PI3K inhibitors also exist, BAY80-6946 (p110α) and GDC-0941 (p110α and p110β) have shown

cytotoxic, anti-proliferative and oncogene IGF-1 inhibition across a number of MM cell lines, with synergy when combined with lenalidomide and dexamethasone in murine xenograft tumour models (Glauer et al. 2013; Munugalavadla et al. 2014).

mTOR inhibitors, such as rapamycin in theory would have benefit in preventing MM cell growth and proliferation by blocking the downstream effects of PI3K and Akt. (Li et al. 2014). Although clinical trials of mTOR inhibition in a number of cancers have occurred, no significant ones involving MM have been documented.

1.2.7 Chimeric antigen receptor T-cells (CAR-T)

CAR-T therapy involves modifying a patient's own T-cells, to express a chimeric protein that targets a specific antigen and then re-infusing the T-cells back into the patient. To date a number of different myeloma cell antigens have been studied, these include B-cell maturing antigen (BCMA), SLAMF7, CD138, NKG2DA and CD19 (Kumar 2017). The most promising target to date is BCMA. In a phase I study, 21 heavily pre-treated patients (median prior lines of therapy 7), where treated in a dose-escalation study. ORR was 89%, with MRD achieved in all patients who had an MRD marker (Berdeja et al. 2017).

1.2.8 Other emerging therapies

Targeted therapies such as the anti-apoptotic protein BCL-2 inhibitor ABT199 (venetolcax) has shown potency in both cell lines and patients with t(11;14), which can be up to 20% of patients (Kumar et al. 2017). However, concerns regarding venetolcax toxicity have been raised with the recent FDA warning. Enrolment of patients onto the venetolcax arm of the BELLINI trial for RRMM has been halted due to excess deaths in the venetolcax arm (FDA 2019).

The kinesin spindle protein inhibitor dinaciclib and the pan PIM kinase inhibitor LGH-447, are other drugs which are potentially showing promising single agent activity in the RRMM setting (Rajan and Kumar 2016).

1.2.9 Supportive care

Recent British Society of Haematology (BSH) guidelines has put huge emphasis in the supportive care of myeloma patients both at diagnosis and during treatment (Snowden et al. 2017). The guidance includes strategies to reduce infection, prevention of thrombosis, pain management and treatment of bone disease. Bisphosphonates, such as zoledronic acid, are routinely given to myeloma patients as treatment for bone disease. They have been shown to preserve bone density and reduce skeletal fractures through their osteoclastic inhibition as well as prolong progression-free and overall survival (Morgan et al. 2013). The mechanisms for improved OS are not clear, but likely involves modification of the bone marrow microenvironment as well as direct anti-myeloma activity (Aparicio et al. 1998; Silbermann and Roodman 2013). Other treatments for bone disease include localised radiation, which can be effective for bone pain, treatment of unstable spinal disease and solitary plasmacytomas.

Addition of prophylactic antibiotics, can also have a dramatic impact in preventing infections. Many serious infections occur within the first few months of diagnosis, due to the combined effects of chemotherapy, impaired normal immune function and the impact of spinal bone disease has on impaired breathing leading to chest infections. The 2019 results of the TEAMM trial, showed that both the number of infections and deaths were reduced if patients received 12 weeks prophylactic levofloxacin upon diagnosis of MM (Drayson et al. 2019). Other anti-microbial treatments include the anti-viral acyclovir, used with proteasome inhibitors to prevent shingles and herpes simplex infections.

1.3 Mechanisms of drug resistance

MM is characterised by cycles of remission and relapse, which infers that eventually all forms of treatments will fail, or the disease becomes resistant to treatment. The mechanisms of drug resistance and how myeloma cells acquire them are complex. They include genetic, epigenetic or transcriptional changes usually involved in survival or apoptotic pathways. These changes can either be acquired or pre-existing, either way the selective pressures caused by drug treatment drive the emergence of drug-resistant sub-clonal populations.

1.3.1 Clonal evolution

The concept of 'clonal tides' was born from the monitoring of MM sub-clones and their changes in relative frequency through the course of a single patient's disease from diagnosis to death (Keats et al. 2012). Through PCR analysis of the IgH VDJ region, multiple clones were identified at diagnosis. At each stage of disease treatment and upon relapse, the percentage frequency of these clones was monitored. The terminal clone most predominant at death (following progression to leukaemic phase of the disease) was shown to be present at diagnosis but represented a very small proportion of the original cancer bulk (<1%). This model of tumour evolution seemingly went against traditional paradigms of cancer evolution such as the unicellular origin linear model, where sequential acquisitions of NS-SNV (Non-Synonymous-Single Nucleotide Variant) mutations that drive disease progression.

Thus, newer clonal paradigms of disease evolution that attempt to explain Keats' findings, have become either an expansionist model where all mutations are present at diagnosis in multiple sub-clones (Walker et al. 2014), or an intra-clonal heterogeneity model as outlined in Figure 1.3 (Egan et al. 2012). The latter model allows distinct clones to react to selective pressures in a Darwinian response, selecting out clones with survival benefits, either through pre-existing mutations or newly acquired ones, both of which are termed 'driver mutations.' The complexity of this model, makes the treatment and potential cure of MM extremely difficult, as all clones have the potential to further adapt independently through the acquisition of additional driver mutations and thereby obtain drug resistance (Chapman et al. 2011; Egan et al. 2012; Bolli et al. 2014; Walker et al. 2014).

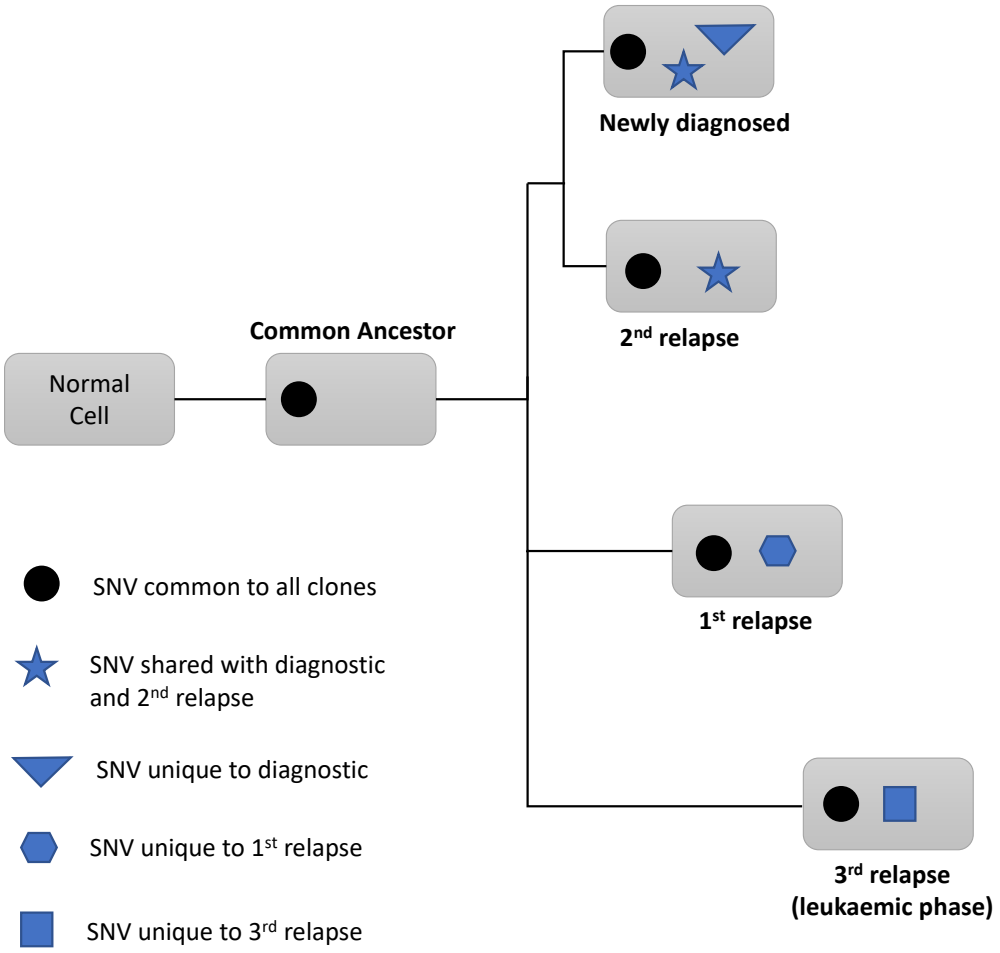

Figure 1.3. Intraclonal heterogeneity model of Multiple Myeloma (MM) development*, adapted from Egan et al. 2012. Cartoon is a phylogram of the different MM clones throughout the course of disease. Distinct PC subclones are present at diagnosis, but the dominant subclone changing with each MM disease progression. All clones contain common Single nucleotide variants (SNVs) indicating a shared common ancestor, but also unique SNV that act as driver mutations. In Egan's example there were 15 common SNV at all time points (●), 6 SNV common to the diagnostic and 2nd relapse (★), while no variants where common to the 1st relapse and 3rd relapse/leukaemic phase. The greatest divergence is that between the 1st and 3rd relapse/leukaemic phase, with 7 unique variants (■ and ⬣) detected in each sample (Egan et al. 2012)*

1.3.2 Glucocorticoid Drug resistance

There are three main mechanisms of glucocorticoid resistance (Schmidt et al. 2004):

i. **Insufficient ligand;** - intracellular GC levels may be reduced by increased levels of steroid binding proteins in the circulation, expression of GC metabolising enzymes or overexpression of cell membrane transporter proteins, thus removing intracellular GC e.g. P-glycoprotein (P-gp). Such resistance can be overcome by using P-gp inhibitors such as ciclosporin or verapamil-based drugs (Bellamy 1996; Karssen et al. 2001).

ii. **GR mutations, splice variants or insufficient expression**; - without the receptor, downstream signalling pathways are unable to be initiated. The lack of GR is thought to be the main mechanism of acquired GC resistance of the MM cell line MM.1R, obtained through long-term exposure to dexamethasone (Greenstein et al. 2003).

iii. **Deficiency in GR-associated proteins;** - these can either be cytoplasmic or nuclear in origin. Mutations or unresponsiveness of GC-regulated genes that are critical for cell death and/or genes that are able to interfere with the GC-induced death pathway could have overall impact on GC-induced apoptosis.

Table 1.5 outlines genes with the greatest microarray expression changes in the MM cell line MM.1S upon exposure to GC. Expression changes in these gene are not exclusive to MM but are seen in many other cell lines (Schmidt et al. 2004).

Identifier	Description	Reg	Other systems gene shared with
Hs.81328	NF-κBα inhibitor (IκB-α)	↑	PreB, S49, WEHI, Jurkat, CEM, thymus-1
Hs.7557	FK506-binding protein 5 (FKBP 51)	↑	PreB, WEHI, EoL, Jurkat, CEM
Hs.420569	GILZ	↑	PreB, CEM, thymus-2
Hs.179526	Thioredoxin interactin protein (TXNIP)	↑↓	PreB, CEM
Hs.442669	Glutamine synthase	↑↓	PreB, thymus-2
D50683	TGF-β II Receptor α	↑	Jurkat, CEM

***Table 1.5. Genes regulated by GC in cells prone to GC-induced apoptosis**, as identified in MM.1S cell line from microarray. Only genes with greater 2-fold change are shown, table adapted from (Chauhan et al. 2002; Schmidt et al. 2004). Genes are listed according to the number of systems wherein regulation was observed; Identifier is either Unigene number (starting with Hs.) or GeneBank accession number (D50683); ↑ and ↓ denote two-fold or greater gene induction or repression, respectively; Cellular Human systems: CEM - various sub-clones of the CCRF-CEM T-ALL cell line; PreB - PreB-697 B-ALL cells; Jurkat - T-ALL cell lines stably transfected with either rat GR^{wt} or rat GR^{LS7}* Mouse*: WEHI - WEHI7.2 lymphoma cell line; S49 - S49.A2 lymphoma cell line; thymus-1 - normal C56BL/6 thymocytes; thymus-2 - 18d foetal thymocytes from C57BL/6 wild-type mice or GR2KO mice.*

1.3.3 P-glycoprotein 1 (P-gp)

P-gp is also known as multidrug resistance protein 1 (MDR1) and ATP-binding cassette sub-family B member 1 (ABCB1). Encoded by the *ABCB1* gene, it is a member of the ATP-binding cassette (ABC) transporter proteins, itself a member of the MDR/TAP subfamily (Ueda et al. 1987). ABC proteins are able to transport various molecules across extra- and intra-cellular membranes and are involved in multidrug resistance. P-gp expression has been shown to increase in cases of MM drug resistance and is thought to act as an efflux pump for xenobiotic compounds with broad substrate specificity, such as glucocorticoids and PI (Grogan et al. 1993; Verbrugge et al. 2012). This can often mediate the origin and subsequent clonal expansion of cancer cells, becoming resistant to anticancer therapy (Karssen et al. 2001; Breier et al. 2013).

1.3.4 Proteasome Inhibitor Resistance

In addition to increasing P-gp expression, a number of differing mechanisms are thought to contribute to PI resistance. One of first reported was the gene mutation *PSMB5*, that codes for the β5 subunit bortezomib binding site (Oerlemans et al. 2008; Ri et al. 2010), thus impairing the ability of PI's to bind to the active subunit. Other mechanisms include (Wallington-Beddoe et al. 2018):

- Aberrant expression of the ubiquitin-proteasome pathway components

- HDAC6 modulated activation of the aggresome autophagy pathway
- Heat shock protein (e.g. Grp78, Hsp90) induction
- Over-expression of *NFE2L2,* resulting in antioxidant response pathway induction
- Reduced expression of the transcription factor Xbp-1, limiting PC differentiation required for PI sensitivity
- Increase in survival signalling pathways such as IL-6, VEGF, c-MET, NF-κB, PI3K/AKT, IGF-1/IGF-1R and EGFR/JAK/STAT

1.3.5 Immunomodulatory Resistance

IMiD resistance is thought to be mainly related to cereblon pathway abnormalities, regarded as the main target of the IMiDs (Ito et al. 2010). The mechanisms can either be due to reduced cereblon expression, therefore less available target for IMiD binding or pathway component mutations, reducing the ability of the IMiDs to bind to cereblon or their associated pathway components (Wallington-Beddoe et al. 2018).

1.3.6 Cell Adhesion Mediated-Drug Resistance (CAM-DR)

The bone marrow (BM) microenvironment allows for MM cell proliferation, survival and protection against cytotoxic agents (Damiano et al. 1999). Drug resistance can also occur through interaction between the adhesion receptors integrins on MM cells and their ligands on BM stromal cells (BMSC) and/or extracellular matrix proteins (ECM) (Hideshima et al. 2007b; Noborio-Hatano et al. 2009). This type of drug resistance has been termed CAM-DR, outlined in Figure 1.4. Both Bortezomib and glucocorticoids have been shown to downregulate expression of VLA-4 thus overcoming the effects of CAM-DR (Tonko et al. 2001; Planey et al. 2003; Webb et al. 2003; Noborio-Hatano et al. 2009).

1.4 Identification and immunophenotypic characterisation of plasma cells in MM

1.4.1 CD138 and CD38 allows for identification of plasma cells

CD138 and CD38 are highly expressed on both normal and disease bone marrow plasma cells. As high expression of CD138 is broadly unique to plasma cells, dual expression of these cell markers are ideal in plasma cell identification (Bataille et al. 2006). CD138, also known as syndecan-1, is a heparan sulfate proteoglycan that promotes cell-surface adhesion of plasma cells involved in their homing to the bone marrow (Katz 2010). CD38 is a cell surface protein that acts both as a receptor and an ecto-enzyme.

1.4.1.1 CD38 expression

The CD38 gene is located on chromosome 4 (4p15) comprising of 8 exons and 7 introns spanning 62kb (Katz et al. 1983). Gene transcription is regulated mainly by CpG islands in the promoter region but also by intron 1 responsive elements of retinoic acid (RA) and peroxisome proliferator-activated receptor γ (PPARγ) (Kishimoto et al. 1998; Song et al. 2012). It is widely expressed on cells of haematopoietic origin, both myeloid and lymphoid, primarily on activated cells and immature cells, with the highest expression generally seen on terminally differentiated plasma cells. Within the normal population and within ethnic groups, there is a wide variation in CD38 expression, with *CD38* gene polymorphisms thought to be a contributing factor to this. Furthermore CD38 expression has been shown to correlate with anti-neoplastic drug sensitivity (Hartman et al. 2010). CD38 expression on MM cells remains high and similar to that seen on normal plasma cells. Unlike CLL, it has not been shown to be a prognostic marker as it is expressed on virtually all MM cells (Hamblin et al. 2002; Lin et al. 2004; van de Donk et al. 2016). Upregulation of CD38 expression is observed in MM patients treated with All Trans-retinoic acid (ATRA) resulting in greater efficacy of the CD38 monoclonal antibody daratumumab (Nijhof et al. 2015).

1.4.1.2 CD38 function

Its function as a receptor helps regulate weak adhesion between CD31 (PECAM-1) on endothelial cells and migrating lymphoid cells (Dianzani et al. 1994). CD31 (the sole ligand of CD38) is also expressed on lymphoid cells, allowing for both cell-cell interaction and migration through the endothelial cell wall (Cesano et al. 1998). The interaction of CD38 and CD31 has also been shown to cause proliferation of lymphoid cells, CXCL12-induced cell migration and lymph node homing (Deaglio et al. 2010; Vaisitti et al. 2010).

CD38 also has enzymatic properties, having cyclase and hydrolase activity (van de Donk et al. 2016). Through the generation of nicotinic acid-adenine dinucleotide phosphate (NAADP+), CD38 is able to regulate Ca^{2+} mobilisation from the cytoplasm, which activates signalling pathways such as PKC and NF-κB resulting in lymphocyte proliferation (Guse et al. 1999; Moreno-Garcia et al. 2005).

1.4.2 Identification of malignant/clonal plasma cells

Additional markers are required to distinguish between normal/polyclonal PC and those of pathological/clonal PC. Molecules involved in the maturation process of PC such as CD19 and CD45 as well as the Ig superfamily molecule CD56, are routinely used in the clinical setting to differentiate between normal and MM plasma cells (Manzanera et al. 2005). Additional molecules such as surface or cytoplasmic immunoglobulin light chains (κ and λ), CD13, CD20, CD28, CD33, CD40, CD52, CD86 and CD117 can also be used as clonal PC identification markers or even as MRD markers (Flores-Montero et al. 2016). Table 1.6 adapted from Bataille et al., compares the immunophenotype of normal and malignant PCs.

Cell Marker	Normal (BM)	MM (BM)	PCL (PB)
CD138	+++	+++	+++
CD38	+++	+++	+++
CD56	-	+++	-
CD19	+	-	-
CD45	+	-	-
CD20	-	+/-	+
CD28	-	+	+

Table 1.6. Comparison of immunophenotype of normal and malignant PC. *(– infers cell marker not expressed, + expressed, +++ strongly expressed). MM – multiple myeloma; BM – bone marrow; PCL – plasma cell leukaemia; PB – peripheral blood. Adapted from (Bataille et al. 2006).*

1.4.3 Cell markers involved in cell migration and adhesion

1.4.3.1 CXCR4, an important cell marker for migration and survival

CXCR4 is the chemokine receptor for CXCL12. The chemokine is highly expressed in various healthy tissues including lung, liver, bone marrow and is secreted by stromal cells as well as malignant cells. The binding of the chemokine to CXCR4 initiates various downstream signalling pathways, resulting in gene transcription, initiating cell migration, proliferation and survival (Ganju et al. 1998; Chatterjee et al. 2013). CXCL12 binding activates two major signal transduction enzymes, phospholipase C-β (PLC-β) and phosphoinositide 3-kinase (PI3K). This ultimately induces the release of Ca^{2+} from intracellular stores, activating protein kinase C (PKC), protein tyrosine kinase 2 (PTK2), paxillin and mitogen-activated protein kinase (MAPK), resulting in the induction of cell migration through reorganisation of the actin cytoskeleton (Mellado et al. 2001).

CXCR4 has also been shown to activate the Ras/ERK and JAK/STAT signalling pathways, leading to changes in gene expression, cell cycle progression and changes in cell morphology required for migration (Chatterjee et al. 2013). Furthermore, activation of PI3K/AKT pathway by CXCR4 has effect on the promotion of cell survival and proliferation. This occurs through inhibition of the pro-apoptotic protein BAD and by AKT stabilising the transcription factor β-catenin, which can then translocate to the nucleus and activate gene transcription (Clevers and Nusse 2012; Mo et al. 2013).

1.4.3.2 CXCR4/CXCL12 in Multiple myeloma

Early in MM disease development, MM cells migrate to the BM through the action of CXCR4 acting as the receptor for the chemokine CXCL12 (Alsayed et al. 2007). Once in the BM microenvironment, CXCR4 is able to regulate MM cell adhesion to stromal cells via its interaction with the integrin VLA-4 (Parmo-Cabanas et al. 2004; Chatterjee et al. 2013).

CXCR4 expression in plasma cell dyscrasia can be very variable, but with a general trend of decreased expression with increasing disease activity (Moller et al. 2003; Alsayed et al. 2007). One study of 227 newly diagnosed patients showed an association between absence of CXCR4 expression with hypercalcemia, bone destruction, occurrence of extramedullary disease and reduced overall survival (Bao et al. 2013). This clinical observation is supported by mouse models, which show reduced CXCR4 expression is associated with bortezomib resistance, extramedullary disease and reduced survival (Stessman et al. 2013).

However, subsequent studies have shown the relationship between CXCR4/CXCL12 expression and prognosis to be far more complex, especially in the role of extramedullary disease. Contrary of Stessman's et al findings, increased expression of CXCR4/CXCL12 has been shown to play a role in the dissemination of plasma cells to extra-medullary sites, through Epithelial-Mesenchymal Transition (EMT) like transcriptional activation (Roccaro et al. 2015). Roccaro speculates the difference in their findings could be related to subclonal variation in CXCR4 expression or up-regulation of CXCR4 through epigenetic changes upon subclonal dissemination to the BM or extramedullary sites. The resulting increase in expression of the subclones leads to proliferation and survival of these cells in their new host environment (Roccaro et al. 2015).

Subclonal CXCR4 variation may explain why in certain MM cell lines and primary samples, CXCR4 antagonists are able to inhibit MM growth and could serve as a therapeutic option in preventing plasma cell to disseminate (Beider et al. 2011). Indeed, such antagonists (e.g. plerixafor) are already used in the manipulation and subsequent mobilisation of haematopoietic stem cells, prior to stem cell collection (Steinberg and Silva 2010).

1.4.3.3 Integrins, pivotal role in plasma cell adhesion

Integrins are transmembrane proteins found on numerous cells, that allow interactions with other cells and/or their extracellular matrix. Each integrin is comprised of a single alpha and a single beta subunit that both penetrate the cell surface membrane with small cytoplasmic domains. In humans, there are 18 different alpha subunits and 8 beta subunits, making a large number of possible combinations. Their function is either related to the direct interaction with other cells/substances in the ECM or the influence they exert on various cytoplasmic signalling/tyrosine kinases/growth factors (Kumar 1998; Martin et al. 2002). They play a role in the following cell functions (some of which are shown in Figure 1.4):

- migration (Sanz-Rodriguez et al. 2001; Parmo-Cabanas et al. 2004)
- differentiation (Kumar 1998; Martin et al. 2002)
- proliferation and regulation of cell cycle (Schwartz and Assoian 2001)
- cytoskeletal reorganisation and cell shape (Aplin et al. 1999)
- wound healing (Zeltz and Gullberg 2016)
- apoptosis (Wang et al. 2011b)
- cancer metastasis (Hamidi and Ivaska 2018)

Each integrin has a specific ligand (e.g. fibronectin, vitronectin, collagen, laminin), that upon binding triggers the activation of transcription within the cell. Vinculin is recruited to the cytoplasmic tail of integrins that are able to regulate kinases such PTK2 and c-Src, but also results in anchoring of F-actin to the membrane forming microfilaments, which essentially link the cell's cytoplasm to the ECM (Parsons et al. 2000; Mitra and Schlaepfer 2006). Uneven distribution of integrins on the cell surface can result in cell migration. When expressed at the front of the cell in the direction of intended travel, upon detachment of integrin substrates, they are absorbed back into the cell, but then reused at the very front of the cell with reattachment of the substrate. This continual process results in a moving or rolling motion of the cell along ligand-coated ECM or blood vessel walls.

1.4.3.4 Specific Integrins/cell adhesion molecules found on MM plasma cells:

- VLA-4; comprised of CD49d (α4) and CD29 (β1), found on many leucocytes as well as MM cells. Binds to fibronectin and VCAM-1 (vascular adhesion molecule) on BMSC, modulated by CXCL12. In MM cells, it can upregulate IL-6 secretion from BMSC, causing proliferation and blockade of apoptosis. MM migration (modulated by the chemokine CXCL12) is a result of upregulation of VLA-4, allowing adhesion to endothelium and thus cell migration (Sanz-Rodriguez et al. 2001; Parmo-Cabanas et al. 2004). It also causes a decrease in osteoprotegrin, which in turn increases RANKL, promoting osteolysis and plays a critical role in CAM-DR of MM cells (Sanz-Rodriguez and Teixido 2001). Both Bortezomib and glucocorticoids have been shown to downregulate expression of VLA-4 thus overcoming the effects of CAM-DR (Tonko et al. 2001; Planey et al. 2003; Webb et al. 2003; Noborio-Hatano et al. 2009).
- VLA-5; comprised of CD49e (α5) CD29 (β1), present on mature PCs. Lack of expression on PCs corresponds to immature and chemotherapy resistant MM PCs.
- LFA-1; comprised of CD11a (αL) and CD18 (β2), interacts with ICAM-1 on BMSC. Expression increases with tumour cell growth
- LFA-3; (CD58) commonly positive on abnormal PC, adhesion to T-cells through CD2. T-cells will produce cytokines necessary for MM growth (Manzanera et al. 2005).

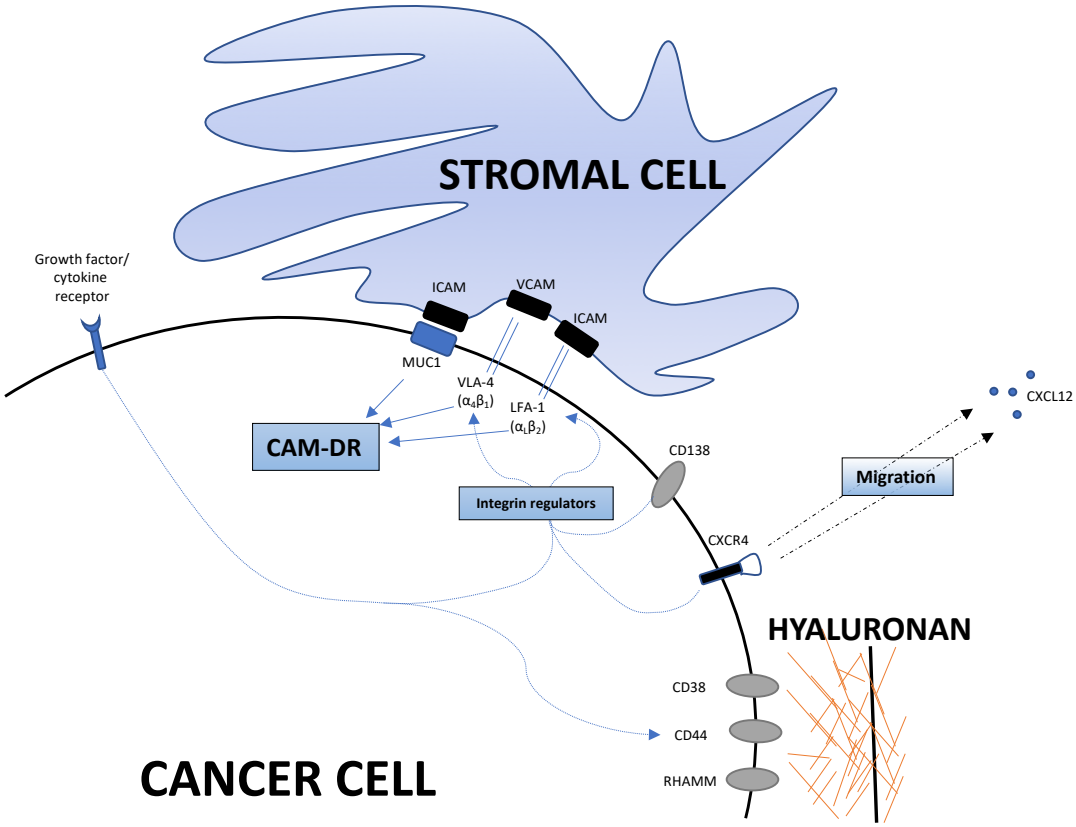

Figure 1.4. Adhesion molecules and integrins within MM bone marrow microenvironment *adapted from Morgan et al. and Katz (Katz 2010; Morgan et al. 2012b). Malignant plasma cells migrate to the bone marrow through the homing of the chemokine CXCL12 (localizes on the surface of stromal cells) to its receptor on MM cells, CXCR4. Upon cancer cells accumulating in the BM, positive cytokine and cell adhesion-mediated feedback loops are established between the cancer and stromal cells, establishing the clone and promoting cell survival, proliferation and mediates drug resistance. Integrin connection between the cancer cell and stromal cell include VLA-4 and LFA-1 adhering to VCAM and ICAM on the stromal cell respectively, with CD138 a key regulator of cell adhesion between MM cells and the ECM including stromal cells. CD44, RHAMM and CD38 mediate MM cells interactions with hyaluronan with expression and activity regulated by intracellular signal pathways and by extracellular factors such as growth factors, the enzymes heparanase and microenvironmental conditions such as hypoxia.*

1.5 Aims of Project

Sub-clonal analysis of MM through immunophenotyping is becoming more relevant in the age of monoclonal therapies such as the anti-CD38 therapy daratumumab. Therapy drives sub-clonal formation and the emergency of CD38 negative MM sub-clones post therapy raises new complexities in understanding drug resistance. We sought to design a complex (10-colour) multi-parameter flow cytometry panel, enabling clonal and sub-clonal immunophenotypic analysis of both primary MM samples and known MM cell lines.
Building upon this initial work, would allow further analysis of any sub-clones discovered with the aim of targeted pharmacological inhibition of MM and to develop a novel cell migration model using MM cell lines. The aims of this project are as follows:

To immunophenotypically characterise myeloma cells related to cell adhesion and migration in both MM cell lines and primary MM bone marrow samples. Thus, aiming to identify the existence of myeloma sub-clones that can be distinguished by their adhesion/migration cell markers.

The goal of achieving a lengthy remission or even a cure in MM, depends on fully understanding the many sub-clones in the disease, how they interact and the sensitivity to differing pharmacological agents. Building upon my initial sub-clonal analysis of MM cell lines, I set out to examine the phenotype, function and genotype of two related commercial cell lines, in order to explore the origins of glucocorticoid drug resistance.

Based upon a novel migratory model used in the study of CLL migration, I aim to develop this model in studying MM cell migration, previously untrialled in such disease. The model would allow to investigate the role of SDF-1/CXCR4, BTK, PI3-k/Akt/mTOR and NF-κB pathways in cell MM migration/adhesion and to assess the impact of pharmacological inhibition of these pathways and ultimately cell survival.

CHAPTER 2:

Materials and Methods

2.1 Tissue Culture

2.1.1 Reagents, media and buffers

RPMI-1640 medium 500ml (Gibco) stored at 4°C.

DMEM high glucose medium 500ml (Gibco) stored at 4°C.

Medium 199 (M199), Earle's Salts 500ml (Gibco) stored at 4°C.

Foetal calf serum (FCS) (Gibco) stored in 50ml aliquots at -20°C.

Penicillin (5000U/ml)/**Streptomycin** (5000µg/ml) (Gibco) stored in 10ml aliquots at -20°C.

L-glutamine 200mM (Gibco) stored in 5ml aliquots at -20°C.

Sodium Pyruvate 100mM (Gibco) stored in 5ml aliquots at -20°C.

Dulbecco's Phosphate-Buffered Saline (DPBS), no magnesium, no calcium 500ml (Gibco).

Trypsin-EDTA (0.5%), no phenol red (Gibco) used at 0.05% concentration, diluted with PBS, stored at 4°C.

Gelatin Solution Type B, 2% (Sigma-Aldrich) stored at 4°C.

Human IL-6 Research grade (Miltenyi Biotec; 130-095-365) 10µg reconstituted in 100µl of deionised sterile-filtered water. Diluted with 900µl PBS, supplemented with 0.1% BSA to give a final concentration of 10µg/ml. 100µl aliquots stored at -20°C.

Histopaque®-1077 (Sigma-Aldrich)

2.1.2 Equipment and tissue culture plastics

Vi-cell XR cell counter (Beckman Coulter), 550µl single cell suspension (or dilutions of) added to Vi-cell sample cups.

Greiner culture flasks, tissue culture treated w/ filtered cap (Greiner Bio-one) – sizes T-25, T-75, T-175

Nunc™ Cell Culture Treated TripleFlasks™ (Thermo Scientific™)

Corning® Cell Scraper (Sigma-Aldrich)

2.1.3 Cell lines

2.1.3.1 Multiple Myeloma (MM)

Cell Line	Disease	Type	Sample	Sex	CD45	Supplier	Catalogue #
JJN-3	MM	$IgA_1\kappa$	PE	F	+/-	DSMZ	ACC 541
MM.1R	PCL	IgA λ	PB	F	-	ATCC	CRL-2975
MM.1S	PCL	IgA λ	PB	F	-	ATCC	CRL-2974
NCI-H929	MM	IgA κ	PE	F	+/-	ECACC	95050415
OPM-2	MM	IgG λ	PB	F	-	DSMZ	ACC 50
RPMI-8226	MM	IgG λ	PB	M	-	ECACC	87012702
U-266	MM	IgE λ	PB	M	+	ECACC	85051003

Table 2.1. List of MM cell lines used in this study and disease type*. MM - multiple myeloma; PCL - plasma cell leukaemia; κ - kappa light chain; λ - lambda light chain; PE - pleural effusion; PB - peripheral blood; F – female; M – male; DSMZ - Deutsche Sammlung von Mikroorganismen und Zellkulturen GmbH; ATCC – American Type Culture Collection; ECACC – European Collection of Cell Cultures;*

Cell Line	IgH T	Target gene	Mutations	Deletions	Reference
JJN-3	t(14;16); t(8;14)	c-Maf		TP53	(Jackson et al. 1989)
MM.1R	t(14;16); t(8;14)	c-Maf	KRAS (*G12A* - het); TRAF3 (*K536* - hom)	CDKN2	(Moalli et al. 1992)
MM.1S	t(14:16); t(8;14)	c-Maf	KRAS (*G12A* - het); TRAF3 (*K536* - hom)	CDKN2	(Moalli et al. 1992)
NCI-H929	t(4;14)	MMSET/ FGFR3	NRAS (*G13D* - het);		(Gazdar et al. 1986)
OPM-2	t(4:14)	MMSET/ FGFR3	FGFR3 (*K650E* - het); TP53 (*R175H* - hom)	CKKN2	(Katagiri et al. 1985)
RPMI-8226	t(14;16); t(8;22)	c-Maf	KRAS (*G12A* - het); TP53 (*E285K* - hom)	TRAF3	(Matsuoka et al. 1967)
U-266	t(11;14)	CCND1	BRAF (*K601N* - het); RB1 (*E419X* - hom*);* *K228R* - hom); TP53 (*A161T* - hom); TRAF (*K550I* - hom)		(Nilsson et al. 1970)

Table 2.2. MM cell line genetic characteristics. *IgH – Immunoglobulin heavy chain; T – Translocation; MMSET - multiple myeloma SET domain; FGFR3 - fibroblast growth factor receptor-3; HD - homozygous deletion; het - heterozygous mutation; hom - homozygous mutation; CCND1 - cyclin D; CDKN2 - cyclin dependent kinase inhibitor 2; TRAF3 - tumour necrosis factor*

2.1.3.2 Fibroblasts and Endothelial cells

Cell line	Cell type	Description	Supplier/Catalogue #
HS-5	Human stromal	GFP and non GFP tagged	ICR, London*
HUVEC	Human endothelial	Virally transfected with hTERT by lentivirus containing cDNA of telomerase, immortalising cell	Invitrogen, CLL group, Cardiff University**
MRC-5	Human fibroblast	Source of SDF-1/CXCL12 secretion (Kang et al. 2005)	CLL group, Cardiff University**
CD40L	Mouse fibroblasts	Transfected embryonic fibroblast L-cells expressing CD40L	CLL group, Cardiff University**
NTL	Mouse fibroblasts	Non-transfected L-cells (Willimott et al. 2007)	CLL group, Cardiff University**

***Table 2.3. Non-myeloma cell lines used in this study**. *Kindly provided by Dr Faith Davis, Institute of Cancer and Genetics, London. **Kindly provided by Dr Elisabeth Walsby, CLL Group, Cardiff University*

2.1.4 Maintenance of cell lines

All Myeloma cell lines are IL-6 independent and except for JJN-3 were cultured in RPMI-1640 growth medium supplemented with 10% FCS, 2mM L-glutamine and antibiotics (100U/ml Penicillin and 100μg/ml streptomycin). JJN-3 was cultured in DMEM supplemented with 1mM pyruvate, non-essential amino acids, antibiotics (as per RPMI medium) and 20% FCS. The cell lines were grown in incubators containing 5% CO_2 at 37°C, maintaining cell densities between 0.3 - 1.0x10^6 cells/ml, thus requiring sub-culturing 2-3 times a week. MM.1R and MM.1S cells were semi-adherent to the plastic culture flasks and were thus removed with aid of a cell scraper. HUVEC, MRC-5 and HS-5 cells were maintained in M199 media, supplemented with 20% FCS and antibiotics (as per myeloma cell lines). Cells were cultured in 3 tier flasks, HUVEC flasks were coated with 0.2% gelatin for 30 minutes before use. Media required replacement every 3 days, with sub-culturing at least once a week. Cells were harvested using 0.05% trypsin due to adherence to flask.

All cell lines were cryopreserved at low passage number, at a density of 1x10^7 cells/ml in complete growth media containing 10% DMSO. If short term storage (less than three months) was anticipated cells were kept at -80°C, otherwise they were stored in liquid nitrogen. All cells were discarded after approximately 10-12 weeks of use. Regular laboratory-wide mycoplasma PCR testing was undertaken and all cells used in this study remained mycoplasma-free.

2.1.5 Cell proliferation and viability

Cells were seeded at $0.5x10^6$ cells/ml in 24-well plates. At 24h intervals, cells were counted on a Vi-Cell XR (Beckman Coulter).

2.1.6 Liquid co-culture, microscopy and camera

Co-culture experiments involved seeding $0.5x10^6$ fibroblasts/endothelial cells (HUVEC, HS-5, MRC-5, CD40L and NTL) into 6-well plates (HUVECs required wells to be coated with 0.2% gelatin prior to seeding) in 3.5ml M199 medium. In every case, cells were left for 3 hours to allow adherence to plastic before $5x10^6$ myeloma cells added to wells (ratio of 10:1).

In experiments where adhesion was assessed, plates were kept at 37°C in a 5% CO_2 atmosphere. Whole wells were analysed at 24h, 48h, 72h and 96h. This was done by removing all the media, 0.5ml was analysed by the Vi-cell XR cell counter, thus counting non-adhered cells and validated by flow cytometry analysis on pre-determine SSC and FSC gates, specific to myeloma cells, using 0.1ml of media. 1ml of fresh M199 media was placed back onto the adhered cells to allow camera screen shots (attached to a microscope) to be taken, using Q-Capture software. Adherent myeloma cells, were removed from wells using 0.05% trypsin and counted by both Vi-cell and flow cytometry methods as described above. Adherent myeloma cells were also phenotypically characterised by flow cytometric analysis having being immunostained. The percentage of adherent cells was expressed as a function of the total number of myeloma cells in the culture (i.e. both adherent and non-adherent cells).

2.2 Flow cytometric analysis

2.2.1 Reagents and materials

Propidium Iodide (PI) (Sigma-Aldrich) x30 stock reconstituted in PBS, used at 50µg/ml for cell cycle analysis and 20µg/ml for apoptosis analysis. Stored at 4°C.

2% Paraformaldehyde (PFA) (Sigma-Aldrich) prepared by dissolving 2g of reagent grade PFA in 100ml PBS at 50°C. Stored at 4°C in dark to prevent depolymerisation. 200µl added to fix stained samples and stored at 4°C until analysed.

Annexin V- Fluorescein Isothiocyanate (FITC) Apoptosis Detection Kit (eBioscience/Catalogue # BMS500FI/300CE)

Annexin V- Allophycocyanin (APC) Apoptosis Detection Kit (BioLegend/Catalogue # 640932)

CellTrace™ Carboxyfluorescein Succinimidyl Ester (CFSE) cell Proliferation Kits (Invitrogen; C34570) Stock solution 1mM, stored at -20°C. Stained cells analysed on BD Accuri C6, FL1 channel (488-nm excitation source).

Cell Proliferation Dye eFluor® 670 (eBioscience; 65-0840) Stock solution 5mM, stored at -20°C. Stained cells analysed on BD Accuri C6, FL4 channel (640-nm excitation source).

Fix & Perm® Cell Permeabilization Reagents (Invitrogen; GAS004)

Anti-Mouse Ig, κ/Negative Control Compensation Particles Set (BD; 552843)

RNase A (sigma) stock solution 10µg/ml, aliquoted and stored at -20°C.

BD Phosflow™ Perm/Wash Buffer I (BD Bioscience; 557885)

BD Phosflow™ Perm Buffer III (BD Bioscience; 558050)

BD Pharmingen™ Stain Buffer (BD Bioscience; 554656)

BD Cytofix™ fixation Buffer (BD Bioscience; 554655)

Anti-human IgM (µ chain specific) antibody (Sigma-Aldrich; I 0759) 1mg reconstituted in 1ml PBS to give working concentration of 1mg/ml, stored at 4°C.

Sodium Pervanadate solution prepared by adding 1µl of 30% sodium peroxide (Sigma-Aldrich) to 99µl of 10mM sodium vanadate (sigma-Aldrich)

2.2.2 Equipment and software

BD LSRFortessa™ Cell Analyser (Becton Dickinson) – Data collected on BD Diva software and analysed on FlowJo® software (FlowJo, LLC).

BD Accuri™ C6 Cell Analyser (Becton Dickinson) data collected and analysed on Accuri C6 analysis software.

BD FACSAria™ Cell sorter (Becton Dickinson)

2.2.3 Antibodies

Target	Site	Fluorochrome	Host Isotype / Clone	Catalogue # / Supplier
CD19	CS	PerCP/Cy5.5	Mouse IgG1 κ / HIB19	302230 / BioL
CD25	CS	PE	Mouse IgG2b κ / 4E3	129-001-311 / MB
CD38	CS	PE/Dazzle™ 594	Mouse IgG1 κ / HIT2	303538 / BioL
		FITC	Mouse IgG1 κ / HB-7	356610 / BioL
		PerCP	Mouse IgG1 κ / HB-7	356622 / BioL
CD45	CS	APC	Mouse IgG1 κ / HI30	304012 / BioL
CD49d	CS	BV 510™	Mouse IgG1 κ / 9F10	304318 / BioL
		PerCP/Cy5.5	Mouse IgG1 κ / 9F10	304312 / BioL
CD56	CS	PE	Mouse IgG1 κ / HCD56	318306 / BioL
CD62L	CS	eFluor ®450	Mouse IgG1 κ / Dreg-56	48-0629-42/ eB
CD90[*]	CS	BV 605™	Mouse IgG1 κ / 5E10	328128 / BioL
		PerCP/Cy5.5	Mouse IgG1 κ / 5E10	328118 / BioL
CD138	CS	Alexa Fluor® 700	Mouse IgG1 κ / MI15	356512 / BioL
		PE	Mouse IgG1 κ / MI15	356504 / BioL
CD184[**]	CS	PE-Cy7	Mouse IgG2a κ / 12G5	306514 / BioL
		APC	Mouse IgG2a κ / 12G5	306510 / BioL
CD243[#]	CS	PE-Cy7	Mouse IgG2a κ / UIC2	348610 / BioL
IL-6	IC	Pacific Blue™	Rat IgG1 κ / MQ2-13A5	501114 / BioL
Ki-67	IC	BV 605™	Mouse IgG1 κ / Ki-67	350522 / BioL
		FITC	Mouse IgG1 κ / 20Raj1	11-5699-42 / eB
MMP-9	IC	FITC	Mouse IgG2b κ / 56129	IC9111F / R&D
MUM-1	IC	FITC	Mouse	0601 / Dako
p-Syk	pY348	PE	Mouse IgG1 κ / I120-722	558529 / BD
p-Tyr	pY99	Alexa Fluor®488	Mouse IgG2b κ / PY99	SC 7020 / SC
SyK	IC	FITC	Mouse IgG2a κ / 4D10	552476 / BD

Table 2.4. Anti-Human antibodies used in this study *all stored at 4°C. PerCP - peridinin-chlorophyll-protein; Cy – cyanine; FITC - fluorescein isothiocyanate; APC – allophycocyanin; PE – phycoerythrin; BV – Brilliant Violet; BioL – Biolegend Inc; R&D – R&D Systems®; SC – Santa Cruz Biotechnology, Inc; BD – BD Bioscience; MB – Miltenyi Biotec; CS- cell surface; IC – intracellular; *also known as thy1; **also known as CXCR4; [#]also known as Mdr-1;*

2.2.4 Cell surface and intracellular immunostaining

Depending on the experiment, between 0.5-1x10^6 cells were harvested for cell surface staining. Cells were washed and re-suspended with PBS to a volume of 200µl. 5µl of antibody (Table 4) would be used to stain 1x10^6 cells. Samples were incubated in dark for 15 mins, and further washed in PBS before being analysed. If intracellular staining was required, the Invitrogen Fix & Perm® protocol was followed, which involved fixing the samples in 100µl of reagent A, followed by permeabilising the samples in 100µl of reagent B together with the addition of 5µl of antibodies and 0.6µl NP-40. Optional final fixation in 200µl of 2% PFA allowed the samples to be stored at 4°C prior to analysis. Unstained controls were always used, prepared in exactly the same manner but without the addition of antibodies. Multi-colour flow cytometry was then employed using a BD LSRFortessa instrument. The panels were set up using compensation beads (BD), such that aliquots of beads were labelled with a 5µl aliquot of each antibody and then auto compensation was applied prior to analysis.

2.2.5 Phosphoylation analysis and B-cell stimulation

The 'BD Phosflow™ protocol for Human PBMCs' was followed. If cell surface marker staining was required, BD Phosflow™ Perm/wash buffer I was used without cytofix, otherwise Cytofix buffer and Perm/Wash buffer III was used as per the protocol, starting with a single cell suspension of 1x10^6 cells/ml in 0.5ml of media. Cells were starved of FCS in FCS-free media for 24h before analysis. Where the effects of B-cell stimulation on phospho-protein levels were investigated, cells were stimulated with 10µg/ml anti-human IgM antibody for 10 mins. Pre-treatment of cells with 10µl of freshly prepared sodium pervanadate solution for 15 mins served as a positive control of phospho-protein expression.

2.2.6 Viability and cytotoxic assays using annexin V and propidium iodine (PI)

Drug cytotoxic assays were done at 48h (unless otherwise specified), cells were seeded in 24-well plates, at a concentration between 0.4-0.5x10^6 cells/ml in fresh media. Samples were stained with 5µl Annexin V (APC or FITC) and 10µl PI (20µg/ml) as per the kit's protocol and samples were analysed on BD Accuri C6 using CFlow software. Cell viability was calculated by first gating out debris and doublets and then acquiring 5,000 events. Viable cells were negative for both Annexin V and PI and were enumerated using quadrant gating.

2.2.7 Cell cycle analysis

Cells for analyse were harvested, washed and re-suspended in a single cell suspension in PBS with 2% FCS at 0.1x10^{6}cells/ml. 1ml ice-cold 70% ethanol was added to each cell pellet and the cells were resuspended and then stored for at least 1h at -20°C. Cells were then washed in PBS and 50µl of RNase A stock solution was added prior to incubation for 45 mins at 37°C. 0.5ml of PI staining solution was added and incubated for a further 15 mins at 37°C before analysis on BD Accuri C6. Data was analysed using FlowJo cell cycle analysis software.

2.2.8 Cell Proliferation analysis by cell tracing reagents

The Invitrogen CellTrace experimental protocol was followed but was optimised for a final cell concentration of 1x10^{6}cells/ml. The procedure was started with single cell suspension in 1ml PBS, desired amount of CSFE or eFluor 670 was added to form a final working concentration of 5µM for CSFE dye and 25µM for eFluor 670 dye. The samples were then incubated in the dark for 20 mins at 37°C. 10ml of culture medium was then added to the cells and incubated for further 5 mins, thus removing any free dye from the solution. Cells were then pelleted by centrifugation and re-suspended in fresh pre-warmed complete culture medium at the desired volume. 50µl samples were analysed on a BD Accuri C6 flow cytometer to ensure adequate uptake of dye.

2.2.9 Flow cytometer based Fluorescence-Activated Cell Sorting (FACS)

Phenotypically distinct sub-populations of the myeloma cell line MM.1S were identified based on their differential CD38 expression (CD38^{dim} and CD38^{bright}). Approximately 10 million cells were stained with 50µl of CD38-FITC Fluorochrome (BioLegend) and the cells were then sorted on a BD FACSAria. Conservative gating was applied to the CD38 histogram, such that approximately 7% of the lowest expressing cells and 30% of highest expressing cells were sorted. Cells were sorted into 15ml Falcon tubes coated with FBS. Once collected, cell purity was checked on BD Accuri C6 flow cytometer and the remaining cells were washed and suspended in RPMI media containing 10% FCS. The two new derived cell lines were subsequently termed MM.1S^{dim}, referring to cells sorted from the CD38^{dim} population and MM.1S^{bright}, referring to cells sorted from the CD38^{bright} population.

2.3 Primary Multiple Myeloma samples

Ethical approval was obtained from the South-East Wales Local Research Ethics Committee (approval number 13/WA/0383). Bone marrow samples were obtained from patients who were being investigated for suspected Myeloma at the University Hospital of Wales, Cardiff in accordance with the Declaration of Helsinki. Patient information sheets regarding this study were given to every patient prior to the request for consent (see appendix for information sheets and consent forms). A Material Transfer Agreement (MTA) for transfer of each sample from the clinical setting to the research laboratory was set up as per Cardiff University guidance.

2.3.1 Cell preparation and freezing

Bone marrow mononuclear cells (MB-MNCs) were isolated by density gradient centrifugation, using Histopaque®-1077 (Sigma-Aldrich). $4x10^6$ cells were aliquoted for flow cytometry analysis. The remaining cells were cryopreserved in DMEM media containing 20% FBS and 10% DMSO.

2.3.2 Antibody staining

$2x10^6$ cells were stained with 5µl of the following antibodies (see section 2.2.4 for additional procedure details) using an Invitrogen 'fix and perm' kit. $2x10^6$ cells were used as unstained controls and were prepared using the same method except no antibodies were added. Once the cell staining protocol was completed, cells were fixed in 200µl 2% PFA and stored at 4°C, until analysed on BD LSRFortessa flow cytometer.

Surface Markers - Fluorochrome	**Intracellular Marker - Fluorochrome**
CD19 - PerCP/Cy5.5	**IL-6** - Pacific Blue™
CD38 - PE/Dazzle™ 594	**Ki-67** - BV 605™
CD45 - APC	**MMP-9** - FITC
CD49d - BV 510™	
CD56 - PE	
CD138 - Alexa Fluor® 700	
CD184 (CXCR4) - PE-Cy7	

Table 2.5. Flow cytometry antibody panel used for primary samples *all stored at 4°C.*

2.4 Migration assays

2.4.1 Reagents and equipment

Recombinant Human SDF-1α/CXCL12a (R&D Systems; 350-NS-010) was reconstituted in 100µl of sterile PBS to give a working concentration of 100µg/ml. Aliquots were then stored at 4°C.

Corning® Transwell® polycarbonate membrane cell culture inserts (Sigma) 6.5 mm Transwell with 3.0µm pore polycarbonate membrane insert.

FiberCell® Systems Duet Pump (FiberCell Systems Inc; P3202)

FiberCell® Small Polysulfone Cartridge - pore size 0.1µm (FiberCell Systems Inc; C2025)

2.4.2 Transwell assays

The upper (apical) chamber was seeded with $0.25x10^6$ cells in 250µl of fresh media with or without the addition of investigational drug. The lower (basolateral) chamber contained 500µl of media with the desired concentrations of CXCL12 (standard concentration 100ng/ml unless otherwise specified). Transwell plates were incubated at 37°C for 24h unless otherwise specified. Cells were counted in both chambers of the transwells using a set acquisition volume (100µL) on a BD Accuri C6 flow cytometer. The percentage of migration was calculated from the number of cells counted in the basolateral chamber (migrated) divided by the number of cells originally seeded into the apical chamber.

2.4.3 Dynamic Circulatory model

2.4.3.1 Modifying a hollow fibre bioreactor

Our research group had previously created a dynamic circulatory model for studying migration of leukaemic cells. The model is a modification of a hollow fibre bioreactor as outlined by Walsby et al (Walsby et al. 2014c) and diagrammatically shown in Figure 2.1. The bioreactor uses a peristaltic pump to create a flow of media at a defined shear force (dynes/cm^2) through a closed system consisting of a reservoir of media, wide tubing, and a polysulfone cartridge containing porous (0.2µm) hollow fibres. The lumen of each hollow fibre was coated with matrix proteins to allow attachment of endothelial cells. The fibres in the cartridge were first activated by 70% ethanol, followed by water, and then exposed to gelatin (0.2% solution; Sigma Aldrich) for 1h, providing a matrix for endothelial cells (HUVEC) to adhere to the insides of the hollow fibres. M199 media supplemented with 20% FCS and antibiotics was used to gently wash unbound matrix protein from the

hollow fibres and to allow its removal from the system. $15x10^6$ HUVECs were then introduced into the hollow fibres and allowed to adhere to the gelatin-coated fibres for 4h (the cartridges were inverted half way through to ensure even coating). Non-adhered cells were then removed from the system and counted. The system was filled with 50 mL M199 media, and circulation was initiated. Once the system was primed with no air bubbles, $5x10^6$ of the CXCL12-secreting fibroblasts MRC-5 (Kang et al. 2005) were introduced into the EVS via one of the EVS ports. Medium was circulated through the system under a shear force of 1.5 dynes/cm^2 overnight before the shear force was increased to 10 dynes/cm^2 for a further 24h. The shear force was increased in increments to encourage the HUVECs in the hollow fibres to form firm adhesion and to align along the fibres to form 'pseudovessels'. Approximately 48h after initial experimental set up, $40x10^6$ myeloma cells (concentration of $0.8x10^6$ cells/ml) were subsequently introduced into the circulating system through port 2 of the cartridge (Figure 2.1). Cells were then circulated for 48h at 37°C. Samples were taken from the circulating compartment and the EVS at 1h and 48h for analysis. Migrated cell were deemed to be those retrieved from the EVS, accessed via either EVS port (Figure 2.1), with non-migrated those remaining in the circulation. Both samples were counted and analysed on a BD Accuri C6 flow cytometer.

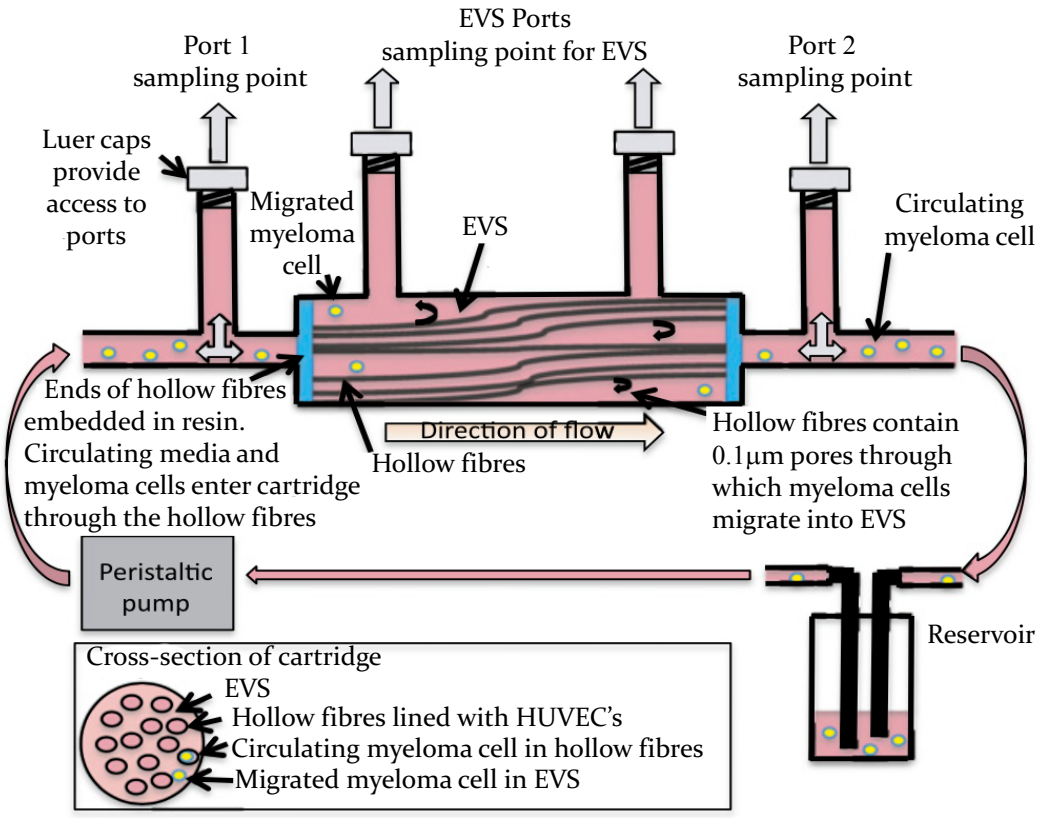

***Figure 2.1. Diagrammatical representation of the circulatory model**, adapted from Walsby et al. 2014. HUVEC cells seeded into the hollow fibres of the bioreactor are exposed to physiologically relevant shear forces through the action of the peristatic pump. In addition, myeloma cells being pumped around the system, will have transient interaction with the endothelial layer. The hollow fibres in the bioreactor have 0.1μm pores through which myeloma cells can migrate into the space outside fibres, attracted to the chemokine SDF-1, secreted by MRC-5; the EVS is shown in the cross-sectional image of the cartridge. Myeloma cells were recovered from the circulating compartment and the EVS of the system via the access ports. EVS: Extravascular space; HUVEC: Human umbilical vein endothelial cells.*

2.4.3.2 Antibody labelling of myeloma cells

After the retrieval of the myeloma cells from the circulating compartment and the EVS, the cells were labelled with the fluorescence-labelled antibodies listed in Table 5. Depending on the experiment, separate samples were labelled with additional antibodies, (CXCR4-APC, CXCR4-PE/Cy7, CD49d-PerCP/Cy5.5, Ki-67-FITC, CD138-PE, CD38-FITC, CD90-PerCP/Cy5.5). Circulated myeloma cells, and where possible migrated cells retrieved from the EVS, were compared with cells maintained under static culture conditions. Flow cytometry was performed on an BD LSRFortessa or BD Accuri C6 and data were analysed using FlowJo software.

2.4.3.3 Migration

Migration of the myeloma cells was measured after 48h by cell counting 100µl samples from the EVS on a BD Accuri C6 flow cytometer. As per the previously described method (Walsby et al 2014), the percentage of the circulating population that migrated was calculated according to the formula:

$$\% \text{ Migration} = 100 \times [N_{P3}/(N_{P2} + N_{P3})]$$

Where N_{P2} is the number of live cells in the circulation compartment and N_{P3} is the number of live cells in the EVS. The total cell number in the entire model was then scaled-up e.g. 100µl of circulation compartment volume analysed, represents 1/500 of the total (50ml) retrieved volume, so the cell count from a volume of 100µl was multiplied by 500 to obtain the total number of cells in the compartment.

2.4.3.4 Inhibiting SyK, CD49d and CXCR4 functionality

In some experiments, the myeloma cells ($40x10^6$) were pre-treated with one or a combination of pharmaceutical agents, listed in Table 2.6, prior to being introduced into the circulating model. In such cases, untreated myeloma cells from the same cell line were introduced into a parallel cartridge as a control.

Drug	**Action**	**Dose**	**Supplier/Cat. #**
Natalizumab (Tysabri)	Anti-CD49d antibody	1µM	Elan Pharma. Ltd
ONO-7161	CXCR4 antagonist	1µM	Ono Pharma. Ltd
GS-9973 (Entospletinib)	Selective SyK inhibitor	5µM-50µM	Selleckchem/S7523

Table 2.6. Pharmaceutical agents used in circulatory model.

2.5 Whole exome sequencing

2.5.1 DNA extraction

DNA extraction of the individual cell lines (MM.1R, MM.1S^{dim} and MM.1S^{bright}) was performed using a DNeasy Blood & Tissue Kit (Qiagen; 69504) as per the manufacturer's instructions. 2.5x10^{6} cells were used per cell line for extraction and extracted samples were stored at -20°C prior to downstream processing and analysis.

2.5.2 Quality Control

2.5.2.1 Nanodrop

Duplicate 1.0µl samples were analysed on a Nanodrop; 1000 Spectrophotometer (Thermo Scientific). This allowed both DNA quantification and purity assessments to be determined. The A260/A280 ratio gives an indication of protein contamination and the 260/230 ratio an assessment of RNA contamination.

2.5.2.2 Gel electrophoresis

Standard agarose gel electrophoresis (100ml), with 5µl ethidium bromide (Sigma-Aldrich) was run for additional DNA quantification, using Fluorescent DNA Quantitation Kit (BioRad) and analysed on the fluorometer QuantiFluor (Promega).

2.5.3 BGI sequencing and bioinformatics

After in-house quality assurance of DNA purity, 4µg of DNA in 1.5ml microfuge tube was centrifuged to generate a dry pellet using a vacuum centrifuge and sent to BGI laboratories in Hong Kong on dry ice. Whole exome sequencing (WES) analysis was generated on an Illumina HiSeq 4000 system at a read depth of x30. Bioinformatics was done using the GATK platform, courtesy of Dr Kevin Ashelford, with mutation analysis performed using Enrichr (Chen et al. 2013). Additional bioinformatics and clonal evolution analysis, including phenotypic analysis and diagrams were courtesy of Dr Tom Connor, Cardiff University.

A copy of the VCF files of the WES can be found on the Research Group shared laboratory protocol folder on Dropbox™, accessed by the following web link:
https://www.dropbox.com/sh/kdrde9xex7zotul/AAB3umWDQOQ-m4YWXLpOTKMTa?dl=0

2.6 Protein Analysis

2.6.1 Equipment

BioTek Cytation 3 image reader

Dry heating block

Orbital Shaker (Stuart-Scientific)

NuPAGE™ 4-12% Bis-Tris Protein Gels, 1.0 mm, 10-well (Invitrogen; NP0321box)

X-cell SureLock™ Mini-cell SDS-PAGE apparatus (Invitrogen)

X-cell II™ Blot module Western Blot apparatus (Invitrogen)

Hybond-P polyvinylidene difluroide (PVDF) membrane (Amersham)

Chromatography paper 3MM Chr (Whatman)

Polyethylene lay flat film 204mm (Jencons)

Powerpac 300 power suppliers (Biorad)

X-OMAT™ LS Kodak film 18 x 24 cm (Amersham)

Konica SRX101A film processor (Konica)

2.6.2 Reagents

Lysis Buffer (2x) containing 100mM HEPES pH7.9, 10mM NaF, 10mM iodoacetamide and 150mM NaCl. Stored at 4°C

Phenylmethosulfonylfluoride (PMSF)

NP-40 (10%)

Protease Inhibitor (Sigma-Aldrich; P8340)

DC Protein Assay (BIO-RAD; CN 500-0116) includes Reagents A, B and S

Bovine Serum Albumin (BSA) 1mg/ml concentration (Sigma)

NuPAGE™ LDS Sample Buffer (x4) (Invitrogen; NP0007)

NuPAGE™ Sample Reducing Agent (x10) (Invitrogen; NP0009)

NuPAGE™ MOPS SDS Running Buffer (x20) (Invitrogen; NP0001) was diluted with deionised water to give a 1x working solution and store at room temperature.

SeeBlue™ Plus2 Pre-stained Protein Standard (Invitrogen; LC5925) supplied as a ready to use molecular weight marker and stored in aliquots at 4°C.

NuPAGE™ Transfer Buffer (x20) (Invitrogen; NP0006) was diluted with deionised water containing 10% analysis grade methanol (Fisher) to give a 1x working solution and stored at 4°C.

PBS-Tween containing 0.2% Tween®-20 detergent in 1xPBS. Prepared and stored at room temperature

Blocking Buffer was prepared by heating PBS-Tween to 80°C and then adding I-Block (Tropix Inc; T2015) to make a concentration of 0.2%. Once dissolved, the solution was allowed to cool and then sodium azide was added to make a concentration of 0.4%.

Pierce® ECL Plus Western Blotting Substrate (Thermo Fisher Scientific; 32132). The product protocol was followed, mixing substrate A and B at a 40:1 ratio.

2.6.3 Cell lysis

$2.5x10^6$ cells were washed in PBS, centrifuged at 4°C and all supernatant removed to leave a semi-dry cell pellet. The pellet was then re-suspended gently in 100µl of freshly made (due to short half-life) cell lysis buffer supplemented with 1% NP-40, 1mM PMSF and protease inhibitor. Cells were incubated for 5 mins on ice and then transferred to 1.5ml microfuge tube, spun at 200 x*g* for 10 mins at 4°C. The supernatant was then decanted into a fresh microfuge tube and stored at -20°C for at least 1 hour before 1D SDS-PAGE.

2.6.4 Measurement of protein concentration

The protein concentration was determined using the Bio-Rad *DC* Protein Assay kit; the Microplate Assay Protocol (section 5.2) was followed. The protein standard used was BSA, at concentrations 1mg/ml, 0.5mg/ml, 0.25mg/ml, 0.125mg/ml and 0.0625 (serially diluted with distilled water). 5µl of samples and standards were pipetted into flat bottomed 96-well plates, in triplicate. 25µl working reagent A (1:50 reagent S to Reagent A) was pipetting into each well, followed by 200µl of reagent B. After 15 mins, the absorbance of each well was read at 750nm using a microtitre plate reader (BioTeK Cytation 3). Standard absorbance (y axis) was then plotted against its concentration (x axis) in a Microsoft Excel spreadsheet. The equation of the straight-line; $y = mx + c$ (where y = absorbance, m = gradient, x = the concentration and c = the y intersect), thus allowed to calculate the concentration of each sample.

2.6.5 Sample preparation

After protein quantification, 3µl of Sample Reducing Agent (Invitrogen) and 7.5µl of LDS Sample Buffer (Invitrogen) was added to 30µg of protein extract in a fresh microfuge tube. The volume was made up to 30µl with deionised water and then placed in a dry heating block at 80°C for 10 mins.

2.6.6 Protein analysis by 1-Dimensional (1D) Sodium Dodecyl Sulphate-Polyacrylamide Gel Electrophoresis (SDS-PAGE)

Pre-cast NuPage™ gels (Invitrogen) were washed with deionised water and inserted into the lower buffer chamber of the Mini-Cell. The gel cassette was locked into place with a Gel Tension Wedge. Approximately 200ml of x1 Running Buffer was added to centre chamber, ensuring the wells were completely submerged. 7.5µl of SeeBlue™ Plus2 Pre-Stained Protein Standard (Invitrogen) was loaded into the first well, followed by 20µl of prepared sample to the subsequent wells. A further 300ml of running buffer was added to the external chambers and lid placed on the cell. Gel was run at 200V (120 mA, 25.0 W) for approximately 55 mins, until the dye front had reached the ridge at the bottom of gel.

2.6.7 Western Blotting

The PVDF membranes were soaked in methanol for 30s before use, rinsed with deionised water and then equilibrated in transfer buffer. The polyacrylamide gel was then removed from cassette and placed onto the PVDF membrane, between 2 pieces of Whatman 3MM filtered paper pre-soaked in transfer buffer. This was placed onto blotting pads pre-soaked in transfer buffer and placed in a X-cell II™ Blot module (Invitrogen). The blotting module was then inserted into the X-cell SureLock™ Mini-cell unit (Invitrogen) and filled with transfer buffer until the gel/membrane assembly was covered. The outer buffer chamber was filled to approximately two thirds with deionised water and the unit was run at 30V (Start 170mA End 110mA) for 90 mins.

2.6.8 Immuno-probing the blot

The PVDF membrane was removed from the module and rinsed with PBS-Tween. The membrane was then placed in a 50ml conical flask and incubated in 15ml of blocking buffer for 60 mins at room temperature on an orbital shaker (Stuart-Scientific). The blocking buffer was replaced with 10ml of fresh blocking buffer and then probed with the primary antibody, diluted to the correct concentration (see Table 2.1). The blots were incubated overnight at 4°C on an orbital roller. Post-incubation, the membrane was washed three times in 15ml PBS-tween for 10 mins. The membrane was then incubated for 60 mins at room temperature with the secondary antibody, diluted in 10ml blocking buffer. The membrane was subsequently removed from the secondary antibody solution and washed three times in 15ml PBS-tween for 10 mins. 10ml of Pierce® ECL Plus Western Blotting Substrate (40:1 Substrate A:Substrate B) was added to membrane and incubated for 5 mins. The membrane was then placed between polyethylene film, with any excess

reagent removed and was exposed to autoradiographic film (Kodak) for 2, 10 and 30 mins. Films were then developed using a Konica film processor (Konica).

Target Protein	Antibody Type	Clone/ Catalogue #	Species	Working Conc.	Supplier
Beta-Actin	Primary	13E5/4970	Rabbit	1:1000	CST
PI3K p110δ	Primary	H-219/sc-7176	Rabbit	1:1000	Santa Cruz
AKT	Primary	/9272	Rabbit	1:1000	CST
Rabbit IgG(H+L) HRP conjugate	Secondary	/31460	Goat	1:10000	Invitrogen

Table 2.7. Antibodies used in protein analysis. *CST - Cell Signalling Technologies; Santa Cruz - Santa Cruz Biotechnologies; Invitrogen - Invitrogen, Thermo Fisher Scientific*

2.7 DNA quantification

2.7.1 Reagents and equipment

TRIzol™ Reagent (Thermo Fisher Scientific; A33250)

Molecular Biology Grade Chloroform (Thermo Fisher Scientific; BPE1145-1)

RNeasy Mini Kit (QIAGEN; 74104)

High Capacity cDNA Reverse Transcription Kit (Applied BioSystems; 4368814) stored at -20°C

Veriti DX Thermal cycler (Thermo Fisher Scientific)

ViiA7 Real-Time PCR system (Thermo Fisher Scientific)

TaqMan® Fast Advanced Master Mix (Thermo Fisher Scientific; 4444556) stored at -20°C

TaqMan® Gene Expression Assays (Thermo Fisher Scientific) stored at -20°C

GAPDH – Hs02786624_g1

PIK3CD – Hs00192399_m1

2.7.2 RNA extraction

1ml TRIzol was added to a dry pellet of $4x10^6$ harvested cells. Sample was stored at -80°C until ready for extraction. Once the sample was thawed, 200µl of chloroform was added and centrifuged at 200 *xg* for 15 mins at 4°C. The aqueous layer on top was gently removed and added to an equal volume of 70% ethanol. 700µl of the sample was then added to an RNeasy spin column and the RNeasy Mini Kit protocol was followed. The elution step used 50µl RNase-free water, which was stored at -80°C until the next step. RNA quantification was assessed using a Nanodrop:1000 Spectrophotometer. Duplicate 1µl samples were evaluated and the RNA concentration, A260/280 ration and A260/A230 ratio obtained.

2.7.3 Reverse Transcription (RT)

Following the Applied BioSystems RT kit protocol, 0.5µg of RNA was added to 0.5ml microfuge tubes containing 10µl master mix and made up to 20µl with sterile RNase-free water. Samples were added to thermal cycler and run as per the kit's protocol. Once the run was complete, 20µl of newly converted cDNA was diluted 5:1 with sterile DNase and RNase-free water to give a total volume of 100µl and a working concentration of 2.5ng/µl. Samples were stored at -20°C.

2.7.4 Real time PCR

The TaqMan Fast Advanced Master Mix kit protocol was followed. Samples were run in triplicate, including a minus RT sample and a minus cDNA sample. Samples were run on a 96-well plate with a running volume 10µl per well. This was composed of 2.5µl of thawed cDNA, 0.5µl primer (GAPDH or PIK3CD), 5µl TaqMan master mix and 2µl of RNA-free water. Samples were run on a ViiA7 Real-Time PCR system using the TaqMan FAST programme. Results were analysed using the Thermo Fisher Cloud software using the Relative Quantification qPCR application.

2.8 Methylation Analysis

2.8.1 Reagents and equipment

DNeasy® Blood & Tissue Kit (QIAGEN®; 69504) stored at room temperature

EpiTect® Bisulfite Kit (QIAGEN®; 59104) stored at -20°C

EpiTect® PCR Control DNA Set (QIAGEN®; 59695) stored at -20°C

PyroMark® PCR Kit (QIAGEN®; 978703) stored at -20°C

PyroMark® CpG assay (QIAGEN; 97846) containing 10x PCR primer set (reconstituted in 550µl of TE buffer) and 10x Sequencing primer (reconstituted in 880µl of PyroMark® Annealing Buffer). See Table 2.8 for additional information.

TE Buffer (10mM Tris·Cl, 1mM EDTA, Ph8.0

PyroMark® Gold Q96 Reagents (QIAGEN®; 972804) stored at 4°C

PyroMark® Q96 Cartridge (QIAGEN®; 979004)

PyroMark® Annealing Buffer (QIAGEN®; 979009)

PyroMark® Binding Buffer (QIAGEN®; 979006)

Streptavidin-coated Sepharose® High Performance (GE Healthcare; 17-5113-01)

PyroMark® Q96 ID (QIAGEN®; 9001525) including PyroMark Q96 ID software

PyroMark® Q96 Vacuum Workstation (QIAGEN®; 9001740)

Veriti DX Thermal cycler (Thermo Fisher Scientific)

2.8.2 DNA extraction

As outlined in section 2.6.1

2.8.3 Bisulfite conversion

1µg of sample DNA (as quantified by Nanodrop; 1000 Spectrophotometer) and 0.2µg QIAGEN unmethylated human Control DNA was bisulfite converted as per EpiTect® Bisulfite Kit protocol, using the Veriti DX Thermal cycler. Carrier RNA solution was not required in view of the relatively large quantity of DNA being converted (as per the protocol recommendation). The final elution step used 20µl of Buffer EB to give a concentration of roughly 50ng/µl. Samples were then stored at -20°C until the next step.

2.8.4 PCR amplification

The PyroMark PCR handbook (May 2009) protocol was followed. Reaction composition per sample included 12.5µl PyroMark master mix, 2.5µl CoralLoad, 2.5µl PCR primers, 20ng of bisulfite converted DNA and RNase-free water to make a total reaction volume of 25µl per well of the 96-well plate. Samples where done in triplicate in addition to EpiTect PCR positive control (methylated human bisulfite converted DNA 10ng/µl) and negative control (unmethylated human bisulfite converted DNA 10ng/µl). The thermal cycling protocol was set as per the handbook; 45 cycles with an annealing temperature of 56°C.

2.8.5 Pyrosequencing

20µl of the 25µl PCR reaction was used for the subsequent pyrosequencing analysis. The PyroMark Q96 CpG Handbook (December 2010) protocol was followed. Immobilisation of 20µl of PCR product was done in the same 96-well plate, using 40µl of binding buffer, 2µl of Streptavidin-coated Sepharose® HP (beads equivalent) and this was made up to a final volume 80µl with RNase-free water. Annealing of the sequence primer to the template was done using the Q96 Vacuum workstation followed by heating the 96-well plate to 80°C to obtain single stranded DNA as per the handbook protocol. The cartridge was loaded with appropriate volumes of Gold Q96 reagents and was inserted into the pyrosequencer in addition to the plate. Quantification of CpG methylation was analysed using PyroMark Q96 ID software.

2.8.5.1 Sequence primers

Qiagen produces two separate PyroMark CpG primer assays for the *PIK3CD* gene. Both of which were used in this thesis. The gene has 3 promoter regions with high CpG activity. Each promoter region has flanking regions either side with minimal or no CpG islands. The middle and largest promoter region (highlighted figure 2.2) is the site of Qiagen's 2 primer assays (termed PIK3CD-1 and PIK3CD-2). The dispensation order for the different CpG assay primers is outlined in Table 2.8.

CpG assay 1	Hs_PIK3CD_01_PM
Catalogue #	PM00093310
Chromosome Location	Chr1:9749264-9749343
Amplicon Length	79
CpG sites	8
Sequence to be Analysed*	AGYGTGYGYGTYGTYGGGGTTTYGYGGT
Dispensation Order	TAGTCGTAGTCGTCGTCGATCGTCGGTTCGTCG
CpG assay 2	Hs_PIK3CD_02_PM
Catalogue #	PM00093317
Chromosome Location	Chr1:9749963-9750155
Amplicon Length	192
CpG sites	3
Sequence to Analysed*	TTTAGGTTTTTTYGTTGTYGTTTTTGATGGGATTYGT
Dispensation Order	ATAGTTCGTCTAGATCGTTGAGTGATCG

Table 2.8. PyroMark CpG Assay information. **Bisulfite converted sequence*

2.9 Telomere Analysis:

Single Telomere Length Analysis (STELA) was performed using a PCR-based method for the determination of telomere length (Baird et al. 2003). Profile was on the XpYp chromosome. All of the data shown were produced courtesy of Professor Duncan Baird's laboratory.

2.10 Statistical analysis

All statistical analysis was performed using GraphPad Prism 6.0 software unless otherwise specified. Continuous variables were analysed by 2-tailed parametric (*t*-test) or non-parametric (Wilcoxon rank sum test) tests as appropriate. Multivariable analyses were performed using 2-way ANOVA Fisher's LSD test, with $P \leq 0.05$ considered to represent statistical significance. All error bars are standard deviation and are calculated by repeated independent experiments (as opposed to technical replicates) unless specified otherwise.

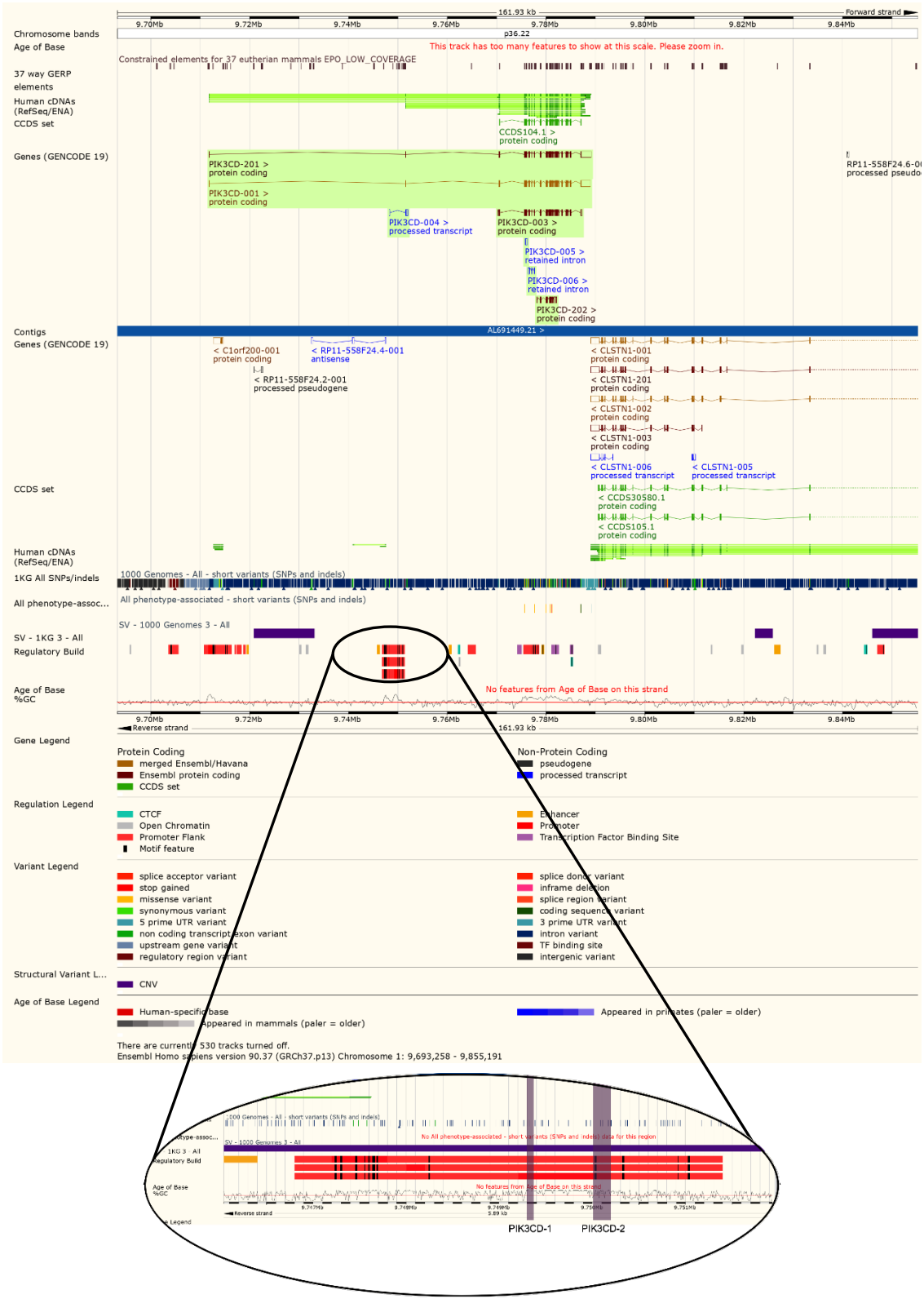

Figure 2.2. Image taken from GRCH37 ensembl showing Chromosome 1:9693258-9855191 *(Yates et al. 2016). Enlarged area is promoter region for the gene, with shaded areas showing the location for the 2 Qiagen PyroMark CpG primer assays, identified as PIK3CD-1 (amplicon length 79bp containing 8 CpG sites) and PIK3CD-2 (amplicon length 192bp containing 3 CpG sites).*

CHAPTER 3:

Immunophenotypic Characterisation of Myeloma

3.1 Introduction:

Immunophenotyping of multiple myeloma (MM) plays an important role for both clinical and research purposes. It is essential for both the diagnosis of MM and the monitoring of minimal residual disease (MRD). In the era of 4-colour flow cytometry, a primary diagnostic panel would include CD38 and CD138 for identification of plasma cells with CD19, CD45 and CD56 distinguishing MM plasma cells from normal plasma cells (PCs). The percentage of aberrant PCs identified alone can define the stage of the disease (e.g. less than 10% for Monoclonal Gammopathy of Undetermined Significance (MGUS), 10-60% for Smouldering MM (SMM) and greater than 60% for symptomatic MM), thus determining if treatment is necessary (Rajkumar 2016). IMWG guidance states that clonality and sub-clonal identification of bone marrow plasma cells are established by showing abnormal κ/λ light-chain ratio of >3:1 or <1:3 by flow cytometry immunofluorescence (Rawstron 2006; Peceliunas et al. 2011).

MRD monitoring by flow cytometry can be obtained in virtually all MM patients, by using the PC diagnostic panel and a combination of aberrant cell markers that include CD81, CD27, CD117, CD28 and CD20 (Rawstron et al. 2008; Rawstron et al. 2013; Rajkumar et al. 2014; Flores-Montero et al. 2016). Munshi et al. meta-analysis showed multi-parameter flow cytometry (MFC) MRD negativity resulted in longer OS (hazard ratio 0.60). Although there is a lack of standardisation in the MFC technique between laboratories and a lower sensitivity (up to 1×10^{-5}) compared to other MRD methods (ASO-qPCR, NGS), it remains the most widely used form of MRD monitoring owing to its relatively low cost, wide availability and short turnaround time (Mailankody et al. 2015; Munshi et al. 2017).

Although cytogenetic analysis remains the prominent prognostic tool, influencing disease course and response to therapy, and forms a key component of the revised international staging system score (R-ISS) (Rajkumar 2016), immunophenotyping has been shown to

provide prognostic value using a range of different cell markers, including CD56, CD45, CD20, CD27, CD28 and CDl17, some of which are linked to cytogenetic abnormalities (Kumar et al. 2010). The advent of polychromatic flow cytometry and CyTOF (cytometry by time-of-flight) technology, as well as the availability of a vast array of monoclonal antibodies, has provided the opportunity to design ever more sophisticated analysis panels, which have wide-ranging research applications. However, to date few complex multi-coloured flow panels have been routinely used on either primary MM samples or MM cell lines. The aims of this chapter were to design a multi-colour flow cytometry panel to immunophenotypically characterise cell adhesion and migration properties in both MM cell lines and primary MM bone marrow samples. I also set out to potentially identify the existence of phenotypically distinct myeloma sub-populations based on differential expression of adhesion/migration markers.

3.2 Designing a MM multi-colour flow cytometry panel

Table 3.1 details the ten cell markers selected for the flow cytometry panel. The panel was broadly divided into two - half of the cell markers were used for PC identification and/or aberrant markers associated with MM - the other half were used to characterise markers associated with adhesion, migration and proliferation

3.3 MM gating strategy

Figures 3.1 and 3.2 show the gating strategies applied to MM cells lines (Figure 3.1) and primary bone marrow cells (Figure 3.2). Samples were analysed on a BD Fortessa flow cytometer. Primary samples, prior to analysis, were red cell lysed and centrifuged on a layer of Ficoll. Plasma cells were identified by CD138 and CD38 positive single gated cells. All samples, were analysed using FlowJo software, calculating MFI (median fluorescence intensity), percentage positive expression compared to unstained control and the presence of distinct sub-populations. Subsets (potentially indicative of sub-populations/sub-clones) were identified by bivariate pseudocolour dot plots. As a minimum, the following dot plots were composed:

i. CD38 vs. CD138
ii. CD19 vs. CD45
iii. CD45 vs. CD56
iv. CD19 vs. CD56
v. CD49d vs. CXCR4
vi. CD49d vs. Ki-67
vii. CXCR4 vs. Ki-67
viii. IL-6 vs. MMP-9

In the event that sub-populations were identified, overlaid histograms were used to illustrate differences in antigen expression and the MFI values for each sub-population were used for quantitative comparison.

Antigen	Function	Purpose
CD138 (syndecan-1)	Heparan sulfate proteoglycan – promotes cell-surface adhesion. High expression broadly unique to plasma cells	Plasma cell gating
CD38	Transmembrane glycoprotein with enzymatic activity, variable expression in B-cells, high in PC	Plasma cell gating
CD45 (Leucocyte common antigen)	Protein tyrosine phosphate – activation of lymphocytes and development. Generally low expression in MM, but increasing expression correlates with higher proliferation and immaturity	Myeloma cell gating/aberrant phenotype
CD19	Pan B-cell marker – regulatory role in expansion of B-cells. Loss in myeloma PCs correlates with altered PAX-5 expression	Myeloma cell gating/aberrant phenotype
CD56 (NCAM)	Glycoprotein of Ig superfamily Weakly expressed on normal PC, strongly positive in 60% myeloma cells, expression loss in PC leukaemia	Myeloma cell gating/aberrant phenotype
CD49d (α4)	Integrin subunit forming VLA-4 (α4/β1), ligates to VCAM on BMSC. Upregulates IL-6 secretions from BMSC	Adhesion marker
IL-6	Induces proliferation (Ras pathway), blocks apoptosis (STAT-3), protects against dexamethasone cytotoxicity (PI3K pathway) Decreases: osteoprotegerin secretion, Increases: expression of RANKL (promoting osteolysis) and antiapoptotic molecules (bcl-2, bcl-xL, Mcl-1)	Survival marker
CXCR4	Chemokine receptor for CXCL12 (SDF-1) Induces chemotaxis of PC towards BM Modulates adhesion activity of VLA-4	Migration marker
MMP-9	Secreted as inactive proproteins, cleaved by extracellular proteinases. Role in breakdown of extracellular matrix, IL-8 induced mobilisation of blood cells from bone marrow, cleavage of chemokines and possible role in cancer-associated tissue remodelling and angiogenesis	Bone marrow micro-environment remodelling
Ki-67	Nuclear marker, necessary for cellular proliferation	Proliferative marker

Table 3.1. Explanation of the ten cell marker fluorochrome panel *used in this chapter, brief function of each cell marker as well as intended purpose are included; PC, plasma cells; PAX-5, paired box-5; NCAM, neural cell adhesion molecule; VCAM, vascular cell adhesion molecule; BMSC, bone marrow stromal cell; IL-6, interleukin-6; STAT-3, signal transducer and activator of transcription 3; RANKL, Receptor activator of nuclear factor kappa-B ligand; MMP-9, Matrix metallopeptidase 9;*

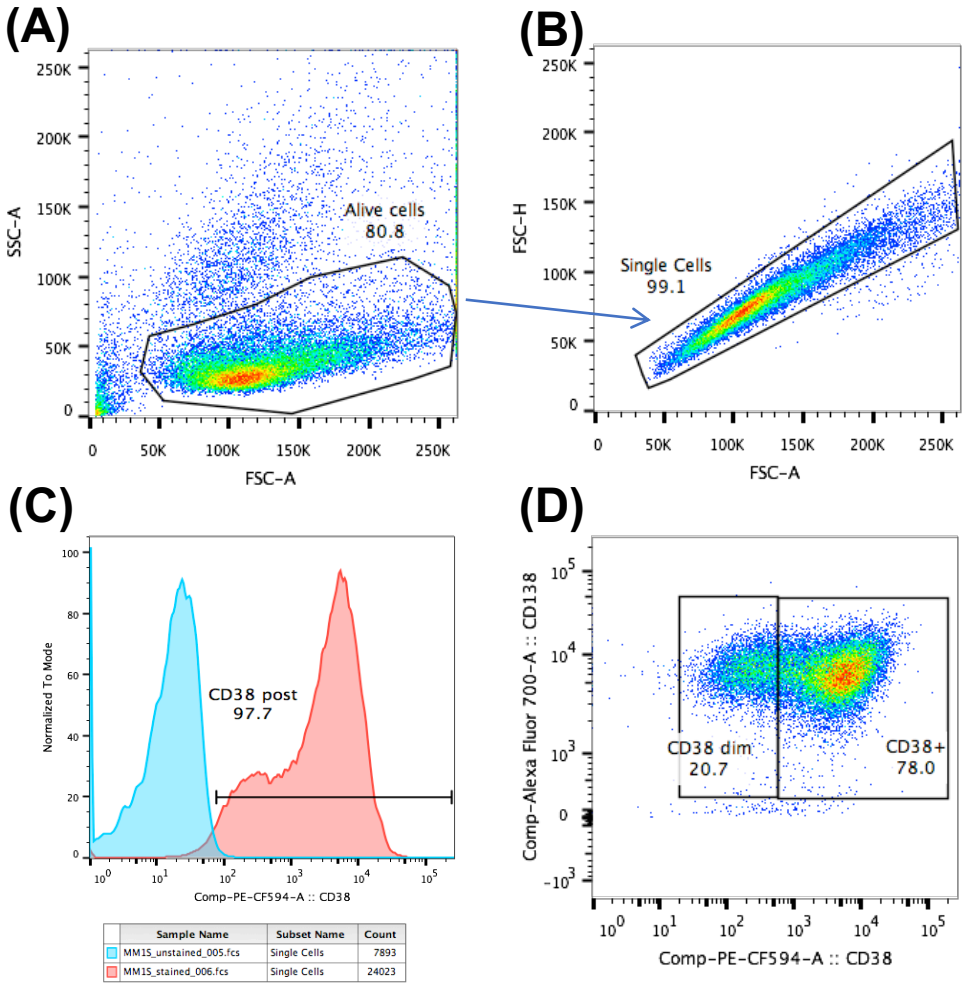

Figure 3.1. Gating strategy applied for each MM cell line flow cytometry Immunophenotyping analysis. *In this example 30,000 events of the cell line MM.1S were recorded (both stained and unstained samples). (A) Alive cells for either sample were gated on side scatter area (SSC-A) and forward scatter area (FSC-A) dot plot, thus removing debris. (B) Of the Alive cells gated events, doublets were removed by single cells gate from FSC-height and FSC-area dot plot. (C) Stained single cells where then analysed by individual cell marker histograms. This allowed for either median fluorescence intensity (MFI) or comparison of percentage positivity staining to unstained sample. In this example 97.7% of the MM.1S cells showed positive expression for CD38. (D) Subset analysis of different cell markers undertaken to identify phenotypically distinct sub-populations, e.g. the bimodal expression of CD38.*

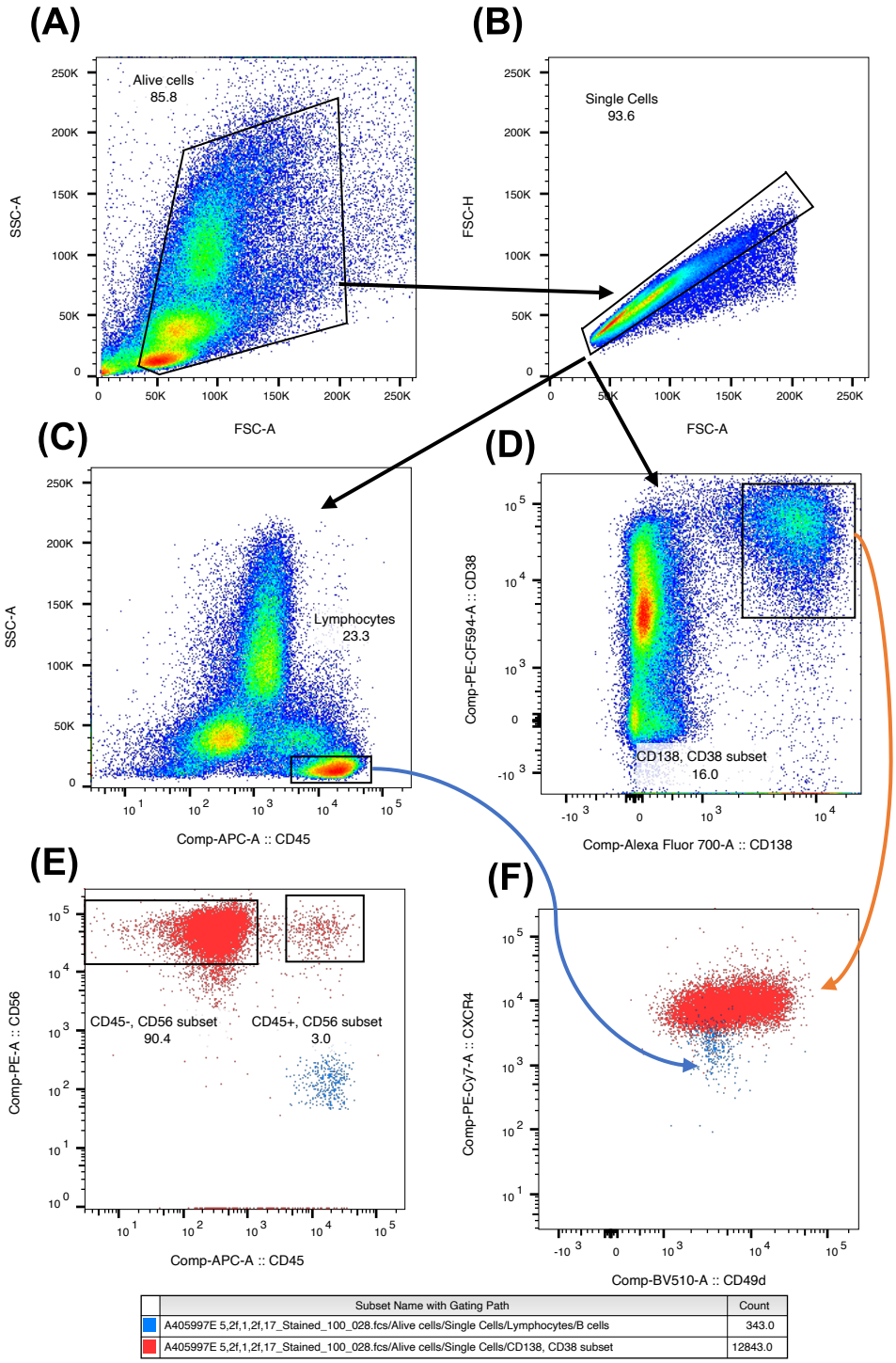

Figure 3.2. Immunophenotyping gating strategy applied for each primary bone marrow sample*. In this example, 100,000 events were analysed from a Ficoll centrifuged bone marrow sample, from a newly diagnosed MM patient and stained with fluorescence-labelled antibodies. (A) Live cells were gated on side scatter area (SSC-A) and forward scatter area (FSC-A) dot plot, thus removing debris. (B) Of the live-cell gated events, doublets were removed by single cell gating using a FSC-height vs FSC-area dot plot. (C) Lymphocytes were gated by CD45 SSC-A dot plots (provided sufficient cell numbers, an additional subset analysis was performed using CD19 to identify B-cells). (D) Plasma cells were identified through gating CD138/CD38 double positive single cells, with MFI and percentage positivity referenced to unstained sample undertaken for each sample (not shown for this example). (E) and (F) Overlaid dot plot immunophenotypic comparison of gated PC from (D) (coloured red) with gated lymphocytes from (C) (coloured blue). (E) Analysis of PC aberrant cell markers CD56 and CD45 to determine if PC are phenotypically abnormal (in this example PC are predominantly CD45-, CD56+, in keeping with the phenotype of myeloma PC, but with a small (3% of PC) CD45+ subset also identified. (F) Additional analysis undertaken looking at other cell markers expression outlined in Table 3.1, in this example PC (red) CXCR4 and CD49d expression was positive and when compared to lymphocytes (blue), had increased CXCR4 expression, but more variable CD49d expression.*

3.4 Characterisation of MM cell lines

Table 3.2 details the six IL-6 independent MM cell lines used in this thesis. The cell lines encompassed the main Immunoglobulin (Ig) heavy chain MM subtypes and the most frequent genetic and chromosomal abnormalities (Table 3.2). U266, RPMI-8266 and JJN3 were already in use by the research group, chosen for their differing genetic mutations affecting the NF-κB signalling pathway. MM.1S and MM.1R cell lines are derived from the cell line MM.1, by the same research centre who created the MM.1 cell line in 1986. In 1990, Steve Rosen's Laboratory subjected the MM.1 cell line to low dose dexamethasone, forming a dexamethasone resistant cell line, which they termed MM.1R. The original dexamethasone sensitive cell line, was subsequently re-labelled MM.1S and both forms are now commercially available from ATCC. Using both these cell lines, provided an opportunity to explore sub-population expansion and cell adhesion mediated drug resistance (CAM-DR) between functionally different cells that originated from the same patient.

Cell Line	**Disease**	**CD45**	**IgH translocation /target oncogene**	**Mutations**	**Deletions**
JJN-3	IgAκ MM	+/-	t(14;16) *MAF* (c-Maf); t(8;14)		*TP53*
MM.1R	IgAλ PCL	-	t(14;16) *MAF* (c-Maf); t(8;14)	*KRAS* (G12A - het) *TRAF3* (K536 - hom)	*CDKN2*
MM.1S	IgAλ PCL	-	t(14;16) *MAF* (c-Maf); t(8;14)	*KRAS* (G12A - het) *TRAF3* (K536 - hom)	*CDKN2*
OPM-2	IgGλ MM	-	t(4:14) *MMSET/FGFR3;*	*FGFR3* (K650E - het) *TP53* (R175H - hom)	*CKKN2*
RPMI-8226	IgGλ MM	-	t(14;16) *MAF* (c-Maf); t(8;22)	*KRAS* (G12A - het) *TP53* (E285K - hom)	*TRAF3*
U-266	IgEλ MM	+	t(11;14) *CCND1*	*BRAF* (K601N - het) *RB1* (E419X - hom) K228R - hom) *TP53* (A161T - hom) *TRAF* (K550I - hom)	

Table 3.2. List of MM cell lines used in this study, their disease type and genetic characteristics. *IgH translocations are present in each cell line, target oncogene is the affected gene that is upregulated through the translocation of the IgH enhancer. MM - multiple myeloma; PCL - plasma cell leukaemia; κ - kappa light chain; λ - lambda light chain; IgH – Immunoglobulin heavy chain; t – Translocation; MMSET - multiple myeloma SET domain; FGFR3 - fibroblast growth factor receptor-3; HD - homozygous deletion; het - heterozygous mutation; hom - homozygous mutation; CCND1 - cyclin D; CDKN2 - cyclin dependent kinase inhibitor 2; TRAF3 - tumour necrosis factor.*

3.4.1 MFI Immunophenotypic analysis

Figure 3.3 shows the different cell markers Median Fluorescence Intensity (MFI) on a logarithmic scale for the six cell lines. Figure 3.3a shows cell markers predominantly used for plasma cell identification (CD138 and CD38) as well as the aberrant cell markers CD45, CD56 and CD19. Between the six cell lines, expression was uniformly high for CD138 (8,106 SD±3,648) and low for CD19 (158 SD±66), whereas a greater variation MFI was observed for CD38 (10,413 SD±16,708) and CD56 (9,186 SD±19,573). In contrast, Figure 3.3b shows that there was little variation in the expression of CXCR4, IL-6, Ki-67 and MMP-9 but a more marked variation in the expression of CD49d (12,059 SD±9,637) between the six cell lines.

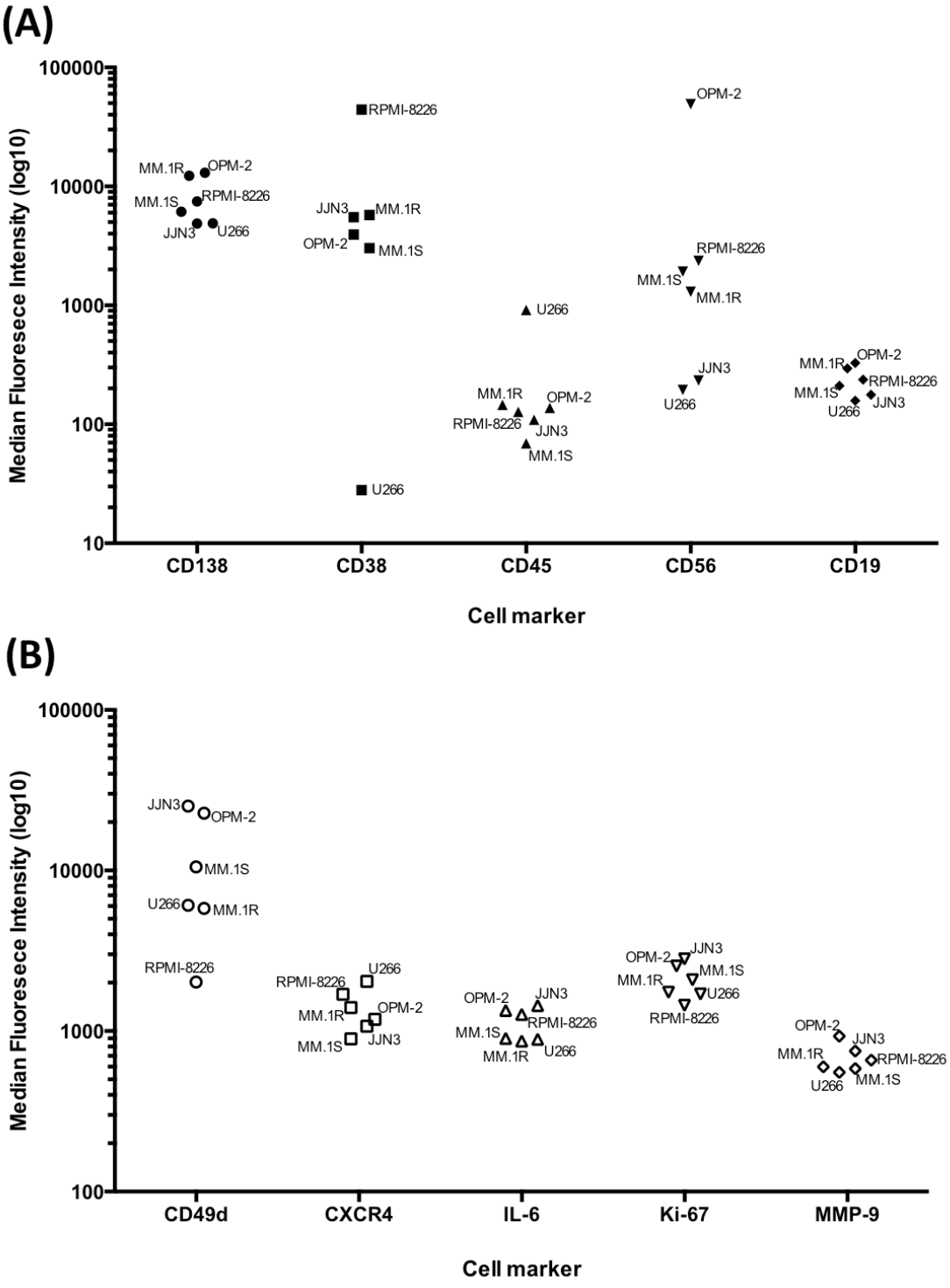

Figure 3.3. Flow cytometric comparison of antigen expression in six commonly used myeloma cell lines*. 1 x 10^6 cells from each of the cell lines were stained with fluorescence-labelled antibodies and data was acquired on a BD Fortessa flow cytometer. (A) Shows the comparison of CD138, CD38, CD45, CD56 and CD19 in the cell lines. (B) Shows the comparison of CD49d, CXCR4, IL-6, Ki-67 and MMP-9. The results are expressed as median fluorescence intensity values and are the product of n = 3 separate experiments.*

3.4.2 Percentage positivity Immunophenotypic analysis corresponds with their MFI except for cell markers IL-6 and MMP-9

Analysis of percentage positivity roughly correlated with MFI (data not shown). U266 percentage positivity for CD38 was 9.9% (MFI 28), whereas all other cell lines were above 90%. CD45 positivity was less than 20% for all cells except U266 (74.5% positivity, MFI 916). CD49d and CXCR4 expression was broadly positive and above 90% in all cell lines except RPMI-8226 (CD49d - 15.4%) and JJN3 (CXCR4 - 75.9%). The only markers where a discrepancy between MFI and percentage positivity was seen were IL-6 and MMP-9, notably in the cell lines JJN3 and OPM-2, which showed high percentage positivity for both MMP-9 and IL-6. Both of these markers showed low uniform MFI expression (Figure 3.3B), but expression was more variable when analysed by percentage positivity (Figure 3.4A) and was shown to have a strong positive correlation (r=0.9539; Figure 3.3B), which was statistically significant (p=0.0031).

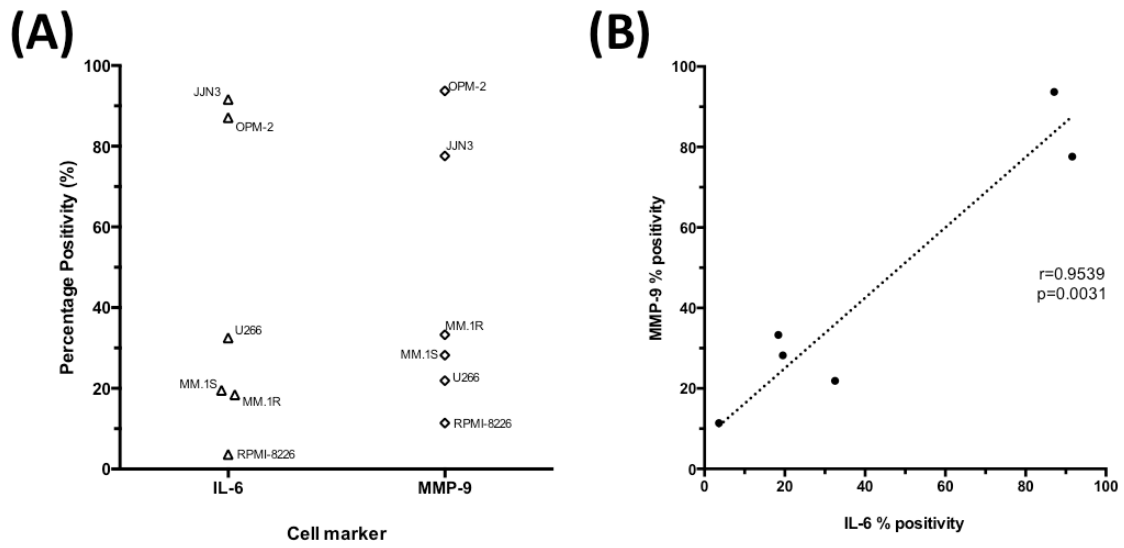

Figure 3.4. Comparison of IL-6 and MMP-9 percentage positivity between the six MM cell lines. Flow cytometric comparison of IL-6 and MMP-9 expression in six commonly used myeloma cell lines*. 1 x 10^6 cells from each of the cell lines were stained with fluorescence-labelled antibodies and data was acquired on a BD Fortessa flow cytometer. (A) Shows the comparison of IL-6 and MMP-9 percentage positivity in each of the cell lines. (B) Shows the correlation between MMP-9 and IL-6 positivity between the six cell lines, Pearson's correlation co-efficient was r=0.9539, with a two-tailed statistical positive correlation of p=0.0031. The results are expressed as percentage positivity relative to unstained control samples of the same cell line and are the product of n = 3 separate experiments.*

3.4.3 Ki-67 expression shows strong correlation with other cell markers.

By individually plotting antigen expression of each cell line with (as done in Figure 3.4B), specific cell marker correlations were able to be identified (Figure 3.5). The proliferative marker Ki-67 expression showed the greatest number of correlations with the other cell markers (Figure 3.5B). There was almost a perfect positive correlation with CD49d expression (r=0.99; p=0.0002). Other cell markers with positive correlation, although not statistically significant, were IL-6 expression (r=0.60, p=0.21) and MMP-9 expression (r=0.68; p=0.138). A negative correlation, although again not statistically significant, was observed with CXCR4 expression (r=-0.68; p=0.13). Previously, CD38 expression has been shown positively correlate with CD49d and Ki-67 in other B-cell malignancies such as CLL (Pittner et al. 2005). However, in this study no significant correlation between CD38 and the other cell markers was observed (Figure 3.5A).

3.4.3.1 Wide variation in CD38 expression but with uniform CD138 expression amongst the cell lines could represent sub-populations/subclones

In an attempt to further characterise the cell lines and identify possible reasons for the lack of correlation of CD38 expression with other cell markers, such as the presence of different sub-sets/sub-populations within each cell line, dot plot comparison of cell markers for each cell line were undertaken as outlined in section 3.3.

As previously outlined in section 3.4.1. CD138 expression was broadly uniformly positive and bright – with roughly 0.5 log difference between the minimum (JJN-3) and maximum (MM.1R) cell line fluorescence intensity (Figure 3.6B). No CD138 expression subsets were identified between any of the six cell lines. CD38 expression in contrast, showed a wide variation (average MFI cell lines 10,576±SD 15,258). Of the six cell lines analysed, U266 cells showed the lowest MFI for CD38 expression, Whilst RPMI-8226 showed the highest MFI for CD38 (MFI 44,251). Furthermore, variation of CD38 expression was also observed within the individual cell lines. This was most prominent for MM.1S cells, with CD38 expression showing a bimodal distribution (Figures 3.6A and 3.6C), which highlighted two distinct CD38 expressing sub-populations within the cell line.

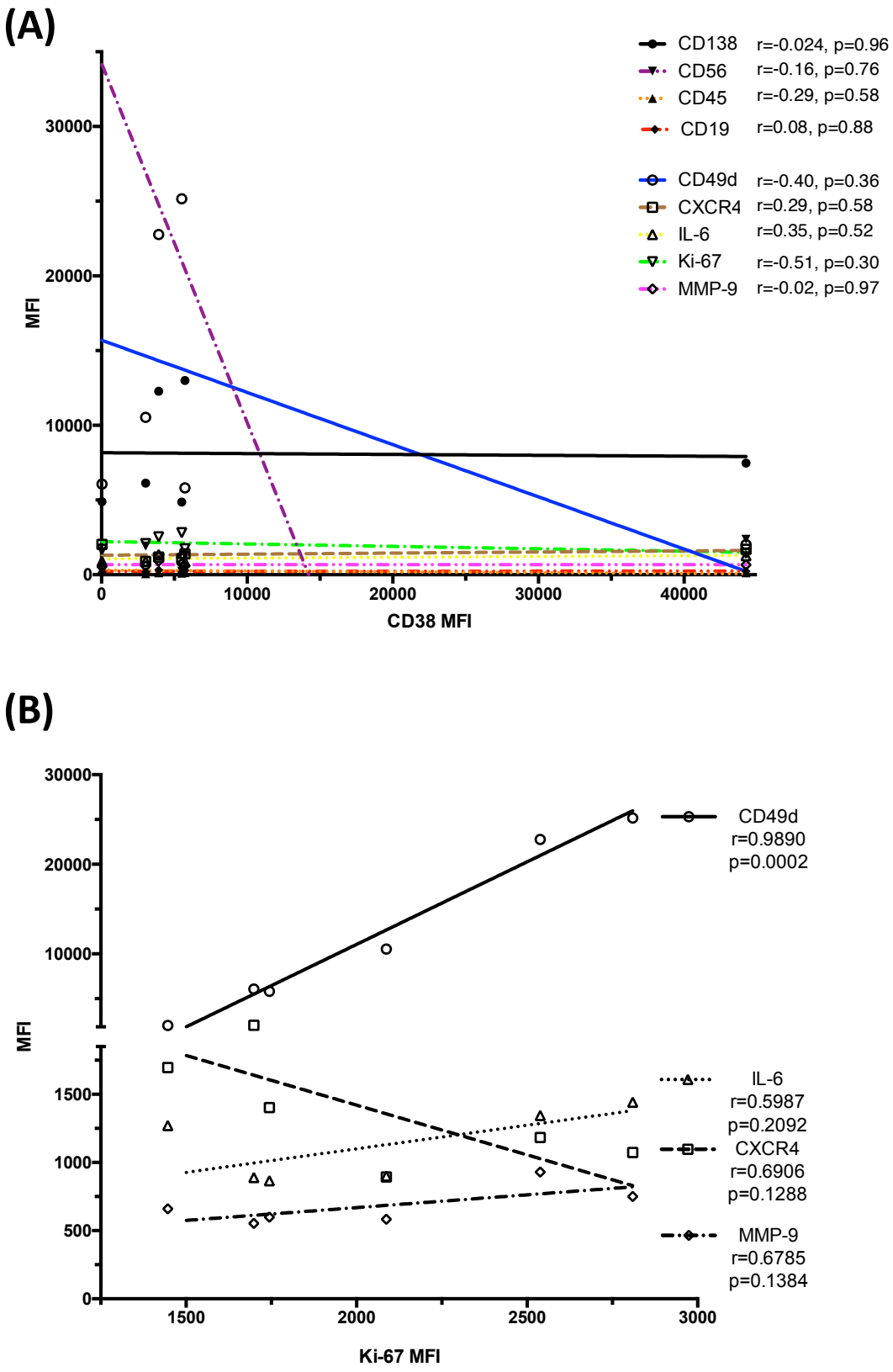

Figure 3.5. Flow cytometric correlation of antigen expression for the six MM cell lines*. 1 x 10^6 cells from each of the cell lines were stained with fluorescence-labelled antibodies and data was acquired on a BD Fortessa flow cytometer. (A) Shows the correlation of CD38 expression with the other 9 antigen expression. (B) Shows the correlation of Ki-67 expression with CD49d, IL-6, CXCR4 and MMP-9. The results are expressed as median fluorescence intensity values and are the product of n = 3 separate experiments, from the same data set as Figures 3.3 and 3.4. Where relevant Pearson's r value is provided and two-tailed p value.*

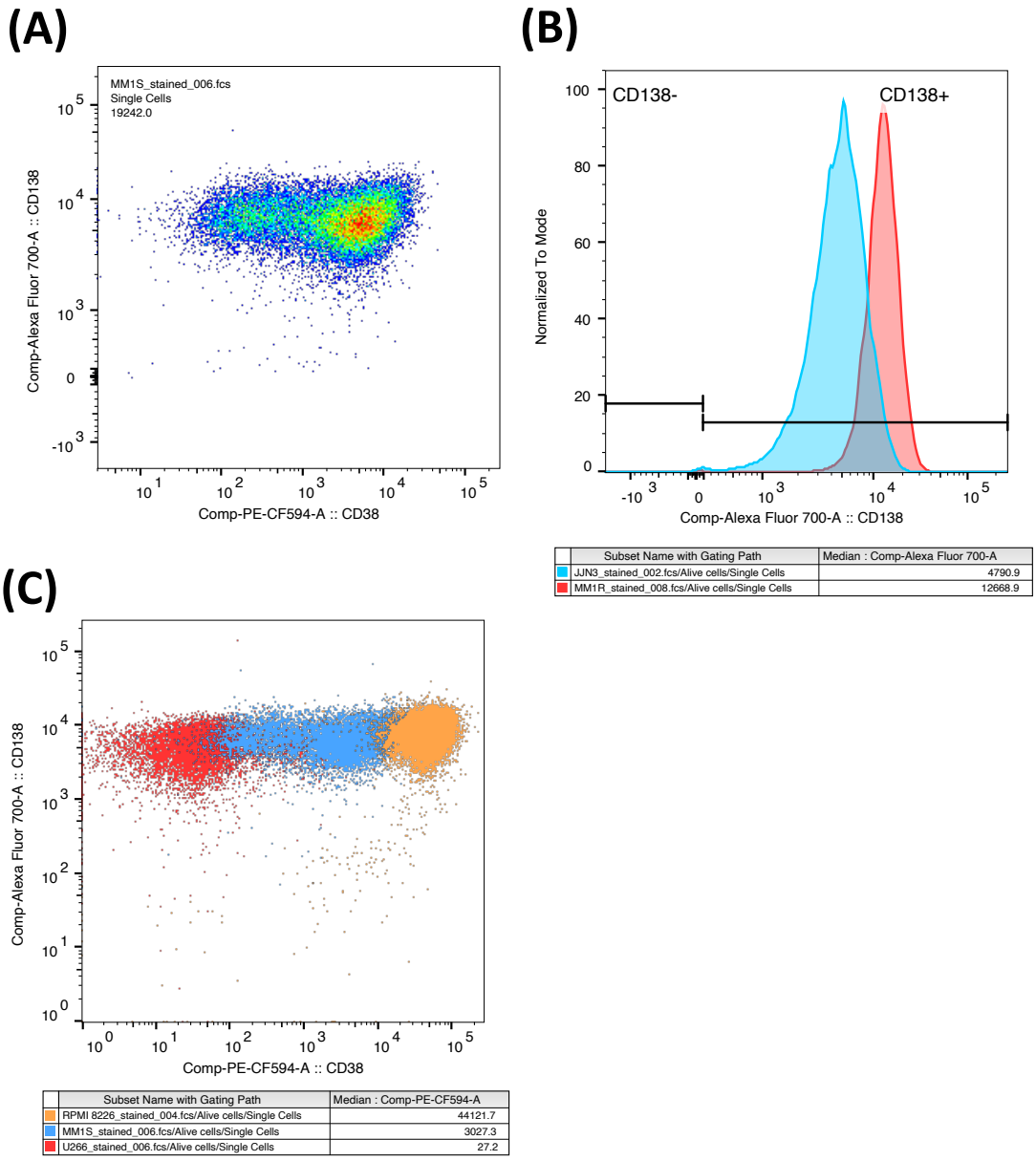

Figure 3.6. Flow cytometric comparison of CD138 and CD38 expression in myeloma cell lines. *1 x 10^6 cells from each of the cell lines were stained with fluorescence-labelled antibodies and data was acquired on a BD Fortessa flow cytometer. (A) Shows a pseudocolour dot plot of CD138 and CD38 expression in the cell line MM.1S. (B) Overlaid histogram of the highest (MM.1R red) and lowest (JJN3 blue) CD138 expression of the six MM cell lines used. (C) overlay dot plot comparing CD138 and CD38 expression between the lowest CD38 expressing cell line (U266 red), the bimodal population (MM.1S blue) and the highest CD38 expressing cell line (RPMI-8226 orange).*

3.4.3.2 Analysis of CD56/CD45/CD19 expression of the cell lines, reveals distinct immunophenotypic populations, indicative of sub-clonal co-existence

Analysis of CD56, CD45 and CD19 expression not only allows for distinction between normal PC (CD45+/CD19+/CD56-) and clonal myeloma PC (CD45-/CD19-/CD56+), but also for detection of additional myeloma sub-populations that do not conform to either immunophenotype. Thereby providing support to the concept of numerous immunophenotypic sub-clones co-existing within an individual cell line, as postulated in section 3.4.3.1. With the exception of OPM-2 cells, all of the cell lines showed evidence of intra-cell line sub-populations (Figure 3.7). In four of the six cell lines (OPM-2, MM.1S, MM.1R and RPMI-8226) the largest immunophenotypic population was that typically seen in myeloma plasma cells (CD45-/CD19-/CD56+). The exceptions, U266 and JJN-3, were CD56-; a phenotype characteristic of plasma cell leukaemia (Harada et al. 1993), although both contained small sub-populations (<10%) that were CD56+ (Figures 3.7A and B). The most notable example of distinct sub-populations was found in U266 cells, which demonstrated distinct expression patterns of CD19. In addition, four distinct CD45/CD56 expressing sub-populations were also evident (Figure 3.7A). This polytypic profile is suggestive of clonal evolution although the necessary genetic profiling of the distinct sub-populations was not performed. The MM.1S cell line, in which distinct bimodal CD38 expression existed, was shown to have variable CD56 expression. This was particularly apparent when compared to cell lines OPM-2 and U266 (Figure 3.7B). Although this variation in CD56 expression did not correlate with the bimodal CD38 expression (data not shown), it again emphasises the heterogeneity of immunophenotypic expression within an individual cell line.

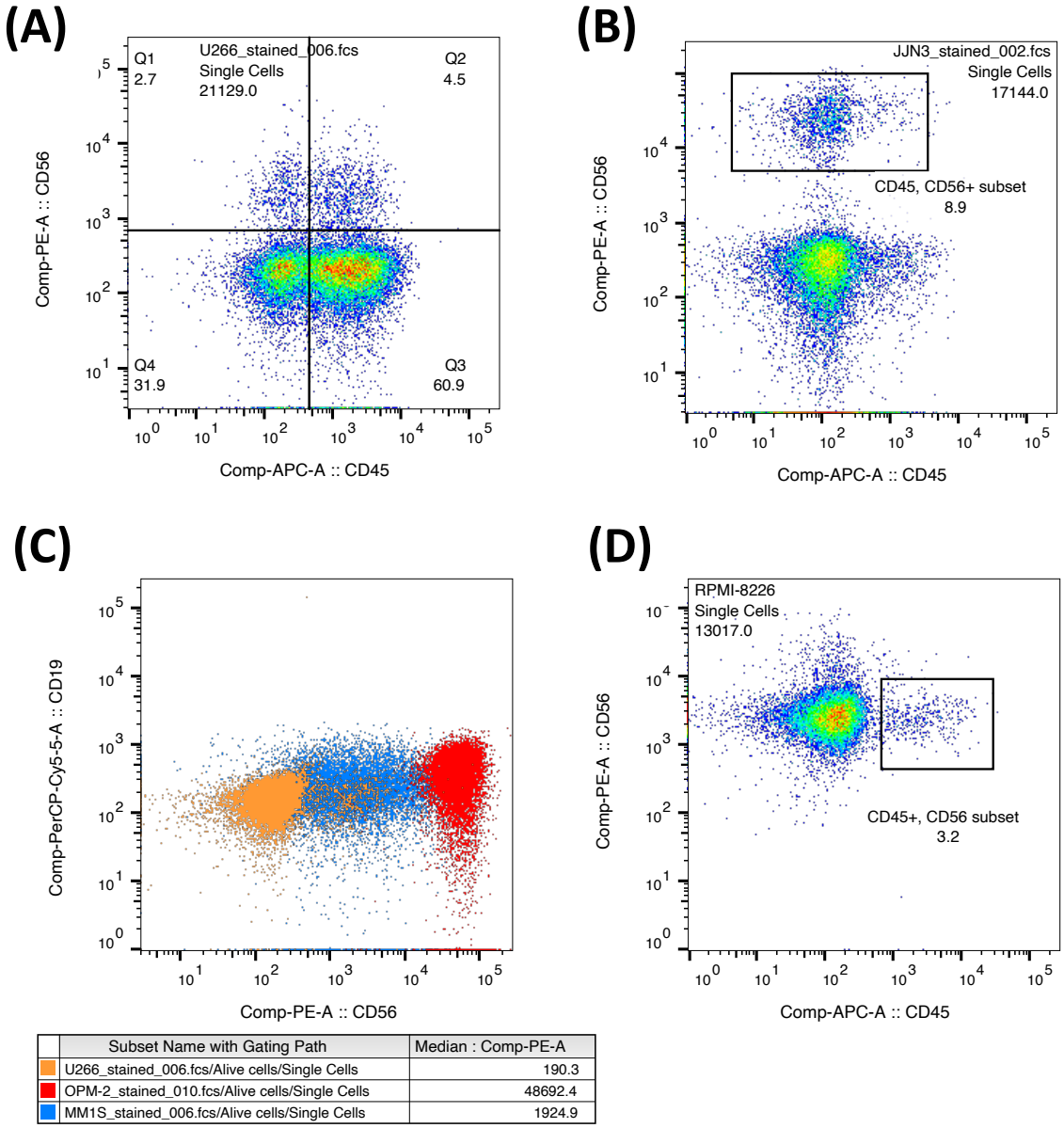

	Subset Name with Gating Path	Median : Comp-PE-A
	U266_stained_006.fcs/Alive cells/Single Cells	190.3
	OPM-2_stained_010.fcs/Alive cells/Single Cells	48692.4
	MM1S_stained_006.fcs/Alive cells/Single Cells	1924.9

Figure 3.7. Flow cytometric dot plots of CD56, CD19 and CD45 expression of MM cell lines*. 1 x 10^6 cells from each of the cell lines were stained with fluorescence-labelled antibodies and data was acquired on a BD Fortessa flow cytometer. (A) U266 cell line CD56 and CD45 pseudocolour dot plot. Shows 4 separate populations, split into quadrants with % populations provided. (B) JJN-3 cell line CD56 and CD45 pseudocolour dot plot. The largest population was CD45-/CD56-, but a distinct CD45-/CD56+ population was also observed, representing 8.9% of the cell line. (C) Overlaid dot plot comparing CD19 and CD56 expression between 3 separate cell lines, all cell lines were uniformly negative for CD19, CD56 was much more variable - U266 (orange) lacked CD56 expression, MM.1S (blue) had variable expression and OPM-2 (red) strongly expressed CD56. CD56 MFI is provided in table below figure. (D) RPMI-8226 cell line CD56 and CD45 pseudocolour dot plot. The largest population was CD45-/CD56+, but a distinct CD45+/CD56+ population was also evident, representing 3.2% of the cell line.*

3.4.3.3 Identification of MM cell line sub-clones through immunophenotypic markers of adhesion, migration and microenvironment remodelling

Having shown distinct immunophenotypic populations within most of the cell lines for the commonly used plasma cell markers (CD56, CD45 and CD19), additional analysis looked for similar distinct populations in the other cell markers used. Although a wide variation in CD49d expression was observed between the six cell lines tested (Figure 3.3a), CD49d expression within each individual cell line was fairly uniform (Figure 3.8), except for RPMI-8226 cells, which contained a brighter CD49d expressing sub-population, which accounted for ~10% of the cell line. CXCR4 expression for each cell line was much more variable, especially within the cell lines JJN-3 and OPM-2 (Figure 3.8). Subtle immunophenotypic differences were observed between MM.1S and MM1.R cell lines in terms of CD49d and CXCR4 expression. In contrast, no obvious MMP-9 or IL-6 sub-populations were identified.

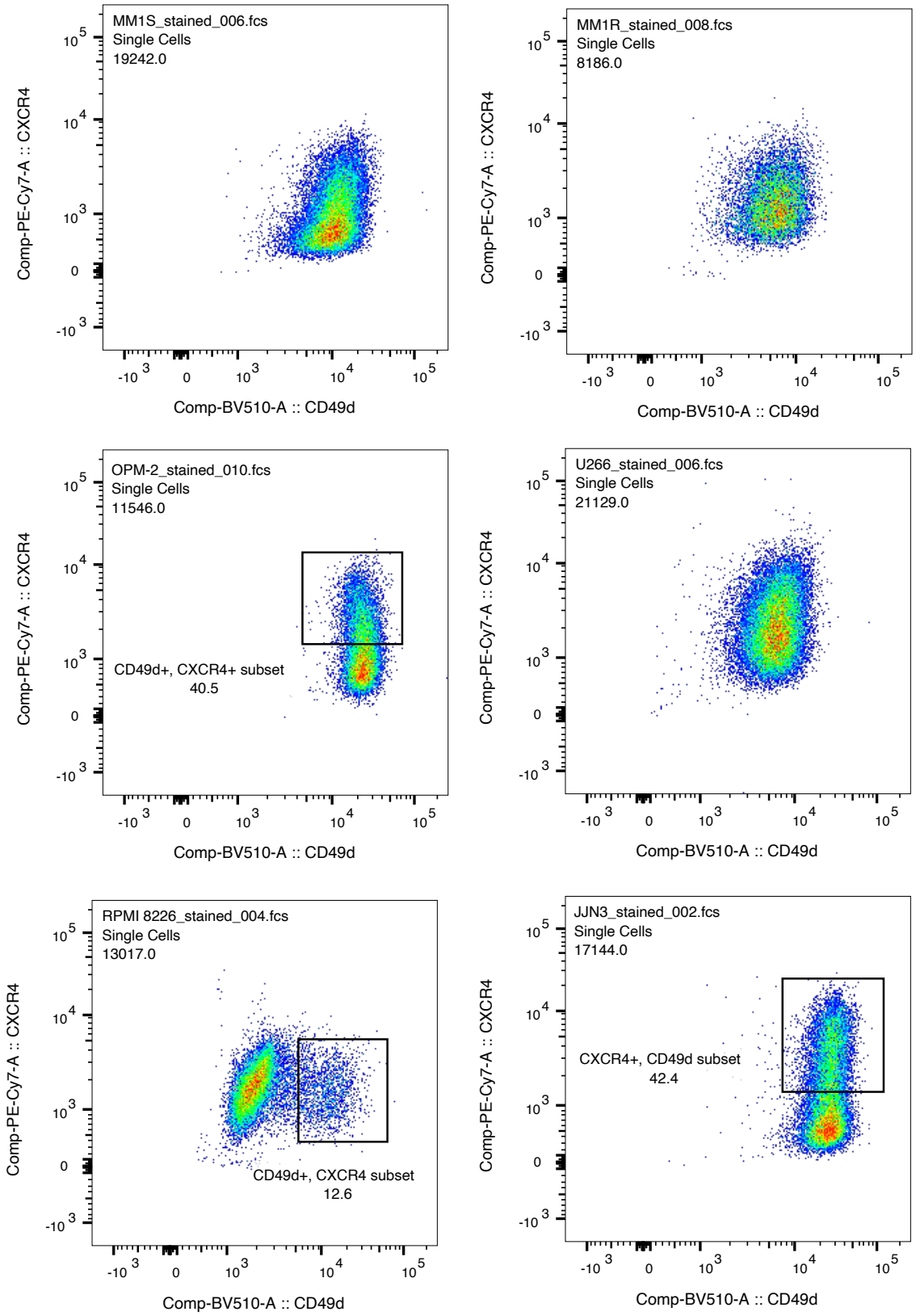

Figure 3.8. Flow cytometry pseudocolour dot plots comparison of CXCR4 and CD49d expression of six MM cell lines. *1 x 10^6 cells from each of the cell lines were stained with fluorescence-labelled antibodies for the cell markers CXCR4 and CD49d. Data was acquired on a BD Fortessa flow cytometer. The cell line is stated in the top left corner of each figure. Where a distinct sub-population was identified (OPM-2, RPMI-8226 and JJN-3), it was gated with the percentage of each population stated.*

3.4.4 CXCR4 expression a marker of migratory potential

The chemokine CXCL12 and its receptor CXCR4 are known to play a key role in MM cell migration and regulation of CD49d (Sanz-Rodriguez et al. 2001; Moller et al. 2003). The variability in CXCR4 expression both between the cell lines but also individually, could imply different migratory capacities of the cell lines, but also of the existence of sub-clones with differing migratory potential.

To identify whether baseline CXCR4 expression or indeed any of the other cell marker expression (outlined in Table 3.1) correlated with MM cell line migration, 24h Transwell (3μm membrane pore size) migration assays, against a CXCL12 concentration gradient were undertaken. Transwell migration assays (Costar; Corning, Acton, MA) are a recognised method of assessing CXCL12 induced MM migration (Tai et al. 2003; Alsayed et al. 2007). The static chambers are separated by a membranous film with numerous micropores that allow migration of cells in theory in the direction of a homing stimulus such as CXCL12. Cells are usually suspended in the upper chamber, with the migratory stimuli in the lower chamber, with the migrated cells recovered from the lower after a period of time.

In my experiments, minimal migration (0.1% of total cells) was observed for the cell lines U266 and RPMI-8226 (Figure 3.9A). In contrast, MM.1S cells showed the greatest cell migration (4.04%±0.82), followed by the related, steroid resistant, cell line MM.1R (3.26%±1.34). The difference in migration between these two lines was not statistically significant ($p=0.18$). Interestingly, there was a negative correlation between cell line percentage migration and baseline CXCR4 expression (prior to migration experiment) ($p=0.0436$; Figure 3.9B). No correlation was observed between CD49d, CD38 and Ki-67 baseline expression (Figure 3.9b), all of which have been previously shown to play a role in migration in B-cell malignancies (Moller et al. 2003; Vaisitti et al. 2010).

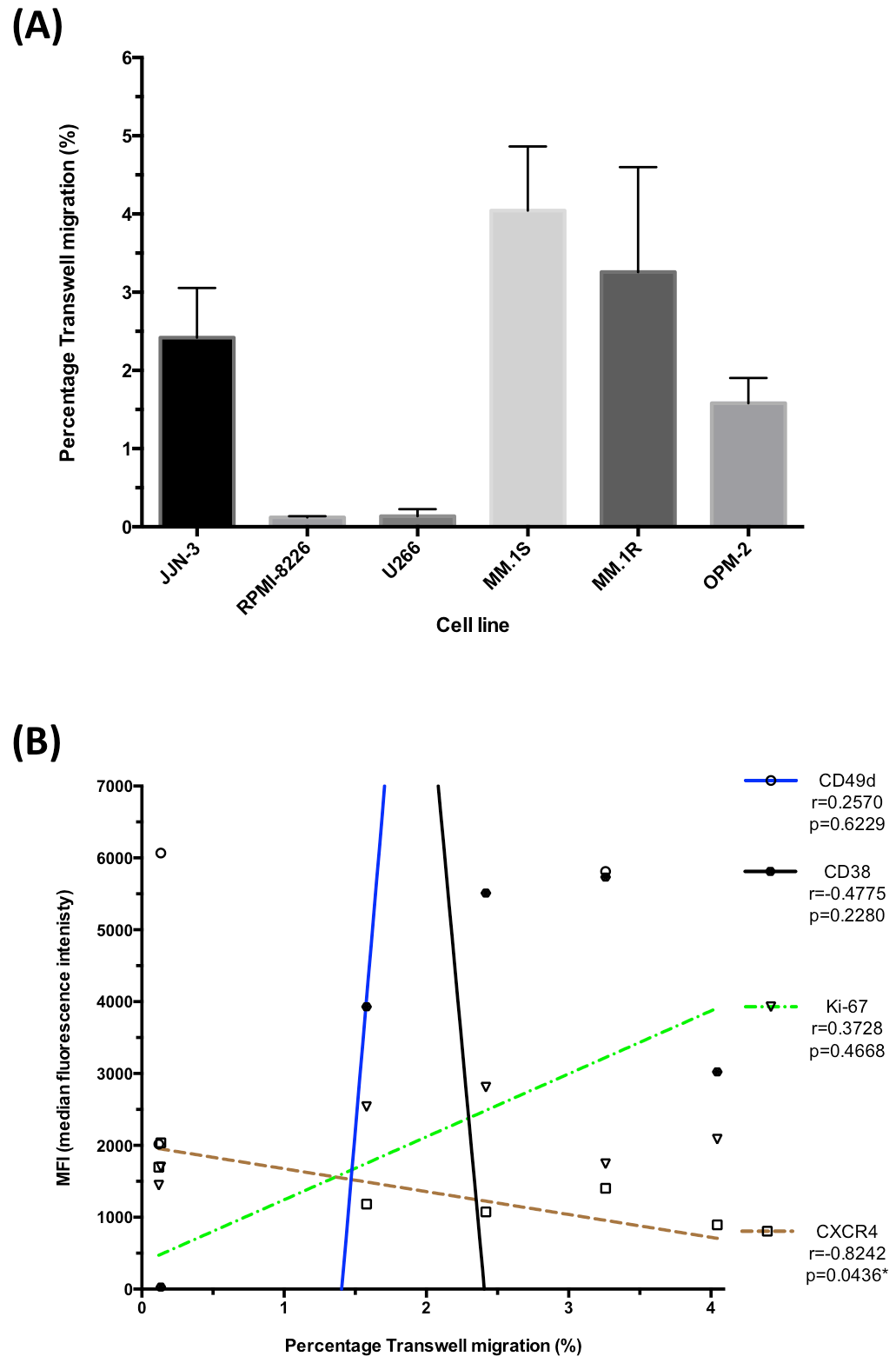

Figure 3.9. Comparison of MM cell line CXCL12 induced migration and correlation with CXCR4 expression. *(A) 0.25x10^6 cells were placed in the apical chamber of a 3μm transwell plate. Migrated cells where retrieved from basolateral chamber of transwell at 24h. Migration was stated as a percentage of the total number of cells inserted into transwell. Cell lines analysed, JJN-3 (n=5), RPMI-8226 (n=3), U266 (n=8), MM.1S (n=8), MM.1R (n=8) and OPM-2 (n=6). (B) MM cell lines correlation between percentage transwell migration at 24h (at stated in figure 3.9A) and cell markers baseline CXCR4, Ki-67, CD38 and CD49d expression (MFI). A statistically significant negative correlation was observed for CXCR4 expression. (r=-0.8242; p=0.0436). Each legend also states Pearson's correlation (r) and whether the correlation was statistically significant (P<0.05). Error bars are standard deviation and calculated by repeated independent experiments.*

3.5 Immunophenotypic comparison of primary bone marrow plasma cell dyscrasia samples

Of the findings obtained from the immunophenotypic analysis of MM cell lines (section 3.4), I aimed to establish if the discoveries could also be applicable to primary samples of patients with plasma cell dyscrasia. In particular I aimed to confirm if large variation in CD38 expression is seen and correlation with other cell markers. Such analysis would also allow for the confirmation of CD38 negative or weakly expressive populations. In addition, I aimed to identify the degree of immunophenotypic sub-populations within individual primary samples as well as showing if statistical correlation of cell marker expressions existed, as seen in the MM cell line analysis. My data would also allow for sub-group analysis between MGUS, newly diagnosis MM and Relapsed/Refractory MM (RRMM).

3.5.1 Sample characteristics

36 samples were immunophenotypically analysed stained with 10-colour panel in Table 3.1. 22 were of newly diagnosed MM, 9 MGUS and 5 RRMM. Table 3.3 shows baseline characteristics of primary bone marrow samples.

	MGUS*	Newly Dx. MM	RRMM
Total number	9	22	5
Type of plasma cell dyscrasia			
IgGκ	7	7	5
IgGλ	1	4	-
IgAκ	-	5	-
IgAλ	-	1	-
Plasma cell leukaemia	-	3	-
Plasmacytoma	-	2	-
Smouldering Myeloma	1	-	-
R-ISS stage			
I	-	9	-
II	-	6	-
III	-	7	-
No. analysed for cytogenetics	2 (22.2%)	18 (81.8%)	4 (80.0%)
Normal	1	7	3
p53	-	-	1
t(4:14)	-	1	-
CKS1B (+1q)	1	9	-
CDKN2C (-1p)	-	3	1
Extra copy 11q (CCND1)	-	1	-
Loss of IGH	-	3	-
Extra copy IGH	-	-	1

Table 3.3. Baseline characteristics of primary marrow samples analyses. *MGUS – monoclonal gammopathy of unknown significance; RRMM – relapsed refractory multiple myeloma; PCL – plasma cell leukaemia; *Includes one low risk Smouldering myeloma. Cytogenetics analysed by Cytocell IGH breakapart probe, interphase score 200 analysed - other probes – p53 and CKS1B (+1q)/CDKN2C (-1p).*

3.5.2 Immunophenotypic variation at different stages of disease

Figure 3.10 compares the 10-cell marker expression, for the different stages of plasma cell disease (MGUS, newly diagnosed MM and RRMM). Although only 5 RRMM samples were obtained, statistically significant expression differences between the different stages of disease were seen. Consistent with the MM cell line expression data, CD138 was uniformly bright for each of the three sub-groups of plasma cell disorder, with a statistically lower difference in CD138 expression between newly diagnosed MM and RRMM ($p=0.031$). This could either imply CD138 is shed and/or sub-populations of plasma cells expressing lower levels of CD138 are selected for during treatment.

Consistent with the MM cell lines data, there was a large variation in CD38 expression for all stages of disease (Figure 3.10a). The average MFI for all newly diagnosed MM was 40,345 (SD±24,637), 43,561 (SD±22,868) for MGUS and 19,563 (SD±26,976) for RRMM. Although, a decrease in CD38 expression was seen in RRMM compared to newly diagnosed MM, no statistical difference existed ($p=0.097$). Other statistical expression differences between the three groups included reduced CD56 expression in RRMM compared to newly diagnosed MM (MFI 15,569 vs. 450, $p=0.04$) and CD19 expression, showing a general trend of decrease expression as disease progressed (MGUS 5,629 vs. newly diagnosed MM 1,585 ($p=0.0007$) and MGUS vs. RRMM 1,185 ($p=0.0064$)). Wide variation in CD49d and CXCR4 expression was seen for all stages of disease, especially newly diagnosed MM (CD49d MFI 7,791±3,879 and CXCR4 MFI 7,159±4,489). CXCR4 expression was lower in relapsed disease compared to newly diagnosed ($p=0.0059$). Ki-67 expression was statistically lower in RRMM compared to MGUS ($p=0.042$) and newly diagnosed MM ($p=0.027$). MMP-9 expression upon relapse was statistically higher than at diagnosis ($p=0.026$) and for MGUS ($p=0.022$).

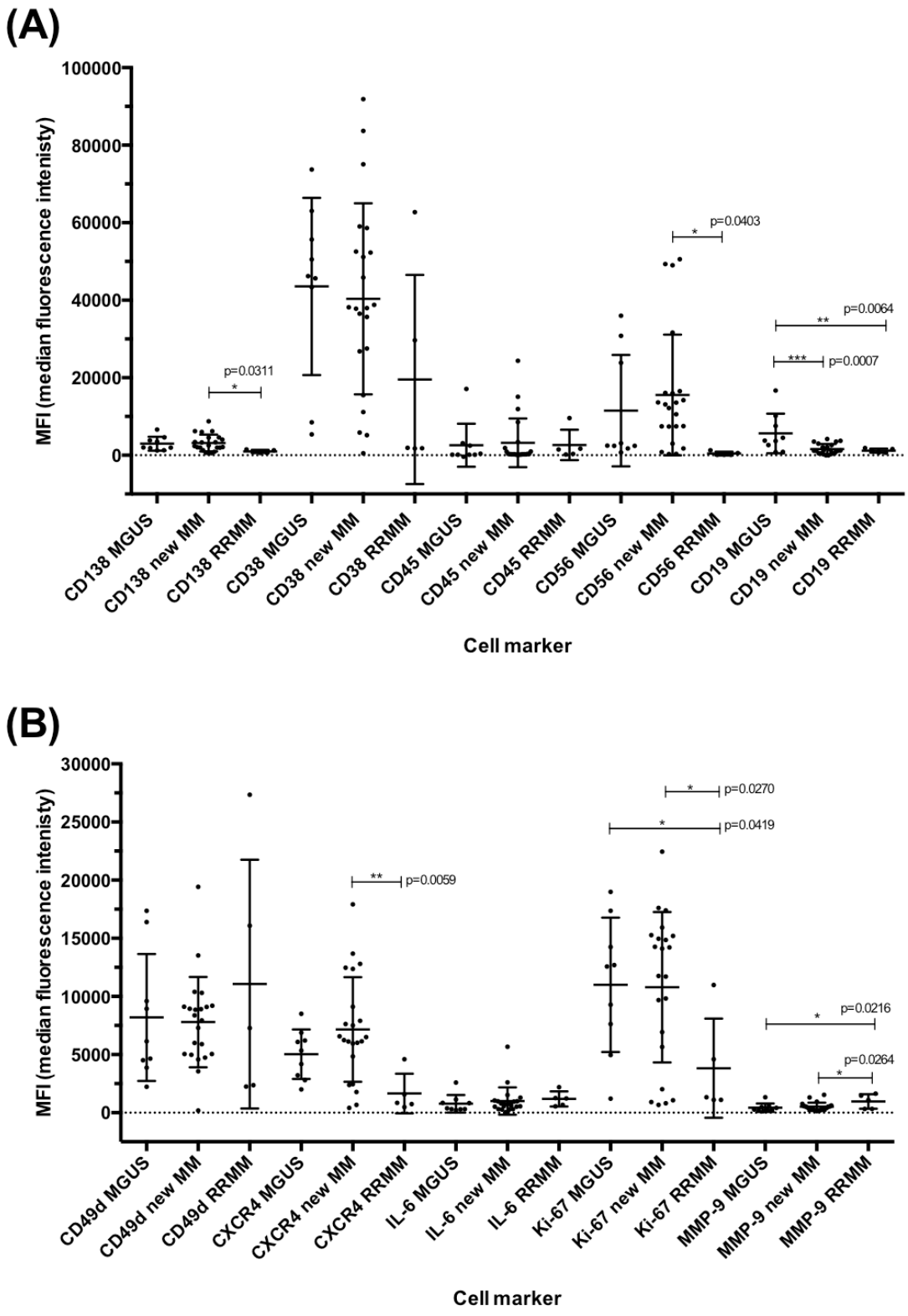

Figure 3.10. Scatter plot flow cytometric comparison of antigen expression in plasma cell dyscrasia primary bone marrow samples. *Bone marrow samples were separated into mononuclear cells by Ficoll centrifuge. 1 x 10^6 cells were stained with fluorescence-labelled antibodies and data was acquired on a BD Fortessa flow cytometer. (A) Shows the comparison of CD138, CD38, CD45, CD56 and CD19 in the primary samples. (B) Shows the comparison of CD49d, CXCR4, IL-6, Ki-67 and MMP-9. The results are expressed as median fluorescence intensity values and are the product of n = 36 separate experiments. Analysis of each cell marker was further divided into separate plasma cell dyscrasia sub-group (MGUS n=9, newly diagnosed MM n=22 and RRMM n=5). Each scatter plot has SD error bar lines, with mean. Where a statistical difference between the same cell marker and different plasma cell disease stage, an ordinary one-way ANOVA Fishers LSD test p value is provided.*

Table 3.4 shows the mean percentage positivity between the cell markers and the different stages of disease. A complimentary method of presenting expression data to MFI, similar patterns were observed to the MFI values. As seen with the MFI data, RRMM CD56 percentage positivity (34.6%) was statistical lower compared to both MGUS (98.0%, p<0.0001) and newly diagnosed MM (97.1%, p<0.0001). The only conflicting data comparison between MFI and percentage positivity was for RRMM CD49d expression (MFI 11,067, 56.5% positive). Here, percentage positivity was statistically lower compared to MGUS (83.3%, p=0.048) and newly diagnosed MM (92.5%, p=0.0038), a trend that was not observed in MFI data (MFI 8,191 and 7,791 respectively). The reason for the discrepancy is likely due to small numbers within the RRMM group, and also the inclusion of an outlier sample (MFI 27,344, 99.9% positive).

Cell marker	MGUS (9)	New MM (22)	RRMM (5)
CD138	100% (±0.0, p=0.53)	99.1% (±4.4)	97.1% (±3.9, p=0.31)
CD38	100% (±0.0, p=0.50)	97.8% (±10.2)	100% (±0.0, p=0.59)
CD45	38.4% (±46.5, p=0.60)	47.5% (±42.4)	48.9% (±35.8, p=0.95)
CD56	98.0% (±4.3, p=0.89)	97.1% (±9.9)	34.6% (±40.8, p=<0.0001***)
CD19	80.4% (±26.7, p=0.013*)	52.5% (±27.7)	34.6% (±24.3, p=0.19)
CD49d	83.3% (±22.9, p=0.33)	92.5% (±17.3)	56.5% (±43.3, p=0.0038**)
CXCR4	99.9% (±0.2, p=0.79)	98.6% (±5.2)	41.4% (±34.6, p=<0.0001***)
IL-6	18.3% (±24.1, p=0.11)	39.9% (±38.1)	10.8% (±22.4, p=0.090)
Ki-67	96.3% (±7.7, p=0.98)	96.2% (±14.3)	52.0% (±44.1, p=<0.0001***)
MMP-9	23.2% (±13.4, p=0.10)	44.5% (±37.0)	41.1% (±30.1, p=0.83)

Table 3.4. Mean percentage positivity (±SD) of cell markers at different stages of disease; *(Monoclonal Gammopathy of underdetermined significance (MGUS), newly diagnosed Multiple Myeloma (MM) and Relapsed/refractory MM (RRMM)). P values are two tailed ANOVA comparison of percentage positivity with newly diagnosed MM and MGUS or RRMM.*

3.5.3 Primary plasma cell dyscrasia samples, show strong correlation with Ki-67 and CD38 expression:

When MFI data for the three-plasma cell dyscrasia groups were combined, specific cell marker correlations were able to be identified by individually plotting antigen expression of each sample (figure 3.11). Unlike the MM cell line MFI data, CD38 expression exhibited strong correlations with a number of cell markers (figure 3.11A), the strongest correlation being between Ki-67 (r=0.89, p=<0.0001). Statistically positive correlations were also seen in CD56 (r=0.36, p=0.029), CXCR4 (r=0.57, p=0.003) and CD19 (r=0.37, p=0.025). The strong correlation between CD38 and Ki-67 expression also inferred statistical positive correlation with CD56 (r=0.58, p0.0002), CXCR4 (r=0.53, p=0.0008) and CD19 (r=0.44, p=0.007) (figure 3.11B). The only other statistical correlation observed was between IL-6 and CD49d (r=0.51, p=0.0016).

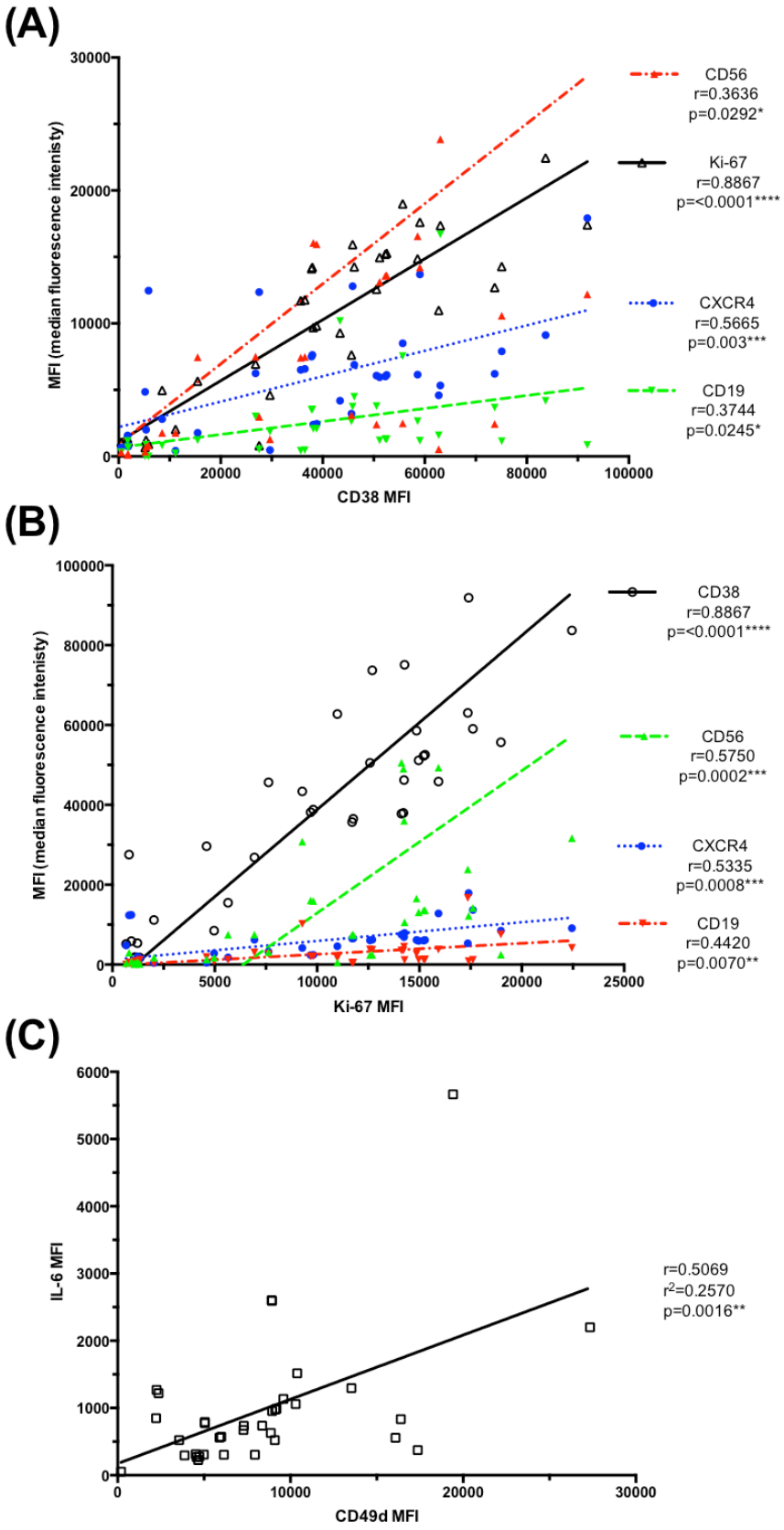

Figure 3.11. Flow cytometric correlation of antigen expression for primary bone marrow samples. *The mononuclear fractions were isolated from Bone marrow samples by density gradient centrifugation. 1 x 10^6 cells were stained with fluorescence-labelled antibodies and data was acquired on a BD Fortessa flow cytometer. (A) CD38 MFI correlation between MFI of CD19, CD56 and Ki-67 (B) Ki-67 MFI correlation between MFI of CD19, CD56 and CD38. (C) CD49d MFI correlation between IL-6 MFI. The results are expressed as median fluorescence intensity values and are the product of n = 36 separate experiments, where relevant Pearson's r value is provided and two-tailed p value.*

3.5.4 Confirmation of existence of CD38 negative expressing plasma cell populations, from primary bone marrow samples that are immunophenotypically distinct

The discovery of a CD38 dim sub-clone within the MM cell lines (MM.1S and U266) was of particular interest due to its role in cell migration and activation, but also in light of the clinical emergence of anti-CD38 therapy. Analysis of all of the primary data looked for CD38 expression variability. Of the 36 samples, one newly diagnosed MM patient (previously diagnosed with SMM), exhibited a CD38 dim and CD38 bright population (Figure 3.12A). The CD38 dim population represented 1.7% of the total nucleated cells and expression was more akin to normal B-lymphocytes (MFI 4,913 vs. 4,527). This expression was much lower than CD138+/CD38+ gated plasma cells (MFI 56,231). Additional immunophenotypic analysis between the two plasma cell populations showed them to be very different (Figure 3.12). The CD38 dim population was CD19-/CD45weak/CD56-; the opposite to the CD38 bright population (Figure 3.12B). In addition, the CD38 dim population appeared less activated, with lower Ki-67, CXCR4 and CD49d expression than the CD38 bright population (Figures 3.12C and 3.12D). The CD38 bright population appeared to also demonstrate bimodal expression for IL-6, with the lower expressing subset representing 36.6% of the population; IL-6 expression that was more like that seen in the CD38 dim population.

3.5.5 CD45 sub-population analysis of the plasma dyscrasia primary bone marrow samples, reveals the possibility of multiple sub-clones co-existing

Additional examination for sub-clones within the primary samples, showed 17 of the 36 (47%) samples had evidence of differing CD45 expressing sub-sets, with only 3 of them having the phenotype of normal PC (CD45+/CD56-/CD19+). Figure 3.13 shows examples of 4 separate CD45 expressing sub-sets, that did not conform to a normal PC phenotype. Such sub-sets are likely to be clonal and I have shown that there are differences in expression of functional cell markers (IL-6, CXCR4, MMP9 and CD49d), between the larger and smaller CD45 populations.

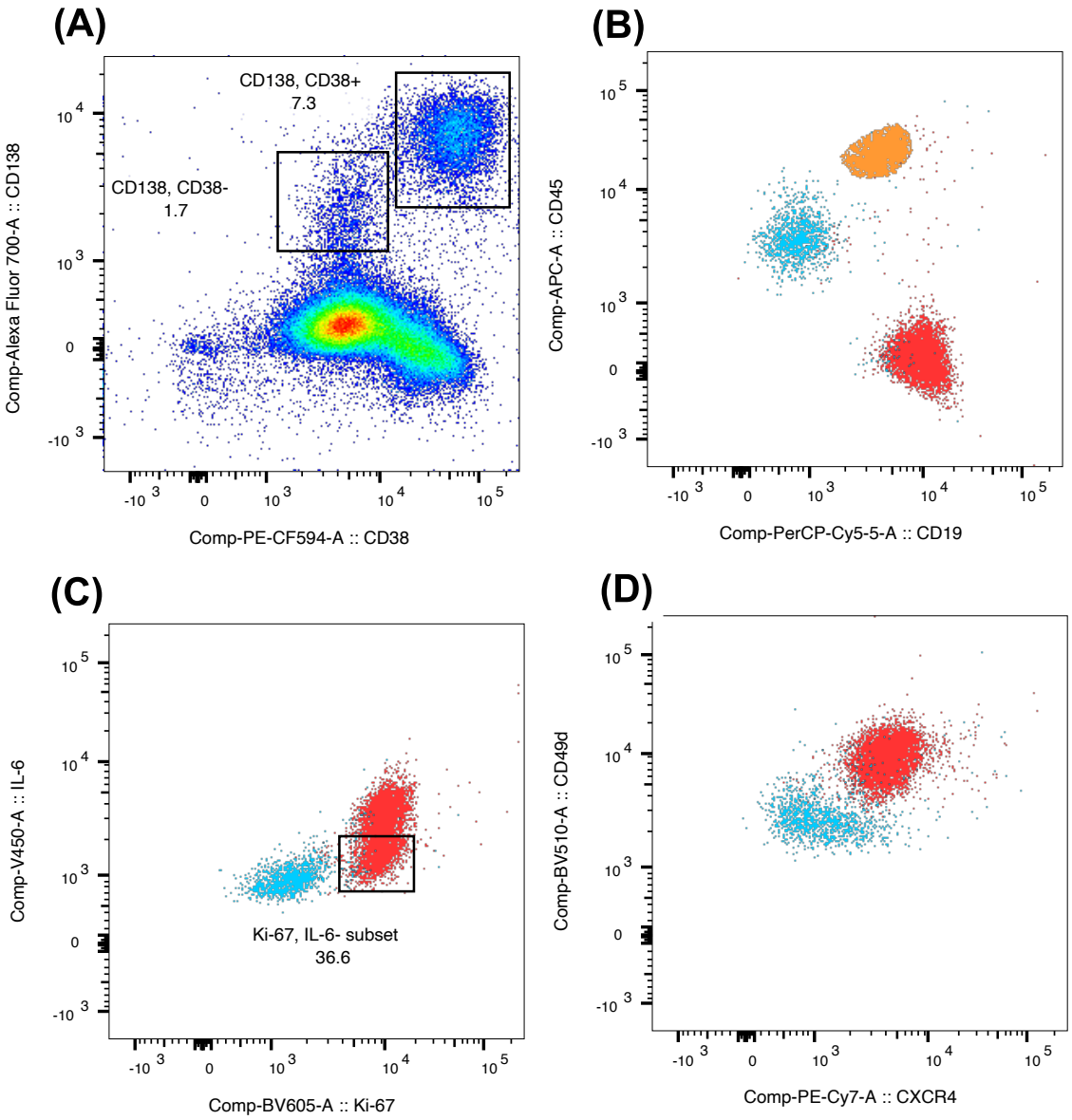

	Subset Name with Gating Path	Count	Median : Comp-PE-CF594-A
	A411410V 4,2f,11,2f,16_Stained_100_005.fcs/CD45, SSC-A subset/B-lymphocytes	3298.0	4527.8
	A411410V 4,2f,11,2f,16_Stained_100_005.fcs/Alive cells/Single Cells/CD138, CD38-	1359.0	4913.3
	A411410V 4,2f,11,2f,16_Stained_100_005.fcs/Alive cells/Single Cells/CD138, CD38+	5703.0	56231.2

Figure 3.12. Immunophenotypic evaluation of a CD38 weakly expressing sub-population. *Analysis was from a newly diagnosed MM bone marrow sample and the mononuclear cells were isolated by density gradient centrifugation. 1 x 10^6 cells were stained with fluorescence-labelled antibodies and data was acquired on a BD Fortessa flow cytometer. (A) Pseudocolour dot plot of stained bone marrow mononuclear cells, showing MFI CD138 and CD38 expression. Two distinct CD38 populations that were positive for CD138 were identified; the larger (7.3% of total cells) was CD38 bright. Neither clone fitted into either a typical MM or normal PC phenotype as shown in (B). Overlaid dot plots were used for comparison of the MFI expression of the CD38 dim (blue), CD38 bright (red) populations and B-lymphocytes (orange), which showed that they are immunophenotypically distinct for CD45 and CD19 expression, (C) IL-6 and Ki-67 expression and (D) CD49d and CXCR4 expression.*

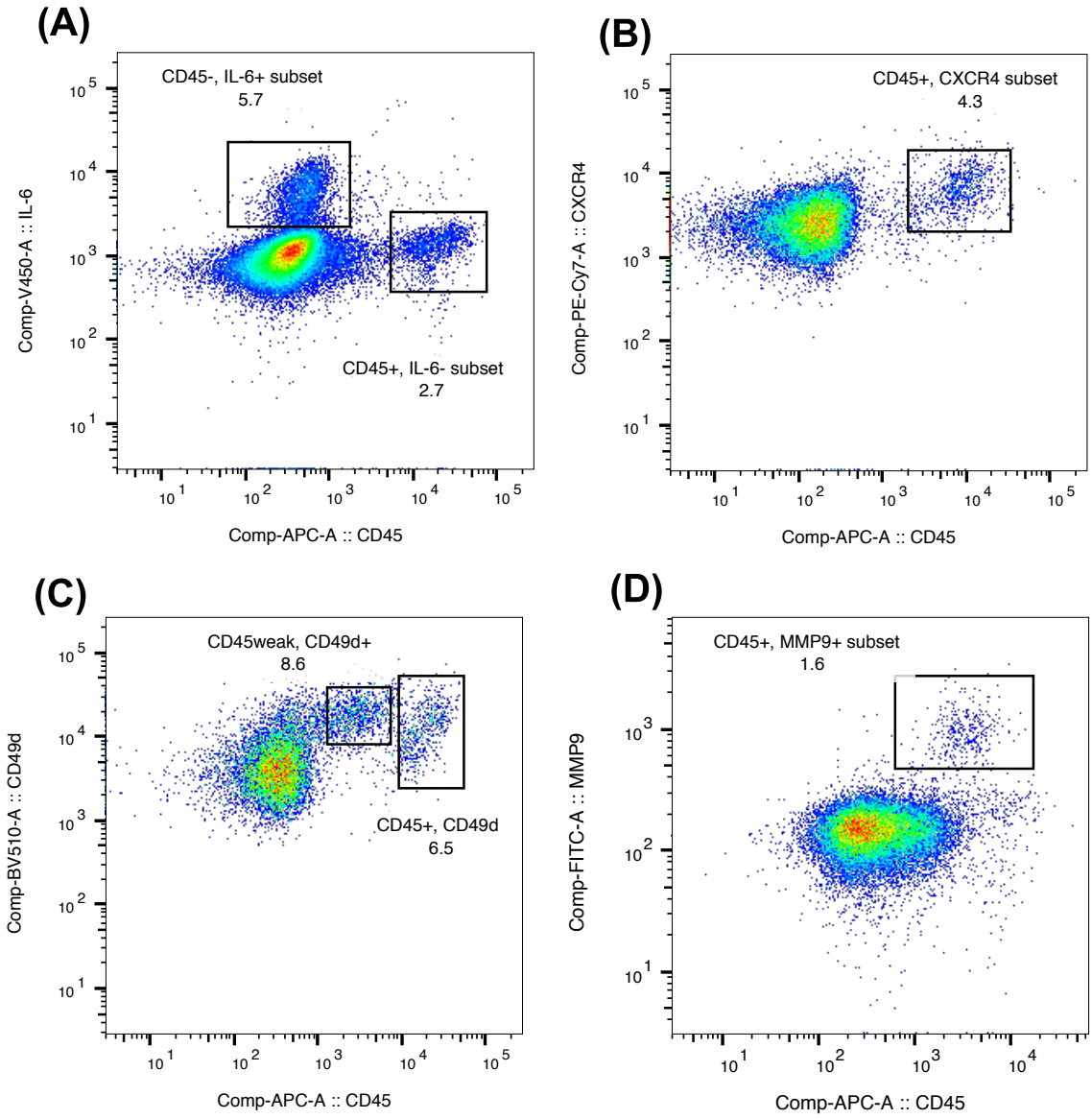

Figure 3.13. Examples of CD45 expressing sub-populations in the same plasma cell dyscrasia bone marrow sample. *The mononuclear cells were isolated by density gradient centrifugation. 1 x 10^6 cells were stained with fluorescence-labelled antibodies and data was acquired on a BD Fortessa flow cytometer. Each example is CD138, CD38 gated plasma cells from MM patients bone marrow. All are from separate patients. (A) 3 distinct IL-6 CD45 populations, largest population is CD45-/IL-6-, there are 2 separate smaller populations, IL-6+/CD45- and a CD45+/IL-6-. (B) CD45+ population has a higher CXCR4 expression that the more dominant CD45- population. (C) 3 distinct CD45 populations all with varying CD49d expression. (D) CD45 weak expressing sub-set, with much higher MMP-9 expression than dominant CD45- population.*

3.6 Discussion

Although immunophenotypic comparison of MM cell lines already exists, for example a comparison of MM.1S and MM.1R revealed CD25 and HLA-DR were both more highly expressed on MM.1S cells (Greenstein et al. 2003). To my knowledge, no systematic intra-cell line immunophenotyping has been done. The complexity of a 10-colour flow cytometry panel allows for detection of distinct myeloma sub-populations co-existing together as well as immunophenotypic characterisation of these populations, that can relate to functional elements such as migration, adhesion and survival/activation within their microenvironment. Greater number of fluorochromes allows for better characterisation, but can also lead to increased fluorochrome spectral overlap, that requires more complex fluorescence compensation. Insufficient or incorrect compensation will result in inaccurate MFI expression levels recorded and misleading results.

Measures were taken to reduce the variation in sample analysis and assure proper compensation. This involved using compensation controls consisting of unstained cells as well as singly-stained tubes with fluorescent probes and compensation beads. Due to limited size of the primary samples, FMO (fluorescence minus one) staining was not routinely employed. Ensuring that autofluorescence artefact was accounted for in each primary sample was very difficult as no two samples had the same proportion of mononuclear cells. However, the same compensation settings were used for each primary sample analysis. Compensation was based on CD138 and CD38 positive cell, so only cells with identical autofluorescence characteristics to plasma cells were able to be viewed correctly. In the event of reduced expression of these markers, compensation settings required post-acquisition adjustment using Flow-Jo software, but this was minimised as much as possible. B-Lymphocyte gating based on SSC-A-/CD45+/CD56-/CD19+ made for a good immunophenotypic reference to malignant PC comparison.

The choice of fluorochrome for the antibody is a key factor in designing a successful panel. Pairing cell marker expression with the correct fluorochrome brightness will ensure subtle differences in expression between populations are easily identified. For example, MMP-9 and IL-6 expression used low brightness fluorochromes, as a result MFI variation was subtler for these markers and why percentage positivity differences, showed greater variation in expression that was not apparent for the MFI data. In addition choosing a high brightness fluorochrome for highly expressing antigens can result in difficulties in

maintaining a standard PMT voltage. PMT voltages were attempted to be standardised for both cell lines and primary samples, with the aim of both negative and positive antigen expressing population within the axis in every channel. However, this was not possible, because of the variation in cell size (cell lines tending to be larger) and expression variation in the higher brightness fluorochromes (most notably CF594 fluorochrome on the anti-CD38 antibody). This meant that generally, primary samples PMT voltages appeared too low and cell lines PMT voltage, most notably RPMI-8226, appeared too high. Therefore, different PMT voltages where used for cell lines and primary samples, but were standardised within their group.

Although CD38 expression was predominantly positive for cell line and primary data, a wide variation in expression was observed for both, each showing evidence of CD38 negative/weak populations (including the cell lines U266 and MM.1S). The presence of CD38 weakly or negatively expressing clones are estimated at less than 2% but are becoming more prevalent in the advent of anti-CD38 therapy (Minarik et al. 2017). Thus, the study and understanding of CD38 negative clones are becoming more relevant in the attempt of developing novel myeloma treatment. Additional understanding of CD38 function in MM can also be obtained from expression correlation. Although no correlation was observed from the cell line data, statistical positive correlation between CD38 expression and other cell markers was observed in the primary bone marrow samples. The strongest correlation was with Ki-67 expression ($r=0.89$, $p=0.0001$) and although such relationship has been well described in other B-cell malignancies such as CLL (Pittner et al. 2005), it has not been for MM. The positive correlation of Ki-67 and CD38 expression in MM emphasises CD38 function as a marker of activation/proliferation, highlighted in Figure 3.12C, showing the comparison of CD38 expressing sub-populations with Ki-67 expression greatly reduced in the weakly expressing CD38 sub-population. CD38 correlation was also seen for CXCR4, and to a lesser extent CD19 and CD56. I am unaware of published data that shows these correlations, in CLL it has been shown that CD38 increases CXCL12/CXCR4 axis mediated migration (Vaisitti et al. 2010) and it is possible that similar mechanisms occur here. A larger cohort of primary samples and sub-group analysis would strengthen these correlations.

In contrast to CD38 expression, CD138 expression within each primary sample sub-group (MGUS, MM and RRMM) was fairly uniform, but with statistical decrease in expression in the relapsed/refractory group compared to newly diagnosed MM ($p=0.031$). This has been previously described in the literature (Kawano et al. 2012) and attributed to increase in

CD138 negative clones, which can be up to 30% in the relapsed/refractory setting (Bataille et al. 2006; Reid et al. 2010; Kawano et al. 2012), although I did not identify any obvious negatively expressing populations in my data set.

CD138 negative clones both at diagnosis and relapse have also been shown to contain a greater proliferative ability and subsequently greater clonogenic expansion (Reid et al. 2010) and may partly explain why CD138 expression is reduced at relapse. It was therefore surprising that Ki-67 expression was statistically lower (p=0.027) in the RRMM group and is contradictory to what has been previously described in the literature (Drach et al. 1992). Reasons for this could be that although CD138 expression was lower, no true CD138 negative expression sub-populations were observed. However, this may not fully explain why Ki-67 expression for RRMM was reduced and the difference may be inaccurate due small numbers of RRMM samples (n=5), the difference in age of samples and methodological variation in intracellular staining. In view of CD38 expression also being lower in the RRMM group (although not statistical, p=0.097), would suggest the RRMM samples for whatever reason did indeed have a lower proliferative propensity and where not as activated as would be expected. By increasing the cohort of RRMM samples, potentially would change the findings. One statistical finding which is more in keeping with RRMM pathophysiology is the increased MMP-9 expression compared to MGUS or newly diagnosed. Increased MMP-9 expression is associated with remodelling of the bone marrow microenvironment and of a more aggressive disease state (Barillé et al. 1997).

Primary bone marrow samples expression of CD19/CD45/CD56 remains a crude and simple 3-colour panel for differentiating between normal PC, disease PC and possible sub-clones. The immunophenotypic data was largely consistent with that expected for its stage of disease (i.e. MGUS, MM or leukaemic phase), but many samples co-existed with small distinct immunophenotypic sub-populations. CD45 expression usually decreases with disease progression, but expression can be variable and may represent differing sub-clone formation at different stages of disease. In one study, 44% of MM patients were shown to contain a CD45 positive sub-clone that was at least 20% of the total malignant plasma cell population (Kumar et al. 2005). My data is strongly supportive of this study, with 47% of samples containing a CD45 sub-population. In addition, I showed the CD45 sub-populations to be phenotypically distinct, highlighting the potential of immunophenotyping in identifying sub-clones that may have functional differentiation (e.g. migration and adhesion).

My data saw a statistical decrease in CD19 expression from MGUS group to both newly diagnosed MM (p=0.007) and RRMM (p=0.0064). This is an expected occurrence where CD19 expression decreases through B-cell maturation and a change in phenotype from normal to malignant plasma cell (Zandecki et al. 1995). CD56 expression was reduced in the RRMM group compared to newly diagnosed (p=0.040) and in keeping with the immunophenotype of plasma cell leukaemia or the leukaemic phase of MM (CD56 negative), a disease state that the majority of cell lines including MM.1S and MM.1R arise from and are predominantly CD56 weak/negative (Pellat-Deceunynck et al. 1998).

The statistical difference in lower CXCR4 expression in relapsed disease compared to newly diagnosed, is in keeping with the published literature, where CXCR4 expression is downregulated through disease progression (Moller et al. 2003). In addition, a larger variation in CXCR4 expression was observed within the newly diagnosed primary samples compared to other stages of the disease and the cell lines data. Although no distinct CXCR4 expressing sub-populations were identified within my primary sample data, the wide expression variation observed potentially represents cells/clones at different stages of disease progression. Cells with lower CXCR4 expression possibly signifying cells/clones becoming more autonomous of the bone marrow microenvironment and developing migration mechanisms independent of CXCR4-CXCL12 axis. Serial measurements of CXCR4 expression for the same patient at different stages of disease/treatment would provide additional information into the role of CXCR4 in relapsing disease and whether CXCR4 expression can be regulated or is clone dependent, especially in view that CXCR4 expression has been shown to be a prognostic factor in relapsed disease, especially those treated with bortezomib (Alsayed et al. 2007; Stessman et al. 2013).

Although myself and others have shown MM cell lines such as MM.1S, MM.1R and OPM-2 migrate across a CXCL12 gradient in Transwell assay conditions (Fedyk et al. 1999), I have shown MM cell lines expression levels of CXCR4 do not positively correlate with chemotactic responsiveness to SDF-1, indeed contrary to other studies I showed a negative correlation between transwell migration and CXCR4 baseline expression. The cell lines U266 and RPMI-8226 I showed to have poor migratory CXCL12 potential, (figure 3.9A), which for U266 is in keeping with the results of others (Moller et al. 2003), yet RPMI-8226 has shown by some to migratory respond to SDF-1 stimulation (Tai et al. 2003). Reasons for these findings could be due to differing experimental conditions. Notably, my experiments used smaller Transwell transmembrane pores (3μm compared to 8μm) and I did not use fibronectin or endothelial layers on the transmembrane unlike the

aforementioned referenced research groups. Ideally, I would conduct the same experiments with additional MM cell lines and primary samples for confirmation as well as measure CXCR4 expression post migration, to confirm if SDF-1 blockage of the antigen occurred or even if CXCR4 is upregulated. Possible explanations for this finding could be that reduced CXCR4 expression is a marker of disease progression to leukaemic phase with migratory mechanism becoming independent of the CXCR4-CXCL12 migratory axis, as seen in extramedullary disease (Stessman et al. 2013).

The cell line migratory work implied that SDF-1 induced migration is independent of CD49d expression ($r=0.26$, $p=0.62$), indicating migration occurs through different mechanisms within these cell lines. However, the relative limited number of cell lines used and the selection bias means that migration correlation with CD49d expression still may exist for other MM cell lines and/or primary samples. Provided with greater time and resources, other cell lines transwell migratory experiments could occur, that would provide greater confidence in saying whether certain markers had definite correlation with migration or not, such as CD38 expression ($r= 0.48$, $p=0.23$), which has been shown to regulate migration for other B-cell malignancies (Vaisitti et al. 2010).

In summary, I have shown the complexity of sub-clonal populations that exist in both myeloma cell lines and primary myeloma samples. Although the concept of MM clones is not novel, I have shown that both primary samples and MM cell lines exhibit wide variation in CD38 expression and multiple sub-populations and that they have variable expression of functional markers within my flow panel (CXCR4, MMP-9, CD49d, IL-6). Thus, identification of sub-clones by immunophenotyping has the advantage over other clonal identification methods, in that very small sub-clones can be accurately identified and functional differences, that can result in possible selection advantages, driving clonal evolution can be explored. This work confirms the heterogeneity of the disease and that multiple treatment strategies are required to treat and even cure the disease.

CHAPTER 4:

A Novel Model of Investigating Multiple Myeloma Cell Migration

4.1 Introduction

Migration of myeloma cells is a key step in the development of the disease as clonal plasma cell require homing to the bone marrow niche, essential for providing myeloma cells with signals for cell survival and proliferation (Hideshima et al. 2001). The presence of both lytic disease in bones and circulating myeloma cells in more than 70% of patients (Billadeau et al. 1996), is indicative of active trafficking of myeloma cells between the bone marrow and peripheral blood. Binding of SDF-1 (CXCL12) to the chemokine receptor, CXCR4, has been shown to promote homing of circulating myeloma cells back to the bone marrow and use of CXCR4 antagonists reduces CXCL12-induced cell migration (Alsayed et al. 2007). The rationale of inhibiting migration and disrupting the myeloma cell and bone marrow microenvironment has led to clinical studies involving CXCR4 inhibitors. For example, the inhibitor AMD40 was shown to increase the number of peripheral circulating myeloma cells, indicating its ability to disrupt bone marrow homing and/or retention. In addition, AMD40 was synergistic with the proteasome inhibitor bortezomib (Azab et al. 2009b). The clinical relevance of CXCR4 expression was further demonstrated by the fact that lower expression was seen in extramedullary disease and was associated with poorer survival outcomes, especially in those treated with bortezomib (Stessman et al. 2013). This is consistent with the tumour becoming independent of the bone marrow niche. However, it implies that treatment strategies employing CXCR4 antagonists may not be appropriate or effective for extramedullary disease.

Cellular integrins, particularly CD49d, are key regulators of cell-to-cell adhesion. They modulate the interaction between bone marrow stromal cells and myeloma cells and play a role in a mechanism of drug resistance termed CAM-DR (cell adhesion-mediated drug resistance) (Springer 1994; Damiano et al. 1999). Disruption of CD49d in myeloma can prevent transendothelial migration as well as inhibit recruitment of other immune cells

into the tissues (Podar et al. 2011). Given the importance of myeloma cell migration both in disease development and drug resistance, several research groups have developed migration models with each having their advantages and disadvantages (Urashima et al. 1997; Podar et al. 2001; Hideshima et al. 2002a; Mitsiades et al. 2003). In this study MM cell migration was assessed using conventional transwell assays and a novel, circulating model system containing endothelium-lined 'pseudo-vessels' through which the myeloma cells were circulated under physiological shear forces. This novel model, uses a modified Fibercell bioreactor, allowing cells to circulate under shear force and for migration to occur within the 'C2025' cartridge, packed with hollow fibres with an internal radius of 350μm. The hollow fibres contain pores of 0.1μm along their length to allow the exchange of medium (and potentially cells) with surrounding enclosed space termed the extravascular space (EVS). To migrate, cells have to adhere to a pre-layered endothelial lining, travel through the pseudovessels and move through a 0.1μm pore into the EVS. The comparative pore size of transwells range from 0.4μm-8μm. The EVS can be set up to contain cells, chemokines, cytokines or whatever is desired to attract circulating cells. This chapter sets out to investigate the role CXCR4 and CD49d blockade on myeloma migration in a novel in-vitro migratory model.

4.2 Developing the modified hollow fibre bioreactor as a model for MM migration

Walsby et al. successfully established a circulatory transendothelial migration model, to investigate the effects of shear force and transient endothelial cell interactions on CLL cell migration. In this model C2025 cartridges were endothelialised, with the aim of forming 'pseudo-vessels', providing the matrix for migration (Walsby et al. 2014c). This was done by coating the lumen of each hollow fibre with gelatin to allow attachment of approximately $15x10^6$ endothelial cells (HUVEC). To ensure that the majority of endothelial cells had adhered to the lumen of the hollow fibres, non-adhered HUVEC were removed from the system by gentle PBS washing (see section 2.4.3 and figure 2.1 for greater detail) and counted using a Vi-cell XR instrument (Beckman Coulter). If more than 10% of the total input endothelial cells were recovered, the endothelisation process was repeated. The system was then incubated for 48h in cell culture media under a shear force that encourage the HUVECs in the hollow fibres to spread and form 'pseudovessels'. At which point, migratory experiments could occur between the circulating system and the EVS. Shear force was set to a higher value (minimum 5 dynes/cm^3) than described by Walsby et al. due to the unexpected issue of cells pooling in the reservoir of the system. This was likely as a result of MM cells being larger than CLL cells, however the shear forces

were still within the expected physiological conditions found in trabecular bone and capillaries (Metzger et al. 2015). Note, no HUVECs were inserted into the EVS and none were found to migrate, thus ensuring any cells obtained from the EVS, would be either migrated cancer cells (e.g. CLL or MM) or any pre-inserted cells/fibroblasts (e.g. CXCL12 secreted MRC-5 cells).

For this study and the investigation of MM migration, the bioreactor model aimed to represent the migration of MM cells from the peripheral blood to the bone marrow. For this, the endothelial lining (HUVEC) aimed to represent the barrier between peripheral circulation and the bone marrow microenvironment. And in an attempt to replicate the bone marrow microenvironment, MRC-5 cells (a fibroblast cell line known to secrete CXCL12 (Kang et al. 2005)) were introduced into the EVS. Walsby et al. previously showed (figure 4.1) that a sufficient concentration gradient of CXCL12 was created by $5x10^6$ MRC-5 cells (Walsby et al. 2014b).

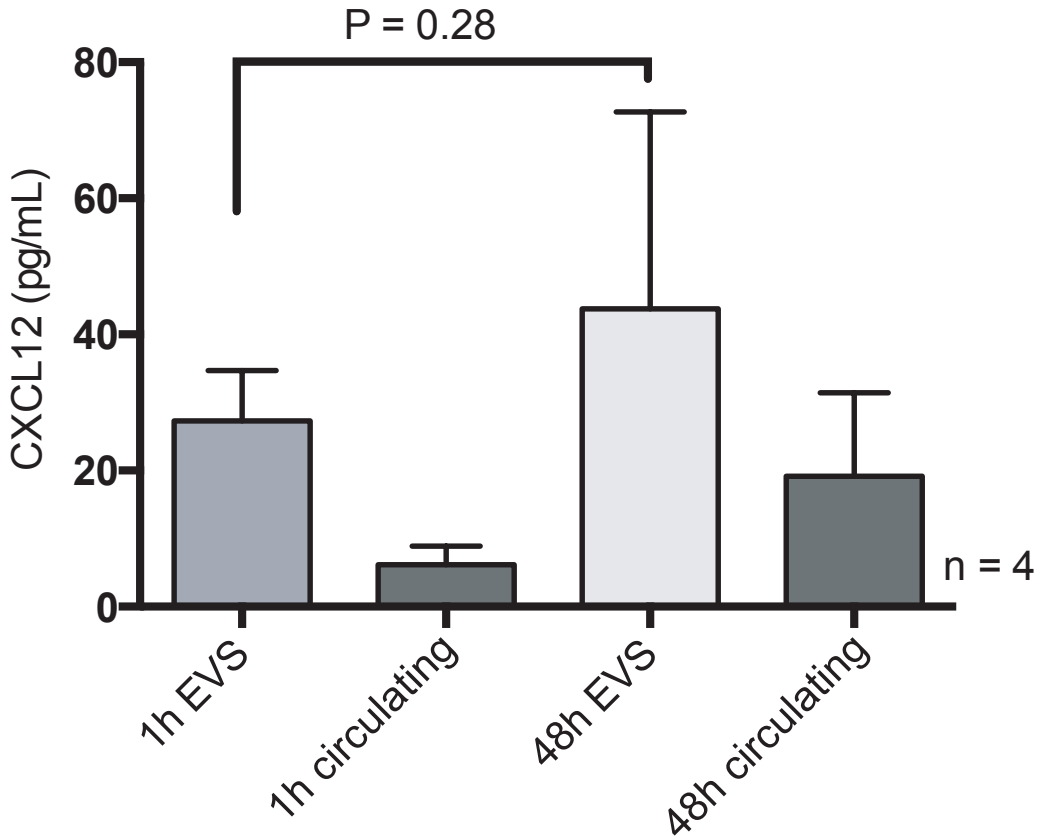

Figure 4.1. CXCL12 expression in dynamic migratory model. *CXCL12 concentration as measured by ELISA, at 1h and 48h, comparing EVS to circulation, after $5x10^6$ MRC-5* cells were seeded into EVS*. No statistical difference existed between CXCL12 levels at 1h and 48h, inferring continual steady state secretion of CXCL12. Mean CXCL12 concentration was higher in the EVS than circulation at both time points, inferring continual concentration gradient persisted. Figure courtesy of Dr Elisabeth Walsby, manuscript awaiting publication. Error bars show standard deviation and are calculated by repeated independent experiments.*

4.2.1 The addition of CXCL12-secreting cells to the EVS significantly enhances myeloma cell migration

In the knowledge that a CXCL12 concentration gradient could be replicated between the EVS and circulation, I set out to prove that the CXCL12-secreting fibroblasts were necessary for MM migration. The hollow fibre bioreactor was prepared as for CLL migration experiments outlined by Walsby et al. (2014) and described in greater detail in chapter 2. Briefly, the cartridge was lined with gelatin before $15x10^6$ HUVEC were seeded into the circulating compartment of the system, with an optional $5x10^6$ MRC-5 seeded into EVS. Gradual increase in shear force was applied to the model over 48h, before $40x10^6$ MM cells were added to the circulating compartment, making a concentration of around $0.8x10^6$/ml. After 48h of circulation, media within the EVS was harvested and migrated cell were counted using an Accuri flow cytometer as outlined by Walsby et al. (2014). Preliminary migrated data (results including within section 3.2) suggested the MM cell line OPM-2 (CXCR4 expression 99.9% positivity, section 3.4) had one of the greatest CXCL12 migration potential, making it an ideal cell line to measure the effects of MRC-5 induced migration. I previously showed (section 3.4.4) that the cell line was responsive to CXCL12-induced transwell migration. Figure 4.2 shows the difference in migration between experiments with and without the addition of MRC-5. Mean migration for MRC-5 containing group was 2.82% (n=10), compared to without MRC-5 0.03% (n=5), p value was 0.0007, inferring that the difference was statistically significant.

4.2.2 Addition of IL-6 to independent cell lines does not affect migration

In an attempt to identify whether migration in this model could be optimised, IL-6, a key component of myeloma cell regulation and migration, was added at a concentration of 1ng/ml. At this concentration, the effects of IL-6 are thought to be maximised and are roughly the recorded levels seen in the most aggressive forms and leukaemic phases of the disease (Bataille et al. 1989; Podar et al. 2001; French et al. 2002).

The cell lines MM.1S and MM.1R were chosen as the had comparatively the lowest expression of IL-6 of all the cell lines used in this thesis (see chapter 3). No significant difference in migration was observed between the cell lines with the addition of IL-6 ($p>0.99$ for both cell lines). Mean migration for MM.1R was 0.65% and 0.58% for IL-6 addition. This compared to MM.1S mean migration of 0.30% and 0.39% with addition of IL-6. Although mean migration was over 2-fold higher in MM.1R, this was not statistically significant ($p=0.25$).

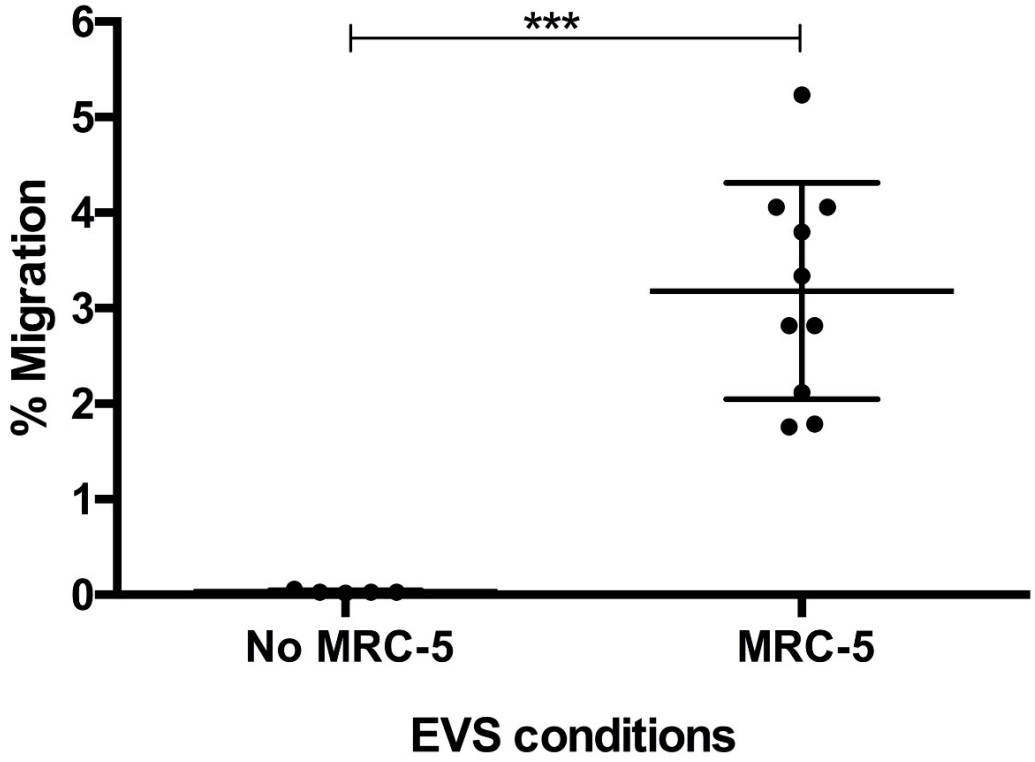

Figure 4.2. The effect of MRC-5 cells on MM cell migration. *Myeloma cell line OPM-2 percentage migration at 48h with addition of MRC-5 in EVS (n=10) and without MRC-5 (n=5). Migration was measured by flow cytometry cell counting, within a strict alive cell gate, of 100μl of EVS and circulation media. The cell count was then multiplied to give estimated count of total retrieved from the EVS as a percentage of the total number of cells seeded into the circulating compartment. Error bars indicate mean ± SD. Mann-Whitney U-test compared the 2 groups, showing a statistical difference in migration, p=0.0007. ***<0.005*

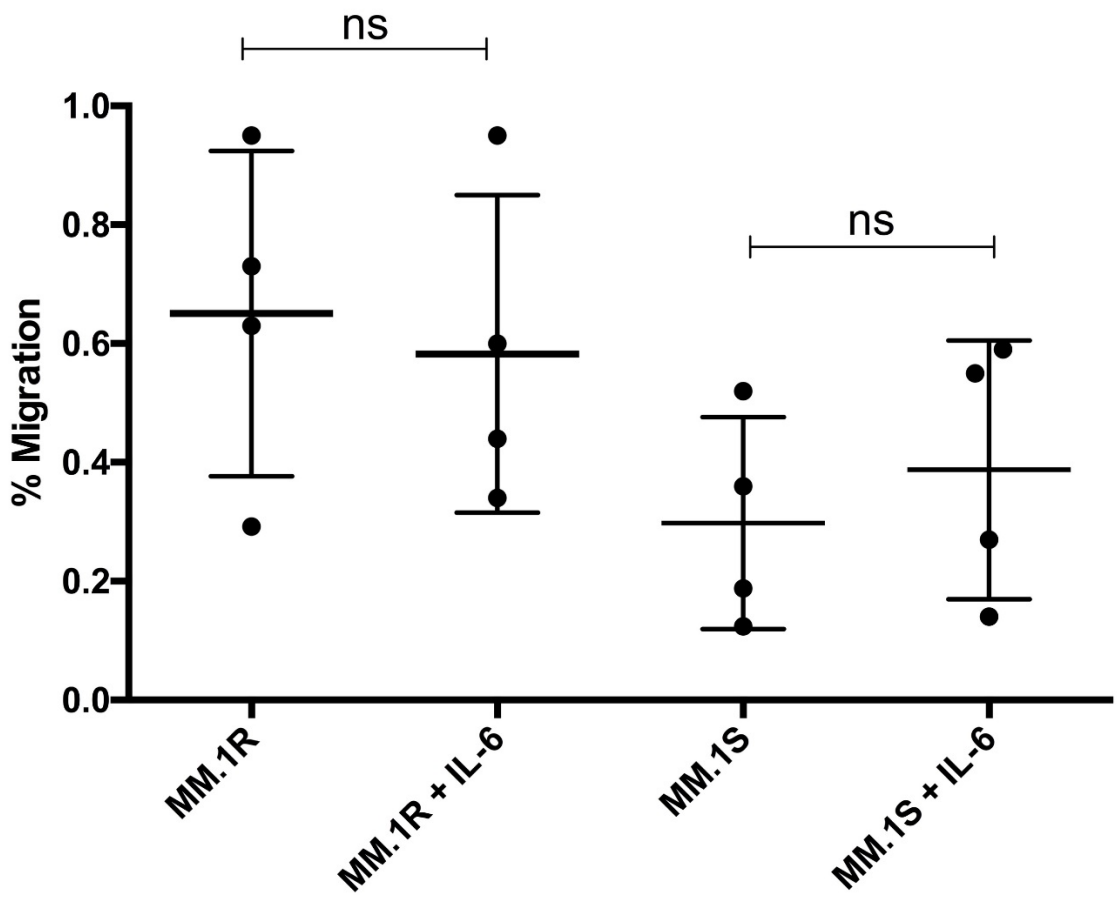

Figure 4.3. The effect of IL-6 of MM cell line migration. *Paired 48h migration experiments of MM.1R and MM.1S (n=4), comparing the effect 1ng/ml of IL-6 has on migration. Migration was measured by flow cytometry cell counting, within a strict alive cell gate, of 100μl of EVS and circulation media. Cell count was then multiplied to give estimated count of total retrieved EVS and circulation volumes. Error bars indicate mean with SD and are calculated by repeated independent experiments. Mann-Whitney T-test compared the 2 groups*

4.2.3 Ensuring correct identification of migrated Myeloma cells

The addition of approximately $5x10^6$ CXCL12-secreting MRC-5 cells into the EVS raises the difficulty of identifying migrated myeloma cells from "resident" MRC-5 cells. Although MRC-5 cells are naturally adherent to plastic, a certain degree of non-adherent MRC-5 could be expected especially when the cells become confluent. Thus, the retrieval of cells from the EVS at 48 hours to determine myeloma cell migration could potentially include the fibroblasts. The collection process involved gentle flushing with PBS (as opposed to trypsin) through the 2 EVS ports with the aim to collect all migrated cells in suspension, plus cells loosely attached to MRC-5 fibroblasts. The process of flushing, instead of the use of the proteolytic trypsin for cell removal, aimed to reduce disruption of MRC-5 adhesion, thereby limiting 'contamination' as much as possible. Concern also existed that myeloma cells could adhere loosely to MRC-5 due to their chemokine attraction (see appendix, co-culture experiments showing myeloma cells adhere to MRC-5), thus simply aspiration of the EVS suspension may not be sufficient for retrieving all migrated MM cells.

The Vi-cell XR cell counter provided a quick and easy method of calculating migration through a cell count (trypan blue staining) and subsequent concentration of cells from the media retrieved from the circulation and EVS. A significant disadvantage of this method was that the instrument could not reliably differentiate between different cell types found in the sample. Thus, cells retrieved from the EVS could not be guaranteed to be migrated MM if MRC-5 cells were added into the EVS. Walsby et al. (2014) addressed the potential 'contamination' of fibroblasts in their CLL migratory experiments, by applying a tight 'lymphocyte' gating strategy during flow cytometric analysis. CLL cells are smaller than MRC-5 cells (typically 8-10μm compared to 15-17μm respectively) and can therefore be easily discriminated between each other through forward scatter (FSC-A) and side scatter (SSC-A) flow cytometry plots.

Immunophenotyping cells offer another method of positively or negatively identifying cell. However, concerns are raised to the integrity of cell markers following active migration of myeloma cells through a 0.1μm pore, whereby possible physical stress to the cell membrane could occur. CD138 (syndecan-1) is a well-documented antigen that is highly expressed on normal and malignant plasma cells. This makes it a useful antigen for myeloma identification (Paiva et al. 2010). However, it is regarded as a very fragile antigen, easily shed either due to cell ageing or physical stress (Jourdan et al. 1998; Yang et al. 2007; Sanderson and Yang 2008). The extracellular bone marrow environment of patients with

myeloma tend to stain very heavily for CD138, which is thought to be caused by the shedding of the antigen from malignant plasma cells (Bayer-Garner et al. 2001). Alternatively, CD90 is a cell surface protein expressed on T-cells, mesenchymal cells and fibroblasts, with no documented expression on MM cell (Kisselbach et al. 2009).

The following section and experiments aimed to identify if this method was robust enough for MM cell identification from MRC-5 cells in media collected from the EVS or if further methods were required. For standardisation purposes, the cell line MM.1R was used as a model for quantifying the migration of myeloma cells.

4.2.3.1 Cell size is a good discriminator of cells used in model, with EVS cells smaller than MRC-5 cells and also their circulatory counterparts

Although MM cells are larger than CLL, I showed that they are still statistically smaller than MRC-5 cells (figure 4.4B). The mean cell size of MM.1R and MRC-5 cells in static co-culture were measured using a Vi-cell XR instrument (12.16μm and 15.22μm respectively, $p<0.0001$). Although mean cell size of MM.1R was slightly higher within the circulation model than static culture (12.70μm vs 12.16μm), the difference was not statistically significant ($p=0.13$). However, when compared to the cell size of cells retrieved from the EVS, a statistical difference was observed (EVS 10.47μm v Circulation 12.70μm $p<0.0001$). An additional observation was a positive correlation between Vi-cell XR recorded viability (measured by trypan blue staining) and cell size (figure 4.4A). The greatest correlation was observed in MM.1R, followed by HUVEC then MRC-5 (Pearson r value 0.90, 0.84 and 0.53 respectively).

Having proven the difference in cell size between MM cells and MRC-5, figure 4.5 shows that applying a tight gating strategy for forward and side scatter on the flow cytometry analysis could remove the majority of MRC-5 cells (up to 95%). Thereby ensuring a very minimal 'contamination' of MRC-5 cells in the MM cell counts.

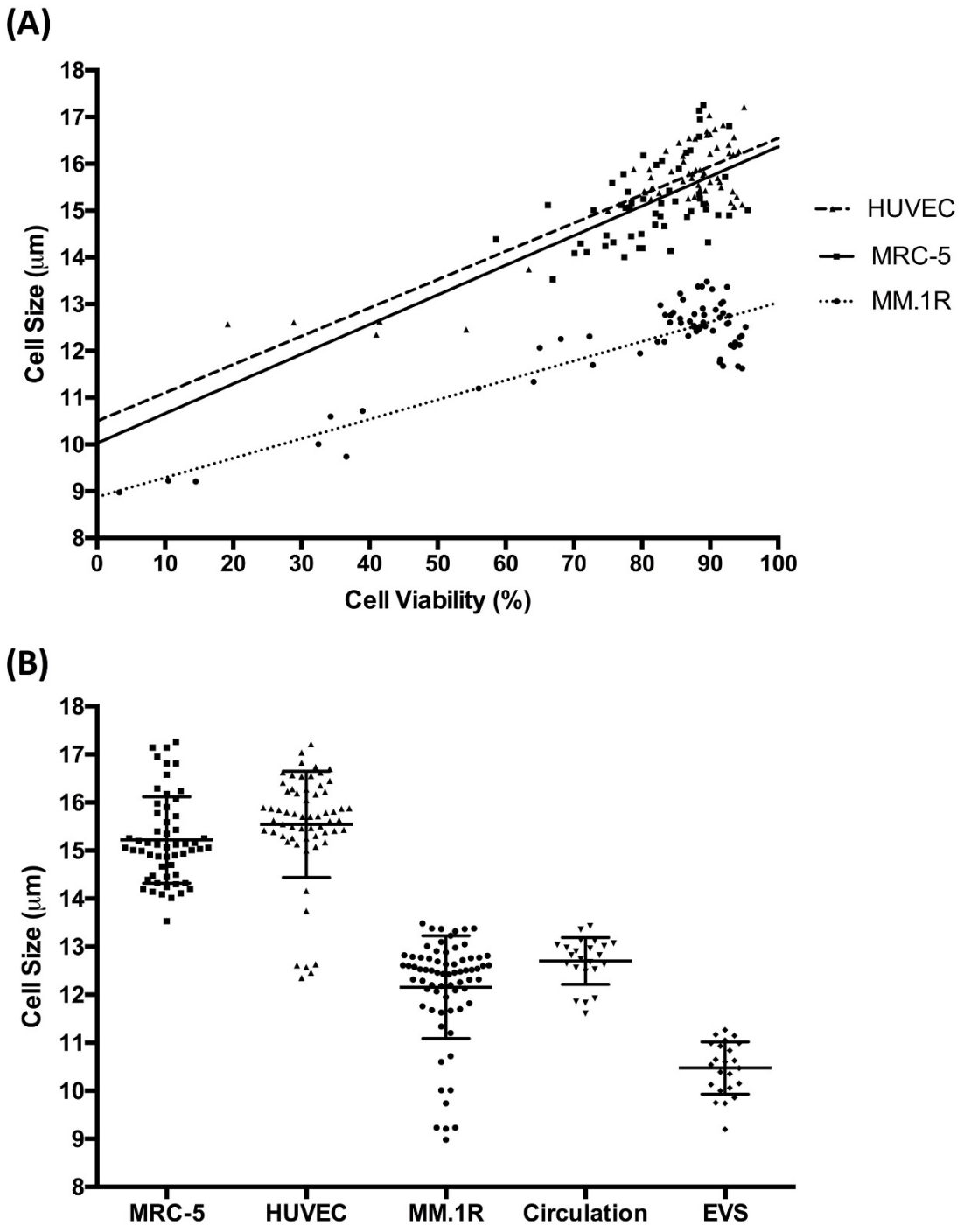

Figure 4.4. Comparison of cell size of the various cell types used in the dynamic circulatory migratory model. *(A) shows the correlation between cell viability and size. Linear regression best fit line shows the relationship between cell size and cell viability for the cell lines. (B) Scatter plots of each cell size measurements shown as the mean ± standard deviation (SD) and are calculated by repeated independent experiments. Cell size and viability were measured using a Beckman Coulter Vi-cell XR. Each point is a separate Vi-cell sample measurement; HUVEC (n=56), MRC-5 (n=61), MM.1R (n=70) and paired MM.1R samples derived from the circulation (n=23) and EVS (n=23). Viability was assessed by Trypan Blue exclusion and data points represent the mean of 50 separate analysed images.*

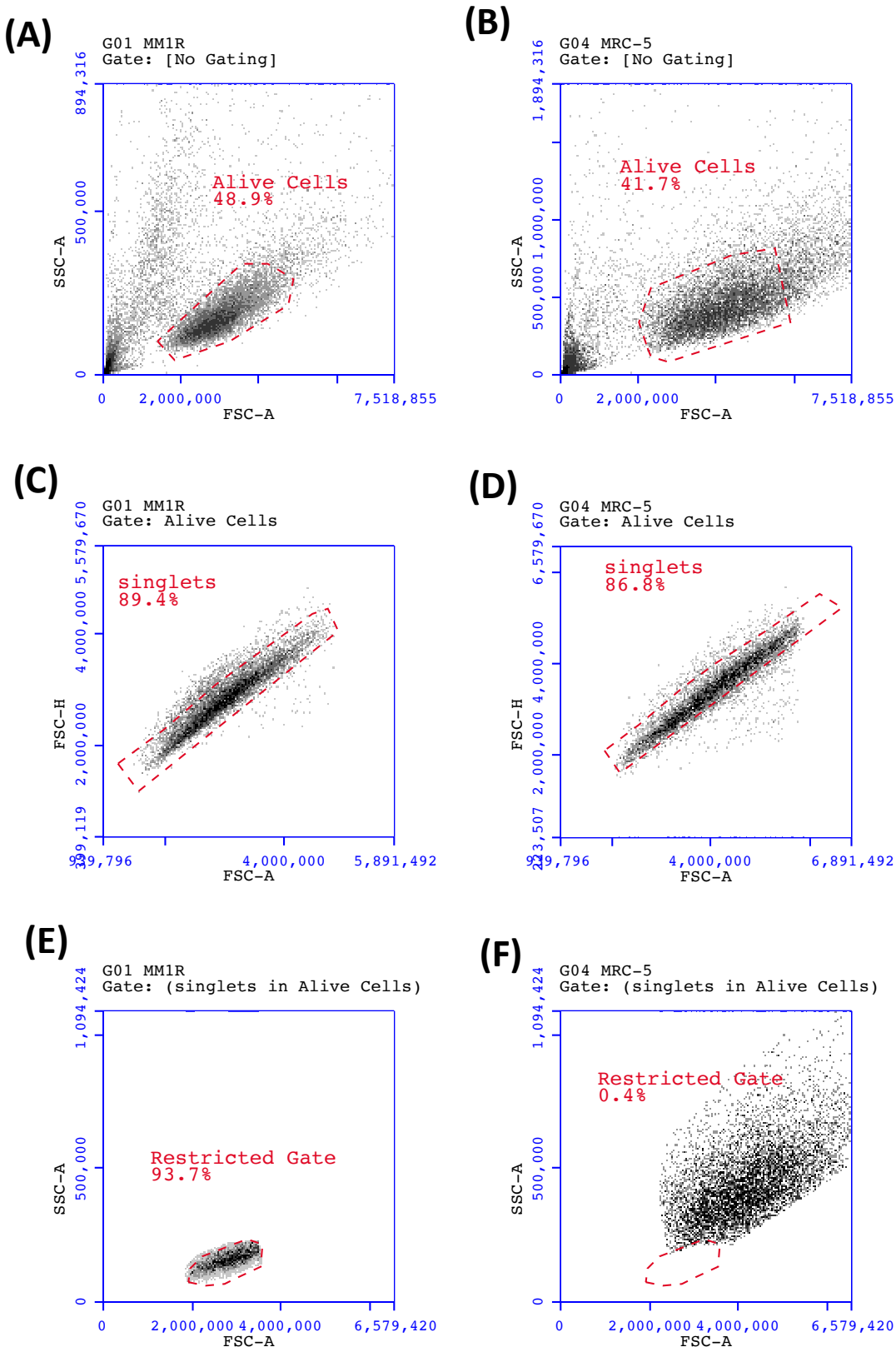

Figure 4.5. Flow cytometry restricted gating of MM.1R and MRC-5 cells results in minimal overlap of two different cell types*. Analysis on Accuri flow cytometer of static co-cultures containing MM.1R and MRC-5 cells. FSC-A and SSC-A 'Alive cell' gating strategy of MM.1R* ***(A)*** *and MRC-5 cells* ***(B)****; Singlet gating of MM.1R* ***(C)*** *and MRC-5 cells* ***(D)****;* ***(E)*** *singlet 'Alive cells' gated FSC-A and SSC-A of MM.1R cells, of which 93.7% are included in a 'restricted gate' gating strategy;* ***(F)*** *singlet 'Alive cells' gated FSC-A and SSC-A of MRC-5 cells, of which 0.4% are included in the same 'restricted gate' gating strategy as in figure (D).*

4.2.3.2 CD138 and CD90 are cell markers differentially expressed on cells used in circulatory model, with CD138 expression reduced in migration

Figure 4.6 shows the expression differences between CD90 and CD138 in HUVEC, MRC-5 and MM.1R cells from static co-cultures. There was a 1.5 log difference in CD90 expression between MRC-5 and myeloma cells. With a similar log difference in CD138 expression between myeloma cells and HUVEC/MRC-5. The contrasting expression of these two markers for MRC-5 and myeloma cells makes them candidates for the positive identification of migrated cells retrieved from the EVS. No HUVEC cells would be expected to be recovered from the EVS as non-adherent HUVECs were removed from the system prior to the introduction of shear. The addition of shear causes the flattening and spreading of HUVECs along the length of the lumen of the hollow fibres.

Although CD138 was an excellent identification marker for myeloma cells recovered from the circulating compartment of the dynamic model, cells recovered from the EVS showed a reduced CD138 expression (figure 4.7). To determine if the retrieved cells were migrated MM with loss of CD138 expression, but had the capacity to upregulate expression, cells obtained cells from the EVS were placed in fresh media culture for a further 48h. This allowed for cell replication or re-synthesis of antigen, with repeat immunophenotypic analysis showing a clear population of CD138 positive cells (figure 4.7D). Therefore, the use of CD138 expression and immunophenotypic analysis as a positive identification of migrated MM was thus deemed unreliable. To further guarantee that cells retrieved from the EVS were migrated MM cells, other confirmatory methods were employed.

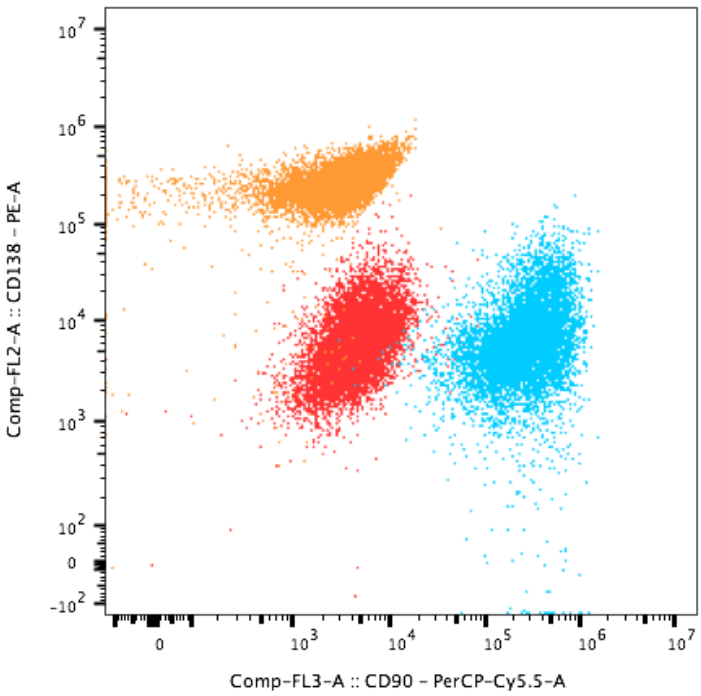

	Subset Name with Gating Path	Median : Comp-FL2-A	Median : Comp-FL3-A
	A02 MM.1R.fcs/Alive cells/Single Cells	262051.5	3533.3
	E02 MRC-5.fcs/Alive cells/Single Cells	6125.4	284993.3
	D02 HUVEC.fcs/Alive cells/Single Cells	5398.9	4515.4

Figure 4.6. Overlay dot plot comparison of Immunophenotypic expression of CD90 and CD138*. 1 x 10^6 cells from the cell lines MM.1R (orange), MRC-5 (blue) and HUVEC (red) were stained with fluorescence-labelled antibodies and data was acquired on a BD Fortessa flow cytometer. Legend states the MFI of CD138 (FL2) and CD90 (FL3) of each of the cell lines.*

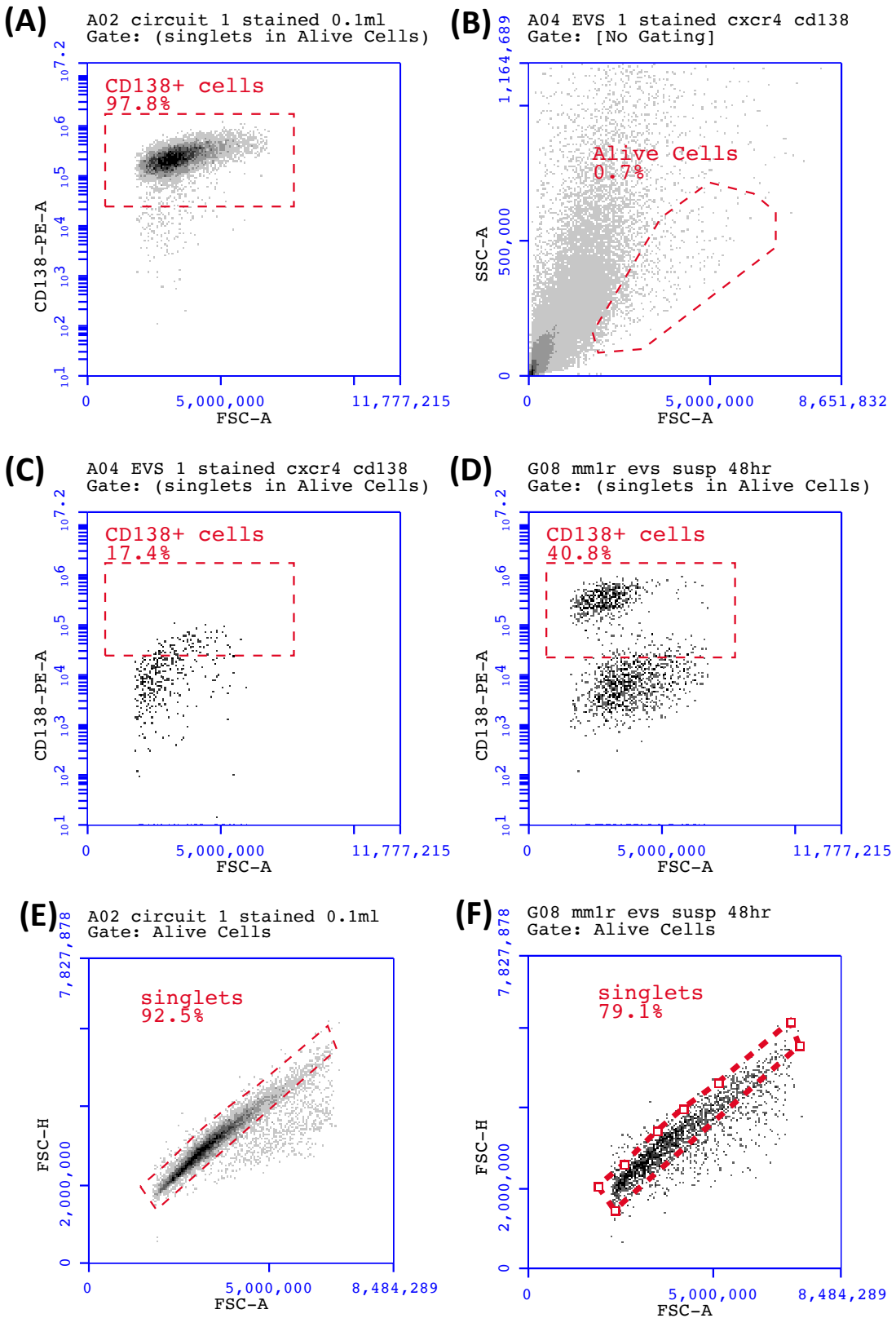

Figure 4.7 CD138 expression of MM cells at different stages of dynamic circulation migration model*. MM.1R cell line used in experiment, were stained with fluorescence-labelled antibodies and data was acquired on a BD Accuri flow cytometer. (A) Dot plot shown is of CD138 expression and forward side scatter of gated alive singlets. Approximately 0.5 x 10^6 circulating cells at 48h were stained with CD138 fluorescence-labelled antibodies. (B) ungated flow cytometry analysis of 100µl EVS at 48h. (C) additional 100µl of EVS was stained with CD138 fluorescence-labelled antibodies and gating applied on alive singlets. (D) of collected EVS cells at 48h, grown in fresh culture media for further 48h and CD138 fluorescence-labelled antibodies stained and gated as in (C). Singlet gating for (A) and (D) shown in figures (E) and (F) respectively.*

4.2.3.3 Direct visualisation and cytogenetic analysis of EVS cells confirm the presence of migrated MM cells

Figure 4.9B shows the presence of myeloma cells taken from the EVS as indicated by red arrow. The addition of the fibroblasts MRC-5 were also shown (blue arrow) as well as myeloma cells loosely adhering to the fibroblasts (black arrow). As a reference, figure 4.9A shows the MRC-5 and MM.1R cells in static co-culture and the tendency of the cells to clump or adhere to the fibroblasts.

MM.1R cells retrieved from the EVS and circulation at 48h were tested for the presence of the IGH/MAF rearrangement (t(14:16) q32q23), a translocation known to be present in the cell line (Greenstein et al. 2003). FISH analysis showed that all myeloma cells in circulation contained this translocation (100 out of 100 cells). Of the retrieved EVS cells, 19 out of 100 cells contained the translocation (figure 4.8).

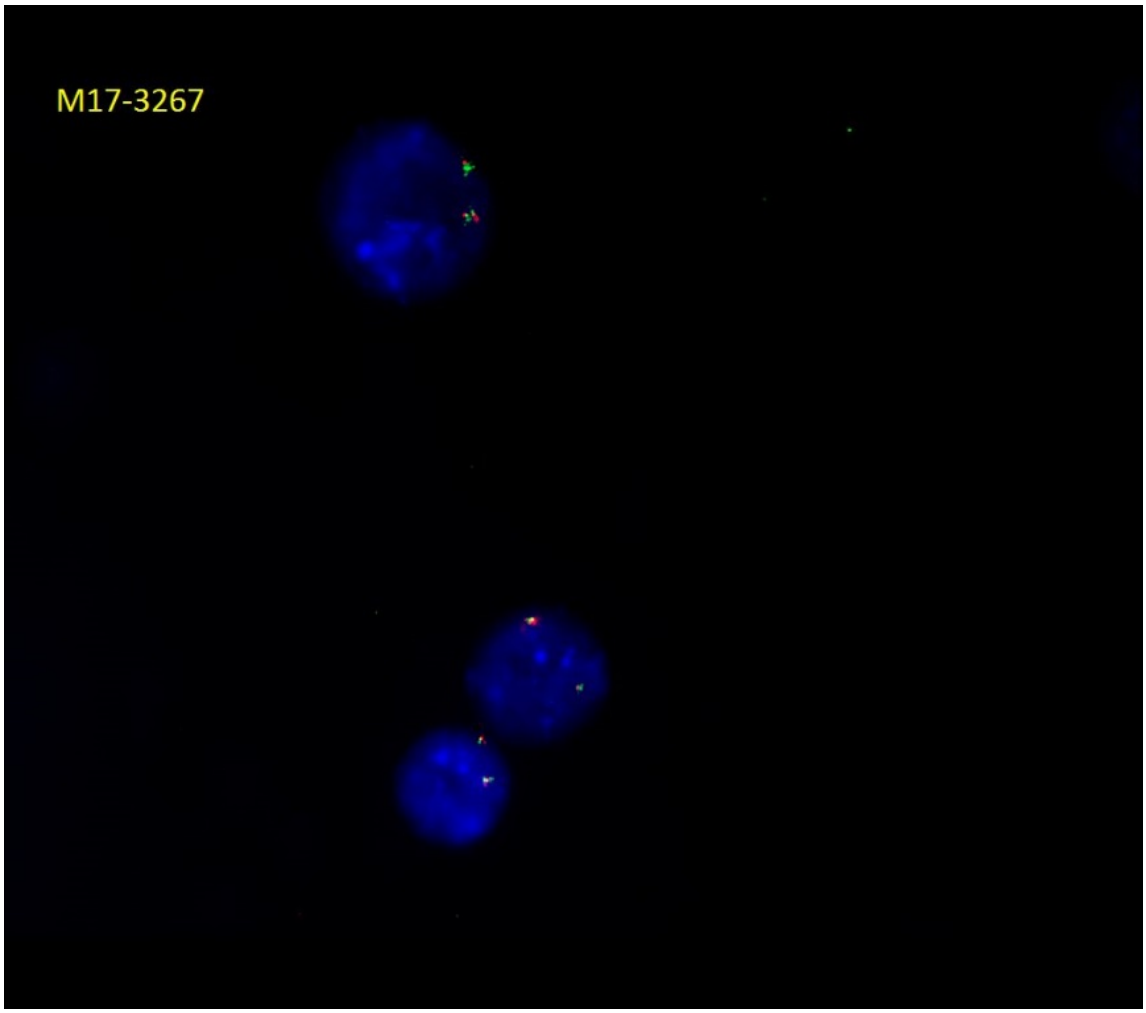

Figure 4.8 FISH analysis of MM.1R cells *(courtesy of Medical Genetics Service of Wales) of MM.1R EVS at 48h using the Cytocell Aquarius IGH/MAF dual fusion translocation probe. The image shows IGH/MAF rearrangement t(14:16) q32q23) in all three cells shown.*

(A)

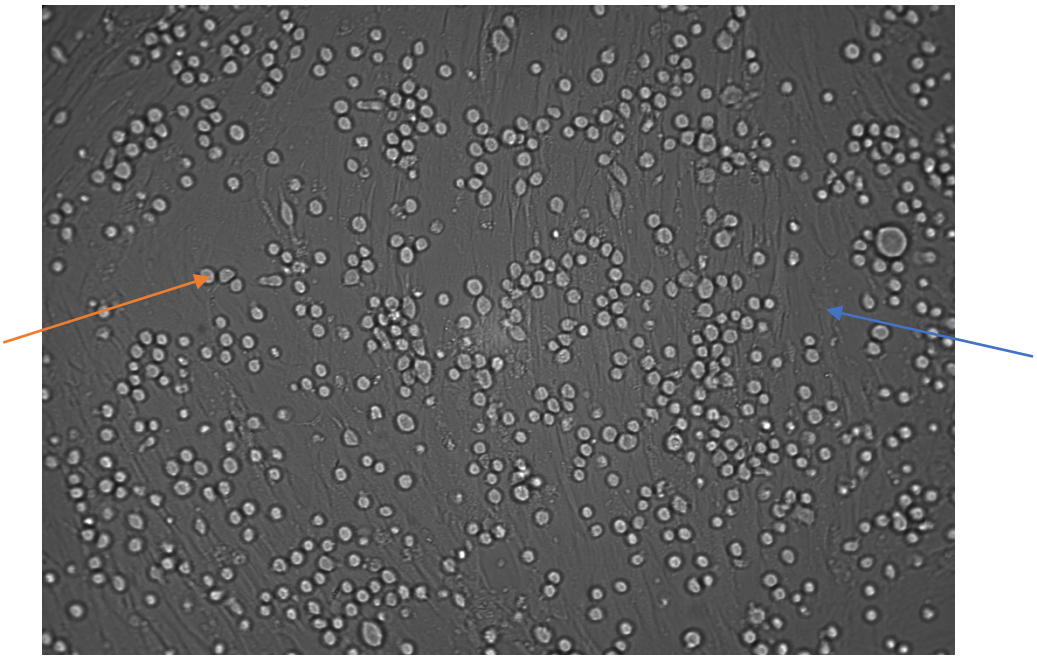

(B)

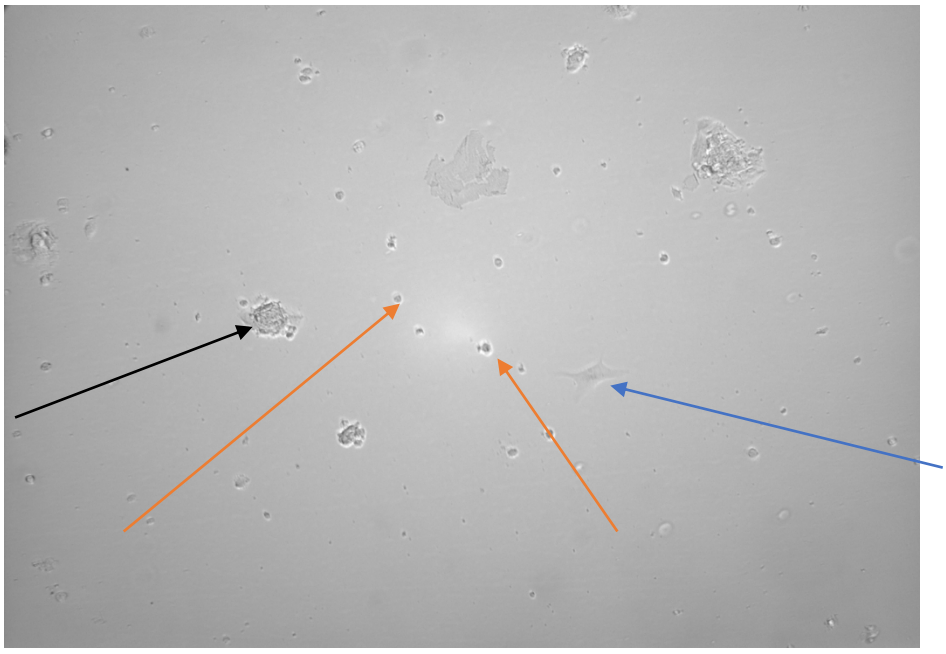

Figure 4.9. 40x high power magnification of myeloma cells MM.1 and Fibroblasts MRC-5. *(A) static liquid co-culture of confluent MRC-5, with adhered MM.1R cells. (B) of total retrieved EVS liquid from MM.1R migrated experiment, equally divided into 6 well plates and grown as static co-cultures. Red arrows indicate myeloma cells, blue arrows indicate adherent MRC-5 cells and black arrow indicate non-adhered MRC-5, with myeloma cells surrounding it.*

4.3 Cell migration varies amongst myeloma cell lines

Having successfully validated the methodology of the modified hollow fibre bioreactor as a model for MM migration, I felt the most accessible and easiest method to use for quantification of myeloma cells remains flow cytometry, which was applied for the rest of chapter.

I next set about comparing the migratory potential of various MM cell lines. Figure 4.10 shows the variation in CXCL12 induced migration of 7 different myeloma cell lines. OPM-2 cell line has the greatest propensity to migrate across a CXCL12 concentration gradient; mean migration was 3.94% (SD±3.56, n=12) of cells seeded into the circulating compartment migrated into the EVS over 48h. The cell line with the lowest propensity to migration was JJN-3, where only 0.75% (SD±0.75, n=7) of total cells migrated. Two cell lines which I had previously not shown to be responsive to CXCL12-induced transwell migration (U266 and RPMI-8226) did show some cell migration, U266 1.66% (SD±1.33, n=5) and RPMI-8226 1.41% (SD±1.41, n=3), comparable to the CXCL12 responsive transwell migration cell line MM.1S, 1.62% (SD±0.51, n=17).

4.3.1 Potential sub-clones within the same cell line can have a differing propensity for cell migration

An additional intriguing finding was the difference in migration for the MM.1-related cell lines (MM.1S, MM.1R and MM.1S^{dim}). A statistical difference in migration (p=0.0056, unpaired 2 tailed *t*-test) was observed between MM.1S (1.62%±0.79, n=17) and its dexamethasone resistant counterpart MM.1R (3.16%±1.9, n=17). When comparing MM.1S cell sorted sub-population, a CD38 expressing negative sub-populations (termed MM.1S^{dim} and further explored in chapters 5 and 6) was statistically not as migratory as its parent cell line (0.86%±0.51, n=5, p=0.027).

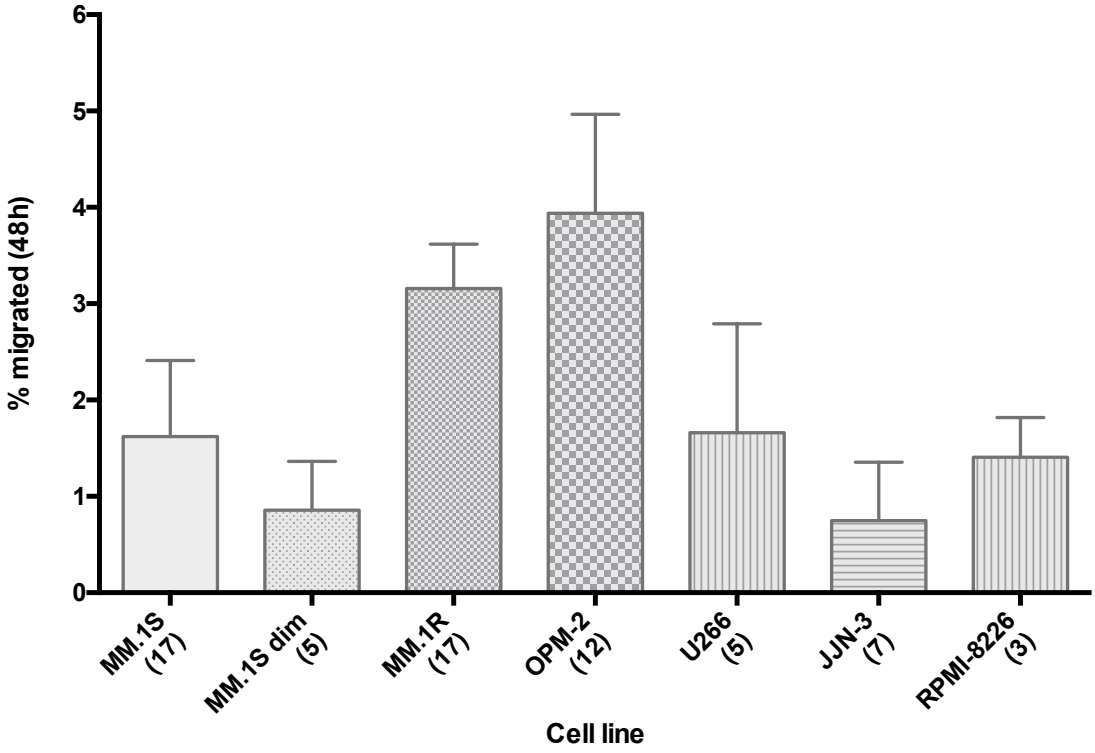

Figure 4.10. MM cell line migration at measured by modified hollow fibre bioreactor model*. Migration measured at 48h and calculated by the number of cells retrieved in the EVS as a percentage of cells retrieved from the circulation. Roughly 40x10^6 MM cells were inserted to the circulating compartment and 5x10^6 MRC-5 cells into the EVS. Migration at 48h was measured by both Vi-cell XR and flow cytometry methods but this figure only shows the percentage migration for each cell line as measured by Vi-cell XR. The data are presented as mean ± SD with the number of replicate independent experiments shown in brackets.*

4.4 The role of the CXCL12 receptor CXCR4 and the integrin CD49d in myeloma cell migration

Having confirmed that the dynamic circulatory migratory model was able to demonstrate MM migration, my next aim was to investigate the expression changes of CXCR4 and CD49d within the model. In addition, the effects on migration of inhibiting these molecules was also investigated in order to determine whether they represent useful targets for myeloma treatment. Although these cell markers are known to be key in MM migration (Katz and Tavor 2009), relatively little research has been undertaken into their potential as therapeutic targets. To explore the importance of CXCR4 and CD49d in MM migration, the cell lines MM.1S and its dexamethasone resistant clone MM.1R were to be used. These cell lines were chosen for several different reasons:

i. Both cell lines expressed (analysed by immunophenotyping) both proteins (figure 4.1l).
ii. The cell lines have been shown to be responsive to CXCL12-induced migration, and the effects of CXCR4 inhibitors have been studied (Alsayed et al. 2007).
iii. Although both cell lines originating from the same patient/clone, expression differences are observed, more pronounced in CD49d with MM.1S having greater expression for both markers (Figures 4.1l). I have already shown the different migratory potential of the cell lines but could also correspond to different sensitivity to drug inhibition within "sub-clones".
iv. Despite the common origin of the cell lines, observed functional and phenotypical differences exist. One area of interest is the PI3K/AKT pathway, a key regulator of CXCL12/CXCR4 induced migration (Hideshima et al. 2007a). Differing expression levels of PI3K could result in varying susceptibility to PI3K inhibition and/or could be an indicator of different migratory potential and responsiveness to inhibition of CXCR4 or CD49d.

Pharmacological inhibition of CXCR4 would be through the small molecule inhibitor ONO-7161, whereas CD49d inhibition would be through the monoclonal antibody Natalizumab.

The CXCR4 inhibitor ONO-7161

Several commercially available CXCR4 inhibitors were considered. Plerixafor (AMD3100-Genzyme) is the most widely accessible as it is licensed for stem cell mobilisation for a number of haematological conditions (including myeloma), prior to autologous stem cell transplants. It has also been used in limited circumstances for the treatment of relapsed

multiple myeloma. Phase II trials using Plerixafor in combination with bortezomib have been undertaken at the Dana-Faber Institute (Ghobrial et al. 2014). The rationale for combining these drugs is that CXCR4 inhibition would induce de-adhesion of myeloma cells, removing them from their protective microenvironment and thus sensitising the cells to bortezomib. Whether such inhibition changes the clinical behaviour of mobilised plasma cells is unclear, but when the effects of CXCR4 inhibition has resolved, plasma cells/stem cells return to their bone marrow microenvironment niche. ONO-7161, like plerixafor, is a small molecule inhibitor of CXCR4. It was developed by ONO-pharmaceuticals but to date it has not been developed beyond pre-clinical studies undertaken in CLL (Walsby et al. 2014b), within our research laboratory. Despite the apparent lack of development into clinical studies, Walsby et al, showed that ONO-7161 is a more potent inhibitor of CXCR4 expression than plerixafor and inhibits CXCL12-induced CLL migration, both in transwell assays and in the dynamic circulatory model used in this thesis. Inhibition of migration was observed at a concentration of 30nM and is non-cytotoxic up to concentrations of 10μM.

The CD49d monoclonal antibody Natalizumab

Natalizumab is a purified, recombinant, humanised monoclonal antibody (IgG4 subclass) that binds to the α4 subunit (CD49d) of integrin α4β1 (also known as VLA-4), thus blocking the binding of ligands VCAM and MadCAM to VLA-4 and to the α4β7 integrin (Leger et al. 1997). The IgG4 class of antibodies demonstrates reduced binding to Fcγ receptors and lack of ability to fix complement *in vitro*. It is also characterised by a shorter hinge region in comparison to antibodies of the IgG1 subclass, leading to a reduced flexibility of the hinge region. Produced in non-immunoglobulin secreting murine myeloma cells it has a molecular weight of 149 kilodaltons (Leger et al. 1997). Natalizumab was initially developed for use in inflammatory disorders, where inhibition of immune cell recruitment to inflamed tissues had obvious appeal and was initially granted license by the FDA in 2004 for use in such conditions (more information available at www.accessdata.fda.gov/drugsatfda_docs/label/2008/125104s106lbl.pdf). However, this licence was temporarily revoked after cases of progressive multifocal leukoencephalopathy (PML) were reported (Kappos et al. 2007). The licence was eventually reintroduced in conjunction with European Medicines Agency (EMA) findings, but solely approved for multiple sclerosis, as the benefits, on balance outweighed the risks of PML at a dose of 300mg or 3 mg/kg every 24 days, roughly equating to a concentration of 400nM (European Medicines Agency 2007).

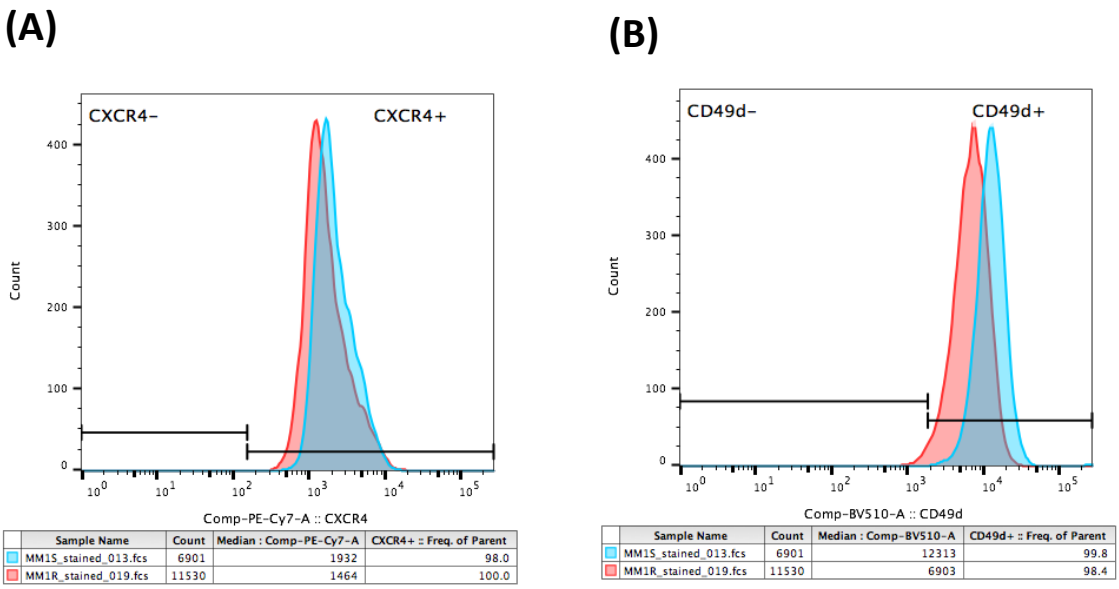

Sample Name	Count	Median : Comp-PE-Cy7-A	CXCR4+ :: Freq. of Parent
MM1S_stained_013.fcs	6901	1932	98.0
MM1R_stained_019.fcs	11530	1464	100.0

Sample Name	Count	Median : Comp-BV510-A	CD49d+ :: Freq. of Parent
MM1S_stained_013.fcs	6901	12313	99.8
MM1R_stained_019.fcs	11530	6903	98.4

Figure 4.11. CXCR4 and CD49d MM.1S and MM.1R expression. *Overlay histograms showing (A) expression of CXCR4 and (B) expression of CD49d of MM.1R (red) and MM.1S (blue). Legend for each histogram shows the number of events analysed (count), median fluorescence intensity (MFI) and percentage positivity (%). 1 x 10^6 cells were stained with fluorescence-labelled antibodies and data was acquired on a BD Fortessa flow cytometer.*

4.4.1 Migrated cells up regulate expression of CXCR4 and Ki-67 but not CD49d

Table 4.1 and figure 4.20 outlines the variation of CXCR4 and CD49d expression between circulating (non-migrated) and migrated MM cells after 48h in the dynamic circulatory model. The experiment included the seeding of MRC-5 cells into the EVS, thus creating a CXCL12 concentration gradient. CXCR4 expression changes of the two cells lines are broadly similar. After 48h of cells circulating within the dynamic model, those circulating cells still within the circuit, CXCR4 expression was lower than compared to baseline expression in static culture (MFI as a percentage of baseline - MM.1S 85%, MM.1R 95%, see table 4.1). However only in MM.1S was the decrease in expression statistically significant (p=0.0039 vs p=0.47). Meanwhile, migrated cells retrieved from the EVS (at 48h) showed a statistically significant upregulated of CXCR4 expression for both cell lines compared to control circulating cells (MM.1S MFI 138% of baseline, p=0.039 and MM.1R MFI 156% of baseline, p=0.047).

Both cell lines showed a reduction in CD49d expression on circulating control cells at 48h compared to static culture; MFI percentage of baseline expression (n=8), MM.1R 79% (MFI 43,627 to 29,303) and MM.1S 57% (MFI 48,606 to 23,900), however, the differences were not significant (MM.1S p=0.27, MM.1R p=0.19). MM.1S (higher baseline CD49d expression) CD49d expression of migrated cells (MFI 19,201 n=5) were similar to expression of circulating cells and almost half the MFI of static culture CD49d expression (57.6% vs. 57.4% - normalised to baseline). Whereas MM.1R showed an increase in CD49d expression (19,117 n=5) of migrated cells retrieved from EVS compared to static culture baseline, however the wide variation in MFI results (SD±93%) meant no statistically significant was shown.

	MFI (%)	SD	No. pairs	Paired *t*-test	p-value	Summary
MM.1S CXCR4						
Baseline	100	65.59				
Circulation	84.61	9.07	9	Baseline	0.0039	**
EVS	138.30	71.97	9	Circulation	0.039	*
MM.1S CD49d						
Baseline	100	56.25				
Circulation	57.40	18.82	5	Baseline	0.27	ns
EVS	57.61	32.08	3	Circulation	0.31	ns
MM.1R CXCR4						
Baseline	100	61.67				
Circulation	94.65	10.22	7	Baseline	0.47	ns
EVS	151.50	69.18	7	Circulation	0.047	*
MM.1R CD49d						
Baseline	100	52.52				
Circulation	79.32	19.58	5	Baseline	0.19	ns
EVS	107.30	93.41	5	Circulation	0.81	ns

Table 4.1. Median fluorescence intensity (MFI) and statistical data of MM.1S and MM.1R CXCR4 and CD49d expression *taken at 48h post experiment from either static culture (Baseline), control circulating system (Circ), Control EVS (EVS) or from paired Circulating and EVS containing drug (ONO-7161/Natalizumab or in combination). MFI values were normalised to paired static culture sample under same experimental conditions and calculated as a percentage. T-test are Wilcoxon paired, 2 tailed non-parametric. Number of pairs are stated in table and MFI was measured on BD Accuri, with approximately 0.5x10^6 cells stained with fluorescence-labelled antibody. In the event of EVS, 100μl of retrieved media was stained with antibody without washing.*

4.4.1.1 Migrated MM cells show increased Ki-67 expression

As well as upregulation of CXCR4, Ki-67 (a key intracellular protein associated with active proliferation) was also shown to be upregulated in migrated MM after 48h derived from the circulatory model. Table 4.2 shows Ki-67 expression as a total percentage compared to unstained MM cells for MM.1S and MM.1R as well as the cell line OPM-2 (the highest migratory cell line – figure 4.10) as a comparison. Comparisons were made between static culture, cells harvested from the circulating compartment and migrated cells retrieved from the EVS.

A statistically significant increase in Ki-67 expression was shown for each cell line between circulating and migrated cells (MM.1R 3.63% p=<0.0001; MM.1S 2.83% p=0.0008; OPM-2 4.25% p=0.0002). The Ki-67 percentage positivity in the migrated MM cells correlated with overall migration, with OPM-2 the highest cell line migrator, also showing the

highest mean Ki-67 percentage positivity. However, this did not correspond to the highest fold increase in Ki-67 expression between circulating and migrated cells with the greatest difference observed in MM.1R (3.8-fold increase in Ki-67 positivity). Although static culture Ki-67 expression was higher than circulation for each cell line, none of the differences were significant, with fold changes ranging from 1.3 (OPM-2) to 1.8 (MM.1S).

The increase in Ki-67 expression in migrated cells compared to their non-migratory counterparts was consistent with data generated by Elisabeth Walsby using CLL cells (personal communication of unpublished data).

Sidak's multiple comparisons test	Mean Ki-67 %	Fold-change	P Value	Summary
MM.1S				
Circulation vs. Static culture	0.90 vs. 1.63	1.8	0.22	ns
Circulation vs. EVS	0.90 vs. 2.83	3.1	0.0008	***
MM.1R				
Circulation vs. Static culture	0.95 vs. 1.47	1.5	0.41	ns
Circulation vs. EVS	0.95 vs. 3.63	3.8	< 0.0001	****
OPM-2				
Circulation vs. Static culture	1.88 vs. 2.35	1.3	0.55	ns
Circulation vs. EVS	1.88 vs. 4.25	2.3	0.0002	***

Table 4.2. Statistical data of Ki-67 expression with the myeloma cell lines MM.1S, MM.1R and OPM-2*. Sidak's multiple comparison test used to show statistical differences between Ki-67 expression. Approximately 0.5x10^6 cells for circulation and static culture were intracellularly stained with Ki-67 labelled fluorescence antibodies, whereas 100µl EVS sample was intracellularly stained. Samples analysed on BD Accuri and percentage positivity set as a percentage positivity compared to negatively stained sample, prepared by same method apart from addition of fluorescence antibody. Each Ki-67 percentage is the mean of three separate experiments*

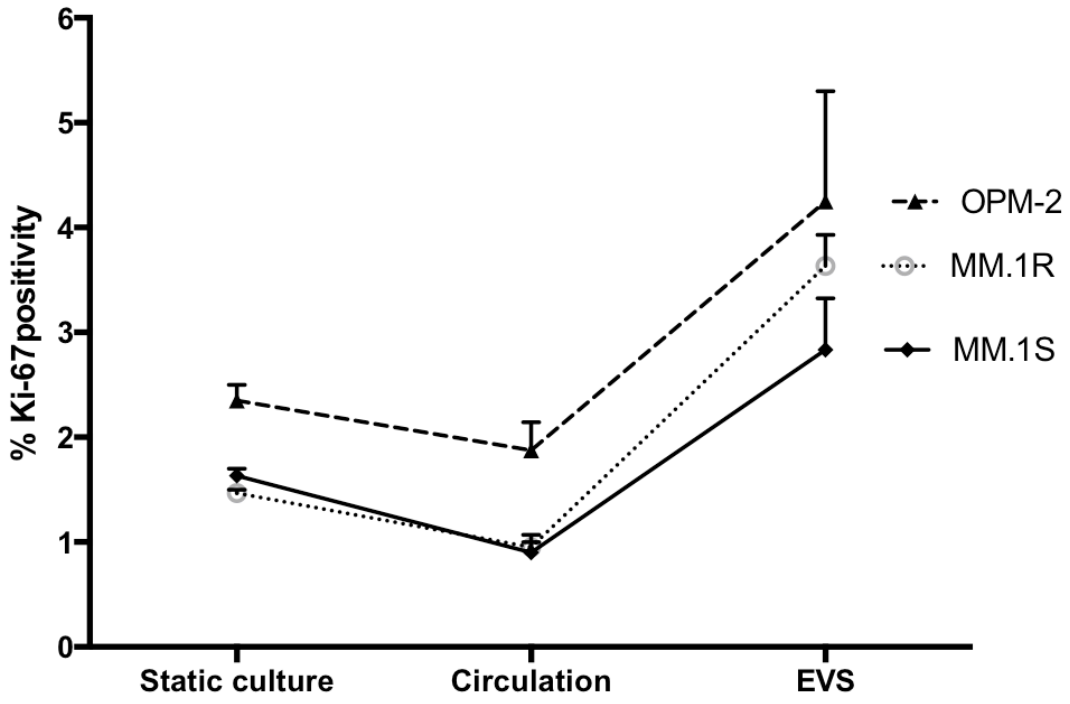

Figure 4.12. Proliferative marker Ki-67 expression for 3 different cell lines*. Difference in expression of the cell lines OPM-2, MM.1R and MM.1S in static culture, cells exposed to 48h of shear force in circulation model and migrated cells retrieved at 48h from the EVS. Error bars show standard deviation and are calculated by repeated independent experiments.*

4.4.1.2 Emergence of a bimodal CXCR4 expressing migrated population as possible explanation for upregulated CXCR4 expression

Of the retrieved migrated cells obtained from the EVS, CXCR4 expression on several occasions appeared to have a bimodal population. Figure 4.13 provides such an example, of an overlaid histogram comparing CXCR4 expression of circulating cells (red outline) with migrated cells (blue outline). The more dominant EVS population (82.9%) had lower expression of CXCR4 and akin to circulating cells CXCR4 expression. The higher expressing CXCR4 EVS population for this example accounted for 17.1% of the cells, with almost a log difference in expression. This CXCR4 upregulation was seen in the majority of control migration experiments, with statically significant increases in CXCR4 expression for both MM.1S (53.69% absolute increase, $p=0.039$) and MM.1R (58.85% absolute increase, $p=0.047$).

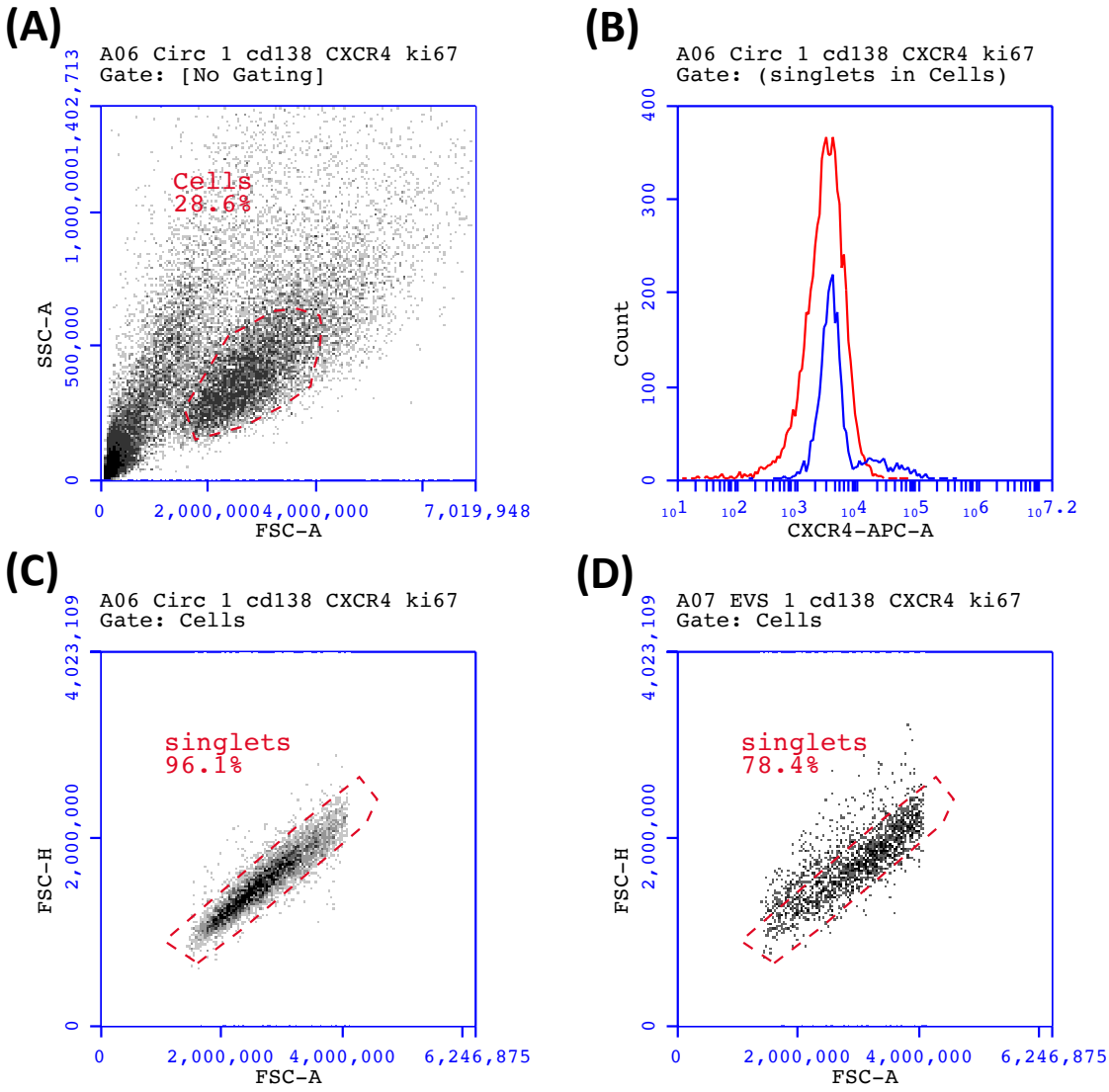

Figure 4.13. Comparison of CXCR4 expression between migrated and non-migrated MM cells. *(B) Overlaid histogram comparing CXCR4 expression between MM.1R cells retrieved from EVS (blue line) and Circulation (red line). Analysed on BD Accuri, 0.5x10^6 circulated cells and 100µl of EVS media stained with immunofluorescence antibodies. Experimental method as of section 4.1, with the EVS containing 5x10^6 MRC-5 cells. The bioreactor hollow fibres were seeded with 15x10^6 HUVEC and 40x10^6 MM cells entered into circulation (in addition with drug) and migration measured at 48h using a BD Accuri flow cytometer and employing the same FSC v SSC 'tight' gate (as shown in figure (A), circulating cells) as described previously. Singlet gating (FSC-H and FSC-A) is shown in figures C (circulating cells) and figure D (EVS).*

4.4.2 Pharmacological inhibition of CXCR4 and CD49d in transwell migration

Having shown that CXCR4 expression is upregulated in migrated MM cells, I next aimed to identify if pharmacological inhibition of the CXCR4 receptor would affect MM migration. Although no statistical changes in CD49d expression was shown in MM cell migration within the dynamic model, I also set out to determine if CD49d pharmacological inhibition affected MM migration and if any migratory synergy existed between the inhibitors.

I decided to conduct preliminary migratory work using static transwell plates rather than undertake repeated dynamic circulatory model experiments in an attempt to identify the optimal drug concentrations to inhibit MM migration. This strategy would have a number of advantages. Firstly, it would be more cost effective, and less time consuming but it would also allow easier reproducibility of my experiments, with the aim of finding drug concentrations that either inhibit migration and/or provide synergy. These results would better inform me in deciding ONO-7161 and Natalizumab drug concentrations to be used within the dynamic circulatory model to either confirm or identify migratory synergy.

4.4.2.1 ONO-7161 and Natalizumab are non-cytotoxic to myeloma cell lines, but only ONO-7161 decreases expression of its target

Maximum suppression of CXCR4 expression was achieved at a dose of 1μM ONO-7161 after 1h exposure (see figure 4.15), in an apparent dose–dependent manner for both cell lines. CXCR4 MFI at this concentration for MM.1S was 683 (1.2% positivity) from a baseline of 2,218, whereas MM.1R MFI was 705 (1.9% positivity) from a baseline of 1,870 (figure 4.14). Suppression of CXCR4 expression was maintained for 48h (see figure 4.15), MM.1S MFI 813 (2.1% positivity), MM.1R MFI 949 (2.1% positivity). At concentrations of 50μM and above, cytotoxic effects of ONO-7161 started to become apparent, with mean viability of MM.1S 60.75% (±11.05) and MM.1R 56.70% (±12.5) at 100μM.

The cell lines MM.1S and MM.1R highly express CD49d (percentage positivity of MM.1S 99.5% and MM.1R 91.6%, figure 4.11). The small difference in expression positivity between the cell lines is represented by a much greater difference in Median Fluorescence Intensity (MFI) (MM.1S = 9,035±845, MM.1R = 4,784±753, n=2). Natalizumab was non-cytotoxic to both cell lines (maximum dose of 50μM for 48h, figure 4.16) and did not statistically alter either the MFI expression or positivity of the cells at 1h or 24h.

This raises either the possibility that Natalizumab does not affect CD49d expression or that the antibody used for immunostaining has a different epitope target to Natalizumab. Data from multiple sclerosis patients receiving Natalizumab showed up to a 50% decrease in PBMC CD49d expression (using the same CD49d antibody clone – 9F10, as used in this study), in most but not all patients. This was maintained after a number of repeated infusions (Defer et al. 2012).

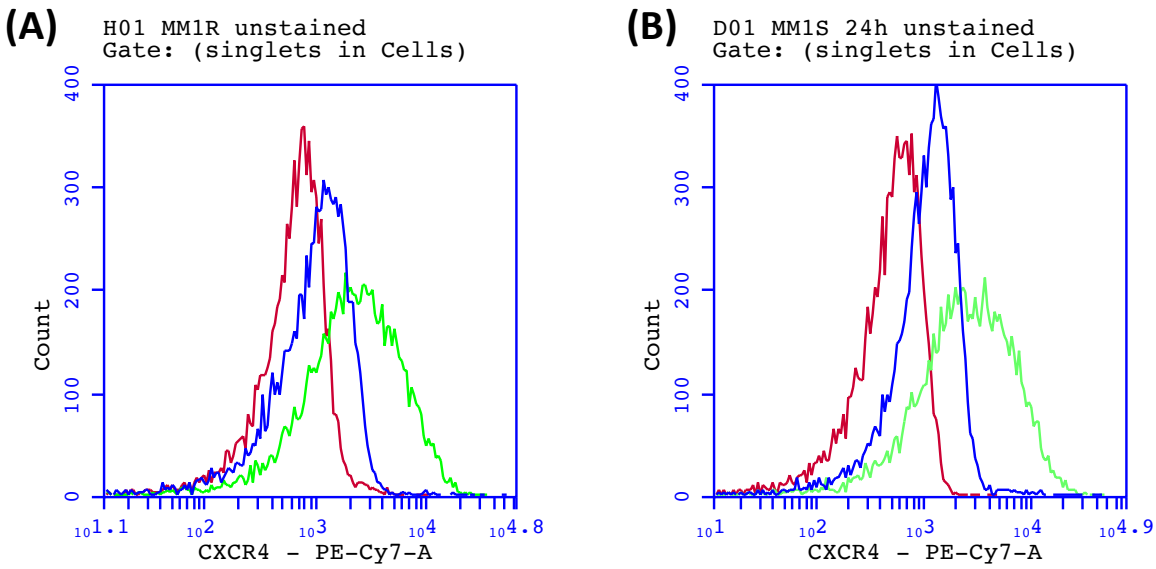

Figure 4.14. Effect of ONO-7161 on CXCR4 expression. *Overlaid histograms showing CXCR4 expression for (A) MM.1R (B) MM.1S. For both histograms,* ***red*** *outline represents unstained control,* ***Green*** *outline represents stained control and* ***blue*** *outline represents 24h exposure to 1μM ONO-7161 in static culture. For CXCR4 staining, 1 x 10^6 cells were stained with fluorescence-labelled antibodies and data was acquired on a BD Accuri flow cytometer.*

4.4.2.2 ONO-7161 inhibition of CXCR4 expression does not correlate with reduced CXCL12-induced transwell migration

Both cell lines have been shown to possess a migratory potential across a CXCL12 transwell barrier (chapter 3). MM.1S was shown to be the better migrator with 3.97% (±0.39) of total cells migrating after 24h compared to MM.1R 3.28% (±0.83). However, this difference was not statistically significant (p=0.48). Upon exposure to ONO-7161, at lower doses (10nM and 100nM), both cell lines showed a slight increase in migration compared to baseline (figure 4.15D), although this difference was not significant. Maximum inhibition of CXCR4 expression occurred at 1μM of drug for both cell lines, however at this dose, migration was not affected (MM.1S 4.64%, p=0.97; MM.1R 3.42%, p>0.99). MM.1R migration, unlike MM.1S did fall with higher concentrations of drug (50μM and 100μM) but again neither was significant (1.52% ±0.31 p=0.36; 1.63% ±0.51 p=0.35 respectively, figure 4.15D). In addition, concerns of off target effects of drug at the higher concentration (100μM) were raised, as viability started to fall, therefore no further dose increased in the drug occurred.

4.4.2.3 Natalizumab reduces, but does not completely prevent, myeloma cell transwell migration

Figure 4.16D shows that a reduction in CXCL12-induced 24h transwell migration started to be seen at 10μM of Natalizumab (percentage migration MM.1S 3.28%, MM.1R 3.54%), although at this dose reduction in migration was not statistically significant (MM.1S p=0.086 and MM.1R p= 0.07). However, a statistical difference was observed at 50μM when percentage migration was normalised to its baseline without Natalizumab. MM.1S total percentage migration was 2.51% (p=0.02 compared to baseline) and MM.1R 2.51% (p=0.07 compared to baseline).

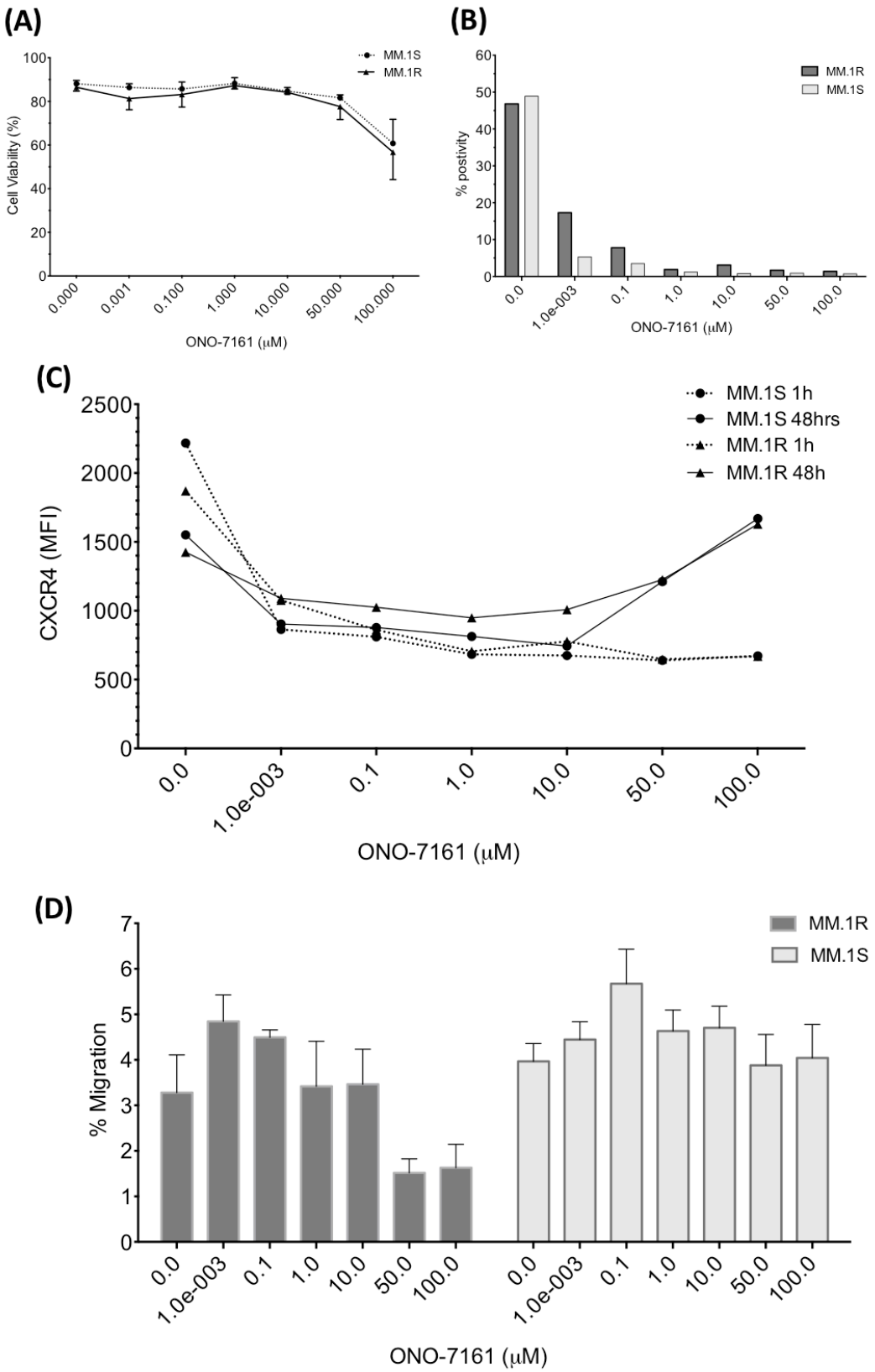

Figure 4.15. Effect of the CXCR4 inhibitor on the cell lines MM.1S and MM.1R. (*A) Cell line viability after 48h exposure to ONO-7161 in static culture (n=2) as measured by annexin V and PI staining and analysed on BD Accuri flow cytometer. (B) The percentage positivity of CXCR4 expression, as determined by gating on unstained cells, after 1h exposure of ONO-7171 in static culture, as measured on BD Accuri flow cytometer (n=2). (C) Comparison of CXCR4 median fluorescence intensity (MFI) at 1h and 48h exposure to ONO-7161. (D) 24h percentage transwell migration (CXCL12-induced) at different concentrations of ONO-7161 (n=4)*

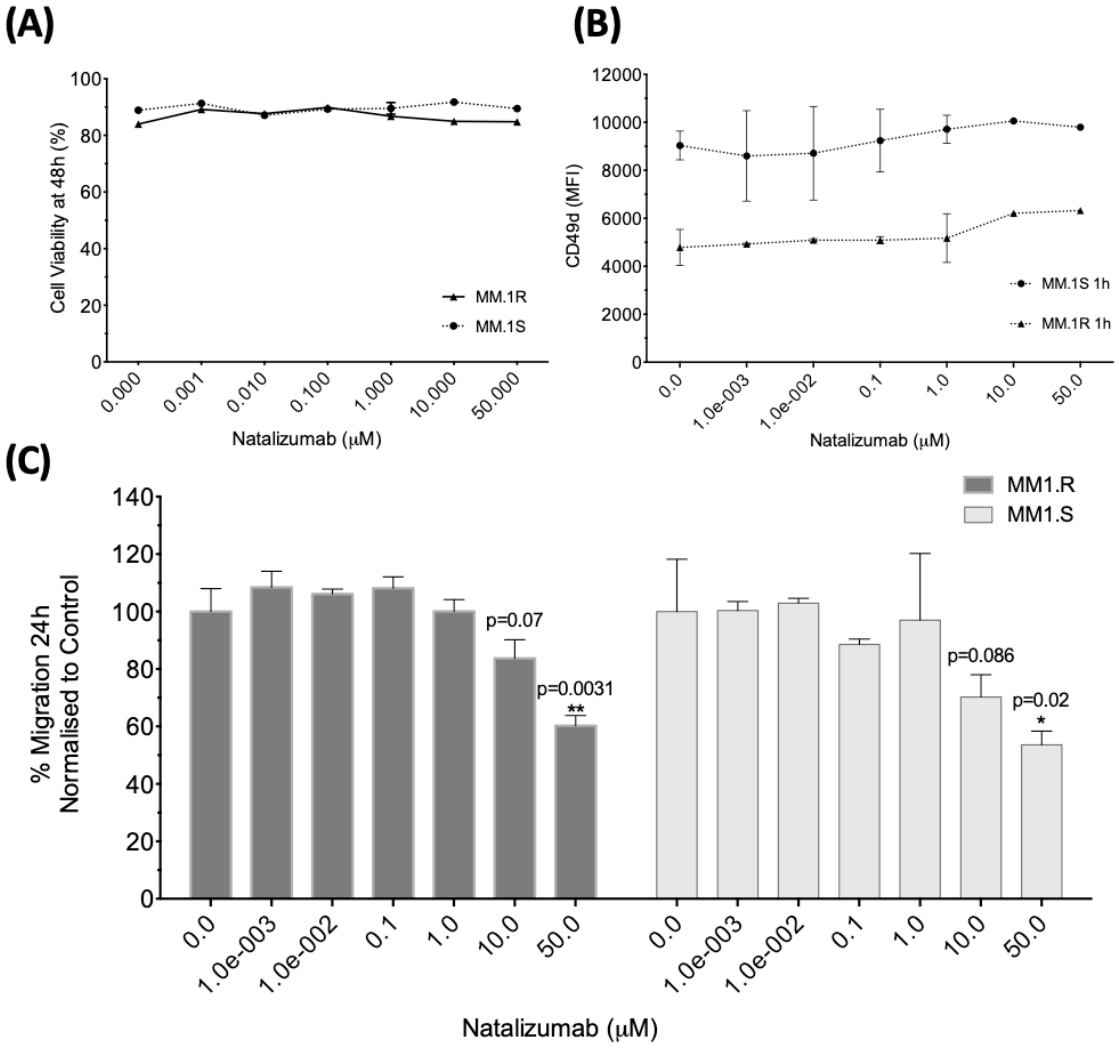

Figure 4.16. Effect of the monoclonal anti-CD49d antibody Natalizumab on the cell lines MM.1S and MM.1R. (*A) Cell line viability after 48h exposure to natalizumab in static culture (n=2) as measured by annexin V and PI staining analysed on BD Accuri flow cytometer. (C) Comparison of CD49d median fluorescence intensity (MFI) after 1h exposure to Natalizumab, approximately 0.5x10^6 cells stained with fluorescence labelled CD49d antibody and measured on BD Accuri flow cytometer. (C) 24h percentage transwell migration (CXCL12-induced), normalised to control at different concentrations of Natalizumab (n=4). Error bars show standard deviation and are calculated by repeated independent experiments.*

4.4.2.4 Transwell migration experiments provide evidence of the synergist effect of CXCR4 and CD49d inhibition

To show if a possible synergistic effect of the two agents in inhibiting migration existed, repeat transwell experiments were undertaken combining Natalizumab and ONO-7161. Resources and time restraints meant that full synergistic experiments at fixed ratios were unable to be conducted. A dose of 1μM for ONO-7161 was decided upon, as this was the lowest concentration that showed complete expression inhibition of CXCR4, with no cytotoxic effects. Natalizumab concentration was more problematic to decide upon as the drug seemingly had no effect on expression and although statistically significant migration inhibition was shown at 50μM, this dose was much higher than the approved clinical use of between 400-800nM, above which concentrations concerns of PML occur. Therefore, a dose of 1μM (0.14mg/ml, a similar level to approved drug concentration and the same dose as used by Walsby et al, in their CLL experiments (Walsby et al. 2014c)) was decided upon.

Figure 4.17 shows a number of effects ONO-7161 and Natalizumab have on MM cell lines when combination both at a fixed dose of 1μM. Combination therapy had no effect on cell viability or the expression of the proliferative marker Ki-67 at 48h. However, when the drugs were combined and 24h MM cell transwell migrations experiments across a CXCL12 concentration gradient were undertaken, a statistically significant reduction in migration was observed. Migration (normalised to control) for MM.1R fell to 63.76% ($p=0.0043$ compared to control) and MM.1S migration fell to 57.34% ($p=0.0005$ compared to control). No inhibition of transwell migration was identified in single agent use and was comparable to the previous experiment (figure 4.15 and 4.16).

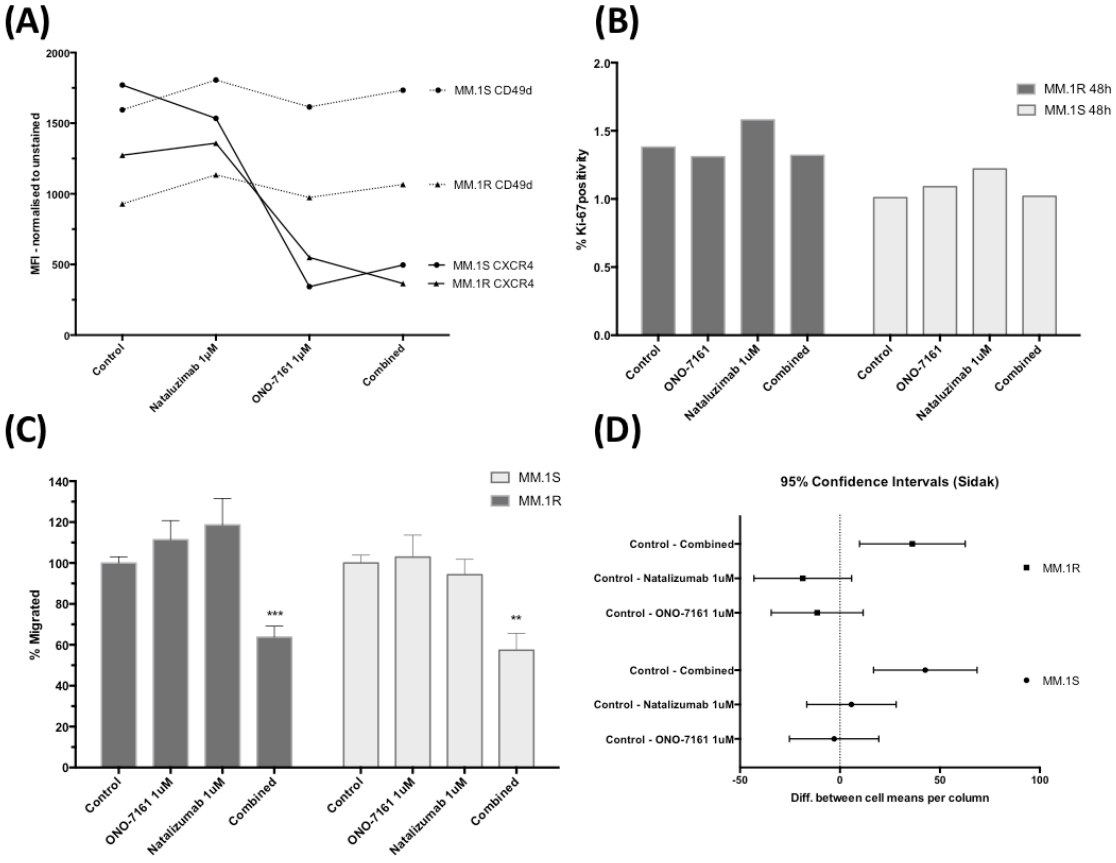

Figure 4.17. Effects of combination ONO-7161 and Natalizumab has on MM cell lines, MM.1S and MM.1R *(A) CXCR4 and CD49d MFI (normalised to unstained) of cell lines MM.1S and MM.1R after 48h of drug exposure. (B) Percentage Ki-67 positivity of the 2 cell lines after 48h of drug exposure in static culture. Cells were intracellularly stained with fluorescence labelled antibody and analysed on BD Accuri flow cytometer (C) Percentage CXCL12 induced transwell migration at 24h (normalised to control) of cell lines MM.1S and MM.1R, with single agent drugs and in combination (n=4). (D) box and whisker plot showing 95% confidence intervals (Sidak) between control and drug combination. Error bars show standard deviation and are calculated by repeated independent experiments.*

4.4.3 Inhibition of migration investigated in the dynamic circulatory model

Transwell migration experiments showed that single agent ONO-7161 and Natalizumab, at concentrations that would otherwise not affect CXCL12 induced MM migration, could potentially combine synergistically to inhibit MM cell migration. My next aim was to see if such drug combination could also affect migration for MM cells within the dynamic circulatory model. Fixed concentration of 1μM for both drugs were to be used, based on the results of the transwell experiments (Section 4.3.2.4), as it was at these doses that promising synergistic effect in inhibiting transwell migration were observed and also at a dose of Natalizumab that limited the concerns of PML. As for the transwell experiments, MM.1S and MM.1R cell lines were to be used to add continuity and also to possibly identify if any migratory difference exists between the cell lines.

4.4.3.1 CXCR4 inhibitor (ONO-7161) and the CD49d inhibitor (Natalizumab) are non-cytotoxic either as single agent or in combination.

As observed with the transwell experiments, neither agents either as single or in combination (1μM) was toxic to circulating cells or to cells retrieved from the EVS (figure 4.18). No statistical difference was seen between the MM cell viability of circulating cells with or without either drug (mean cell viability 77.23% v 76.54% p=0.99). Likewise, no statistical difference was seen in cell viability between cells retrieved from EVS in either control or drug (mean cell viability 68.59% v 70.84% p=0.91). A difference was seen between circulation control and EVS control cell viability (p=0.0085), but not between the circulating compartment and the EVS with addition of drug (p=0.49).

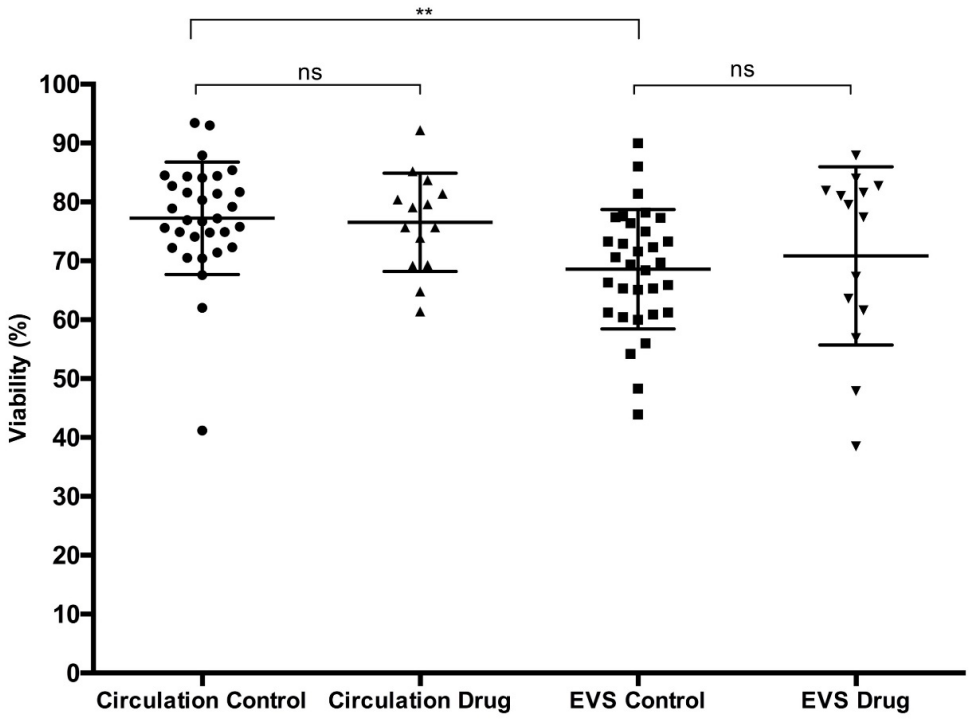

Figure 4.18. Viability of MM cells within the dynamic circulatory model*. Collective scatter plots comparing cell viability between the different compartment of dynamic circulatory model and between drug included (either in combination or single, both drugs at a concentration of 1μM) and without. Plots include mean and SD of cell viability (measured by Beckman Coulter Vi-cell XR) of cells retrieved from circulation and EVS and are of a by-product of MM.1S and MM.1R experiments combined. Experimental method as of section 4.1, with EVS containing 5x10^6 MRC-5, bioreactor seeded with 15x10^6 HUVEC and 40x10^6 MM cells entered into circulation (in addition with drug) and migration measured at 48h.*

4.4.3.2 The pharmacological agents ONO-7161 and Natalizumab in combination inhibit migration

When MM.1R and MM.1S were subjected into the circulation of the dynamic migratory model (with CXCL12 secreting MRC-5 as a chemoattractant within the EVS), mean migration for the cell lines without pharmacological agents was MM.1R 0.51%±0.51 (n=25) and MM.1S 0.33%±0.31 (n=23). The difference between the two cell lines was not statistically significant (p=0.30, unpaired t-test n=12, table 4.3 and figure 4.19). These results were in keeping with dynamic circulatory experiments from section 4.1.2 (note migration in figure 4.10 was calculated by Vi-cell cell counter for standardisation purposes between all cell lines).

In contrast to the Transwell migratory experiments, inhibition of migration occurred with the addition of the single agent pharmacological agents ONO-7161 (1μM) and Natalizumab (1μM). MM.1R mean migration with ONO-7161 was 0.23%±0.066 (n=3) and Natalizumab 0.31%±0.12 (n=3), whereas MM.1S mean migration with ONO-7161 was 0.13%±0.058 (n=3) and Natalizumab 0.25%±0.14 (n=3). These results indicate ONO-7161 resulted in greater

reduction in migration than Natalizumab for both cell lines with relative reduction in migration being 55% vs 24% for MM.1R and 61% vs 39% for MM.1S. However, the reduction in migration caused by 1μM ONO-7161 compared to control without drug was non-significant (MM.1R p=0.44, MM.1S p=0.053, n=3).

When the pharmacological agents were used in (1:1) combination (1μM ONO-7161 and 1μM Natalizumab), a statistically significant reduction in migration was seen when compared to control, (MM.1R 0.13% p=0.036, MM.1S 0.07% p=0.002). The relative reduction in migration was comparable between the 2 cell lines (MM.1R 75% vs. MM.1S 79%).

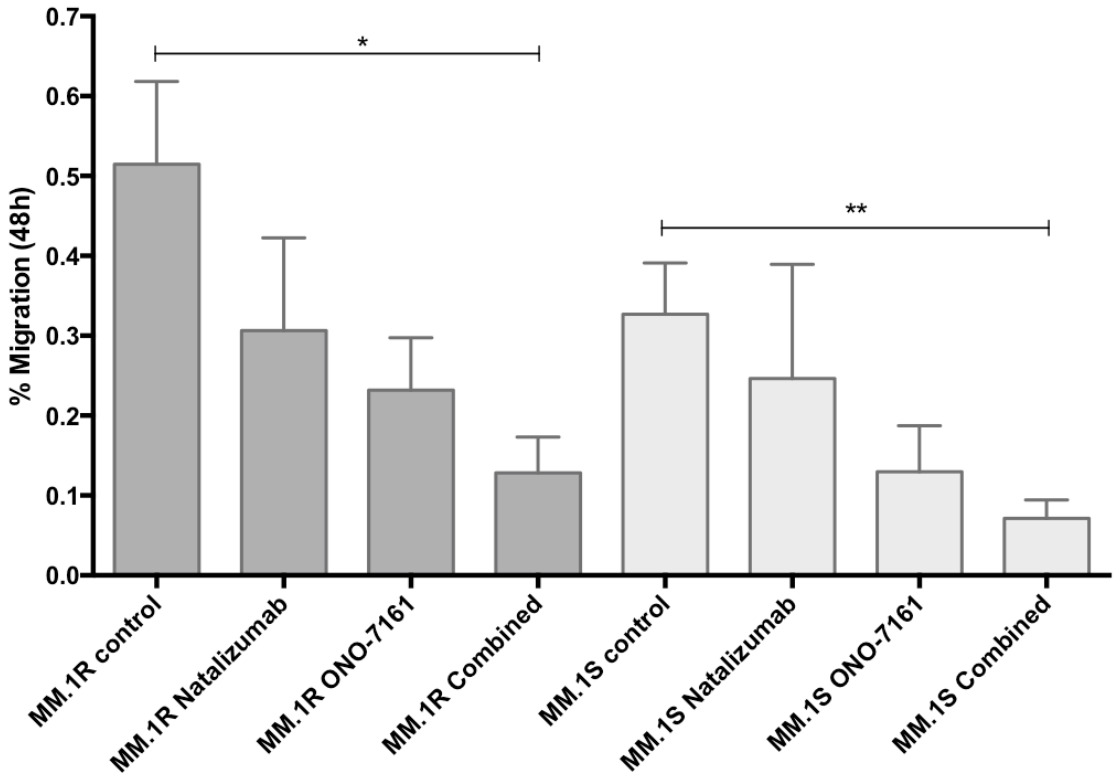

Figure 4.19. Percentage migration in the dynamic circulation model at 48h*. Table 4.3 shows statistical data from these experiments. The experimental method used was as described in section 4.1: the bioreactor seeded with 15x10^6 HUVEC, the EVS containing 5x10^6 MRC-5 and 40x10^6 MM cells introduced into circulation (in addition with drug). Migration was measured at 48h using a BD Accuri flow cytometer using FSC v SSC 'tight' gating as previously described. The data are shown as mean ± SD of three independent experiments, with each experiment a pair of control (untreated) and treated samples.*

	Mean migration	SD	SEM	p-value	Summary
MM.1R					
Control (n= 12)	0.51%	0.52	0.1	0.30^{+}	ns
Natalizumab 1μM (n=3)	0.31%	0.23	0.12	0.65	ns
ONO-7161 1μM (n=3)	0.23%	0.13	0.07	0.44	ns
Combination (n=3)	0.13%	0.11	0.04	0.036	*
MM.1S					
Control (n=12)	0.33%	0.31	0.06	0.30^{+}	ns
Natalizumab 1μM (n=3)	0.25%	0.29	0.14	0.33	ns
ONO-7161 1μM (n=3)	0.13%	0.14	0.06	0.053	ns
Combination (n=3)	0.07%	0.06	0.02	0.002	**

Table 4.3. Statistical data from experiments outlined in figure 4.17*. Mean percentage migration of the cell lines with combination of drugs in dynamic circulation model. P-value are Mann-Whitney paired T-test with control of the same cell line, except for (+) which is unpaired T-test between all of MM.1S control and MM.1R control comparing migration of the two cell lines without pharmacological agents (i.e. the controls). SD – standard deviation; SEM – Standard error of the mean; Cont. – control; Nat. – Natalizumab 1μM; ONO. – ONO-7161 1μM; Comb. – Combined (Natalizumab 1μM and ONO-7161 1μM); ns – non-significant.*

4.4.3.3 Combined ONO-7161 and Natalizumab inhibits CXCR4 but not CD49d expression in circulatory model

CXCR4 expression at 48h in the combined ONO-7161 (1μM) and Natalizumab (1μM) treated circulating cells was reduced compared to non-treated circulating cells. Relative percentage reduction of CXCR4 expression for MM.1S was greater and statistically significant than for MM.1R (35% p=0.031 vs. 26% p=0.063 respectively). Although CD49d expression in the circulation (both with and without pharmacological agents) was reduced compared to static culture (see figure 4.20), there was comparably no statistical difference in CD49d expression between the circulating compartment and the EVS for either MM cell line (MM.1S p=0.75 n=3 and MM.1R p=0.25 n=3).

Of the small number of EVS retrieved cells for the pharmacologically treated experiments (ONO-7161 and Natalizumab), small increases in CXCR4 expression were seen for both cell lines, but neither were statistically significant, MM.1S (44.25% absolute increase, p=0.47) and MM.1R (27.44% absolute increase, p=0.31). Figures 4.21C and 4.21D, give an example of CXCR4 expression of migrated cells under conditions containing combination drugs ONO-7161 and Natalizumab. Although much reduced in number, a bimodal population still exists, but this time the larger population (61.1%) is the more brightly expressing CXCR4, compared to CXCR4 expression in migrated cells without pharmacological agents (figures 4.21E and 4.21F). The same cautionary conclusive remarks apply for CD49d expression as well and although no statistical changes in expression of either cell line was observed, of the pharmacologically treated migrated cells retrieved, CD49d expression decreased for both cell lines (relative reduction from static culture baseline, MM.1S 39.4%, MM.1R 36.3%), with the difference approaching significance (p=0.063 for both cell lines).

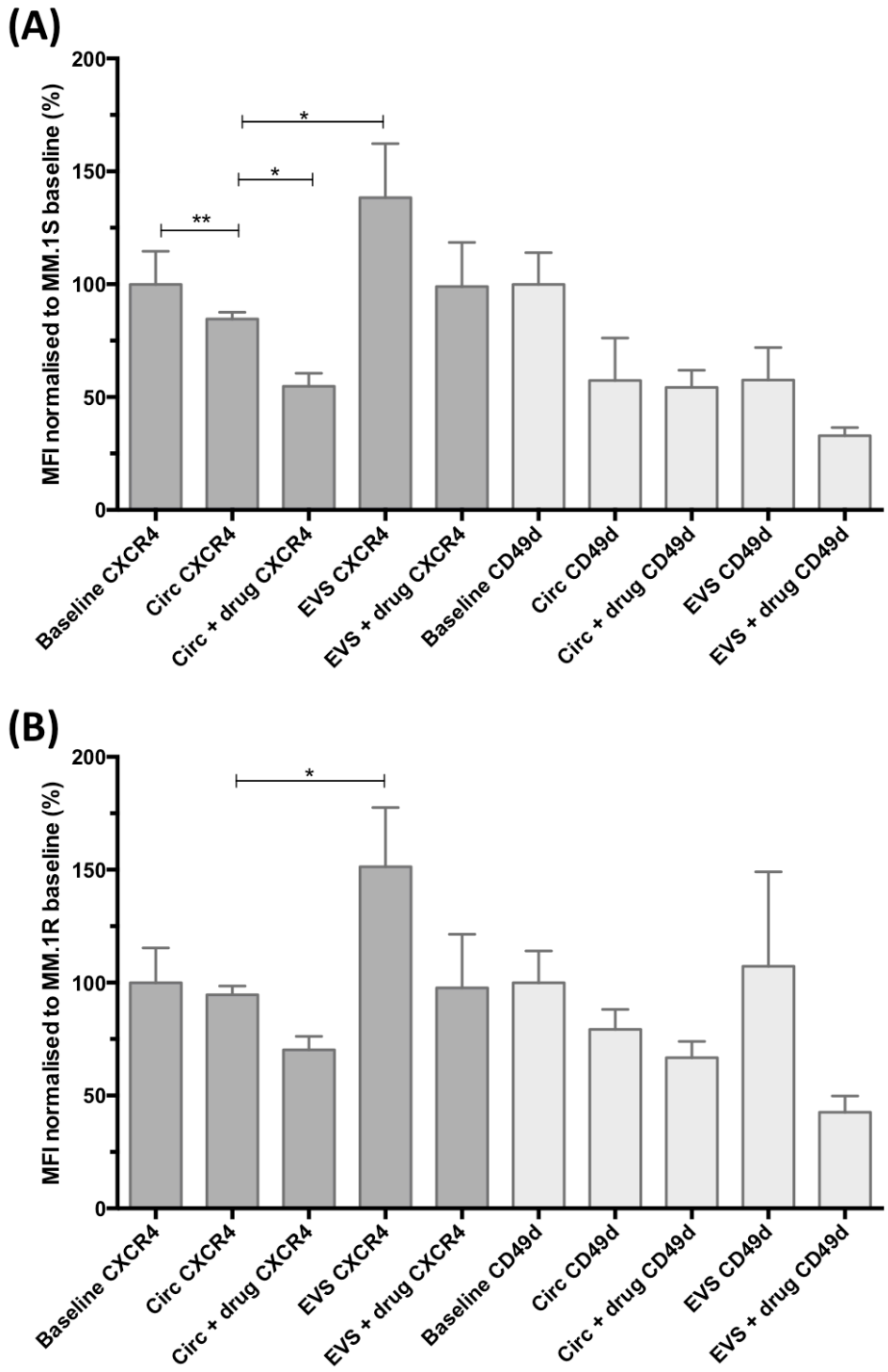

Figure 4.20. Diagrammatic representation of percentage MFI changes within pharmacologically treated dynamic migratory experiments*. Comparison of CXCR4 and CD49d expression with each bar corresponding to different experiment conditions (circulation, EVS, baseline, drug containing (ONO-7161 and Natalizumab) or not), cell lines ((A)-MM.1S, (B)-MM.1R) and cell marker (CXCR4 or CD49d). MFI has been normalised to static culture untreated baseline MFI and represented as a percentage. Median fluorescence intensity (MFI) and statistical data of CXCR4 and CD49d expression taken at 48h post experiment from either static culture (Baseline), control circulating system (Circ), Control EVS (EVS) or from paired Circulating and EVS containing drug (ONO-7161/Natalizumab or in combination). Statistical evaluations were performed using the two tailed Wilcoxon signed -rank test. The number of pairs are stated in the table and MFI was measured on BD Accuri flow cytometer, with approximately 0.5x10^6 cells stained with fluorescence labelled antibody. In the event of EVS, 100μl of retrieved media was stained with antibody without washing. Error bars show standard deviation and are calculated by repeated independent experiments.*

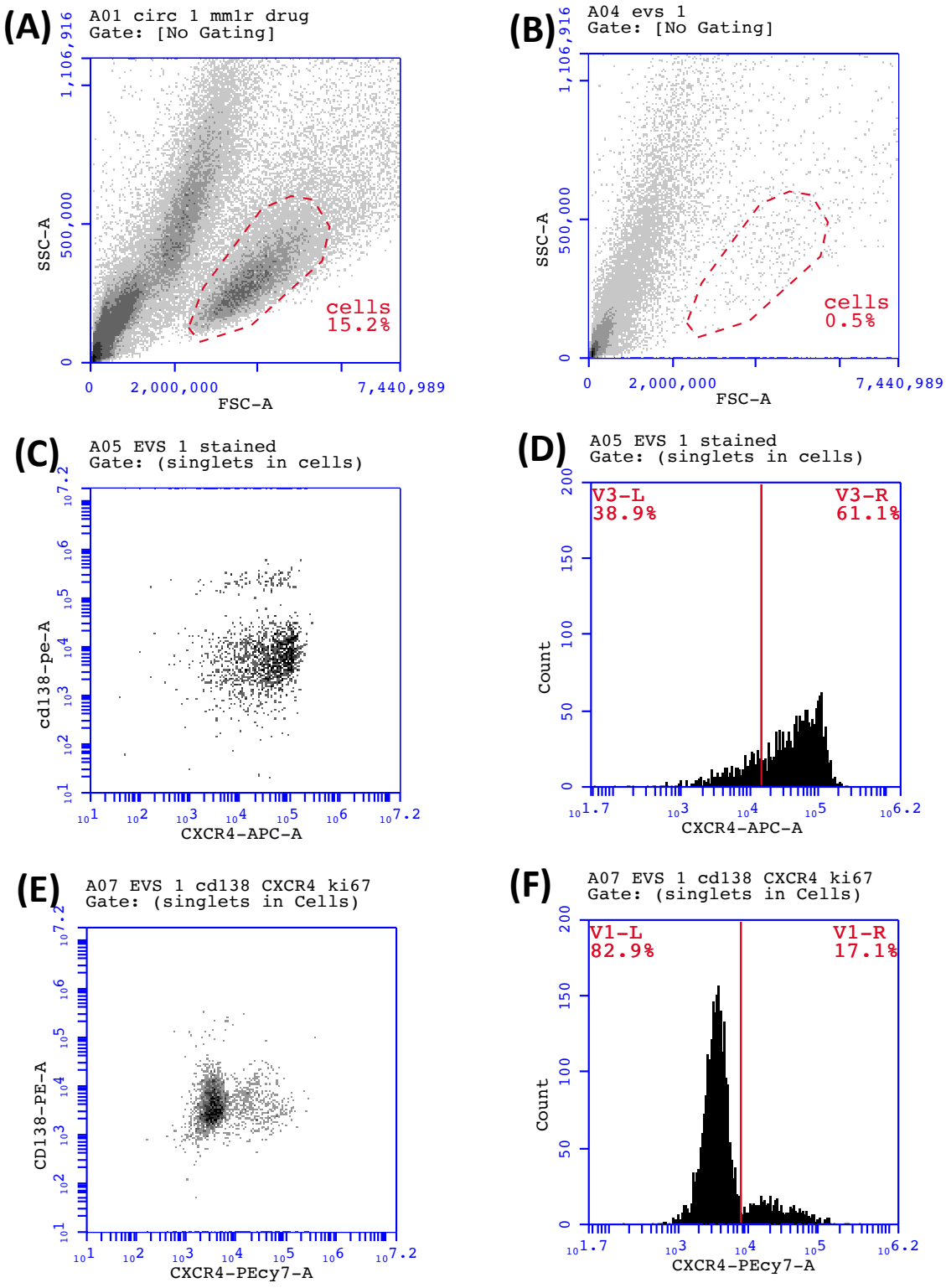

Figure 4.21. Flow cytometry plot comparison of CXCR4 expression of migrated MM.1R cells *treated with ONO-7161 and natalizumab (figures A-D) and those not treated (figures E-F). Experimental conditions are those outlined in section 4.3.1 – EVS containing 5x10^6 MRC-5, bioreactor coated with 15x10^6 HUVEC and 40x10^6 MM cells entered into circulation (with or without pharmacological agents). Samples taken at at 48h, stained with immunofluorescence antibodies (EVS 100µl sample, circulation 0.5x10^6 cells. Analysed by BD Accuri flow cytometer using a FSC v SSC 'tight' gate. (A) + (B) 48h FSC-A and SSC-A flow cytometer using same alive MM gate strategy analysed sample of (A) ONO-7161 and natalizumab treated circulation sample and (B) 48h EVS sample from same experiment as (A). (C) CD138 and CXCR4 stain of EVS shown in (B). (D) CXCR4 histogram of same sample as (C). (E) Control MM.1R experiment without combined pharmacological agents, EVS-derived cells were stained with CXCR4 antibody and the bimodal histogram is shown in (F)*

4.5 Discussion:

My results have shown that the dynamic circulatory model initially applied to CLL cells developed by Walsby et al, can be applied to MM. I have proven than MM cells with the addition of MRC-5, HUVEC's and shear force are able to create a model that allows MM cells to migrate from one compartment to another across a CXCL12 concentration gradient. The model is more physiological representative than transwell assays and has the capacity to study the effects of migration inhibitors on MM cell lines. In an attempt to optimise the model specifically for MM, addition of IL-6 was proposed. Early commercially available MM cell lines required the addition of the cytokine to ensure cell survival and proliferation and although the majority of commercially available MM cell lines today (including MM.1S and MM.1R) have been selected and cultivated to be IL-6 independent, thereby assisting in cell culturing (Goldman-Leikin et al. 1989), studies have shown the addition of IL-6 to MM.1S can still activate key pathways and pro-survival protein such as Mcl-1 (Zhang et al. 2003). Nevertheless, the addition of IL-6 did not appear to influence cell survival or migration and was not further used.

The initial concern of the dynamic migratory model was how to ensure retrieved cells from the EVS were migrated Multiple Myeloma (MM) cells. The recorded cell diameter of retrieved cells from the EVS by a Vi-cell cell counter, revealed that the cells to be smaller than both static culture MRC-5's and circulating MM cells is suggestive that these cells are unlikely to be the fibroblasts MRC-5. This is supported by cytogenetic proof that retrieved EVS cells contain the known MM cytogenetic translocation of the MM.1 cell lines and were also visualised through high power light microscopy. MM.1R and MM.1S are known to have the IGH/MAF rearrangement (t(14:16) q32q23) (Greenstein et al. 2003). Analysis confirmed that all myeloma cells in circulation contained this translocation. Of the cells retrieved from the EVS, the presence of the same translocation was identified, confirming the presence of MM cells and the ability of MM cells to migrate into the EVS. Although the actual number of cells with the translocation was lower than circulation (19 out of 100 for MM.1R), the purpose of this experiment was simply to confirm the migratory potential of MM.1 cells within the EVS and not an estimation of total number of migrated cells or migration percentage. Inevitably MRC-5 would have been included in EVS sample and although I did not test MRC-5's for the t(14:16), ATCC cell line characteristics state it has a normal karyotype (Jacobs et al. 1970), giving confidence that the translocations identified in the retrieved EVS cells were that of migrated MM.1R. Through these different methodologies, I was able to confirm the presence of migrated MM cells within the EVS and hence confirm the robustness of the dynamic circulatory migratory model. On this

basis it shows myeloma cells can remarkably migrate through pore sizes of approximately 0.1μm, or around 1% of the cells' diameter. The ability of a cell to migrate through this narrow space is remarkable and is far smaller than documented in-vitro transwell migration work, where pore size of between 3-8μm is traditionally used. The static nature of the transwell assay, in addition to relatively large pore size makes it a less than ideal model for studying cell migration and in no way replicates leukocyte movement from blood to tissue or bone marrow to blood. In-vivo migration is a dynamic process of transendothelial migration through capillary beds, where cells first attach to an endothelial cell and move through the tight junction of a process termed diapedesis (Johnson-Leger et al. 2000), a process that is much more represented in our dynamic model, where shear force and HUVEC, allow for circulating cells to attach to the inner tube lining of the cartridge and from there, trans-migrate into the EVS, attracted by CXCL12 (SDF-1) secreting fibroblasts. Published studies investigating CXCL12 induced myeloma migration using transwells (Tai et al. 2012) have tended to see higher percentage migration, but using greater pore size (8μm), not much smaller than the average myeloma cell (11-13μm). Such transwell migratory studies should be interpreted with caution. The Fibercell reactor used in my studies represents a much more novel, more physiological accurate template for investigating migration. A pore size of 0.1μm infers cells that migrate must have a strong potency to do so.

The disadvantage of having such a small pore size for migration to occur through could be that overall migration is decreased, or that physical strain caused by the act of migration results in altered cell surface antigen expression and/or potential cell death. And is potentially a reason why there is a discrepancy between percentage migration between the two migratory models used. Syndacan-1/CD138 has an important role in cell adhesion, but is also known to be fragile, with expression loss over time (Bayer-Garner et al. 2001) and is shed quickly during early stages of apoptosis. I have shown that the cells migrated both in the Fibercell dynamic model and in transwell plates, have a lower expression of CD138. What I am unable to determine if this represents cell signalling changes related to cell migration, i.e. CD138 is required to be downregulated in order to migrate, thus forming CD138 weakly expressing sub-clones, which are known to exist in MM cell lines (Chen et al. 2016). Studies have shown that that CD138 (syndecan-1) is an important factor in mediating myeloma cell adhesion both directly and indirectly. Thus, in theory CD138 negative or weakly expressing clones would find it harder to attach to the endothelium, making it less likely and more difficult for the cell to transmigrate (Bayer-Garner et al. 2001). However, almost contradictory to this, the loss of its CD138 expression has been

shown to precede intravascular invasion and potentially increase the extramedullary spread of MM (Ridley et al. 1993; Rawstron et al. 1997). i.e. the loss of adhesive properties, releases the cell from its bone marrow microenvironment/attachment to stromal cells, thus allowing for cell migration into the peripheral circulation. The fact that MM.1S and MM.1R are derived from a plasma cell leukaemic phase of the disease (Goldman-Leikin et al. 1989), suggests that these cell lines, like the aforementioned CD138 negative clones lines, have lost their dependency from stromal cells in other ways.

A more likely explanation is that CD138 is being removed or shed from the cell surface either by enzymes from HUVECs lysates (such as heparinase) or simply being "ripped off" by the active process of migrating through a small pore. As already described in section 4.1.3.1, Syndacan-1 is routinely shed within the bone-marrow by heparinase, a known natural proteolytic enzyme that has been shown to be part of HUVECs lysates (Godder et al. 1991; Yang et al. 2007). This explanation is further supported by the fact CD138 expression of migrated MM cells can return back to baseline if re-cultured in media over 48h. Thus, suggestive that the expression changes are reversible and rejuvenation of CD138 occurs provided the correct conditions are present and that the explanation of CD138 loss of expression is not due to CD138 negative clones, but due to MM cell interaction with HUVEC and subsequent cleavage of CD138 by heparanase. Cell sorting MM.1S or MM.1R CD138 negative sub-clones and circulating these cells through the migratory model to see if migration increases could help disprove the CD138 negative migration theory, while measurement of heparinase activity either through an ELISA based assay or high-throughput sequencing/cDNA measurement (Rivara et al. 2016) of EVS substrate would help prove the heparinase activity theory.

The potential shedding of cell surface antigens such as CD138 raises the possibility of other cell surface antigens being shed and could make the interpretation of CXCR4 or CD49d expression of migrated MM cells more difficult and raise scepticism regarding any conclusions. This could be further confounded, as cell size is drastically altered by the act of migration compared to circulating cells (figure 4.4), smaller cell size can have fewer cell markers and thus result in reduce cell marker expression. However, as neither CD49d or CXCR4 expression was downregulated in cells retrieved from the EVS, this would infer that if shedding of CD138 does indeed occur, it appears to be isolated to just this antigen of the ones used in this thesis. Supportive of this point, there does not appear to be antigen loss for migrated CLL cells within the dynamic migratory model (Walsby et al. 2014c) and

hence strengthening the conclusion that the phenomena appear to be specific to MM expression of CD138.

The baseline or static culture difference in CD49d expression between MM.1S and MM.1R is an interesting occurrence. The functional differences of MM.1R compared to MM.1S, such as dexamethasone resistance, increased semi-adhesive properties to plastic and increased migratory potential would lead to believe MM.1R to have the greater CD49d expression of the MM.1 cell line, but it is MM.1S that has the marginally higher CD49d expression, although the difference was never proven to be statistically significant and it is worth noting migrated MM.1R cells retrieved from the EVS have a higher expression of CD49d than the circulating cells (i.e. expression upregulated), that is not observed in MM.1S, where expression levels remain comparable. It is possible MM.1R increased migratory potential compared to MM.1S could be related to its ability to upregulate CD49d expression when required. An additional means of investigating migratory differences and adhesive properties between the cell lines given more time and resources, would be for direct observation of migrating myeloma cells either by a BioFlux cellular light microscopy or in vivo optical imaging models (Runnels et al. 2011). Such models can include the use of fluorescence staining kits of key integrins like CD49d, allowing to directly observe expression differences related to either migration or adhesion to endothelial cells and what effects inhibitory agents such as Natalizumab have on adhesive and migratory properties.

Another interesting property of CD49d not fully explored in this thesis is its role in Cell Adhesion Mediated-Drug Resistance (CAM-DR). Although CD49d is unlikely to be implicated in MM.1 clonal dexamethasone resistance, with the mechanism of resistance widely believed be related to altered expression levels of the Glucocorticoid Receptor (Greenstein et al. 2003), it is plausible that CD49d may be involved in other MM.1 drug resistance/CAM-DR sub-clones, e.g. lenalidomide (Zhu et al. 2019).

Regardless of the subtle CD49d expression differences between the MM.1 cell lines, it remains a strongly expressed cell markers in MM cell lines and patients. Indeed around 85% of patients positively express the integrin, with treatment naïve patients tending to have higher expression and when in conjunction with negatively expressing CD45, exhibit a better prognosis (Suzuki et al. 2013). As to why this occurs is unknown, but the high expression, its important role in migration as well as its role in drug resistance/CAM-DR (Damiano et al. 1999), makes it a promising therapeutic target in myeloma. Despite this

fact, Natalizumab remains the only commercially available CD49d antagonist and its involvement in myeloma is very limited. A Phase I/II clinical trial in 2008 in relapsed/refractory multiple myeloma (RRMM) conducted by Biogen Idec (Identifier: NCT00675428) was terminated due to low enrolment and major concerns remain as to the potential side effects, notably PML. Because of the lack of other CD49d antagonists, it remains to be seen whether PML is specific to Natalizumab or potentially generic to any form of CD49d inhibition. And to add further complexities surrounding the actions of Natalizumab, my results have provided questions regarding the effectiveness of Natalizumab in inhibiting CD49d in MM cell lines, as expression was not affected, even at high doses of the antibody. Although Natalizumab (IgG4 subclass) and the CD49d immunofluorescence labelled antibody (IgG1 subclass) are different IgG subclasses (Leger et al. 1997), this should not have an impact in epitope competition on the assumption the antibodies were competing for the same binding site. In transwells experiments, migration only started to be inhibited (not significantly) at a supratherapeutic dose of 10μM (clinical concentration for Multiple Sclerosis roughly 0.4μM). At this dose, CD49d binding sites should have been fully saturated, preclinical studies showed a single dose of 35nM, α4-integrin saturation was above 90% and decreases slowly in a dose related manner, with a half-life of between 60-90h (Leger et al. 1997). Therefore, assuming that Natalizumab potency was intact, is it likely the binding epitopes of Natalizumab and the CD49d immunofluorescence labelled antibody are different, therefore not in competition. Though it is worth noting data from multiple sclerosis patients receiving Natalizumab showed up to a 50% decrease in PBMC CD49d expression (using the same CD49d antibody clone – 9F10, as used in this study), in most but not all patients. This was maintained after a number of repeated infusions (Defer et al. 2012).

The addition of an endothelial layer (HUVEC) into the dynamic circulatory migratory model, appears to be fundamental in allowing MM cells to migrate, as it provides a surface for the cells to adhere to and subsequently actively migrate. This is possibly why a discrepancy between the migratory models with single agent Natalizumab was observed. As the transwell migration model, not including HUVEC, observed no decrease in migration, whereas the dynamic circulatory model which did include HUVECs, observed a decrease in migration (albeit non-statistical). This would help to explain why Podar et al has showed MM.1S adhesion to fibronectin and endothelial cells is inhibited by Natalizumab at doses lower than used in the transwell (1μg/ml). Podar et al. showed transwell migration was also inhibited at a dose of 1μg/ml, but only with the addition of bortezomib and on fibronectin layer above the transwell membrane (Podar et al. 2001).

Although the study confirmed the MM.1S expression of CD49d by flow cytometry analysis, no mention was made of Natalizumab reducing expression on any of the myeloma cell lines (including MM.1S). These results strongly confirm the requirement of a fibrin contact for MM.1S to adhere allowing migration and that CD49d plays a key role as an integrin in allowing adhesion.

Limited clinical data of Natalizumab use in myeloma patients exists, therefore it is difficult to predict at what concentrations effective migration inhibition will start to occur, especially as myeloma cells have higher expression of CD49d than healthy lymphocytes. which can further increase with acquired drug resistance (Suzuki et al. 2013). Regardless, pharmacokinetics of the drug in healthy individuals are likely to be comparable to myeloma patients. On this presumption, concentration of 1μM (as used in this chapter and greater than the clinical use concentration) of the antibody is sufficient to fully saturate CD49d antigen for 48 hours. Despite CD49d important role in migration and also as a prognostic factor in a number of B-cell malignancies (Shanafelt et al. 2008; Bulian et al. 2014), it is still unclear whether inhibition in cell migration would correspond in prevention of clonal expansion and ultimately improved PFS/OS. Sadly, as CD49d antagonist research is limited with no new drugs coming into clinical trials, in addition to the toxicity concerns of Natalizumab (notably PML) and the discovery of developing anti-natalizumab antibody development (titres up to 1800 μg/ml within 2-3 weeks after administration in primate toxicology studies), the likelihood of CD49d therapy in MM in the near future remains remote.

I successfully showed that ONO-7161 inhibits expression of CXCR4 at low concentrations (1nM), an hour after exposure, with effects still seen after 48h. Its effects appear more potent that plerixafor, where CXCR4 expression was reduced at 6h after exposure of 50μM with effects worn off by 24h (Azab et al. 2009b). Azab et al. have extensively investigated the effect of plerixafor at a dose of 50μM on the cell line MM.1S. Their data suggested when used in combination with bortezomib, it can overcome drug resistance induced by bone marrow stromal cells (BMSC), disrupt adhesion to fibronectin by up to 50%, and significantly inhibit migration in response to CXCL12. Although I have not undertaken adhesion assays, the presumption as with CD49d, is that the ONO-7176 effect on migration is maximised when an endothelial platform is applied to the model. Azab et al data suggests that by inhibiting CXCR4, not only are myeloma cells homing signals lost, but also a mechanism of cell adhesion. The lack of HUVECs within the transwell experiment as for Natalizumab maybe why a reduction in migration was only seen at very

high concentrations of ONO-7161 and surprisingly only for MM.1R. However, minimal CXCR4 expression differences between the two cell lines (MM.1S marginally greater) are observed and another possible explanation for this could be related to the uninhibited receptor CXCR7, a recently discovered additional receptor to CXCL12, that has been shown to be involved in the CXCL12-CXCR4 migration axis and whose inhibition has shown to disrupt MM cell trafficking in the MM.1S cell line (Azab et al. 2014). Measuring CXCR7 receptor expression differences between the two cell lines in transwell experiments would therefore be informative in explaining why only MM.1R migration is affected at higher ONO-7161 concentrations.

Another slightly surprising observation concerning ONO-7161 experiments and CXCR4 expression, was that CXCR4 expression appeared to increase back to baseline at higher drug concentrations (50μM and 100μM – figure 4.15). Presuming that this is a genuine phenomenon and not due to auto-fluorescence or background artefact/signal, this could be related to off target effects, or cell self-upregulation of CXCR4 expression. The cytotoxic effects of the drug start to be observed at 50μM, as higher doses it is possible off-target effects are resulting in cell death, which result in up-regulation of CXCR4 expression, a phenomenon which has been described in AML cell lines (Sison et al. 2013). Unfortunately, no pharmaceutical data exists as to how ONO-7161 works. The suggestion of possible off target effects and cytotoxicity suggests that the drug is likely internalised as a small molecular inhibitor rather than inhibiting the antigen on cell surface.

Alsayed et al. (Alsayed et al. 2007) gave rise to the phrase "dynamic regulation of the CXCR4 receptor", whereby expression of CXCR4 of myeloma cells in the peripheral blood is high but decreases once in the bone marrow where high levels of CXCL12 exist. This contributes to the retention of myeloma cells in the marrow, thus preventing further trafficking. Indeed, this likely explains why there is an apparent decrease in CXCR4 expression when comparing static cell line expression to those in circulation (figure 4.20). The latter cells, exposed to CXCL12, would result in the internalisation of the CXCR4 receptor and thus decrease in expression. However, my migratory expression results are seemingly in contrast to this theory, whereby migrated cells in the EVS have a higher expression of CXCR4. Myeloma cell CXCR4 expression levels are notoriously variable, with other studies giving conflicting results (Hideshima et al. 2001; Moller et al. 2003). My results suggest that migrated cells in the confines of high CXCL12 concentration, do not downregulate CXCR4 expression, but expression is seemingly upregulated in the direction of migration. This is supported by the bimodal CXCR4 expression identified in EVS

retrieved myeloma cells. Serial sampling of CXCR4 expression within migrated cells and attempted cell sorting and cell culturing of the higher CXCR4 expressing population would help establish the existence of CXCR4 sub-clones or whether the occurrence is due to receptor upregulation that allows for migration. Again, it should be noted that my work is on two closely-related cell lines and that true representation could only be obtained by circulating numerous primary myeloma samples. The variability observed in CXCR4 expression amongst primary samples could easily be down to the interaction of different clones, sub-clones, all having different migratory potential. This theory is supported by my own work, where MM.1S^{dim}, MM.1S^{bright} and MM.1R all have varying CXCR4 expression, but all originate from the same patient (see chapter 4). Unlike CD49d, CXCR4 antagonists are at a much more developed stage, with numerous CXCR4 inhibitors already available, all claiming to be more potent than Plerixafor. CXCR4 inhibition in cancer is not exclusive to myeloma, or even other blood cancers (CLL and AML), but is being investigated in solids tumours such as breast cancer (Kang et al. 2005). Inhibitors include other small molecular inhibitors, peptidomimetics and even mono-clonal antibodies (Kashyap et al. 2016; Peng et al. 2016; Abraham et al. 2017) and remain a promising target of inhibition in MM patients.

However, it was not until combination of CD49d and CXCR4 inhibitors within a dynamic migratory model involving shear force (as opposed to transwells), that a statistical reduction in CXCL12-induced MM migration was observed. As with many other forms of MM therapies, it is unclear whether such inhibition could potentially lead to the selection of sub-clones that could escape such inhibition, part of the tidal clones concept (Keats et al. 2012). Indeed, immunophenotypic and/or genetic analysis of the small number of migrated cells retrieved from the EVS where pharmacological inhibition of CXCR4 and CD49d occurred, could determine if such migrated cells are distinct sub-clone that had escaped such inhibition. However, analysis proved difficult due to small cell numbers of migrated cells retrieved from the EVS (on average $<0.1x10^6$ cells in total) in the ONO-6171 and Natalizumab treated experiments. To highlight this point, figure 4.21 shows the difference in cell numbers between 100µl analysed samples of ONO-7161 and Natalizumab treated MM.1R cells in the circulatory compartment at 48h (17,911 events, figure 4.21A) and the EVS at 48h (251 events, figure 4.21B).

In summary, I have shown a potent regimen in preventing MM migration, with the possibility of halting disease progression. A question still remains how migration inhibitors like the ones used in this chapter could be introduced into therapeutic use. A

plausible treatment strategy would be in combination with cytotoxic agents such as bortezomib. Pre-clinical studies have combined similar migratory inhibitors with bortezomib, resulting in additional and synergistic effects on cell cytotoxic and migration (Podar et al. 2001; Ghobrial et al. 2014).

CHAPTER 5:

Phenotypic and genetic analysis of MM.1S sub-populations

5.1 Introduction

The concept of clonal tiding in the field of MM research has become topical over the last few years. The theory is that at diagnosis there are multiple cancer clones either co-existing or competing for survival. Over the course of the disease, clonal selection occurs, usually in response to treatment. Ultimately, this results in the dominance of more treatment-resistant clones that culminates in treatment failure (Keats et al. 2012).

Understanding the pathology of MM and the testing of therapeutic agents has relied heavily on cell lines due to the inability to sustain myeloma plasma cells in long-term *in vitro* culture. The cell lines MM.1S and MM.1R have been extensively used in the field of myeloma research as they provide an isogenic model for the development of glucocorticoid drug resistance. They originate from the same parental cell line (MM.1), derived from the peripheral blood of a female patient with a t(14:16) IgA lambda Plasma cell leukaemia. This cell line carried a number of gene mutations including *CDKN2, KRAS* and *TRAF3* but was originally sensitive to dexamethasone (Moalli et al. 1992). In the 1990's Steve Rosen's laboratory, based at Northwestern University, Chicago, created a dexamethasone resistant cell line from MM.1 by exposing the cells to continuous low dose dexamethasone in cell culture for 3 months. Greenstein et al. showed when the cell line was exposed to dexamethasone, it started to express modified GR mRNA, a variant of which being the hGR-P mRNA, known to be present in a number of blood cancers (Greenstein et al. 2003). After 3-4 months of growth in dexamethasone, the cell line was found to no longer express either mutant GR mRNA or its wildtype GRα (the predominant isoform). This cell line, termed MM.1R, then became commercially available (Sánchez-Vega et al. 2006) and subsequently become a much-studied model of glucocorticoid resistance, focusing on altered GR expression, coded by its gene *NR3C1* (Greenstein et al. 2003; Edwards V et al. 2012). DNA microarray comparison between the MM.1S and MM.1R revealed 12 gene expression changes that were shared. 11 upregulated genes included;

FKBP5I, *GILZ*, growth factor receptor genes for TGF-β and IL-6, enzymes α-2 6-sialyltransferase and prolyl 4-hydroxylase, *IGSG20* (interferon stimulated gene 20) and the apoptosis-related gene *VDUPI*. Only one gene was downregulated, *BCL2L1*, which codes for the anti-apoptotic protein bcl-xL, a member of the Bcl-2 family (Boise et al. 1993). Table 5.1 provides an overview of the genetic comparisons between the two cell lines from Greenstein et al and Edwards V et al.

CGH[1]	mRNA[1]	DNA Microarray[2]	Whole exome Sequence[1]
MM.1R deletion: • chr2:p37.1-37.3 • chr4:q32.3-33 • chr5:31.3 • ? homozygous deletion of *NR3C1* MM.1R amplification: • chr7:q36.3	63 genes with differing expression • *NR3C1* decreased in MM.1R • *MGST1* largest difference, (increase in MM.1R)	Shared expression changes • Increase 11 genes (see text) • Decrease 1 gene *(BCL2L1)* Increase expression in MM.1R; • *BTK, HLSP-1, MIC, HSP28, HSP72, Ubiquitin*	Shared mutations; • 208 non-synonymous mutations (not present in 1KGP) MM.1R mutations; • *PDIA5, TCERG1, ERN1, RANBP9, MMS22L, PHF19, PIGT, AURKB, RNMTL1, GPCPD1*

Table 5.1. Summary of genetic differences between MM.1S and MM.1R *from Edwards V et al and Greenstein et al.; CGH - Comparative genomic hybridisation (copy number differences). [1](Edwards V et al. 2012); [2](Greenstein et al. 2003);*

Although cellular and genetic characterisation of MM.1S and MM.1R has been published, none of the previous studies interrogated these cell lines using polychromatic flow cytometry, next generation sequencing or explored the sub-clonal selection process, a concept (clonal tiding) now widely recognised as a mechanism of drug resistance amongst treated patients (Goldman-Leikin et al. 1989; Greenstein et al. 2003; Keats et al. 2012). Furthermore, the introduction of molecular targeted treatments, including anti-CD38 monoclonal antibodies such as daratumumab (de Weers et al. 2011), make it more likely that resistance will emerge due to the selection of CD38 negative or CD38 weakly expressing sub-clones. Therefore, the availability of CD38 negative/weak sub-clones may be increasingly important in order to provide further insight into the function of the CD38 antigen in MM disease progression and drug resistance.

In both this chapter and the next, I describe the phenotype, function and genotype of the MM.1S and MM.1R cell lines in order to explore the origins of the glucocorticoid drug resistance manifested by MM.1R cells. In addition, I explored the sub-clonal architecture of each cell line and in the next chapter will demonstrate how functional genomics can be

used to preferentially target molecular pathways that are differentially expressed in sub-clonal populations.

The main aims of this chapter were as follows:

i. Determine whether the two distinct $CD38^{bright}$ and $CD38^{dim}$ expressing sub-populations in the MM.1S cell line showed phenotypic and functional differences.
ii. Use whole genome sequencing to establish whether $CD38^{bright}$ and $CD38^{dim}$ expressing sub-populations in the MM.1S cell line are genetically distinct sub-clonal populations.
iii. Explore whether comparative genomics can be used to determine the origin of the glucocorticoid resistance cell line MM.1R.

5.2 Discovery of MM.1S as a potential model of the study of CD38 sub-clonal populations in MM

5.2.1 Differential CD38 expression identifies two phenotypically distinct sub-populations within the MM.1S cell line

As described in chapter 3, the MM.1S cell line demonstrated a bimodal CD38 expression, with a 1.5 log difference in CD38 expression between the two populations (Figure 5.1A). In contrast, the MM.1R cell line was uniformly CD38 bright, with expression being a further 0.5 log higher than MM.1S^{bright} sub-population. The CD38 MFI of the two cell lines in the overlay histogram in figure 5.1A was 60,653 for MM.1R compared to 26,488 for MM.1S. In contrast, the distinct CD38 sub-populations both showed uniformly high expression of CD138, consistent with plasma cells (Figure 5.1B).

Upon receiving the MM.1S cell line from the commercial cell bank ATCC, the minority CD38^{dim} population contributed around 16% of the total cell line with the CD38^{bright} population around 74% (Figure 5.1B). Over subsequent cell passages (4-5), the proportion of the CD38^{dim} population reduced to less than 5% (Figure 5.1C). The rate of CD38^{dim} loss to less than 5%, was found to be even greater (2-3 passages) if only adherent cells to plastic were passaged (i.e. cells in suspension were discarded). Thus, implying different adhesion properties of the CD38 sub-populations in addition to possibly different proliferation capacities.

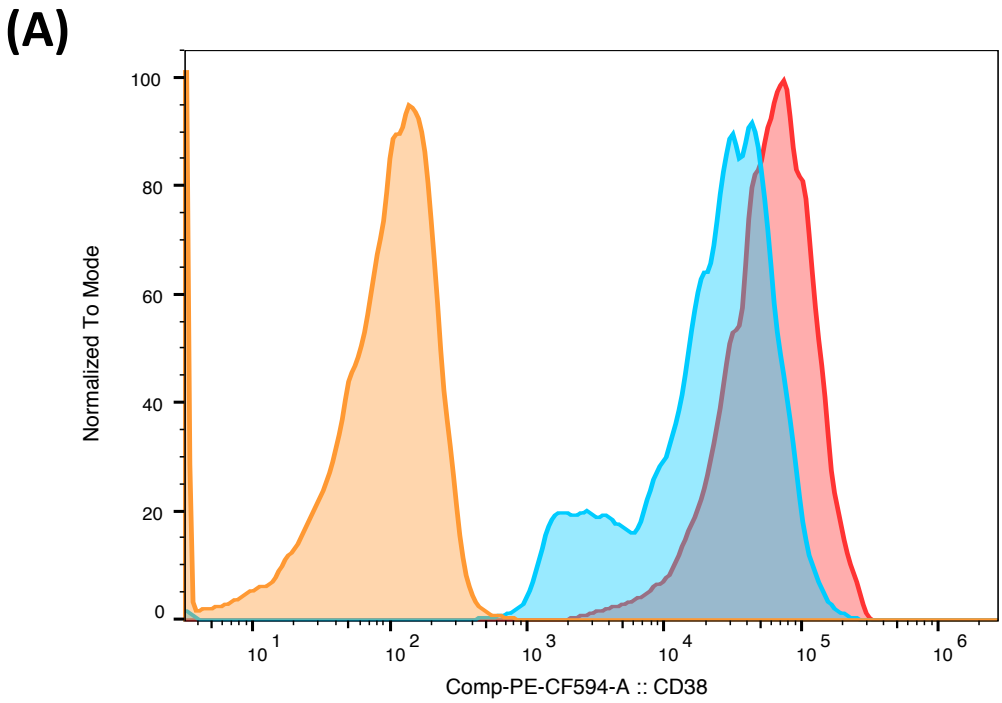

	Subset Name with Gating Path	Count	CD38+ :: Freq. of Parent	Median : Comp-PE-CF594-A	Mean : Comp-PE-CF594-A
	MM1S_Unstained_012.fcs/Alive Cells/Single Cells	6759.0	0.4	89.3	102.3
	MM1S_stained_013.fcs/Alive Cells/Single Cells	6901.0	99.7	26488.4	32211.9
	MM1R_stained_019.fcs/Alive Cells/Single Cells	11530.0	100.0	60652.6	70100.6

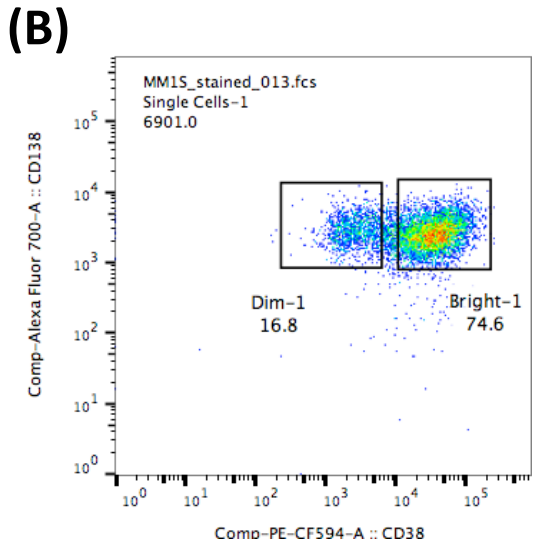

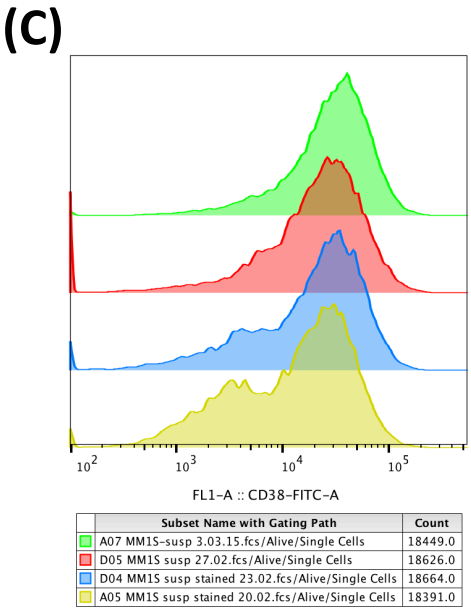

	Subset Name with Gating Path	Count
	A07 MM1S-susp 3.03.15.fcs/Alive/Single Cells	18449.0
	D05 MM1S susp 27.02.fcs/Alive/Single Cells	18626.0
	D04 MM1S susp stained 23.02.fcs/Alive/Single Cells	18664.0
	A05 MM1S susp stained 20.02.fcs/Alive/Single Cells	18391.0

Figure 5.1. Flow cytometry dot plots and overlaid histograms of CD38 expression in the MM.1 cell lines. *(A) Overlaid histograms of CD38 expression, as measured on BD Fortessa, comparing MM.1S and MM.1R and unstained MM.1S; legend states CD38 MFI and percentage positivity. (B) Bivariate dotplot of CD38 and CD138 expression on MM.1S cells, highlighting the percentage contribution of the different CD38 expression populations and the invariant expression of CD138. (C) Shows the loss of the CD38^{dim} population in adherent MM.1S from same culture flask over 14 days. Bottom histogram (yellow) shows CD38 expression of newly acquired MM.1S cells from the ATCC cell repository. Sequential CD38 expression on adherent cells from the same flask; blue histogram +3 days, red histogram +7 days, green histogram +14 days.*

5.2.2 CD38^{bright} expression is a surrogate marker of increased dexamethasone resistance within the MM.1S cell line

Figure 5.2 shows that when MM.1S was exposed to increasing concentrations of dexamethasone, MM.1S CD38^{bright} cells were significantly more resistant to dexamethasone than the MM.1S CD38^{dim} cells (LD_{50} values 62nM v 29nM respectively; p=0.002).

To establish whether the CD38^{bright} sub-population was inherently more resistant to other anti-myeloma therapies, the cell lines were exposed to the proteasome inhibitor, Bortezomib. In contrast to dexamethasone exposure, these subsets showed no significant difference in drug sensitivity (p=0.43; Figure 5.3B). Similar to MM.1S subsets comparison, no difference in Bortezomib resistance was observed between MM.1R and MM.1S (p=0.31; Figure 5.3A).

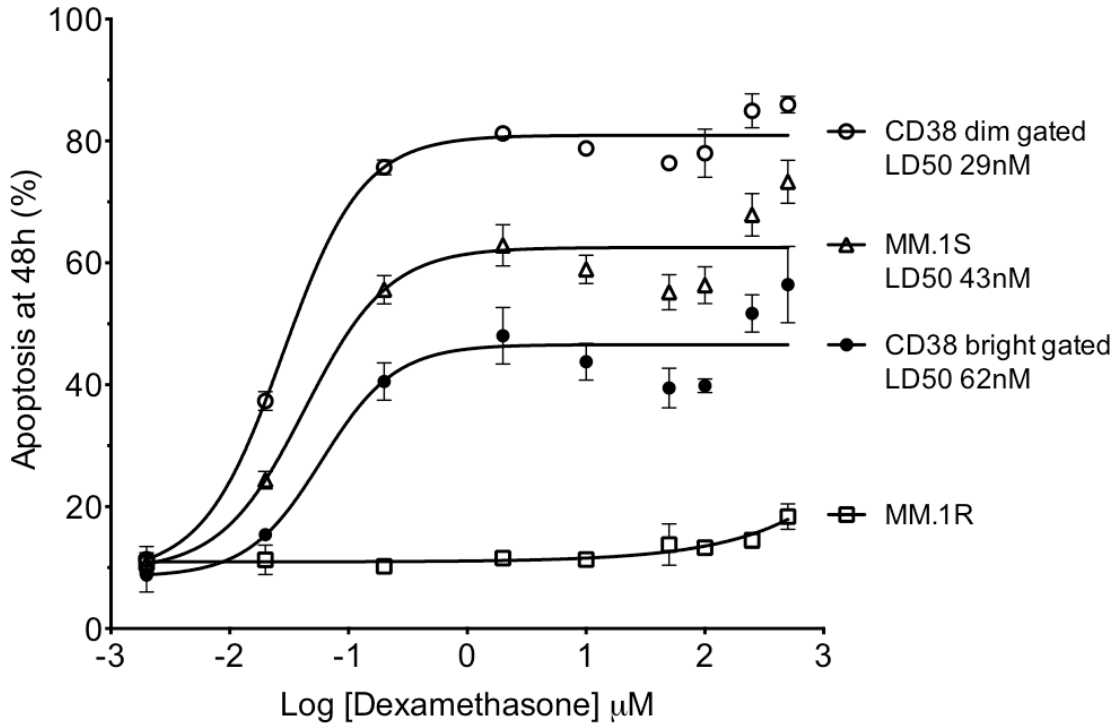

Figure 5.2. Dexamethasone cytotoxic assays *in MM.1S cells, CD38 gated sub-populations (CD38^{bright} and CD38^{dim}) and MM.1R. Cells were exposed to increasing concentrations of dexamethasone for 48h. Cells were then stained with Annexin V, propidium iodide and allophycocyanin-labelled anti-CD38 antibody to enable apoptosis analysis in the CD38^{bright} and CD38^{dim} sub-populations (n=3). Analysis was performed on a BD Accuri flow cytometer using CFlow software. In every experiment, 30,000 events were recorded to ensure adequate accumulation of events in the minority MM.1S CD38^{dim} subset. Paired Wilcoxon non-parametric t-tests were used for comparison of individual LD_{50} values. Error bars indicate mean with SD and are calculated by repeated independent experiments.*

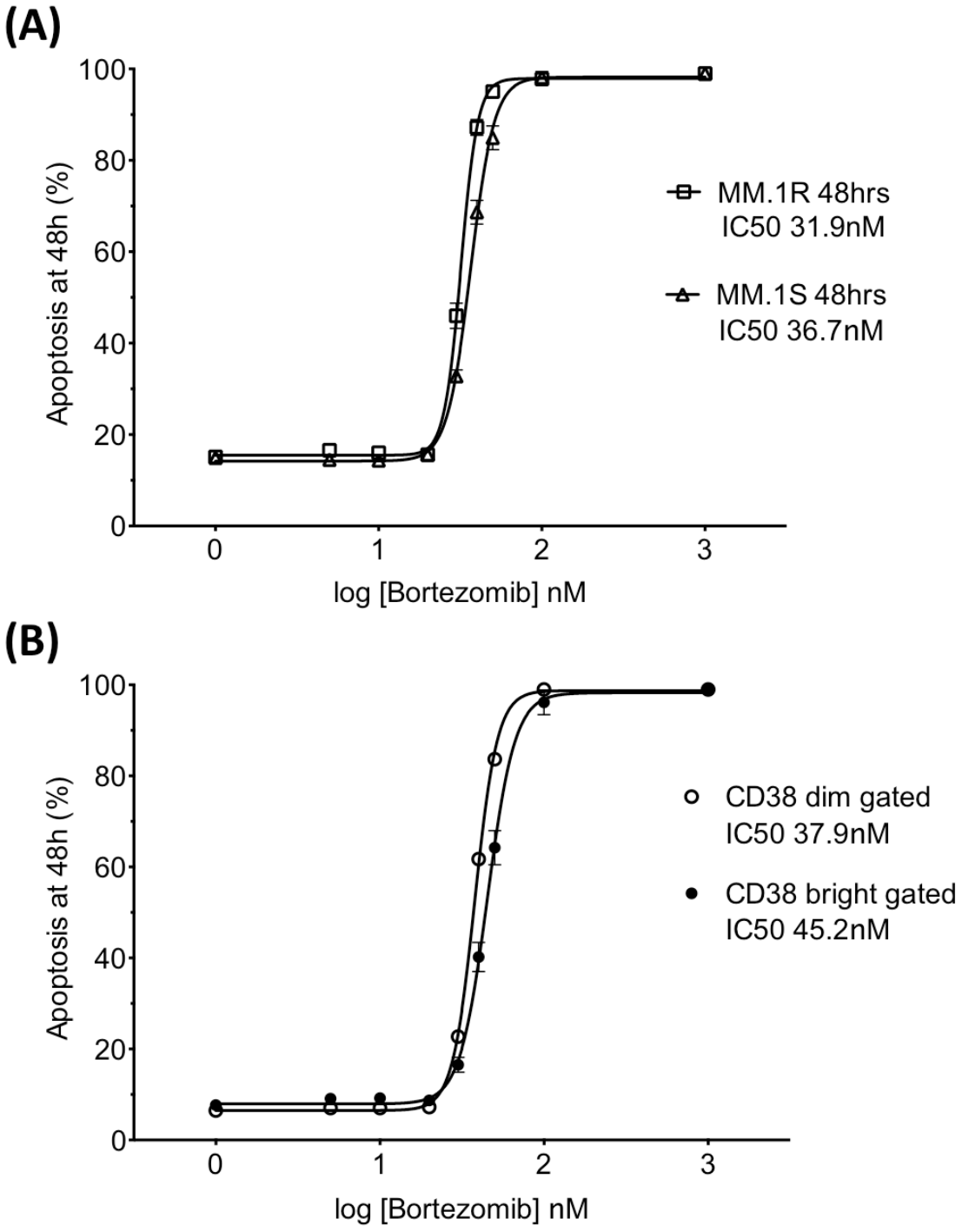

***Figure 5.3*. Bortezomib cytotoxic assays**, *comparison of (A) MM.1S and MM.1R and (B) CD38 gated subsets of MM.1S ($CD38^{bright}$ and $CD38^{dim}$). In all experiments, Cells were exposed to increasing concentrations of bortezomib for 48h. Cells were then stained with Annexin V, propidium iodide and allophycocyanin-labelled anti-CD38 antibody to enable apoptosis analysis in the $CD38^{bright}$ and $CD38^{dim}$ sub-populations (n=3). Analysis was performed on a BD Accuri flow cytometer using CFlow software. In every experiment, 30,000 events were recorded to ensure adequate accumulation of events in the minority MM.1S $CD38^{dim}$ subset. Paired Wilcoxon non-parametric t-tests were used for comparison of individual LD_{50} values. Error bars indicate mean with SD and are calculated by repeated independent experiments.*

5.2.3 To further explore sub-clone characteristics, CD38 sub-populations were isolated by FACS

$CD38^{bright}$ and $CD38^{dim}$ subsets were purified using fluorescence-activated cell sorting (FACS) to allow a more comprehensive phenotypic, functional and genetic analysis. Figure 5.4A shows the gating strategy used for the FACS purification. Figure 5.4B shows the CD38 expression of the two MM.1S sub-populations post purification, together with MM.1R CD38 expression. The brightly expressing CD38 purified population was termed $MM.1S^{bright}$ cells, with the dimly expressing CD38 population termed $MM.1S^{dim}$ cells. Statistical significance of CD38 expression between the two purified population was confirmed ($p<0.0001$), with over 1 log difference in expression (MFI 21,828 vs 1,254). As for comparison, MM.1R had a further 0.5 log higher CD38 expression compared to $MM.1S^{bright}$ (MFI 60,744, $p=0.0002$). Despite the reduced CD38 expression of $MM.1S^{dim}$, the population still retained 62.8% positive expression relative to unstained control (Table 5.1).

It was subsequently discovered over a period of 14 days post cell sorting (5-6 passages), the $CD38^{bright}$ population started to re-emerge within the purified $MM.1S^{dim}$ culture. The percentage of cells within the $CD38^{bright}$ gate had risen to 23.2% by passage 5 and further increased to 50.5% after an additional 14 days in culture or 5 cell passages (Figure 5.4C). Therefore, two further cell purification techniques were performed using more stringent CD38 gating. This ensured purer, more distinct CD38 expressing populations that were maintained up to six successive passages or roughly 14 days (Figure 5.4D).

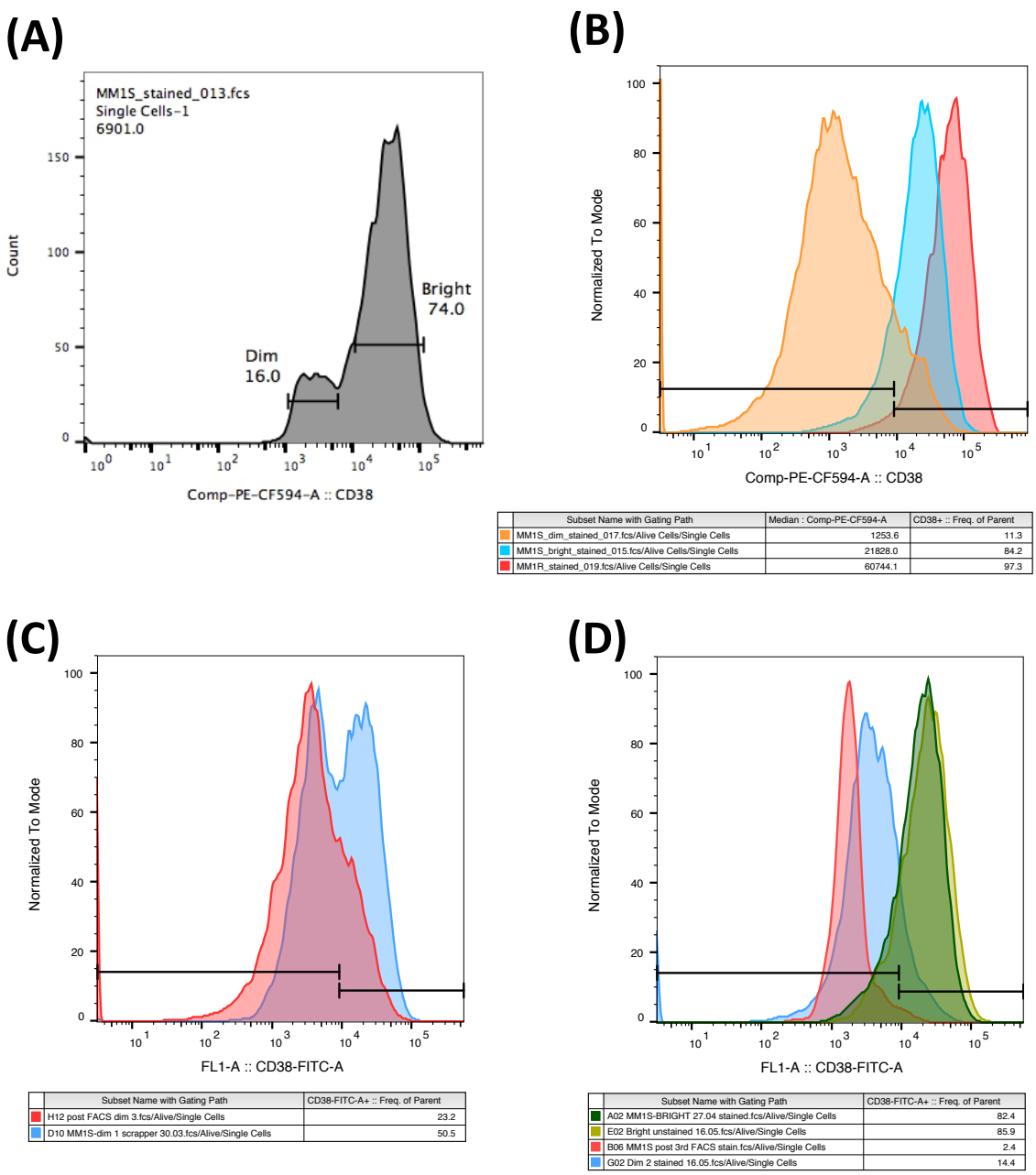

Figure 5.4. *Flow cytometry overlaid histograms of CD38 expression in the MM.1 cell lines. (A) Gating strategy used for FACS on BD FACSAria cell sorter, 10x10^6 MM.1S cells were immuno-stained with CD38 conjugated with PerCP-Cy5.5. (B) Post the first sort, overlaid histograms comparing CD38 expression of MM.1S^{dim}, MM.1S^{bright} and MM.1R, legend records CD38 MFI (median) as well as population frequency within CD38^{bright} gate. (C) Overlaid histograms comparing MM.1S^{dim} CD38 expression of cells from same culture flask 14 days apart post first sort, population frequency within CD38^{bright} gate increased from 23.2% to 50.5%, with re-emergence of CD38^{bright} subset. (D) CD38 histograms with legend stating % frequency of CD38+ population. After 3 consecutive cell sorting, CD38 expression overlaid histograms of MM.1S^{bright} and MM.1S^{dim}, comparing CD38 expression immediately post third sort (indicated on legend as A02-MM.1S^{bright} and B06-MM.1S^{dim}) with 14 days later (indicated on legend as E02-MM.1S^{bright} and G02-MM.1S^{dim}). MM.1S^{bright} CD38 expression mirror each other (population frequency within CD38^{bright} gate remained stable, 82.4% to 85.9%) with no evidence of re-emergence of CD38^{dim} subsets. MM.1S^{dim} CD38 expression did not increase at the rate seen post the first sort, with no evidence of re-emergence of CD38^{bright} subset over 14 days period post third sort (population frequency within CD38^{bright} gate increased from 2.4% to 14.4%).*

5.3 Immunophenotypic analysis of MM.1S CD38 expressing sub-clones reveals additional heterogeneity in antigen expression

Having isolated the two distinct CD38 expressing MM.1S populations, extended immunophenotypic analysis was undertaken to identify any additional immunophenotypic differences. The same 10-colour flow cytometry panel as described in Chapter 3 showed the two populations to be immunophenotypically similar (figure 5.5-5.7). The main exception to this being CD38 expression (figure 5.5 and 5.7) as already described, but also the percentage positivity of the nuclear-specific cell proliferative marker, Ki-67. MM.1S^{bright} showed a statically significant higher Ki-67 percentage positivity compared to MM.1S^{dim} (1.72% (SD±0.13) vs 1.00% (SD±0.29), p=0.0021). Conversely no statistical difference (p=0.73, n=5) was observed between MM.1S (1.58% SD±0.13) and MM.1R (1.54% SD±0.11) in Ki-67 percentage positivity.

Overlay histograms (Figure 5.5 and 5.6) showed subtle expression differences the two populations, MM.1S^{bright} had mildly increased expression compared to MM.1S^{dim} in the migration marker CXCR4 (p=0.87) and reduced expression in CD56 (p=0.52) and the integrin CD49d (p=0.21), although none of the differences were significant (n=3).

Table 5.2 shows the 10 cell markers' average MFI (n=3) and percentage positivity (relative to unstained control) of the two CD38 purified populations compared to MM.1R. Although the majority of cell marker expression were all similar, MM.1S^{dim} CD49d expression (11,764) was higher than both MM.1S^{bright} (10,574) and MM.1R (7,169), the latter being statistically significant (p=0.031).

Antigen	Fluorochrome	MM.1R		MM.1S^{bright}		MM.1S^{dim}	
		MFI	%	MFI	%	MFI	%
CD138	Alexa Fluor 700	6,052	99.8	2,539	99.7	3,061	99.3
CD38	PE-CF594	16,192	100	6,873	99.6	801	62.8
CD19	PerCP-Cy5.5	616	87.0	333	50.0	255	11.3
CD45	APC	118	0.8	73	0.7	104	0.2
CD56	PE	2,491	89.8	1,613	83.6	2,164	86.1
CD49d	BV510	7,169	98.4	10,574	99.5	11,764	99.1
IL-6	V450	829	18.1	870	30.8	844	7.9
CXCR4	PE-Cy7	1,947	100	1,903	100	1,722	99.7
MMP-9	FITC	669	27.3	580	26.8	711	8.8
Ki-67	BV605	2,847	1.7	3,405	1.7	3,453	1.0

Table 5.2. *Mean Fluorescence intensity (MFI) and percentage positivity (referenced to negatively stained sample) of 10 separate cell markers within same flow cytometry panel). Analysis of 10,000 events on BD Fortessa of freshly passaged cell lines. Results are average of 3 separate analysis, n=3.*

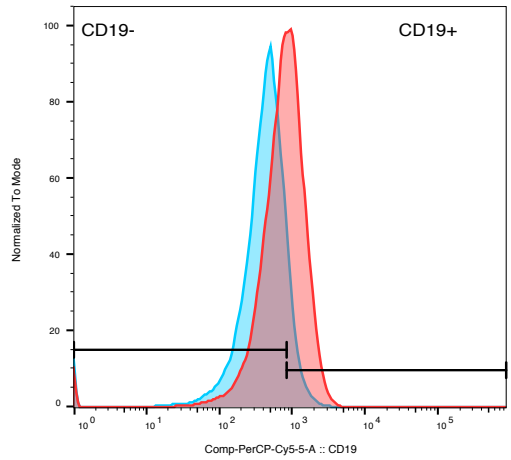

Sample Name	Median : Comp-PerCP-Cy5-5-A	Mean : Comp-PerCP-Cy5-5-A	CD19+ :: Freq. of Parent
MM1S_bright_stained_015.fcs	797.0	894.2	50.0
MM1S_dim_stained_017.fcs	448.2	500.8	11.3

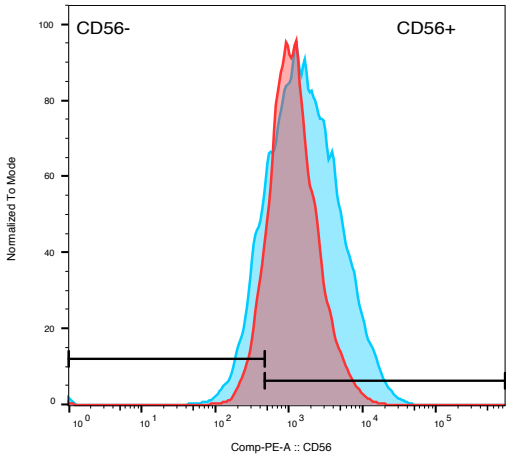

Sample Name	Median : Comp-PE-A	Mean : Comp-PE-A	CD56+ :: Freq. of Parent
MM1S_bright_stained_015.fcs	1093.3	1574.6	89.7
MM1S_dim_stained_017.fcs	1484.8	2788.3	86.1

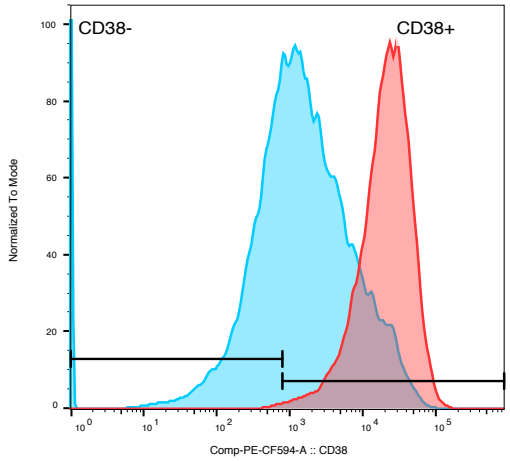

Sample Name	Median : Comp-PE-CF594-A	Mean : Comp-PE-CF594-A	CD38+ :: Freq. of Parent
MM1S_bright_stained_015.fcs	21837.5	25774.3	99.6
MM1S_dim_stained_017.fcs	1253.1	3969.4	62.8

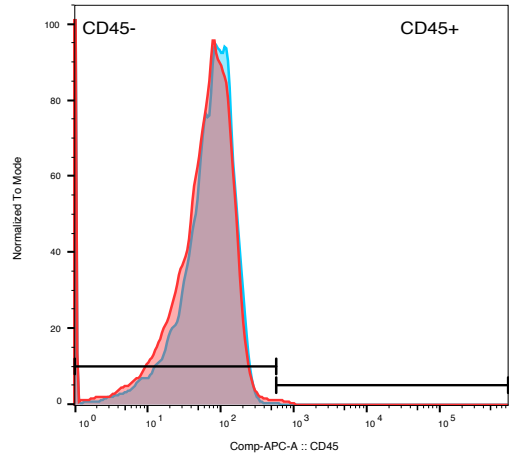

Sample Name	Median : Comp-APC-A	Mean : Comp-APC-A	CD45+ :: Freq. of Parent
MM1S_bright_stained_015.fcs	55.8	68.9	0.7
MM1S_dim_stained_017.fcs	69.3	79.3	0.2

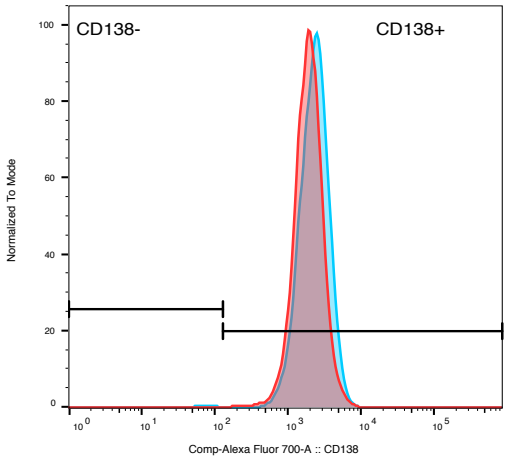

Sample Name	Median : Comp-Alexa Fluor 700-A	Mean : Comp-Alexa Fluor 700-A	CD138+ :: Freq. of Parent
MM1S_bright_stained_015.fcs	1931.2	2091.0	99.7
MM1S_dim_stained_017.fcs	2326.7	2484.8	99.3

Figure 5.5. Overlaid histograms comparing the expression of 5 different MM cell markers *between MM.1S^{dim} and MM.1S^{bright}. Analysis done on BD Fortessa, MM.1S^{dim} 13,920 events counted and MM.1S^{bright} 13,198 events counted. Histograms were normalised to the mode to make expression of the cell lines comparative with individual legend stating Mean and Median Fluorescence Intensity and percentage positivity relative to negatively stained control indicated by black split marker.*

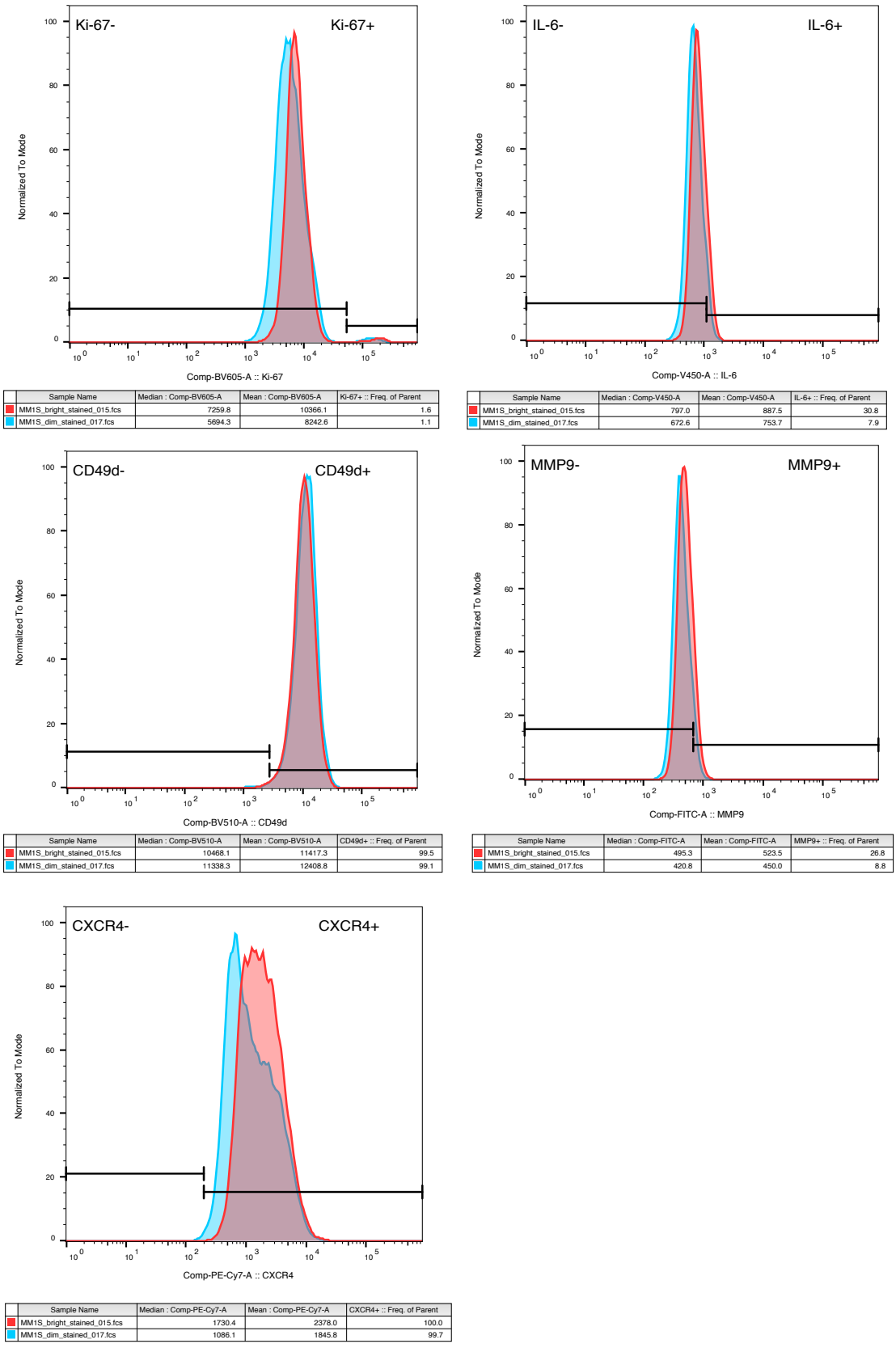

Sample Name	Median : Comp-BV605-A	Mean : Comp-BV605-A	Ki-67+ :: Freq. of Parent
MM1S_bright_stained_015.fcs	7259.8	10366.1	1.6
MM1S_dim_stained_017.fcs	5694.3	8242.6	1.1

Sample Name	Median : Comp-V450-A	Mean : Comp-V450-A	IL-6+ :: Freq. of Parent
MM1S_bright_stained_015.fcs	797.0	887.5	30.8
MM1S_dim_stained_017.fcs	672.6	753.7	7.9

Sample Name	Median : Comp-BV510-A	Mean : Comp-BV510-A	CD49d+ :: Freq. of Parent
MM1S_bright_stained_015.fcs	10468.1	11417.3	99.5
MM1S_dim_stained_017.fcs	11338.3	12408.8	99.1

Sample Name	Median : Comp-FITC-A	Mean : Comp-FITC-A	MMP9+ :: Freq. of Parent
MM1S_bright_stained_015.fcs	495.3	523.5	26.8
MM1S_dim_stained_017.fcs	420.8	450.0	8.8

Sample Name	Median : Comp-PE-Cy7-A	Mean : Comp-PE-Cy7-A	CXCR4+ :: Freq. of Parent
MM1S_bright_stained_015.fcs	1730.4	2378.0	100.0
MM1S_dim_stained_017.fcs	1086.1	1845.8	99.7

Figure 5.6. Overlay histograms comparing the expression of 5 different MM cell markers *(related to adhesion, migration and proliferation) between MM.1S^{dim} and MM.1S^{bright}. Analysis done on BD Fortessa, MM.1S^{dim} 13,920 events counted and MM.1S^{bright} 13,198 events counted. Histograms were normalised to the mode to make expression of the cell lines comparative with individual legend stating Mean and Median Fluorescence Intensity and percentage positivity relative to negatively stained control indicated by black split marker.*

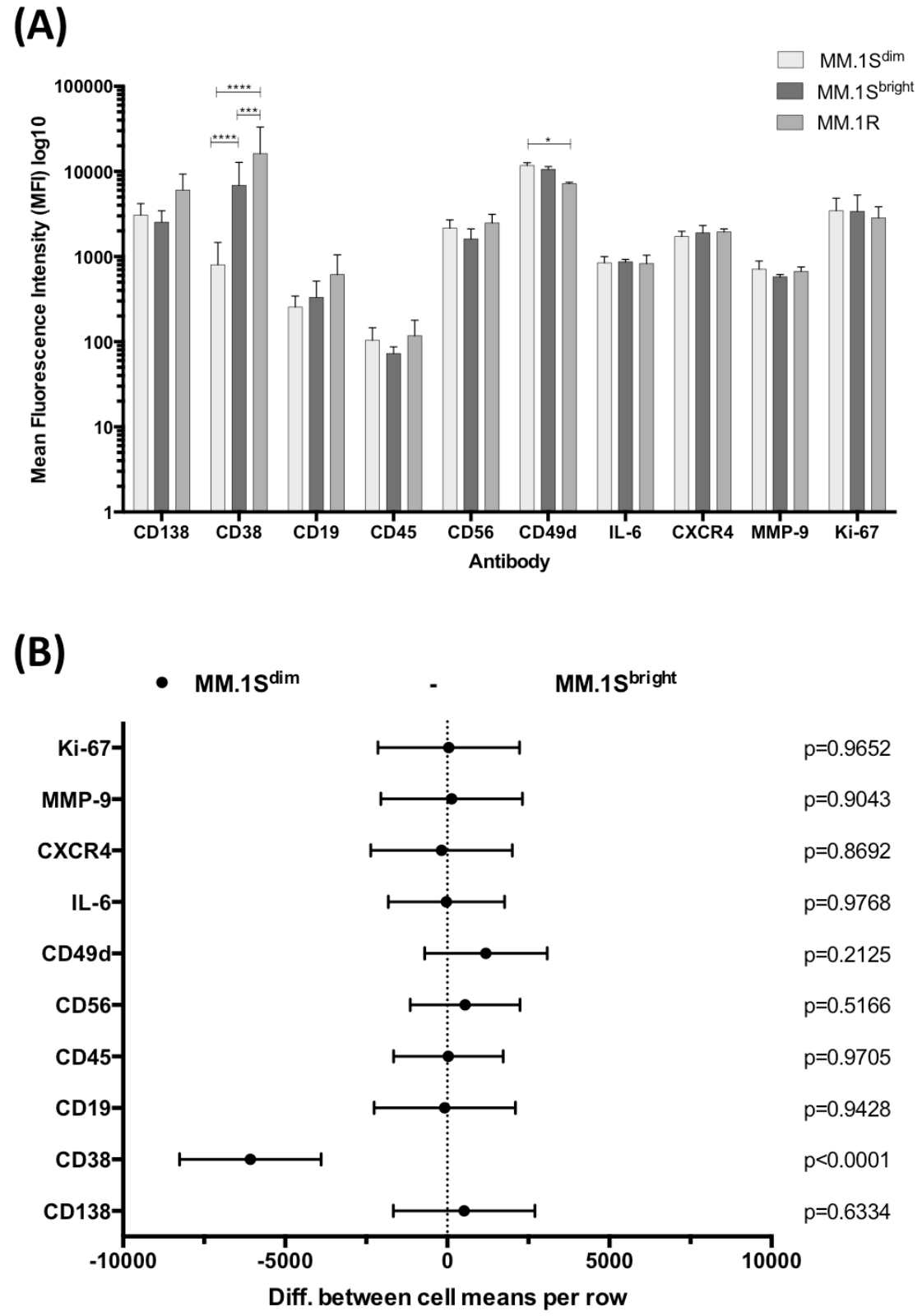

Figure 5.7. Comparison of MM.1S^{dim} and MM.1S^{bright} MFI (mean fluorescence Intensity) of different cell markers*. (A) logarithmic scale of 10 different cell markers MFI comparison between the cell lines MM.1S^{dim}, MM.1S^{bright} and MM.1R, as measured on BD Fortesa. Error bars indicate mean with SD and are calculated by repeated independent experiments (n=3). ****p<0.0001; ***p<0.001; *p<0.05; (B) 2-way ANOVA 95% confidence intervals (uncorrected Fisher's LCD) comparison of MM.1S^{dim} and MM.1S^{bright} cell marker expression, with p-values included for each cell marker.*

5.4 Proliferative differences between the sub-populations could explain the disappearance of sub-clone over time

A statistically significant increase in Ki-67 expression of MM.1S^{bright} compared to MM.1S^{dim}, potentially explains why the CD38^{dim} sub-population diminishes over numerous passages. Therefore, I aimed next to investigate the comparative proliferative properties of MM.1S, its two purified CD38 sub-populations and the MM.1R cell line by differing methods.

5.4.1 Highly expressed Ki-67 cells associated with increased expression of CD38, CXCR4 and CD49d, but no difference between the sub-clones

Dot plot quadrant gating (figure 5.8) inferred a positive correlation exists between Ki-67 and CD38 expression for MM.1S^{bright} and MM.1S^{dim} cells. For both cell lines, there was over a 2-fold increase in Ki-67 expressing cells for the higher CD38-expressing cells (Q2>Q1).

A similar immunophenotypic pattern was observed for CXCR4 and CD49d expression (figure 5.11). Both MM.1S^{bright} and MM.1S^{dim} highly expressing Ki-67 population also inferred higher CXCR4 or CD49d expression. This was more prominent for CXCR4 expression, where highly expressed Ki-67 cells strongly expressed the migration cell marker (Figure 5.11A and B). Although MM.1S^{bright} had a higher Ki-67 expression, the two populations had a very similar pattern of Ki-67 expression with CD38, CXCR4 and CD49d.

5.4.2 MM.1S^{bright} cells proliferate at a significantly higher rate than MM.1S^{dim} cells

Proliferation studies were next performed to confirm whether the differential Ki-67 expression was associated with actual cell growth differences. Figure 5.10A shows the proliferative rates of MM.1S^{dim}, MM.1S^{bright} and MM.1R. MM.1S^{dim} cells had the longest doubling time, 60.08 hours (Y0 0.45 and R^2 0.95), with MM.1S^{bright} the shortest doubling time of 46.68 hours (Y0 0.46 and R^2 0.90). Difference in doubling time (calculated over 72h) between MM.1S^{bright} and MM.1S^{dim} was statistically significant ($p<0.0001$, Figure 5.12B). As for comparison, MM.1R doubling time (48.70 hours) was also statistically significantly shorter than MM.1S^{dim} ($p=0.001$), but no difference existed between MM.1S^{bright} cells ($p=0.29$).

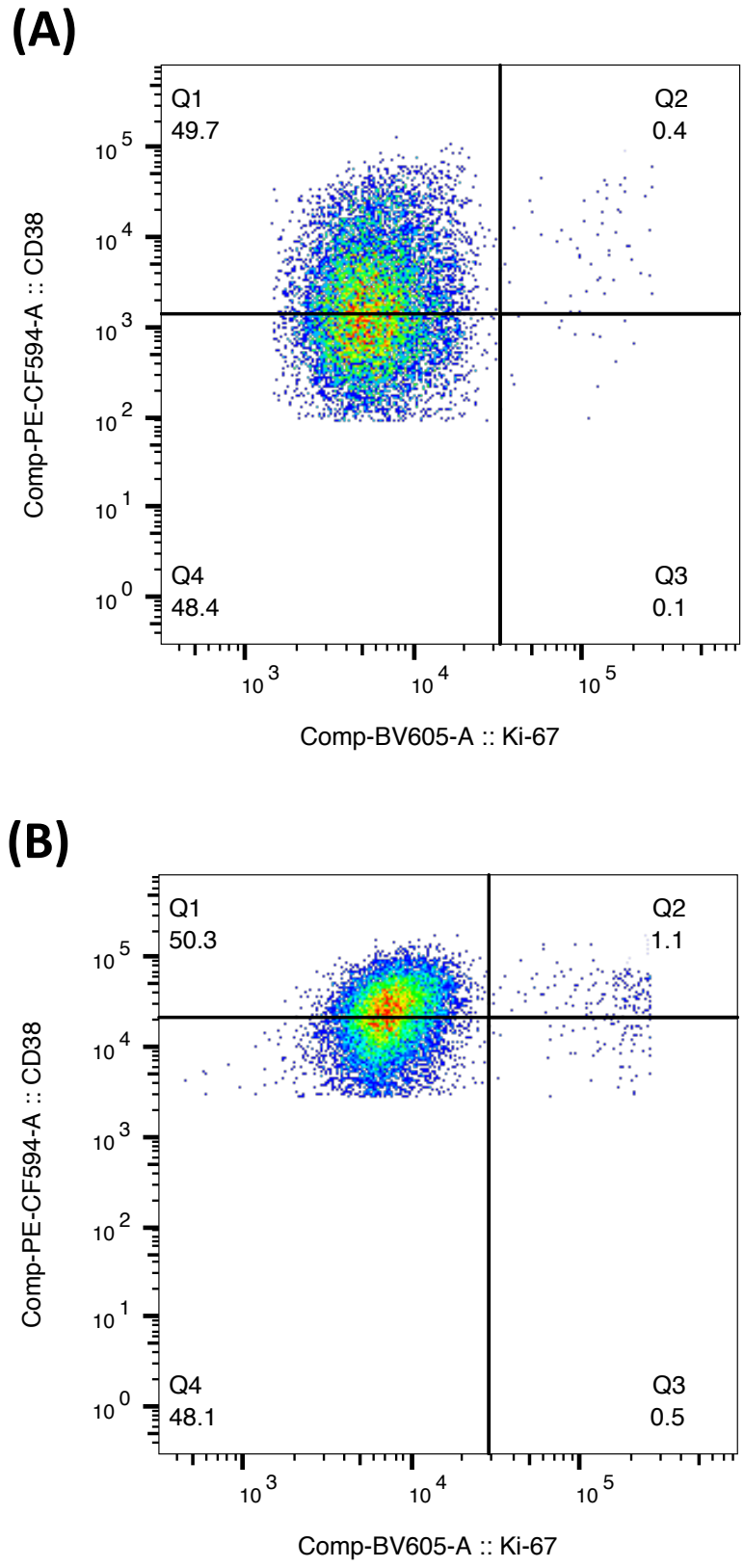

Figure 5.8. Bivariate dotplots of Ki-67 and CD38 expression in MM.1S^{dim} and MM.1S^{bright}cells. *10,000 events for each analyte were collected on a BD Fortessa flow cytometer. The dotplots show CD38-PE-CF594 and Ki-67-BV605 in (A) MM.1S^{dim} (B) MM.1S^{bright}cells. Both figures show arbitrary quadrant gating to evenly divide CD38 expression on Ki-67 negative cells (Q1 and Q4). Q2 therefore represents Ki-67 positive cells in the top half of CD38 expression and Q3, represents Ki-67 positive cells in the bottom half of CD38 expression. Total Ki-67 expression of MM.1S^{dim} was 0.5% (0.4% within higher CD38 expression), and MM.1S^{bright}1.6% (1.1% within higher CD38 expression).*

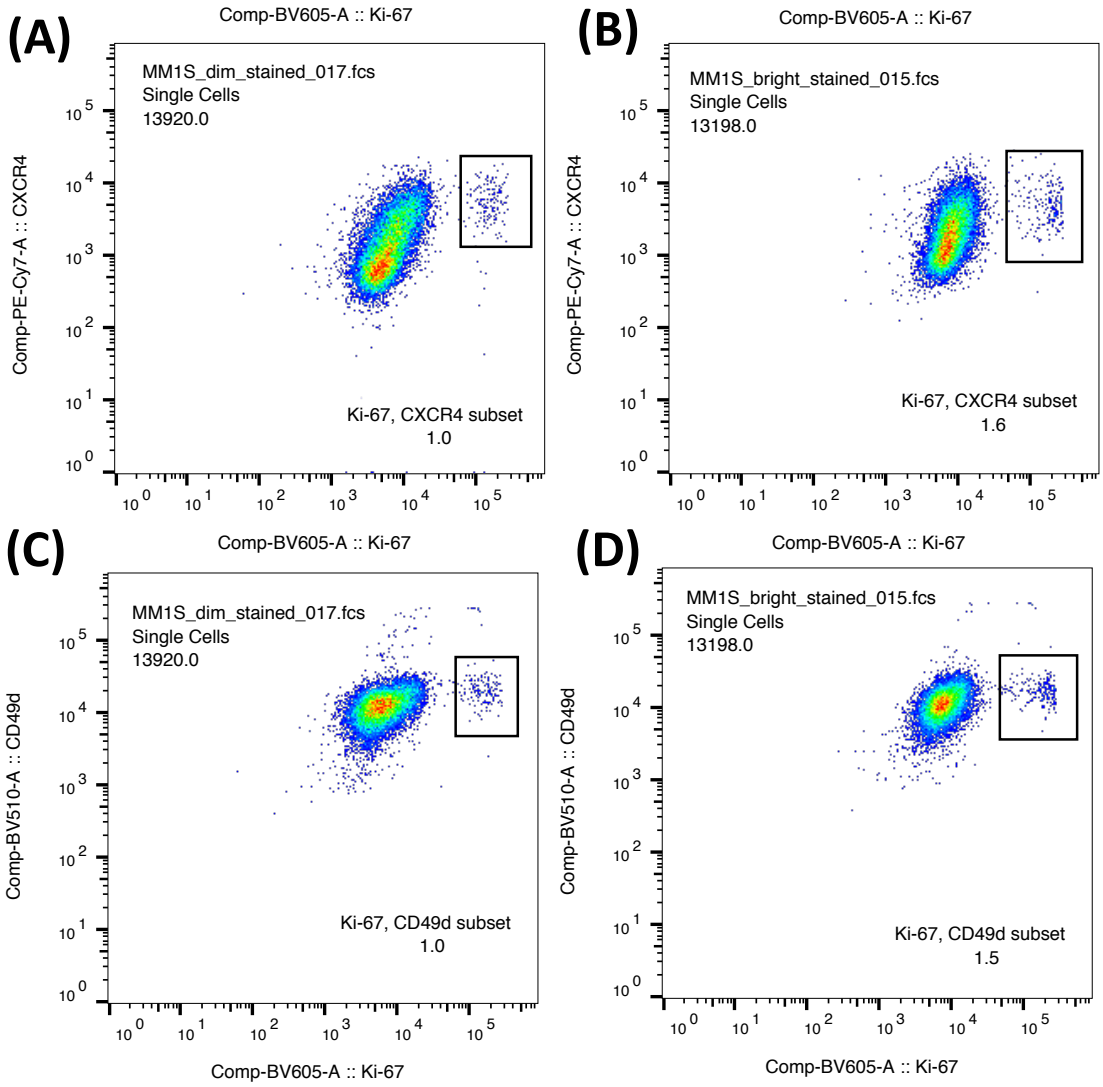

Figure 5.9. Flow cytometry pseudocolour dot plots comparison of Ki-67 expression against either CXCR4 or CD49d expression of the MM.1S CD38 sub-populations. *1 x 10^6 cells from each of the cell lines were stained with fluorescence-labelled antibodies for the cell markers, Ki-67 (BV605), CXCR4 (PE-Cy7) and CD49d (BV510). Data of 10,000 events was acquired on a BD Fortessa flow cytometer. (A) MM.1S^{dim} CXCR4 and Ki-67 expression; (B) MM.1S^{bright} CXCR4 and Ki-67 expression; (C) MM.1S^{dim} CD49d and Ki-67 expression; (D) MM.1S^{bright} CD49d and Ki-67 expression; All figures show the gated Ki-67 positive population together with the percentage positivity.*

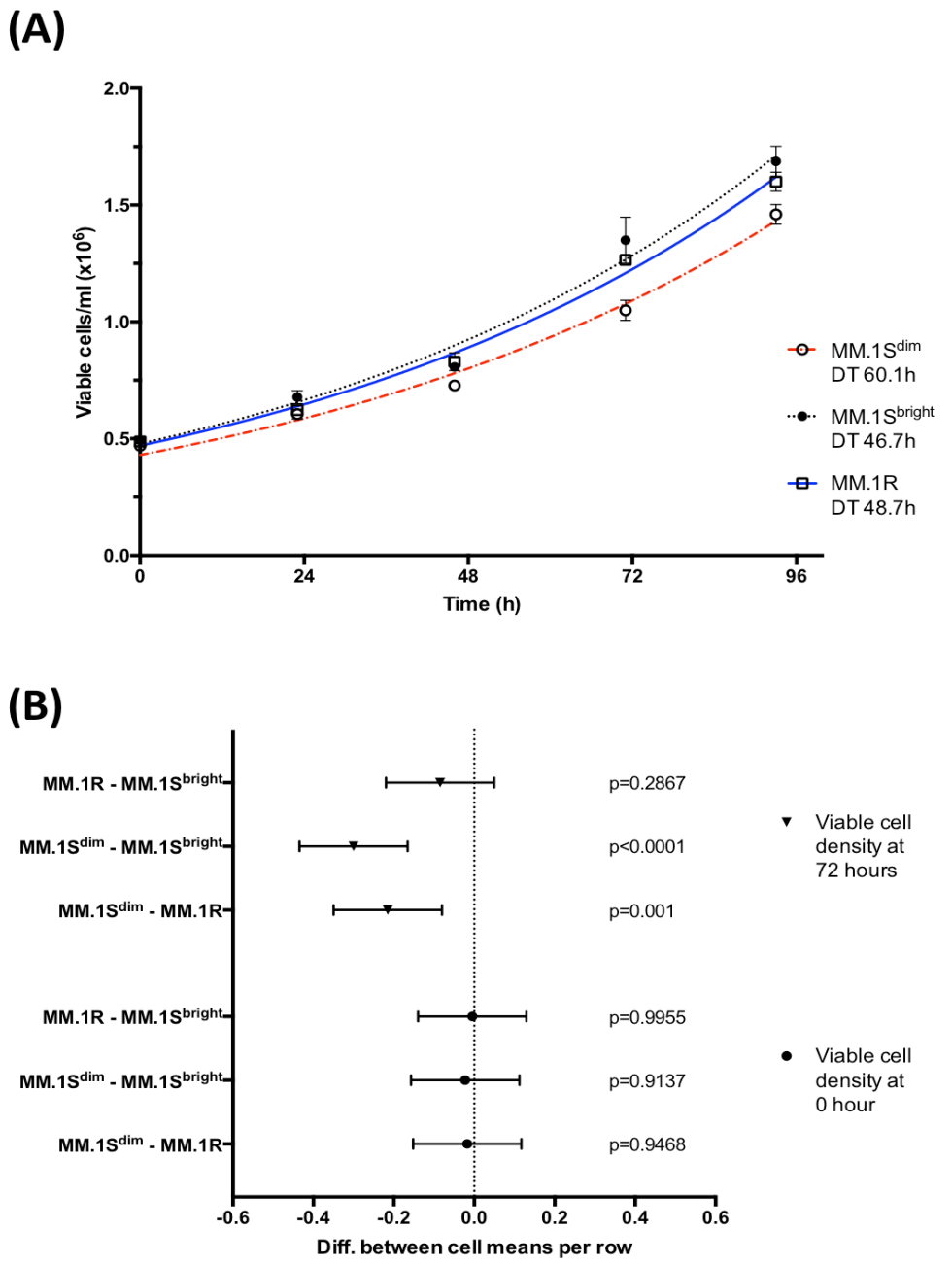

Figure 5.10. Measure and comparison of cell line proliferation over a 96-hour period. *Cell lines were seeded at a density of 0.5x10^6/ml, with density viability measured using a Vi-cell XR at 24h intervals (n=4). (A) Non-linear line of best fit for each cell line over a 96h period was used to calculate DT (doubling time), using exponential growth equations of the data (Prism software 6.0). Error bars indicate mean with SD and are calculated by repeated independent experiments (B) 95% Confidence Intervals (Tukey) comparison of cell lines viability at 0 hour and 72 hours (n=4), p-value comparison between the cell lines were calculated by 2-way ANOVA, with Tukey's correction for multiple comparison.*

5.4.3 The increase in CD38 expression of the MM.1S sub-populations is associated with higher S-phase activity

The S-phase of the cell cycle, represents the stage whereby cells undergoes cell synthesis. Although Ki-67 is not exclusively expressed in S-phase of the cell cycle (also expressed in G1 and G2, but not G0), its levels markedly increase in S-phase. The increase in Ki-67 expression for MM.1S^{bright} compared to MM.1S^{dim} (section 5.3.1) is supported by MM.1S^{bright} having higher S-phase activity (35.6%±2.1 vs. 32.0%±1.6, p=0.051 n=3). Figure 5.11 shows individual cell cycle analysis for each of the MM.1 cell lines and MM.1S sub-populations. MM.1R has the highest S-phase activity (37.4%±2.7), although difference was not statistical (p=0.25, n=3) when compared to MM.1S (32.0%±3.4).

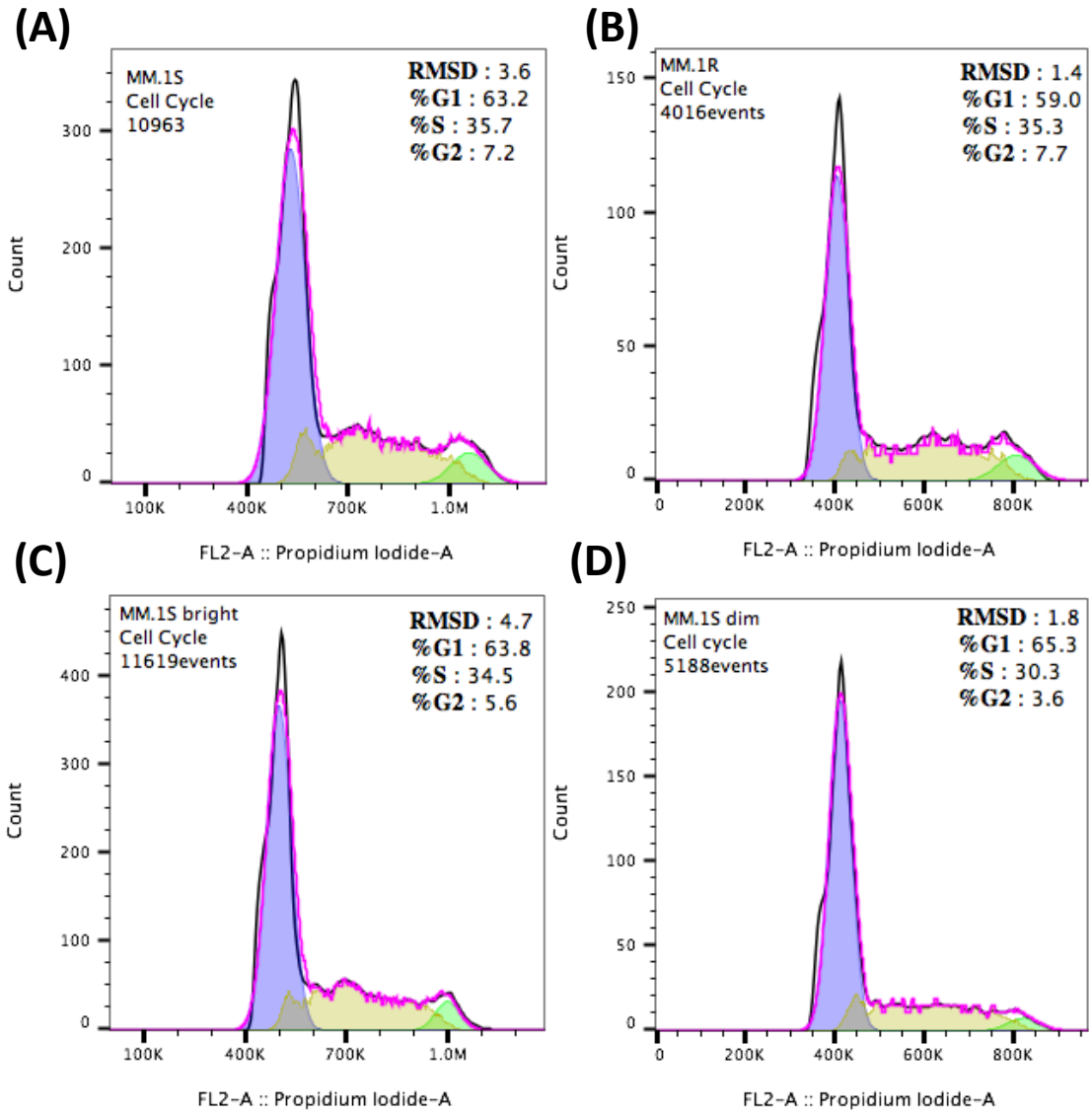

***Figure 5.11*. Propidium iodide (PI) cell cycle analysis.** *Cells were grown in RPMI-1640 cell culture medium with 10% FBS prior to labelling with PI to quantify DNA content and then analysing on a BD Accuri flow cytometer. A live cell gate was serially applied into a singlet discrimination gate prior to cell cycle analysis. Flow-Jo cell cycle analysis software providing RMSD (Root Mean Square Deviation), %G1, %S and %G2. (A) MM.1S, (B) MM.1R, (C) MM.1S^{bright} (D) MM.1S.*

5.4.4 Dexamethasone causes G1 cell arrest in the MM.1S cell lines, with minimal differences between CD38 sub-populations

When subjected to increasing doses of dexamethasone (20nM to 100μM), G1 cell arrest was observed for MM.1S and the two sorted populations, but not for MM.1R (Figure 5.12A). MM.1R cell cycle activity was confirmed to be impervious to dexamethasone, although a minimal increase in G2 with a corresponding drop in G1 was observed at the higher doses of steroids.

Almost complete cell cycle arrest (S-phase percentage plateau) occurred at the lowest dose of dexamethasone (20nM) used for the MM.1S related cell lines and a log lower concentration before the cytotoxic effects of dexamethasone were observed (LD50 roughly at 200nM). There appeared to be no differences in S-phase percentage with increasing doses of dexamethasone between MM.1S^{dim} and MM.1S^{bright}, thus indicating sub-clonal populations within MM.1S that are steroid naïve were dying upon exposure to dexamethasone.

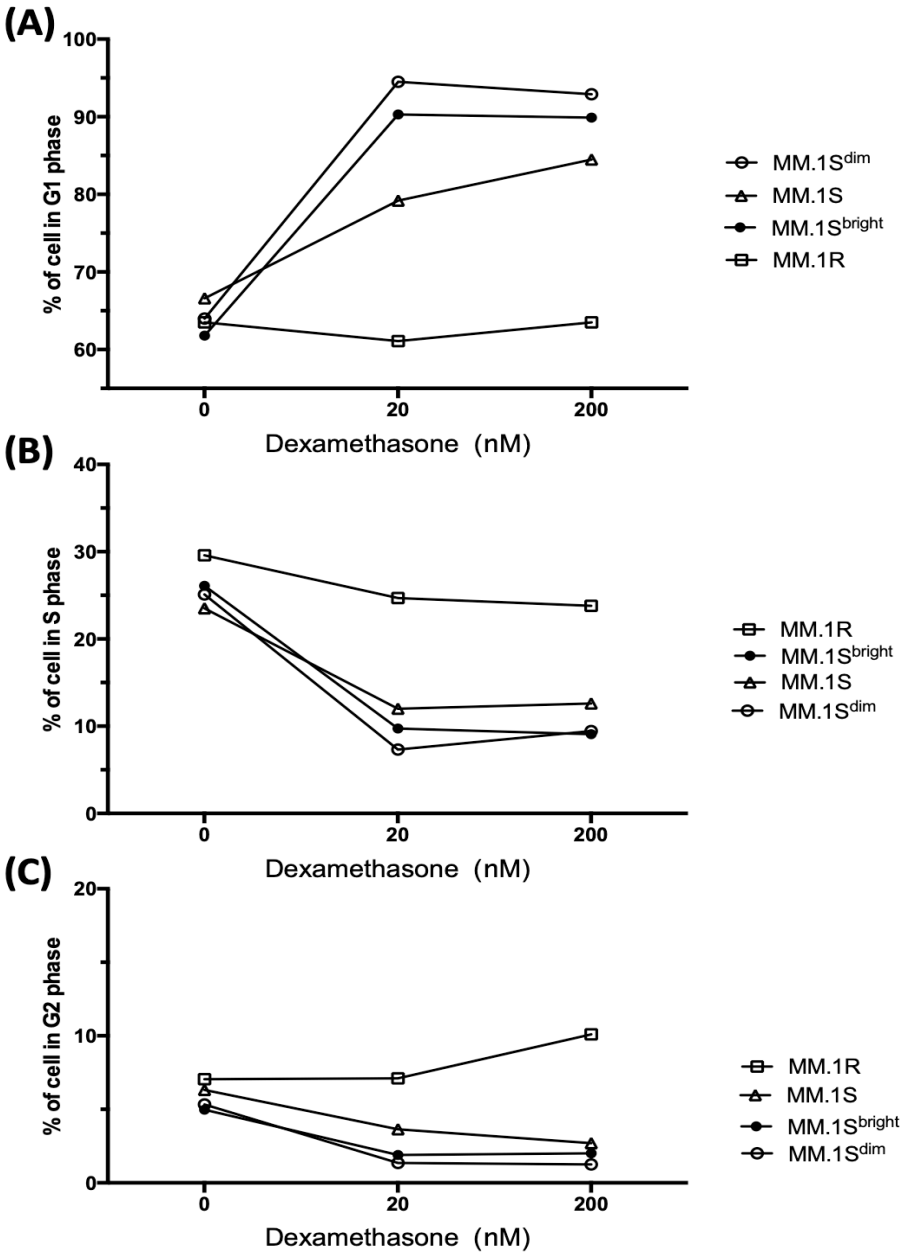

Figure 5.12. Percentage of cell cycle phases of the MM.1 cell lines *with increasing concentrations of dexamethasone, (A) G0/G1-phase, (B) S-phase, (C) G2-phase. Each measurement was only on alive gated cells, percentage cell cycle phase calculated using Flow-Jo cell cycle analysis software. Cells were grown in RPMI-1640 cell culture medium with 10% FBS prior to labelling with PI to quantify DNA content and then analysing on a BD Accuri flow cytometer. A live cell gate was serially applied into a singlet discrimination gate prior to cell cycle analysis.*

5.4.5 Telomere analysis reveals differences in MM.1S^{bright} and MM.1S^{dim} telomere lengths suggestive of differing proliferative propensities

Figure 5.13 shows the comparative telomere lengths of the various MM.1 cell lines. Mean telomere lengths were similar between MM.1S (3.14Kb ±1.23) and MM.1R (3.24Kb ±1.04), analysed from an early passage. However, MM.1S^{bright} when compared to MM.1S^{dim}, of a similar passage and age post purification, had a shorter telomere length (2.51Kb ±0.82 vs 3.26Kb ±1.23). The shorter telomere length of MM.1S^{bright} is confounded by an increased S-phase percentage of cell cycle analysis when compared to MM.1S^{dim}, implying MM.1S^{bright} has a more rapid proliferative history.

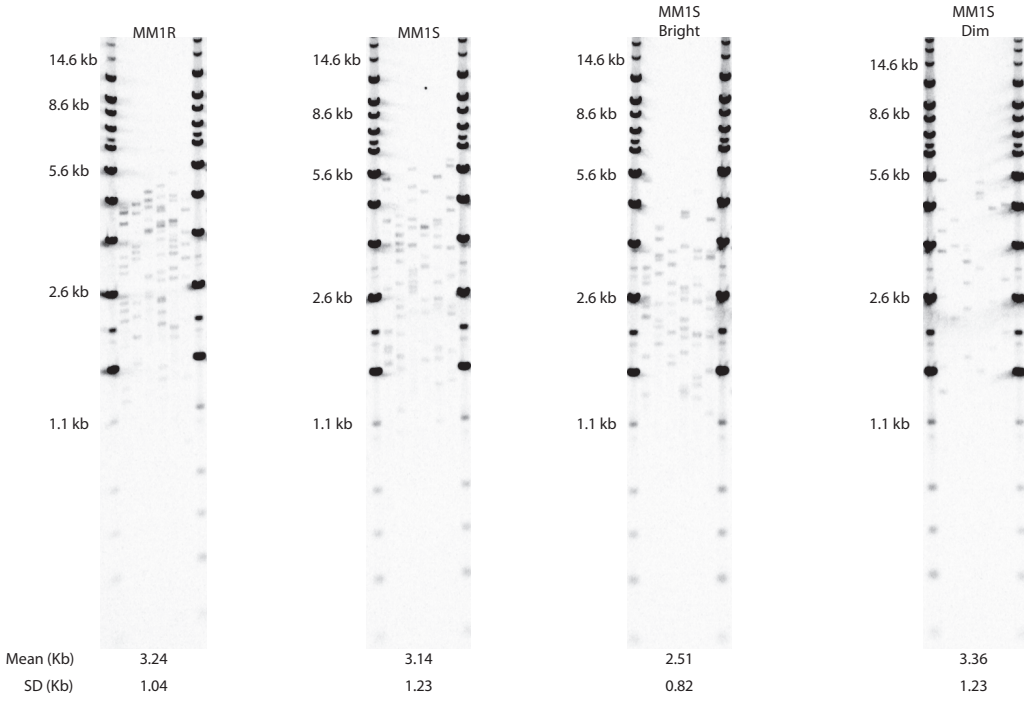

Figure 5.13. Telomere length profiles for the cell lines MM.1S and MM.1R, MM.1S^{dim} and MM.1S^{bright}. *Telomere length was assessed using single telomere length analysis (STELA)-based PCR technique of the XpYp-chromosome. Each STELA profile shows the mean 9Kb) length of telomere and the standard deviation (SD). All of the cell lines were assessed at similar cell passage numbers. The MM.1S^{bright} cells showed significant telomere length shortening compared to the other three cell lines. Assays courtesy of Sam Hyatt.*

5.5 Differing in MM.1S^{bright} and MM.1S^{dim} adherent and migratory potential, emphasises functional variation and potentially of being distinct sub-clones

The immunophenotypic and proliferative difference observed between the two sorted MM.1S CD38 sub-populations and MM.1R, led me to investigate whether further functional differences existed between the cell lines. Myeloma cells (both primary and cell lines) are known to express the chemokine receptor CXCR4 and show homing properties in response to the receptor's ligand, CXCL12 (SDF-1) (Moller et al. 2003). Determining if MM cells have a strong propensity to adhere to the CXCL12 secreting fibroblasts MRC-5 as well the confirmed minor differences in CXCR4 expression between MM.1S^{bright} and MM.1S^{dim}, would be suggestive that the cell lines be susceptible to CXCL12-induced migration, but also discrepancies in migratory potential between the cell lines may exist.

5.5.1 Adhesion

An early observation between the sorted MM.1S CD38 sub-populations and MM.1R was their differential propensity to adhere to plastic culture flasks. MM.1R was observed to be the most adherent, requiring thorough cell scrappage to remove the cells. This was in contrast to MM.1S^{dim} cells which had a greater proportion of cells in suspension, i.e. less adherence. MM.1S^{bright} was more akin to MM.1R, with cells mainly adhered to plastic.

The MM cells were co-cultured with differing stromal or endothelial cells, varying degree of adherence between the cells were observed (see supplementary figures in appendix). Although no functional adherence assays were undertaken, percentage of MM cells adhered to either HUVEC, MRC-5 and HS-5 were calculated. The strongest affinity of adherence was seen with the CXCL12-secreting fibroblast MRC-5, with a statistically significant difference compared to HUVEC's (74.7% ±8.9 vs. 33.0% ±3.6, p=0.012). Thus, the MM cell lines appeared to have a greater adherence propensity to chemotaxis secreting cells (MRC-5) than to endothelial surfaces (HUVEC or HS-5).

The integrin CD49d, is an important adhesion marker in MM and though subtle (but not statistical) expression differences between the cell lines existed (section 5.2), the difference in adherence properties (either to HUVECs or plastic) was unlikely to be attributed to this integrin as MM.1R had the lowest expression, and statistically lower than MM.1S^{dim} (p=0.031). Co-culturing of the cell lines with either the chemokine CXCL12-secreting fibroblasts MRC-5, the human bone marrow stromal cell HS-5 or the endothelial

cell HUVEC, although caused a reduction in expression in CD49d in the MM cells lines when co-cultured (see supplementary figures in appendix), no significant difference was observed between MM.1S^{dim} and MM.1S^{bright}. The greatest reduction in MM CD49d expression with the co-cultured cells was observed for HUVECs. Although VCAM-1 (the endothelial ligand for the integrin α4β1 for which CD49d is a component) was not measured on HUVECs, MRC-5 or HS-5, the HUVECs, as causing the greatest reduction in CD49d expression in MM co-culture, would imply VCAM-1 is expressed at a higher degree on HUVEC and any of the other co-culture cells and emphasising the importance of the CD49d in HUVEC-MM cell to cell interaction.

5.5.2 MM.1S^{bright} cells show increase in migration

Migratory potential between the sorted CD38 MM.1S sub-population was tested in two ways; under static conditions using 3μm pore transwell plates and in a dynamic circulatory migratory model (a novel migratory model as described in detail in chapter 4). In the transwell migratory assay (Figure 5.14), MM.1S^{bright} cells showed significantly higher migration (2.23% SD±0.50) when compared with MM.1S^{dim} cells (1.49%±0.33, p=0.0016).

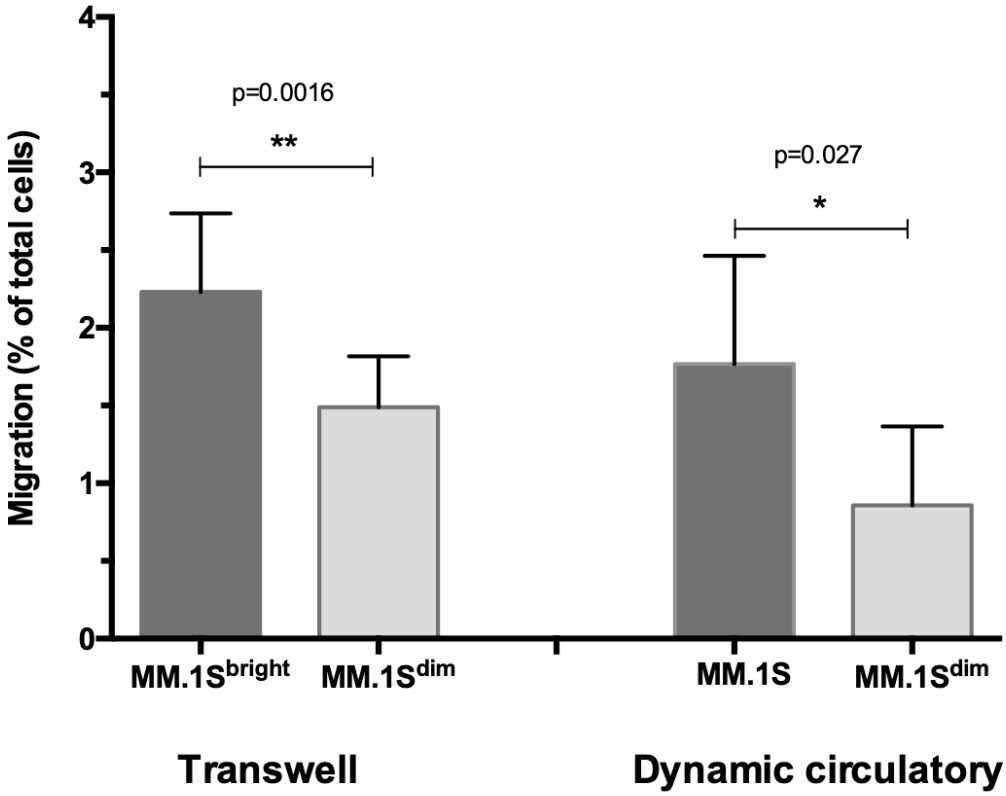

***Figure 5.14*. Comparison of MM.1S and its CD38 sub-populations CXCL12 induced migration.** *Transwell migration ,0.25 x10^6 cells were placed in the apical chamber of a 3μm transwell plate. Migrated cells were retrieved from basolateral chamber of transwell at 24h and counted by BD Accuri flow cytometer. Migration was stated as a percentage of the total number of cells inserted into transwell. Error bars indicate mean with SD and are calculated by repeated independent experiments. Statistical difference was measured by paired two–tailed parametric t-test (n=5). The dynamic circulatory model, 40x10^{6}cells were placed in closed circuit, with migratory cells retrieved from the EVS at 48h. Statistical difference was measured by paired (transwell n=3) unpaired (dynamic circulatory, n=17 MM.1S and n=5 MM.1S^{dim}) two–tailed parametric t-test.*

5.5.2.1 Dynamic migratory model confirms MM.1S^{dim} has a reduced migratory potential and that migrated cells undergo additional cell division

The dynamic circulatory model, as with the transwell assay data (figure 5.14) showed MM.1S^{dim} (0.86% SD±0.51 n=5) to have statistically lower (p=0.027) percentage migration than for the CD38 bright dominant MM.1S cell line (1.62% SD±0.79 n=17). Statistical analysis was conducted on MM.1S rather than MM.1S^{bight}, due to resources and the number of MM.1S previously conducted, thus giving greater power to the statistical analysis. To confirm that co-existence of the two CD38 sub-populations did not affect the other's migratory potential and to observe degree of cell division over 48h period, sorted MM.1S^{dim} and MM.1S^{bright} were simultaneously circulated through the same cartridge in equal proportions. Each cell line was pre-stained with different fluorescence cell markers, MM.1S^{dim} with CFSE and MM.1S^{bright} with eFluor 670. Figure 5.15 shows the overlay histograms of MM.1S^{dim} and MM.1S^{bright} fluorescence as measured on a BD Accuri flow cytometer, over the course of the experiment, lasting 48h. Although only a single experiment, of the migrated cells retrieved from the EVS at 48h, the majority were stained with eFluor 670, the marker of MM.1S^{bright}. Of the total amount of alive cells collected from the EVS, 44.1% matched the fluorescence of efluor 670 (MM.1S^{bright}), 22.6% matched the fluorescence of CFSE (MM.1S^{dim}) and the remaining cells had no fluorescence. Thus, implying roughly twice as many MM.1S^{bright} cells migrated into the EVS than MM.1S^{dim} over 48h period.

The experiment also showed the degree of cell division over the 48h period. Every time a cell division occurs, the amount of cell fluorescence in theory should half. The majority of circulating (i.e. non-migratory) cells experienced a one log loss in fluorescence at 48h. Interestingly, migrated cells recovered from the EVS at 48h showed a further log reduction in fluorescence compared to their circulating counterparts, suggestive that migrated cells undergo an additional cell division compared to non-migrated cells.

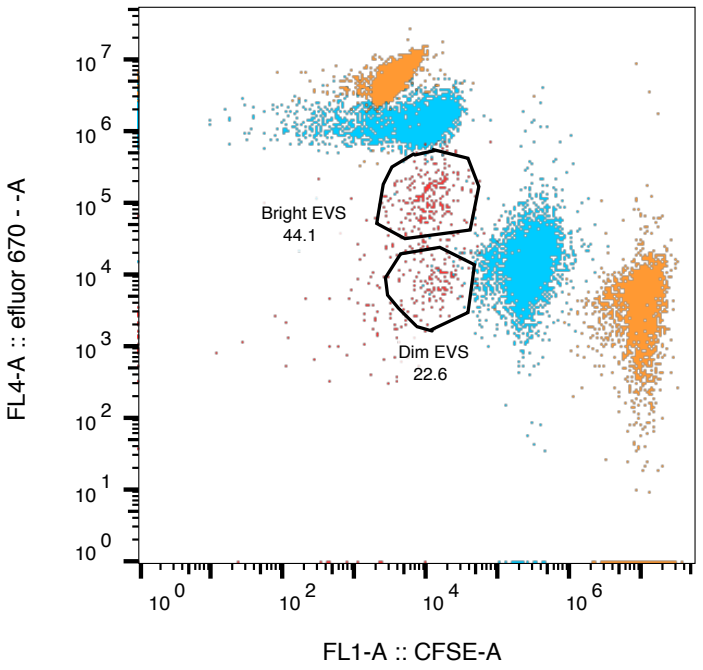

	Subset Name with Gating Path
	G05 mixed dim_bright CFSE che.fcs/Alive cells/Single Cells
	B01 Circuit 2 unstianed 0.1ml.fcs/Alive cells/Single Cells
	B03 EVS-2 unstained 0.2ml.fcs/Alive cells/Single Cells

Figure 5.15. Cell marker stained single cartridge dynamic circulatory migratory model*. 20x10^6 MM.1S^{dim}and 20x10^6 MM.1S^{bright}cells were stained with separate fluorescence cell marker (CFSE-MM.1S^{dim}and eFluor 670-MM.1S^{bright}). At 48h, circulating and EVS cells were retrieved. Figure shows FL-1 and FL-4 overlay dot plot of circulating cells at 0h (G05-orange), circulating cells at 48h (B01-blue) and EVS at 48h (B03-red), measured on BD Accuri. EVS cells are gated as eFluor 670 positive (MM.1S^{bright}) and eFluro 670 negative, weakly CFSE positive (MM.1S^{dim}), with gated percentage proportion of total EVS cells.*

5.5.2.2 Migrated MM.1S^{dim} cells have increased in CD38 expression, which is not observed for MM.1S^{bright}

Having shown that migratory cells undergo further cell division compared to non-migratory cells, is also confirmatory that they are undergoing greater cell activation. CD38 being a recognised marker of cell migratory activation, comparison of CD38 expression between migratory and non-migratory cells were analysed, using the dynamic circulatory model. An increase in CD38 expression of MM.1S^{dim} migrated cells (MFI 174,645 v 47,807, figure 5.16), compared to non-migrated cells was observed. MM.1S^{bright} CD38 expression was not increased and comparable to their non-migratory cells.

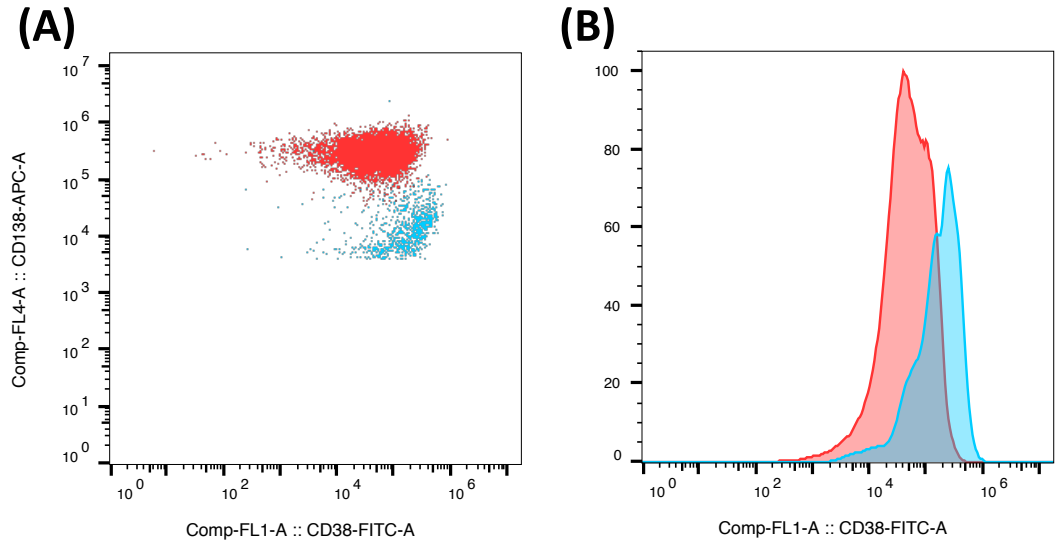

	Subset Name with Gating Path	Count	Median : Comp-FL1-A
	B04 dim circuit 48hr 30.05.fcs/Alive cells/Single Cells/MM1Sdim circulating CD138+	281255.0	47806.6
	B05 dim evs 48hr 30.05.fcs/Alive cells/Single Cells/Myeloma Cells	883.0	175355.4

Figure 5.16. CD38 expression of MM.1S^{dim} migrated and non-migrated cells from dynamic circulatory model at 48h. *(A) Overlaid dotplot of CD38 and CD138 expression of circulating MM.1S^{dim} cells and retrieved EVS cells, serially gated using a live gate and doublet discrimination gate on BD Accuri flow cytometer. (B) overlaid histogram of CD38 expression comparing circulating cells against EVS cells.*

5.6 Mechanism of Sub-clonal variation in dexamethasone sensitivity

The functional and phenotypic differences that I have shown between the MM.1S^{bright} and MM.1S^{dim} sub-populations raised the possibility that they are genetically distinct sub-clones derived from a common ancestor. Although the mechanisms of dexamethasone resistance within the MM.1R cell line are well documented (Greenstein et al. 2003; Sharma and Lichtenstein 2008), no previous analysis of MM.1S CD38 expressing sub-populations has been described. I therefore set out to explain the reasons for the differential dexamethasone sensitivity I identified between the CD38 sub-populations. Potential causes of this may be related to:

i. the glucocorticoid receptor (as for MM.1R)
ii. efflux pumps or protective mechanisms removing or preventing internalisation of the drug
iii. expression differences in molecules that causes cell adhesion mediated drug resistance (CAM-DR)
iv. cytoplasmic or nuclear transcriptional changes, downstream of the GR that ultimately affects the cell's dexamethasone cytotoxic susceptibility.

Currently, it remains inconclusive that a direct correlation exists between the number of glucocorticoid receptors (GR) expressed on lymphoid cancer cells and the degree of glucocorticoid sensitivity (Bailey et al. 2001). The MM.1R cell line was derived from long-term exposure to dexamethasone, which resulted in a complete lack of GR expression. Given that the parental MM.1 cell line has been shown to strongly express GR (Greenstein et al. 2003), it seems unlikely that MM.1S^{bright} and MM.1S^{dim} differential sensitivity to dexamethasone is mediated through altered GR expression.

Alternative mechanisms as outlined above were further investigated. A simple, yet potentially explanatory mechanism for differences in dexamethasone sensitivity would be the efflux of dexamethasone by protein channel pumps. A widely recognised broad substrate efflux pump and a known mechanism of drug resistance is P-glycoprotein (P-gp) (Breier et al. 2013). P-gp has also been shown to play a role in glucocorticoid transport (Gruol and Bourgeois 1997).

5.6.1 P-glycoprotein (P-gp) expression within the MM.1 cell lines in static culture are similar, but vary upon exposure to cytotoxic agents

To determine if the MM.1S subset variation in dexamethasone sensitivity was due to altered expression of an efflux pump, P-gp was measured. In static culture, the MM.1 cell lines uniformly express P-gp, albeit weakly. No statistical difference in MFI was found between MM.1S (2,004±234) and MM.1R (2,047±472) (p=0.85), between the gated MM.1S CD38 populations ($CD38^{dim}$ (2,515 SD±918), $CD38^{bright}$ (2,343 SD±743, p=0.12), or between the sorted $MM.1S^{dim}$ and $MM.1S^{bright}$ cell lines (see table 5.3 and overlay histograms in appendix supplementary figures).

5.6.1.1 Difference in P-gp expression observed between MM.1 sub-populations upon exposure to cytotoxic agents

Having confirmed that P-gp expression was equivalent between the two sub-population in static culture, P-gp expression was explored when exposed to cytotoxic agents at differing concentrations, to see if expression was upregulated and if so, if differences occurred between the sub-populations. Analysis of the sub-populations was applied to unsorted MM.1S and not to the separated cell lines, thus minimising experimental variations such as drug concentrations. Figure 5.17A shows how P-gp expression increased with cumulative dexamethasone concentration for MM.1R (peaking at 0.2mM, MFI 6,114, 16.4% cell death), but remained fairly static for MM.1S and its CD38 sub-populations.

Cells exposed to a concentration of dexamethasone closest to MM.1S IC50 (200nM), a statistical difference in P-gp expression between MM.1R (MFI 3,627) and MM.1S (MFI 1,906) existed (p=0.048, n=3). However, no expression difference at 200nM was observed between the MM.1S CD38 sub-populations (p=0.68, n=3). At concentrations higher than 200nM dexamethasone, substantial (>50%) MM.1S cell death occurred, which made it difficult to interpret P-gp expression accurately due to small number of live cells and significant cell debris.

To identify whether similar P-gp expression patterns existed upon exposure to other cytotoxic agents, the cell lines were exposed to increasing doses of bortezomib for 48 hours (retaining the same experimental conditions as for dexamethasone exposure). Unlike dexamethasone, MM.1R P-gp expression at doses lower than its IC50 (<40nM) did not increase and more akin to MM.1S, with no statistical expression difference (p=0.46, n=3) between them at for a bortezomib concentration closest to its IC50 (40nM). MM.1S CD38 sub-populations bortezomib P-gp expression pattern (up to its IC-50, 40nM), showed a

similar pattern as for dexamethasone, with a fairly static, low level expression and no statistical expression differences between them (40nM p=0.98, n=3). For both cell lines and sub-populations, there appeared to be a slight increase in P-gp expression at 40nM, although substantial cell death was seen (80.3% - 66.3%) at this concentration. Although such results may be artefactual (e.g. increased cell debris), the results could be consistent with sub-populations that have higher P-gp expression that have greater resistance to the cytotoxic effects of Bortezomib. The data is summarised in table 5.3

	MM.1S	MM.1R	MM.1S CD38 gated dim	MM.1S CD38 gated bright
Static culture				
% alive	88.4%	88.9%	87.5%	90.0%
MFI (±SD)	2,004 (±234)	2,047 (±472)	2,5153 (±918)	2,343 (±743)
% positivity (±SD)	6.47% (±5.53)	9.29% (±6.99)	6.42% (±3.17)	5.27% (±3.53)
Dex. 200nM				
% alive	44.6%	88.0%	23.3%	54.5%
MFI (±SD)	1,906 (±272)	3,627 (±427)	2,857 (±372)	2,895 (±252)
% positivity (±SD)	2.94% (±1.02)	18.56% (±4.01)	3.23% (±2.01)	2.96% (±0.78)
Bortezomib 40nM				
% alive	33.7%	28.3%	19.7%	31.6%
MFI (±SD)	3,322 (±1,541)	3,559 (±1,278)	1,883 (±158)	1,884 (±128)
% positivity (±SD)	4.59% (±2.35)	6.97% (±5.52)	5.49% (±4.50)	3.90% (±0.81)

Table 5.3. Comparison of P-gp expression *(MFI and percentage positivity) of alive gated MM.1S and MM.1R including MM.1S CD38 gated subsets. Comparison made between baseline (no drug) and 48-hour exposure of 200nM dexamethasone or 40nM of bortezomib. Standard Deviation are included in brackets and are calculated by repeated independent experiments, n=3. Flow cytometry analysis on BD Accuri. cell markers immunostained with P-gp_PE-Cy7 and CD38-APC. MFI - Mean Fluorescence Intensity; Dex. – dexamethasone. T-Test, parametric paired T-test, fixed ratio 2 tailed; Dex – Dexamethasone;*

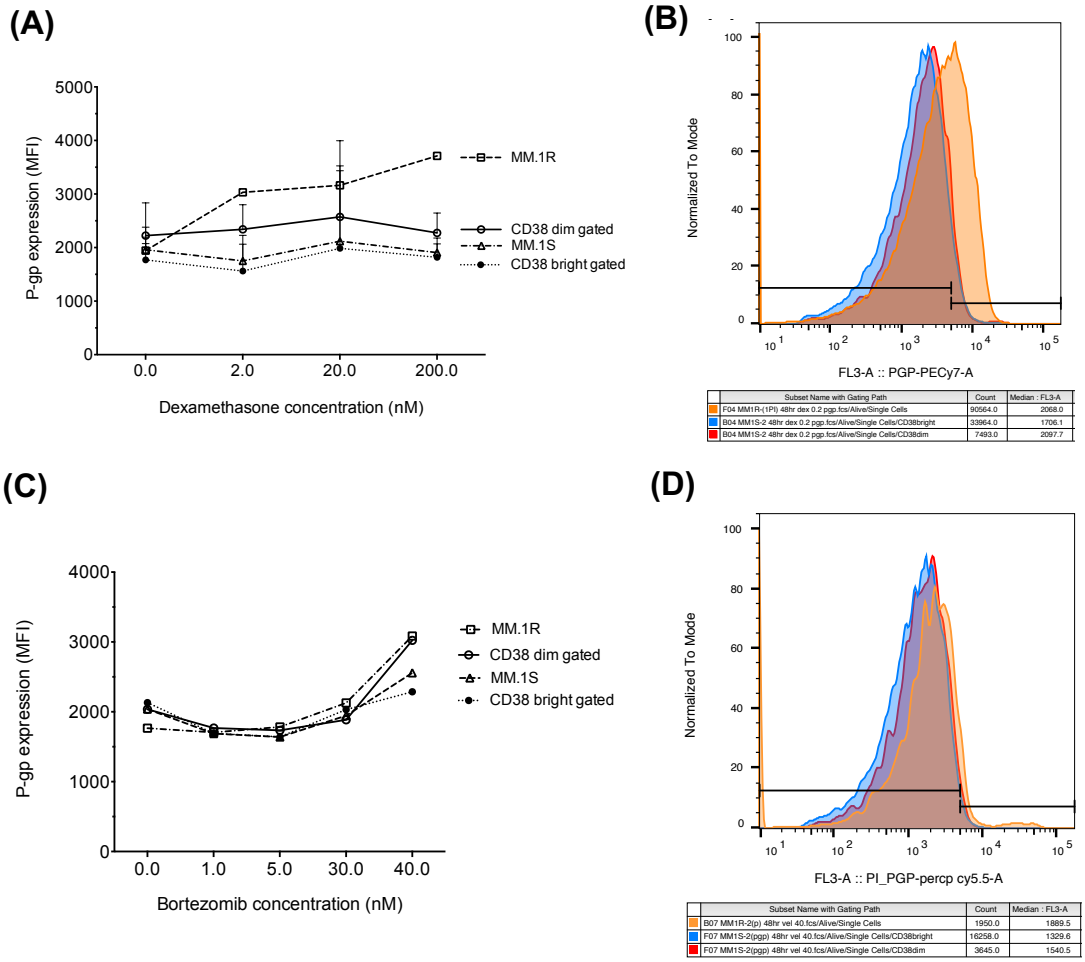

Figure 5.17. MM.1 Alive cells P-gp expression *post 48h exposure of dexamethasone (A & B) and bortezomib (C & D). (A) P-gp expression as MFI (median) of the cell lines MM.1S, MM.1R and MM.1S CD38 subsets, at 48h at increasing concentrations of dexamethasone (n=3). (B) Flow cytometry dot plot of MM.1S at 48h dexamethasone 200nM exposure, showing expression of CD38 (APC) and P-gp (PE-Cy7) as well as CD38 subset gating strategy. (C) P-gp expression as MFI (median) of the cell lines MM.1S, MM.1R and MM.1S CD38 subsets, at 48h at increasing concentrations of bortezomib (n=3). (D) Flow cytometry dot plot of MM.1S at 48h bortezomib 40nM exposure, showing expression of CD38 (APC) and P-gp (PE-Cy7) as well as CD38 subset gating strategy. Flow cytometry analysis on BD Accuri. cell markers immunostained with P-gp_PE-Cy7 and CD38-APC. MFI - Mean Fluorescence Intensity; vel. – Velcade (bortezomib); Dex. – dexamethasone.*

5.6.2 No evidence of CAM-DR as the cause of drug resistance

MM adhesion to bone marrow stromal cells are essential for cell survival and growth (Mahindra et al. 2010), making cell adhesion molecules (CAMs) a key component of these processes. CD49d is known to play a role in cell adhesion mediated drug resistance (CAM-DR) (Damiano et al. 1999) and such differences could bring about varying sensitivities to cytotoxic agents. However, my previous work showed minimal differences in CD49d expression between MM.1S^{dim} and MM.1S^{bright}, and actually a decrease in expression for the steroid resistance cell line MM.1R. My data also showed that co-culture did not upregulate CD49d expression, with no statistical difference between the CD38 sub-populations (see supplementary figures in appendix).

Other important molecular modulators of CAM-DR in MM include integrins such as VLA4 (compromising CD49d), LFA-4 and selectins. Although L-selectin is known to be expressed in MM.1S (Azab et al. 2012) and expression can vary at different stages of the disease as well as being prognostic marker (Terpos et al. 2016), minimal difference in L-selectin expression was observed between MM.1S^{dim} (MFI 2,984) and MM.1S^{bright} (MFI 3,338), with similar overlay histograms (figure 5.18B).

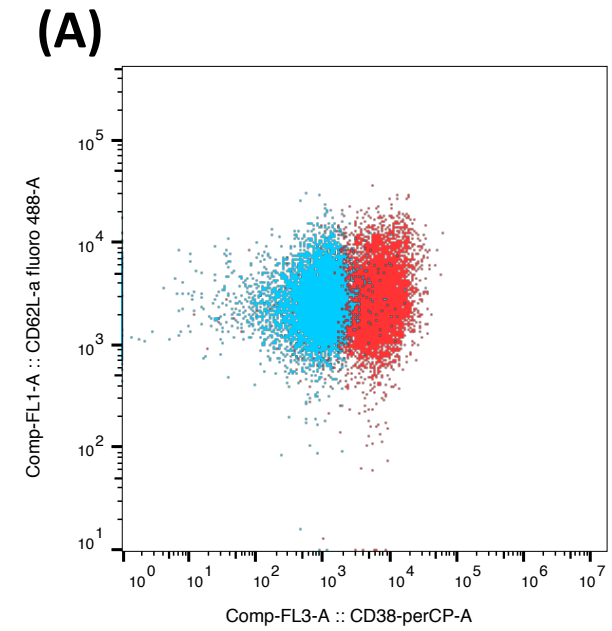

	Subset Name with Gating Path	Median : Comp-FL1-A	Mean : Comp-FL1-A
	B02 Dim stained.fcs/Alive/Single Cells	2409.7	2984.4
	C02 bright stained.fcs/Alive/Single Cells	2422.6	3337.5

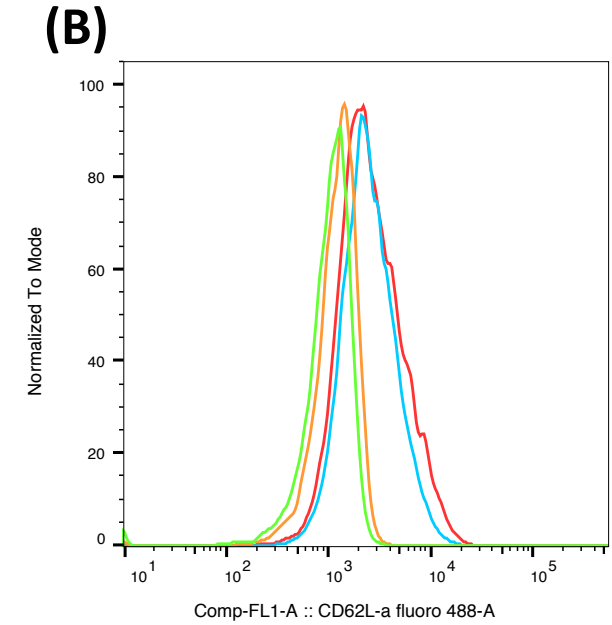

	Subset Name with Gating Path	CD62L-a fluoro 488-A+ :: Freq. of Parent
	C01 Bright unstained.fcs/Alive/Single Cells	0.3
	B01 Dim unstained.fcs/Alive/Single Cells	0.3
	B02 Dim stained.fcs/Alive/Single Cells	33.3
	C02 bright stained.fcs/Alive/Single Cells	41.0

Figure 5.18. CD62L (L-Selectin) and CD38 expression of the cell lines MM.1S^{dim} and MM.1S^{bright}. *Cells stained with Fluoro-488 anti-CD62L antibody and PerCP anti-CD38 antibody. Analysed on BD Accuri flow cytometer, 10,000 cells were acquired for the analysis. (A) Overlaid dotplot comparing the expression of CD62L and CD38 in the two cell lines. (B) overlaid histogram of CD62L expression comparing the two cell lines. Legend shows MFI, both median and mean as well as percentage positivity of CD62L.*

5.7 Genetic Analysis of MM.1S CD38 expressing sub-clones and MM.1R

As I was unable to explain the differences in dexamethasone sensitivity between the MM.1S^{dim} and MM.1S^{bright} sub-populations based on differential efflux pump expression, CAM-DR or GR expression, genetic analysis of the sorted sub-populations appeared the next logical step. This would potentially identify mutations affecting the glucocorticoid receptor pathway and CD38 expression. In addition, it could provide a means to establish the clonal origin of the sub-populations, with particular interest in the origins of glucocorticoid resistance within MM.1S^{bright} cells.

Although epigenetic changes have been assumed to be the accepted cause of absent GR expression within MM.1R cells, clonality is a concept in MM gathering acceptance as to the mechanism of disease progression (Keats et al. 2012). Building upon Edwards V et al genetic data (Edwards V et al. 2012) in identifying differences between MM.1S and MM.1R (Table 5.1), the aim of exome sequencing was two-fold. Firstly, to identify any genetic variation between MM.1S^{dim} and MM.1S^{bright} and how such differences relate to MM.1R, thus examining the clonality of these cell lines. Genetic mutational analysis would enable the construction of an evolutionary tree of the MM.1 cell line sub-clones and test the hypothesis that MM.1R is derived from a sub-clone from MM.1S, that is genetically similar to MM.1S^{bright}. The other objective was to identify genetic mutations that are able to explain the functional and phenotypic differences between MM.1S^{dim} and MM.1S^{bright}, established earlier in this chapter. And whether this data could be used to form a bespoke treatment strategy targeting specific sub-clones based on mutations involved in key MM pathways.

5.7.1 Whole exome sequencing and variation in calling strategies

DNA was extracted from the cell lines MM.1R, MM.1S^{dim} and MM.1S^{bright} with the lowest passage number in order to minimise genetic drift. These samples were then sent to the Beijing Genomics Institute (BGI), Honk Hong, for whole exome sequence (WES) at a sequence coverage of 30X reads. Following massively parallel DNA sequencing, the raw data requires a caller programme to decipher it into a format where it can be interpreted. Four separate variant callers were used, BGI's own caller system, GATK, varscan2 and samtools. Figure 5.19 shows the variation between the different calling programmes. 32,102 separate exonic mutations were called by at least one of the caller programmes, with 19,852 (61.84%) common to all four. This highlights the huge variation in calling

strategies, which is a recognised problem (O'Rawe et al. 2013) indicating that some of the variants identified by a single caller and not by the other callers are likely to be false positives. Although an option for mutational analysis would be to only include variants shared by all 4 callers, it was felt this could exclude important mutations missed by a caller (false negative). GATK caller analysis is the most widely used and felt to be the most conservative of the caller variants, thus reducing false positives and was therefore used as the calling programme for all my subsequent mutational analysis.

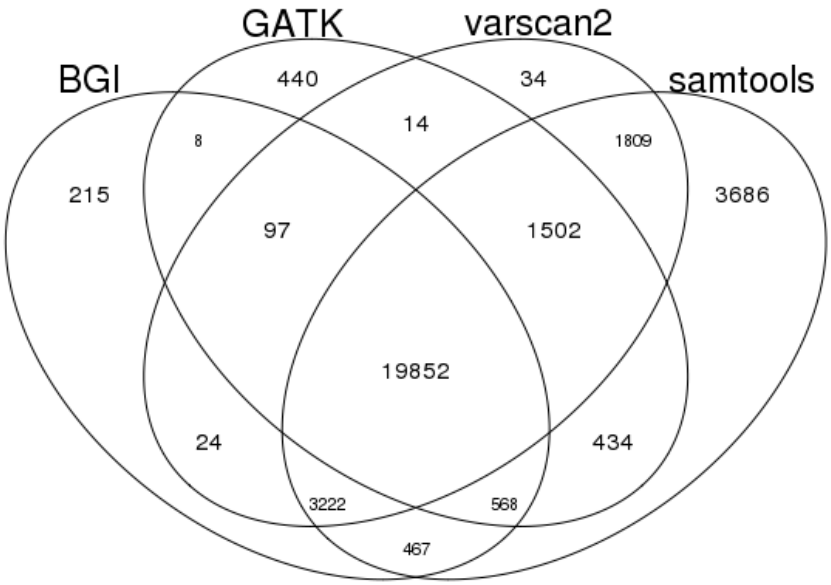

Figure 5.19. Variant calls comparison among four calling strategies. *Between the 4 calling variants a total of 32,102 individual variants were called. Of these variants, 19,852 (61.84%) were called by all four methods. Only variants within exonic regions were considered.*

Gene mutations, as called by GATK, were either 'InDel' (Insertion or Deletion) mutations comprising of both frameshift and non-frameshift mutations or single nucleotide variants (SNV)/point mutations. SNVs were further divided into synonymous (silent mutations where phenotype is not changed) or non-synonymous where phenotype is affected. Non-synonymous mutations in some circumstances were further divided to include 'Missense' where a point mutation results in a different nucleotide and consequently a different amino-acid and 'Nonsense' resulting in premature ending of codon (variations of which include stop-gain, stop-loss, start-loss and splicing). Mutations can be either regarded as constitutional, i.e. passed on through the germline or acquired, so called somatic mutations. 'Driver gene mutations' are more commonly somatic and although my mutational analysis did not specifically aim to differentiate the two groups, my

presumption was that the majority of mutations highlighted through this chapter and the next were somatic.

The mutation analysis broadly took two separate approaches, a 'top down' or a 'bottom-up'. A 'top down' approach involves selection filters being applied to the data, reducing the number of mutations to a manageable amount for additional in-depth analysis. When assessing for functional changes, *exonic, non-synonymous SNP* and *InDel* are the minimal positive selection criteria to be applied. Such mutations will cause an amino acid sequence change invariably resulting in protein structure alteration and thus potentially affecting function. Filtering mutations through reference databases (e.g. Cosmic cell line database) can be also be applied, where common mutations or natural variants are removed. Two widely used reference databases are dbSNP (a reference of common SNP mutations (Sherry et al. 2001)) and 1000 Genomes project (1KGP), a public database of human genetic variants with a frequency of greater than 1% (Birney and Soranzo 2015). The GATK calling is able to reference mutations to either of these databases. Figure 5.20 provides an overview to the filtering strategies I used for my subsequent analysis in this chapter and the next, similar strategies have been used by others in the analysis of MM cell line WES (Leich et al. 2013).

The other approach for mutational analysis, a 'bottom up' or more targeted approach, focuses on genes that are known to affect function and thus aim to identify if mutations exist for a particular gene. And in part can be used to confirm clonality if the gene in question is known to be fundamental to disease progression, survival or expansion.

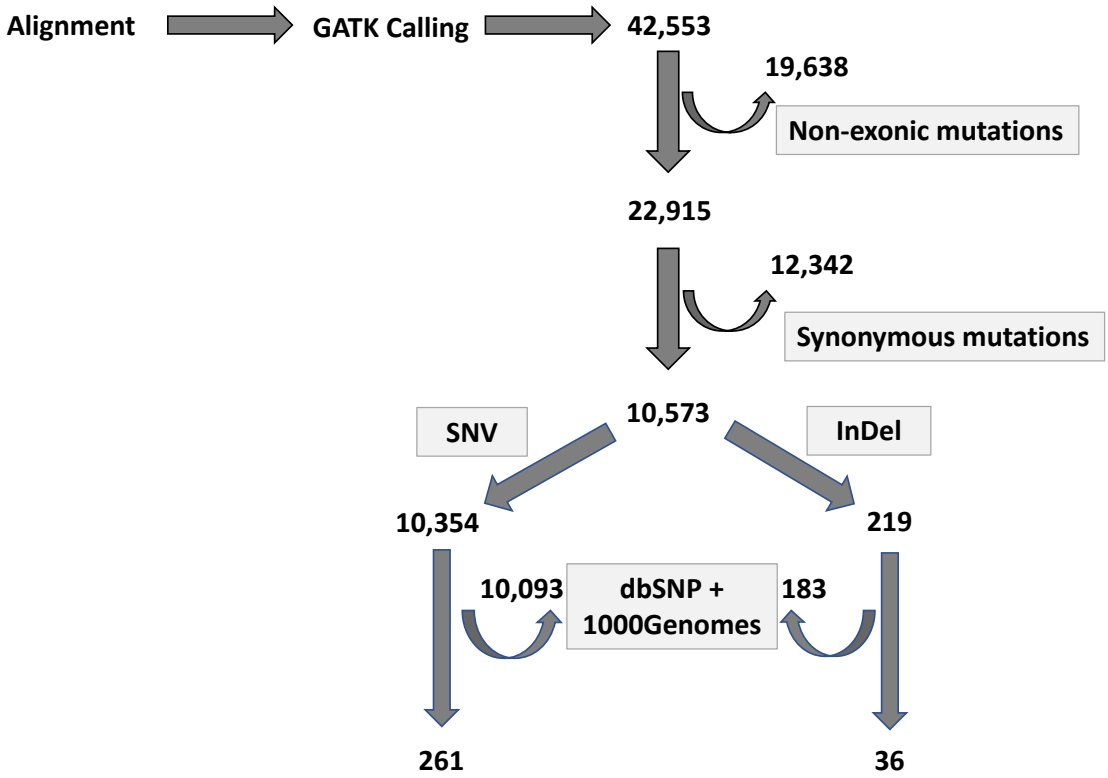

Figure 5.20. Genetic mutation filtering strategy, based on Leich et al. (2013). *After alignment and GATK mutation calling, non-exonic mutations (including introns, splice variants) were filtered. Next, SNVs that did not lead to an amino acid exchange (synonymous mutations) were excluded. Of the remaining, either divided in mutations due to an insertion or deletion of nucleotide (InDel) and non-synonymous SNV. Of the remaining mutations, analysis could be further filtered (as done in chapter 5) by excluding mutations that appear in the databases 1000 genomes or dbSNP, as these are deem to occur in healthy individuals and unlikely to be driver mutations resulting in cancer formation/progression.*

5.7.2 GATK calling reveals the 3 cell lines have high degree of mutations, the majority of which are common

In total 42,553 gene mutations (InDel and SNV) were identified, with 93.05% of them common to all three cell lines. When basic inclusion criteria (mutations that were exonic, non-synonymous or frameshift insertion/deletion i.e. coding regions) were applied, 10,573 mutations were called with 10,050 (95.05%) common to all three cell lines (figure 5.21). The high degree of shared mutations between the three cell lines, inferring a common clonal origin, but each line possessed unique genetic lesions. Of the mutations not common to the 3 cell lines, 92 (0.87%) were identified in MM.1S^{dim}, 53 (0.50%) in MM.1S^{bright} and 91 (0.86%) in MM.1R (see supplementary Table 1 and 2 in appendix for breakdown of type of mutations for each of the cell lines).

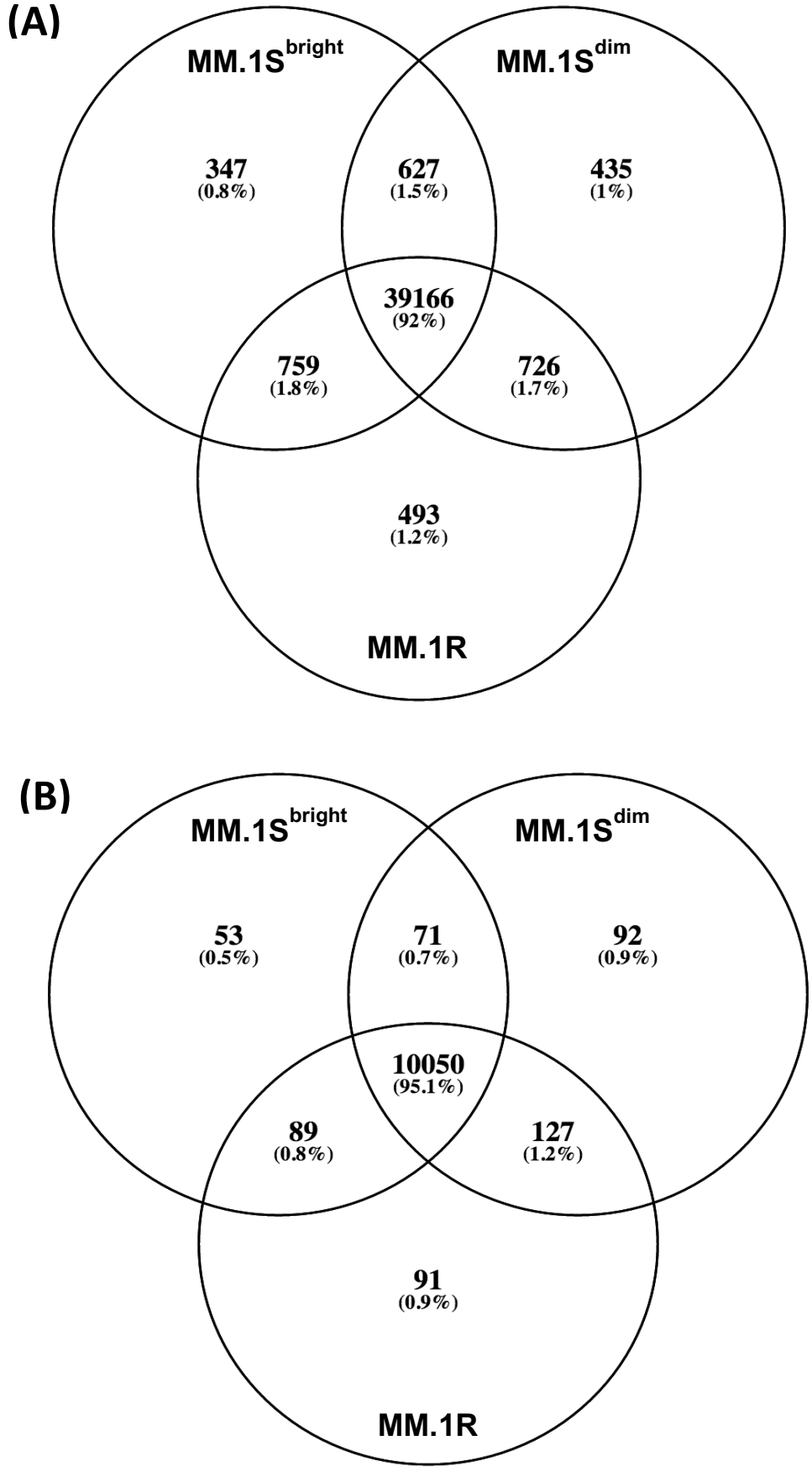

Figure 5.21. Venn diagram showing number of common and unique mutations between the 3 cell lines. *(A) No filters applied. (B) Filters applied – exonic, frameshift insertion/deletion*

5.7.3 Comparison with previous published MM.1S/MM.1R Whole Exome Sequencing confirms own data has many of the same mutations

Exome sequence produces a vast array of data. Cell lines will inevitably have more mutations than primary samples and not all mutations are potentially related to malignant process. Logical methods and screening tools are required to identify key mutation differences. There are a number of databases (Cosmic data base, the 1000 Genome project and GeneCard.org), that allow cross referencing of known cancer related mutations. As a reference point to key genetic mutations, (i.e. distinguishing from acquired mutations through repeated cell culture), it can also inform of cell line contamination through STR recognition. To established consistency of my WES with that of others, I compared my data with two separate (published) sequencing.

5.7.3.1 MM.1S COSMIC database comparison

The Cosmic database (Forbes et al. 2017) holds a vast array of information on somatic mutation relating to human cancers, both on primary samples and cell lines. The cosmic Cell line project aims to provide a comprehensive database on multiple cancer cell lines. The database mutation exclusion criteria can be found at https://grch37-cancer.sanger.ac.uk/cell_lines/about, with the aim of identifying and excluding variants through comparison of over 8000 normal datasets from 4 separate sources (1000 genomes, ESP6500, dbSNP and 'In-house normal set'). Only high confidence variants are considered, classed as 85% or higher likelihood of being real (based on read depth of >15 and mutant allele burden >15%). MM cell lines in the database include RPMI 8226, U266, OPM-2, H929, JJN-3 and MM.1S, but not MM.1R.

Of the 674 COSMIC listed MM.1S mutations, 18 were frameshift mutations (InDel) and 656 SNVs (both synonymous and non-synonymous). 488 (72.4%) of the 674 mutations were present in my WES data in at least one cell lines (15 frameshift and 473 SNV). 379 of the 488 shared mutations were common to all three cell lines (See appendix for table of mutation type subset breakdown).

Table 5.4 lists the 18 MM.1S frameshift mutations from the COSMIC database. These mutations are traditionally thought to have a higher impact on coding changes than non-synonymous SNV. Of the 18 COSMIC mutations, 15 (83.33%) were identified in my sequence data, with 13 common to all three cell lines. Of the two mutations unique to a cell line, and therefore possibly to be considered as a driver mutation, *GRID2IP* was only unique to MM.1S^{dim}, whilst *TEMEM175* for MM.1R. However, neither had a tenable link to

cancer/MM pathogenesis, *GRD2IP* role in Purkinje cell signalling (Matsuda et al. 2006) and *TMEM175* coding for a protein that constitutes a major lysosomal potassium channel (Lee et al. 2017).

Gene	Cell line with mutation	Impact	Gene Description
ABCB5	All	High	ATP-Binding Cassette, Sub-Family B (MDR/TAP), Member 5
BTNL9	All	Moderate	Butyrophilin-Like 9
C19orf33	All	Moderate	Chromosome 19 Open Reading Frame 33
CCNE2	All	High	Cyclin E2
FOXM1	All	Moderate	Forkhead Box M1
OR52K2	All	High	Olfactory Receptor, Family 52 - K, Member 2
SAMD1	All	Moderate	Sterile Alpha Motif Domain Containing 1
SAMD9	All	High	Sterile Alpha Motif Domain Containing 9
TLR6	All	High	Toll-Like Receptor 6
TMC3	All	High	Transmembrane Channel-Like 3
TMEM67	All	High	Transmembrane Protein 67
TRAF3	All	Moderate	TNF Receptor-Associated Factor 3
ZPBP2	All	High	Zona Pellucida Binding Protein 2
GRID2IP	MM.1S^{dim}	High	Glutamate Receptor Ionotropic δ2 Interacting Protein
TMEM175	MM.1R	High	Transmembrane Protein 175
DDX12	None	-	Dead/H-Box Helicase 12, Pseudogene
TNXB	None	-	Tenascin XB
UBE3A	None	-	Ubiquitin Protein Ligase E3a

Table 5.4 Coding InDel mutations as documented by COSMIC cell line mutation database *for cell line MM1.S and if mutation is present in MM1.R, MM.1S^{dim} and MM.1S^{bright} exome sequence and designated impact of mutation.*

5.7.3.2 Comparison with Edwards V et al. ASH 2012 abstract

In 2012, Edwards V et al, published NGS comparison between MM.1S and MM.1R. Table 5.5 lists genes that contained mutations not referenced by the 1KGP, present only in MM.1R and not in MM.1S (Edwards V et al. 2012). Of these 10 genes, my own sequencing data of MM.1R called mutations in 8 of them, with two genes (*MMS22L* and *AURKB*) containing missense moderate impact mutations in all three cell lines.

Gene	**MM.1R**	**MM.1S^{dim}**	**MM.1S^{bright}**
PDIA5	Missense (moderate)	-	-
TCERG1	Nonsense (high)	-	-
RANBP9	-	-	-
MMS22L	Nonsense (high) Missense (moderate)	Missense (moderate)	Missense (moderate)
PHF19	Missense (moderate)	-	-
RNMTL1	UGV-modifier	-	-
AURKB	Nonsense (high) Missense (moderate)	Missense (moderate)	Missense (moderate)
ERN1	Frameshift (high)	-	-
GPCPD1	Missense (moderate)	-	-
PIGT	-	-	-

Table 5.5. List of the 10 non-synonymous or frameshift mutations as described in ASH 2012 abstract being present in MM.1R*. Table also shows if significant impact mutations were identified in my exome sequence and to which cell line. Bracketed implies impact of mutation has on protein coding (low, moderate, high). UGV - upstream gene variant;*

5.7.4 Confirmation of clonality between the cell lines

As the majority of MM.1S and MM.1R genetic mutations identified from the COSMIC database and Edwards V et al. data were present in my exome sequence (table 5.4 and 5.5), this further reassured that my cell lines were non-contaminated and had not experienced too significant genetic drift. However, it did not reveal key mutational discrepancies between MM.1S^{dim} and MM.1S^{bright}, that would explain sub-clonal evolution. Thus, further analysis was required to confirm disease clonality and form a hierarchal picture of the origins of cell lines sequenced. For this purpose, four separate methods were applied.

5.7.4.1 Mutation analysis in known MM driver genes reveals ROBO2 as potential sub-clone driver

Despite the huge genetic heterogeneity found in MM, only mutations arising in a relatively small number of genes are felt to drive the disease or cause new clonal populations to arise. Different genetic mutations arise at different stages of the disease, with each new mutation providing an opportunity for clonal evolution. Table 5.6 outlines the 11 most common and likely mutations that are known to drive clonal evolution at different points of the disease (Bolli et al. 2014; Manier et al. 2017).

Gene Mutation	Exonic Mutations	Mutations comparison between the 3 cell lines
NRAS	-	-
KRAS	2 (nonsynonymous and silent)	Present in all 3 cell lines
BRAF	1 (silent)	Present in all 3 cell lines
TP53	1 (nonsynonymous)	Present in all 3 cell lines
FAM46C	2 (nonsynonymous and silent)	Present in all 3 cell lines
TTN	44 (1 frameshift deletion, 27 nonsynonymous and 16 silent)	Present in all 3 cell lines – 42/44 MM.1S^{dim} + MM.1S^{bright} – 1/44 (silent) MM.1S^{bright} – 1/44 (frameshift deletion)
ROBO2	1 (non-synonymous)	MM.1S^{dim} + MM.1R
PCLO	10 (1 non-frameshift deletion, 5 nonsynonymous and 4 silent)	Present in all 3 cell lines
TRAF3	2 (1 non-frameshift deletion and 1 nonsynonymous)	Present in all 3 cell lines
TET2	5 (2 nonsynonymous and 3 silent)	Present in all 3 cell lines
DIS3	-	-

Table 5.6. Exonic genetic mutation known to cause MM disease progression/formation of subclones and their presence within the 3 cell lines.

Of these 11 genes, only *DIS3* and *NRAS* had no mutations identified. Of the genes with mutations, all expressed non-synonymous mutation except for *BRAF* (silent synonymous present in all 3 cell lines). Majority of these mutations (7 of 9) were present in all three cell lines. However, 2 genes *TTN* and *ROBO2*, mutational variation between the cell lines occurred. *TTN* gene expressed the most mutations (44), 42 common to all 3 cell lines. *TTN* expresses the protein Titin which comprises the highest number of exons (363) of the whole genome (Bang et al. 2001). MM.1S^{bright} contained a unique *TTN* frameshift deletion, not observed in the other cell lines. The other driver gene that mutational variation was observed was *ROBO2*. A non-synonymous SNV was present in MM.1S^{dim} and MM.1R, but not MM.1S^{bright}. *ROBO2* is a tumour suppressor gene, a member of the ROBO family which codes for a protein receptor for the slit homolog 2 protein (Slit2) (Xu et al. 2015). Active Slit2/Robo signalling has been shown to downregulate c-myc and cyclin D1 via the PI3K/Akt pathway in breast cancer cells, with low Slit2 expression in stromal fibroblasts associated with lymph node metastasis (Chang et al. 2012).

5.7.4.2 Mutations in the CD38 gene are not the driver process in MM.1S sub-clonal formation or expression variation of the CD38 antigen

Previous genetic analysis of the *CD38* gene from 3 different non-cancer cell lines, revealed the gene to be prone to mutations (53 SNPs and 1 Indel) (Hartman et al. 2010). An association with CD38 expression and presence of mutations, most notably the 3′-UTR(1363) rs1130169 has been shown and could in theory drive clonal formation through altered expression of the antigen. However, no mutations, intronic, exonic or UTR were observed in any of the cell lines.

5.7.4.3 Inferring clonality between the cell lines is difficult by assessing high frequency gene mutations

The technique of driver gene or sub-clone identification, by analysing genes with a high frequency of mutations has been applied to many different cancers. The theory being, such analysis gives an indication where the genomic stresses are occurring and the most likely site of phenotypically relevant mutations. This method has produced a number of high profile mutation discoveries with clinical implications in haematological cancers, notably the *SF3B1* gene in CLL (Quesada et al. 2011; Wang et al. 2011a) and *CALR* in Myeloproliferative disease (Klampfl et al. 2013; Nangalia et al. 2013). Similar techniques applied to primary myeloma samples have revealed high frequency of mutations in the NF-κB pathway and for mutations causing activation of BRAF (Chapman et al. 2011). A

similar methodology was applied to this data in an attempt to infer the most likely ancestral route for clonal evolution between these three cell lines

22,915 exonic mutations (non-filtered) occurred in 9,739 separate genes. 21,834 (95.3%) of these mutations were common to all three cell lines. Of the mutations that were not common (1,082), only genes with more than 2 mutations were compared between the three cell lines (Figure 5.22). In total, 89 separate genes contained more than one mutation. Of these genes, the chromosome containing the highest amount of separate gene mutations was the X chromosome. The highest number of separate mutations identified on a single gene was 7, both *CROCC* and *COL6A3*. To discriminate the relationship between the cell lines further, a Venn diagram (Figure 5.23), highlighted if mutations were either unique to a particular cell line or at least shared between another. 28 separate genes were identified by these means. 8 of these genes (36.4%) shared exact mutation profile between MM.1S^{dim} and MM.1R, a further 8 genes (36.4%) shared between MM.1S^{bright} and MM.1R and only 2 genes (9.1%) shared between MM.1S^{bright} and MM.1S^{dim}. Of these 28 mutations, MM.1R had the highest number, 19 (67.9%).

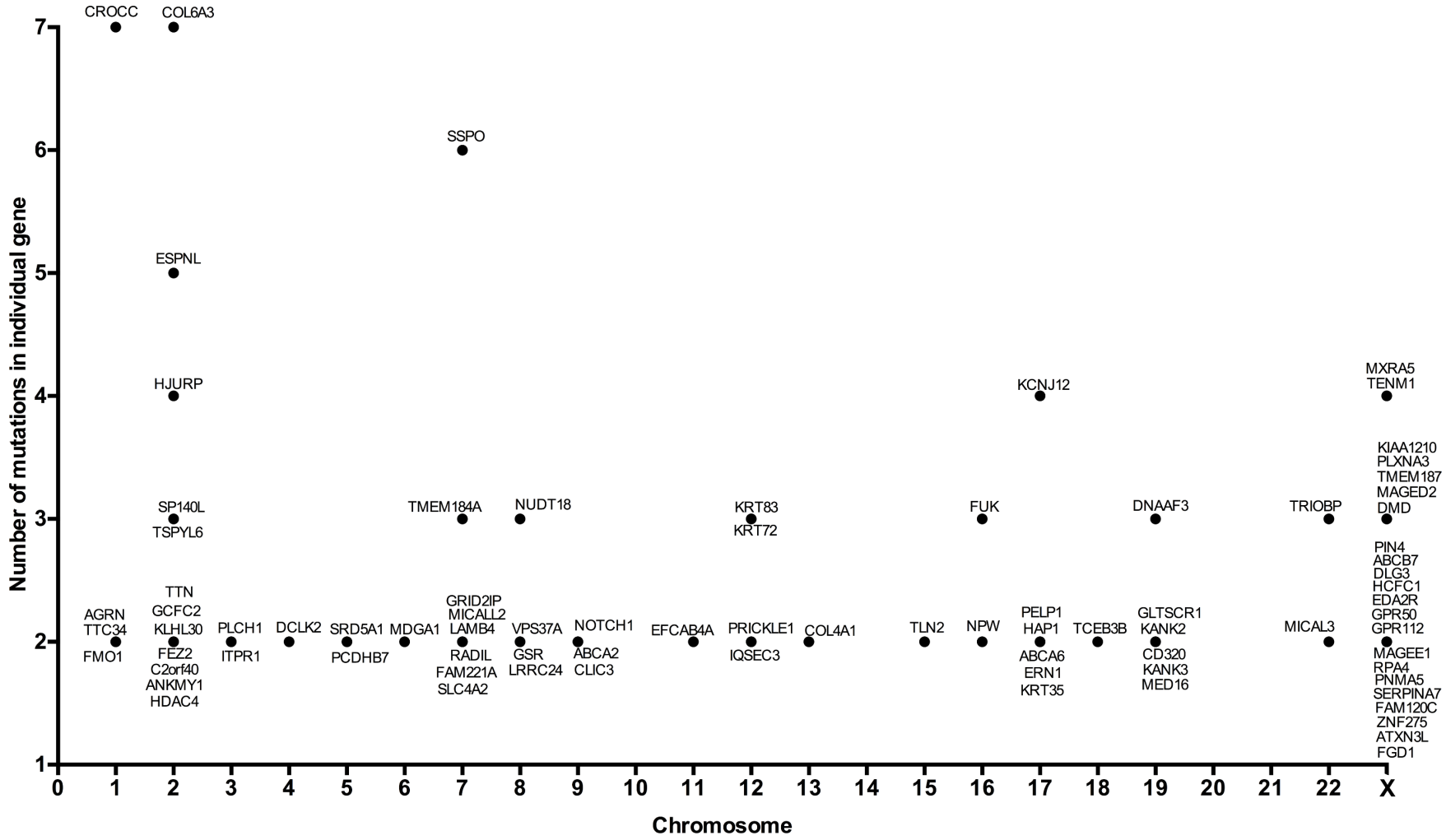

Figure 5.22. Graphic representation of genes that had more than one exonic mutation*. None of these mutations were common to all three cell lines*

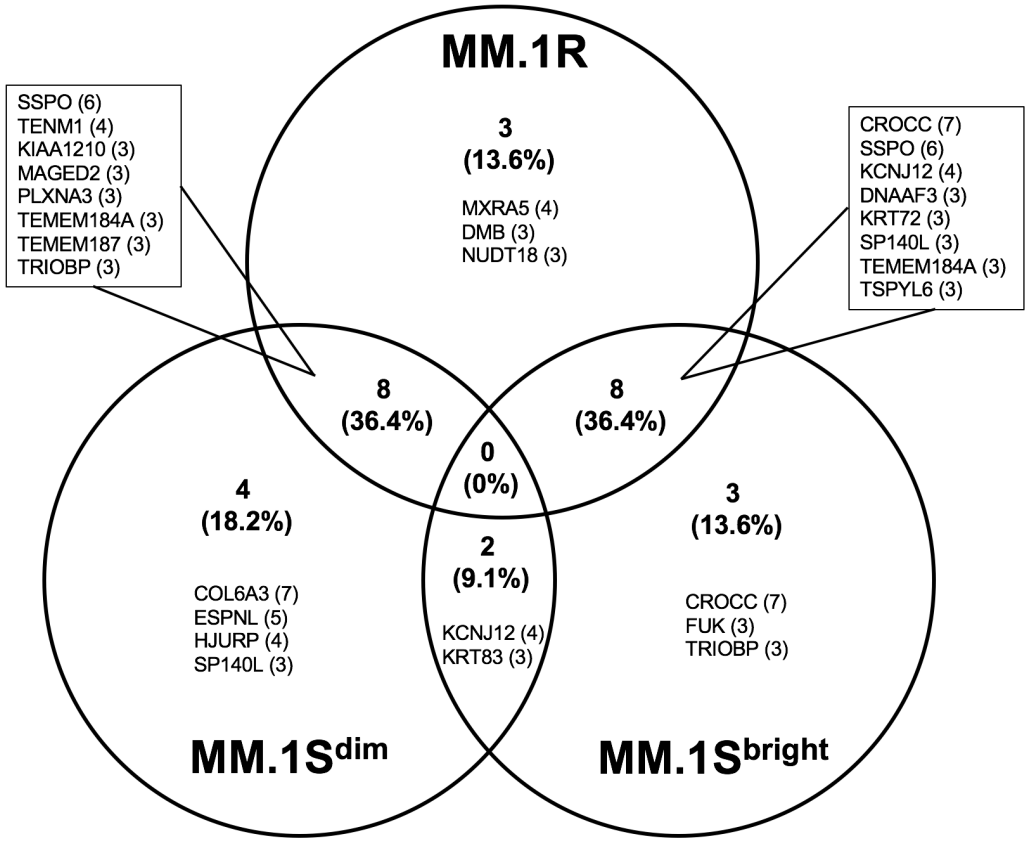

Figure 5.23. Venn diagram of genes with more than 2 mutations with the 3 cell lines. *Number in bracket after each gene name is the total number of mutations identified within that gene.*

Unique mutations found in each cell line, as highlighted by the Venn diagram, could offer potential driver mutations for sub-clonal formation; 4 mutations were unique to MM.1S^{dim}:

i. *COL6A3* contained 7 separate mutations not seen in the other 2 cell lines. This gene encodes for a subunit of Collagen type VI, involved in extra cellular matrix protein binding (Engvall et al. 1986).

ii. *ESPNL* encoded protein is involved in actin filament bundle assembly and a function that is unlikely to drive clonal evolutions in the presence of altered expression or assembly. Such genes I have termed "implausible driver gene".

iii. *HJURP* is involved in chromosome maintenance and stability and centromere function in early G1 phase. It acts to promote mitotic cell-cycle progression (Dunleavy et al. 2009) and plays a role in the immortality of cancer cells, being over expressed in lung cancers (Kato et al. 2007).

iv. *SP140L* encodes for protein that binds to and regulates chromatin found on B-cells (Bloch et al. 2000).

3 mutations unique to MM.1R:

i. *MXRA5* has been shown to have a high somatic mutation frequency in a multitude of cancers most notably non-small cell lung carcinoma. It encodes for a proteoglycan involved in cell to cell adhesion and ECM remodelling (Walker and Volkmuth 2002; Rodningen et al. 2008; Xiong et al. 2012).
ii. *DMB* encodes for the HLA class II histocompatibility antigen, DM β-chain and has been implicated in cell adhesion and antigen processing/presentation in MM cells (Zhang et al. 2015).
iii. *NUDT18* encodes for the protein MTH3, no mutation links have been discovered with MM or other haematological cancers.

3 mutations unique to MM.1S^{bright}:

i. *CROCC* encodes for protein Ciliary Rootlet Coiled-Coil involved in the cytoplasm cytoskeleton structure (Nechipurenko et al. 2016).
ii. *FUK* gene encodes fucokinase, involved in glycolipid synthesis and is likely an "implausible driver gene".
iii. *TRIOBP* is also likely to be an "implausible driver gene", it encodes an actin-bundling protein that is critical for rootlet formation. Mutations are associated with deafness (Kitajiri et al. 2010).

5.7.4.4 Selected dbSNP filter and G1000 mutations not common to all 3 cell lines, offer other potential driver mutations

Using the exclusion criteria outlined in figure 5.20, as well as mutations not shared between the 3 cell lines, 122 separate gene mutations were identified. Of these, listed below are selected genes that are either involved in B-cell physiology or cancer pathogenesis and are suggestive as alternative clonal driver mutations.

Mutation only in MM.1S^{bright}**:**

i. FIP1L1-PDGFRA fusion mutation is seen in a minority of patients with hypereosinophilic syndrome (HES), but who tend to respond extremely well when treated with a tyrosine kinase inhibitor such as Imatinib (Pardanani et al. 2006). Although predominately observed in myeloid malignancies, cases in lymphoid cancer have been reported. The fusion protein activates a number of signalling pathways including PI3K, ERK 1/2 and STAT5 (Gotlib and Cools 2008).
ii. *UGT1A1* codes for enzyme UDPGT that transforms and eliminates potentially toxic xenobiotics and endogenous compounds such as steroids, bilirubin, hormones, and drugs from the cell and has been implicated in cancer drug resistance (Tukey and Strassburg 2000; Holohan et al. 2013).

Mutations only in MM.1S^{bright} & MM.1R:

i. *CD24* encodes for the cell adhesion protein of the same name. It is expressed on most B-cells, promoting T-cell proliferation and can prevent their terminal differentiation into plasma cells, with expression decreasing as B-cells mature (Li et al. 2004; Fang et al. 2010). CD24 has also been shown to regulate CXCR4 receptor in lymphocytes and cancer cells by uncoupling CXCR4 signalling, thus altering cell migration and tumour growth (Schabath et al. 2006).
ii. *UNC13D* plays a role in cytotoxic granule exocytosis in lymphocytes. Mutations of the gene has been identified in malignant melanoma, as well as one of the defining mutations of familiar hemophagocytic lymphohistiocytosis. In this condition, lymphocytes have impaired cytotoxicity and cell apoptosis mechanisms become defective leading to uncontrolled proliferation of lymphocytes, invading healthy organs (Pachlopnik Schmid et al. 2010; Elstak et al. 2012).

5.7.4.5 Phylogenetic relationship between the three cell lines reveals original clone

Using the Human reference genome as an outgroup, phylogenetic relationship between the three sequenced cell lines were attempted, with the aim to infer the descent and relationship of the cell lines. In all cases insertion or deletion (Indel) mutations were excluded, as these are difficult to model phylogenetically. Two different investigation approaches were undertaken, both of which aimed to reduce the inferring of mutation order changes, in determining relationship. The approaches were either to examine sites that were homozygous or heterozygous in all three cell lines.

For homozygous samples there were a total of 43 sites that were variable within at least one lineage, relative to the others. Figure 5.24 shows a phylogenetic tree from the 43 homozygous sites. Amongst these, there were 2 non-synonymous changes within exons that were only found within the MM.1S^{dim} genotype and 1 non-synonymous change within an exon that was only found within the MM.1S^{bright} genotype.

Chromosome and position	Base change*	Variant quality	MM.1R genotype	MM.1S^{dim} genotype	MM.1S^{bright} genotype	Gene id
Chr 6 148869627	G → T	423.51	0/0	1/1	0/0	SASH1
Chr 14 72128103	C → A	373.83	0/0	1/1	0/0	SIPA1L1
Chr 14 22933206	T → A	772.5	0/0	0/0	1/1	TRDC (TRDV2)

***Table 5.7. Homozygous sample mutation**, that form phylogenetic tree. * base change describes the change from reference allele to altered allele; Chr – Chromosome; SASH1 - SAM and SH3 domain containing 1; SIPA1L1 - Signal-induced proliferation-associated 1 like 1; TRDC – T cell receptor delta constant; TRDV2 – T cell receptor Delta variable 2*

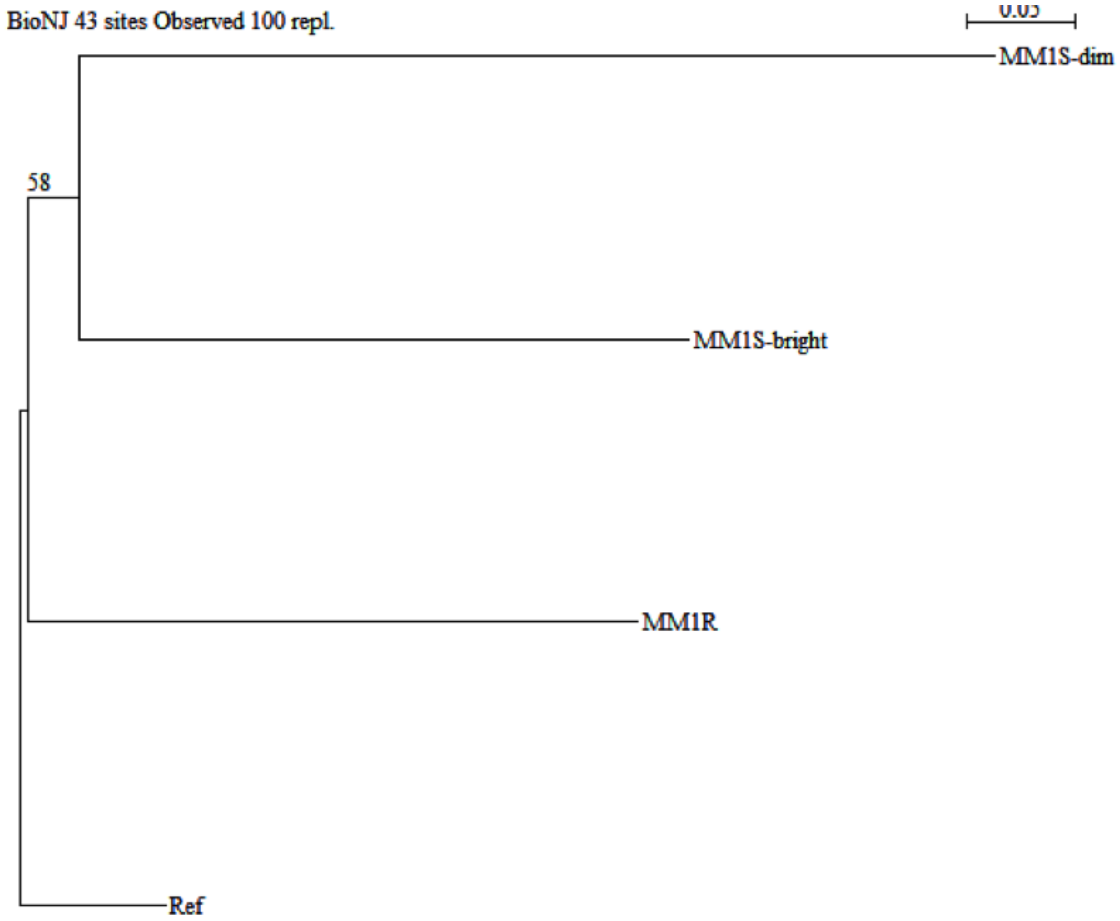

***Figure 5.24.** Phylogenetic tree produced from a SNP alignment of 43 homozygous positions across the three samples, rooted on the reference genome sequence used. Tree drawn using BioNJ in Seaview 4, with 100 bootstrap replicates. Diagram courtesy of Dr Tom Connor, Cardiff University*

The second approach was to examine only sites that were heterozygous, i.e. sites where in at least one of the samples, on one chromosome there was a variant base. This resulted in a larger number of sites analysed, 1,689. Using an algorithm called Maximum Parsimony, 1,155 of these sites were parsimony informative. The prediction showed MM.1R and MM.1S^{bright} samples swap their positions compared to the homozygous phylogenetic tree (Figure 5.25). When examining the dataset with a BioNJ tree, the bootstraps are also low on this much larger dataset (figure 5.26).

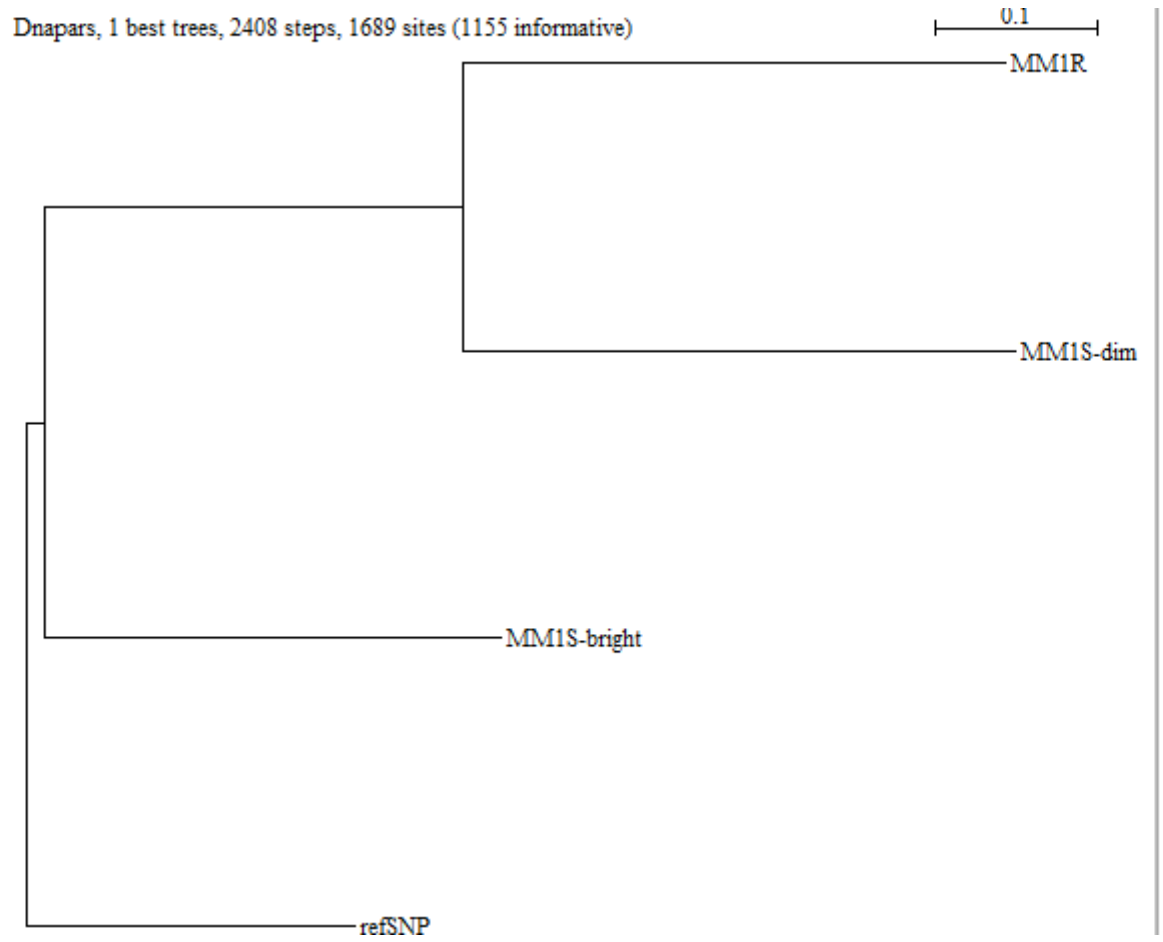

***Figure 5.25**. Parsimony tree of 1,689 heterozygous sites. Diagram courtesy of Dr Tom Connor, Cardiff University*

.

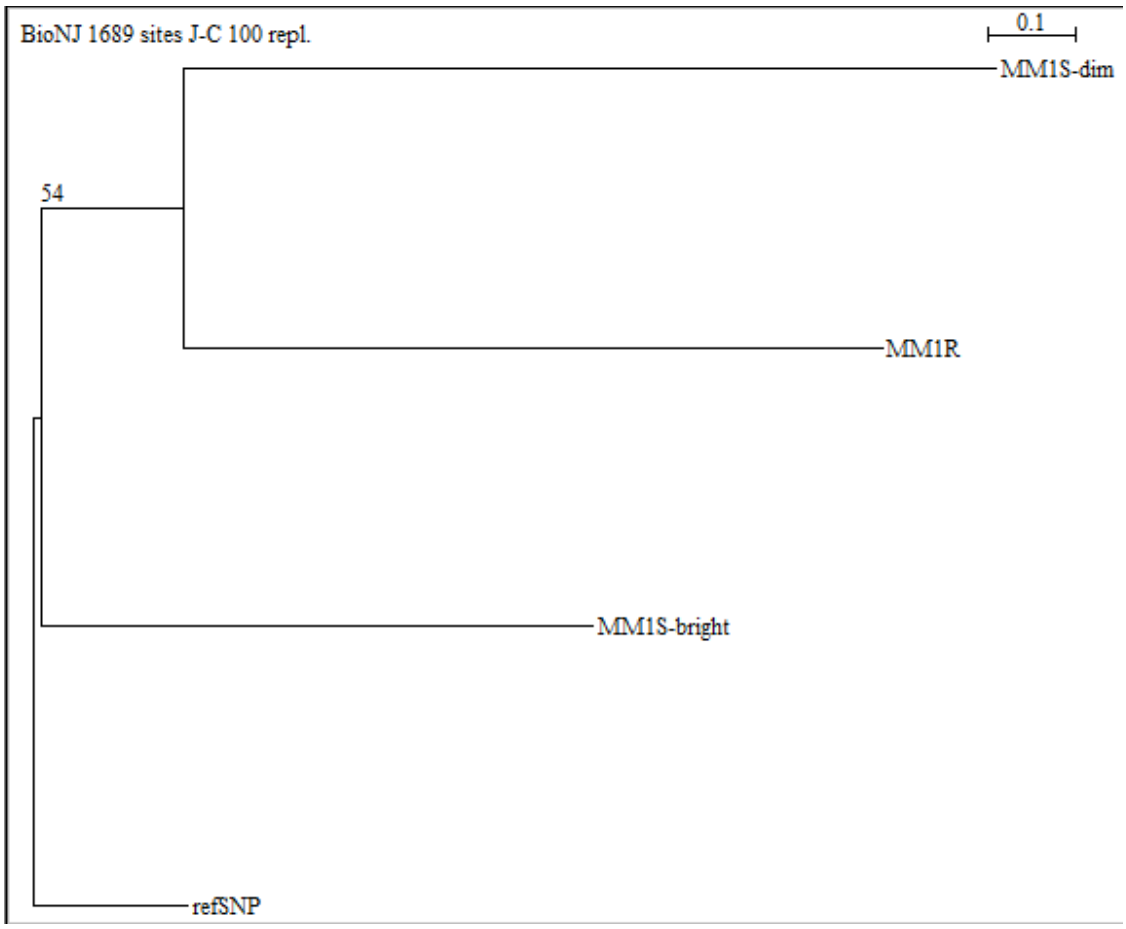

Figure 5.26. *Phylogenetic tree produced from a SNP alignment of 1,689 heterozygous positions across the three samples, rooted on the reference genome sequence used. Tree drawn using BioNJ in Seaview 4, with 100 bootstrap replicates. Diagram courtesy of Dr Tom Connor, Cardiff University*

5.8 Discussion

The advent of highly sensitive deep sequencing MRD monitoring methods such as High-Throughput Nucleotide Sequencing as outlined by Martinez-Lopez et al. has the potential to make MRD or clonal identification by flow cytometry redundant. Although it is widely accepted that flow cytometric MRD monitoring is less sensitive than NGS or PCR based IGH-VDJH, IGH-DJH and IGK gene assays (Martinez-Lopez et al. 2014), I have shown that immunophenotypic differences between sub-populations strongly correlate with functional differences. Therefore, it seems possible that phenotypic differences can be used in conjuncture with NGS to identify clonally distinct drug resistant sub-populations. In my previous chapter, I showed that phenotypically distinct populations 'that could represent differing clones' exist in 6 of the most commonly used MM cell lines. I then isolated two such 'clones' from the MM.1S cell line and showed that they varied in phenotype, drug response and migration. The aim of this chapter was to explore the possibility that MM.1S contained 2 genetically distinct sub-clones distinguishable by CD38 expression and that MM.1R is a sub-clone derived from a CD38 highly expressing clone ($MM.1S^{bright}$) within MM.1S. I confirmed that the variability in dexamethasone sensitivity was associated with CD38 expression and that $MM.1S^{bright}$ cells (which were more resistant to dexamethasone) shared numerous phenotypic characteristics more akin to MM.1R cells than $MM.1S^{dim}$ cells, including similar CD38 expression, adherence, migration and proliferative properties.

5.8.1 Phenotypic analysis

The presence of MM CD38 weak/negative clones do occur but are rare (Minarik et al. 2017). Such clones (unlike CD138 negative) are not well documented, although the Myeloma cell line U266 has virtually no CD38 expression (15.4% CD38 positivity – data not shown). This inevitably raised concern that the presence of CD38 weak subpopulation inferred cell contamination. Initial concerns were partly addressed upon MM.1S (containing both CD38 sub-clones) dexamethasone cytotoxicity assays, resulting in an IC50 consistent with the literature (0.045μM vs. 0.05μM respectively) (Chauhan et al. 2002). This provided reassurance that pre-existing research on MM.1S by others could well have involved both sub-clones and I was not working with a contaminated cell line. However, concerns remain as to why no other researcher has described a MM.1S CD38 bimodal population. Few have published immunophenotypic characteristic on MM.1S or MM.1R since Greenstein et al. initial paper where the dexamethasone resistance cell line MM.1R was acquired through long term low dose dexamethasone exposure (Greenstein et

al. 2003). Flow cytometry analysis on the two separate cell lines by Greenstein, claimed them to be immunocytochemically identical, CD38 expression 96.1% positive in MM.1S and 97.5% positive for MM.1R. I have shown this to be misleading. Greenstein et al. provided no mention of CD38 expression distribution. Indeed, although my two sorted populations have quite clearly different levels of CD38 expression, the MM.1S^{dim} can be still regarded as having a high level of CD38 expression (62.8% positivity). Thus, highlighting why describing immunophenotyping expression as percentage positivity can be flawed and would have otherwise neglected such bimodal expressions that I have gone onto extensively analyse.

The clinical relevance of varying CD38 expression in myeloma, is not as pronounced as for CLL, where it is a prognostic marker. However, it has become a very promising therapeutic target with the monoclonal antibody daratumumab showing encouraging clinical results leading to accelerated approval by the FDA in 2017 (Bhatnagar et al. 2017). The importance of CD38 in MM has therefore become more apparent and the need to study CD38 negative clones all the more important, as already the emergence of CD38 negative clones in the post daratumumab era are being reported (Nijhof et al. 2016a; Minarik et al. 2017). As to the cause of the reduced CD38 expression in MM.1S^{dim}, no mutations were detected that could have resulted in down regulation of gene. The study by Hartman et al. of variable CD38-expressing lymphoblastic cell lines and drug sensitivity with antineoplastic agents (gemcitabine and cytarabine) showed a negative correlation that was caused by non-exonic mutations (Hartman et al. 2010). Intronic sequencing as well as CD38 promoter methylation analysis would aid in confirming if expression variation was due to gene alteration/mutation or post-transcriptional modification/signalling.

FACS sorting provided a means to further analyse the CD38 sub-populations. Initial phenotypic analysis was done by flow cytometry. Immunophenotyping of three separate samples confirmed the difference in CD38 expression between the MM.1S sub-populations ($p<0.0001$). Although overlaid histograms showed subtle differences in expression of CD19, CD56 and CXCR4 between MM.1S^{dim} and MM.1S^{bright}, no statistically significant difference was observed for these or any other of the cell markers. CD49d expression difference of over 1,000 MFI between the cell lines (MM.1S^{dim} 11,764 vs. 10,574) was seen, but was not significant ($p=0.21$) and indeed overlay histograms did not show an obvious difference. The low number of replicates, combined with technicality variability of a 10-colour flow cytometry panel meant that statistical differences were hard to achieve if

genuine small expressions did exist. Increasing the number of repeats would confirm if genuine differences in expression between CD19, CD56, CXCR4 and CD49d existed.

To provide an explanation as to why the proportion of $CD38^{dim}$ cells seemingly diminished through successive cell divisions, proliferative differences between the sub-populations were investigated extensively using four different methods: doubling time, Ki-67 expression, cell cycle analysis and telomere length. The reduced proliferative propensity of the $CD38^{dim}$ sub-population provides an explanation as to why other research groups have never commented on a MM.1S CD38 bimodal population, as the $CD38^{dim}$ sub-population is overgrown by the $CD38^{bright}$ population. Whole exome sequencing allowed the identification of potential mutations in genes essential for G0/G1 cell cycle progression, such as the key proliferative protein Ki-67, which was mutated in $MM.1S^{dim}$ but not in $MM.1S^{bright}$. Although Ki-67 is a recognised nuclear cell marker for cell proliferation (Scholzen and Gerdes 2000), it has also been shown to correlate with MM angiogenesis, cell growth as well as being a prognostic marker (Alexandrakis et al. 2004a; Alexandrakis et al. 2004b). Indeed, additional evidence to $MM.1S^{dim}$ being the more passive or susceptible of the two sub-population, is from $MM.1S^{dim}$ being more sensitive to the reversible G0/G1 cell cycle arrest effect of dexamethasone (Goya et al. 1993; Mattern et al. 2007), whereby $MM.1S^{dim}$ had greater G0/G1 cell cycle arrest than $MM.1S^{bright}$ upon exposure to sub-toxic levels of the steroid.

Although the telomere lengths of all 4 cell lines are roughly of similar length, the subtle differences between them is further proof of the differing proliferative propensities of the sub-populations. The measurement of telomere lengths can be regarded as a measure of proliferative history over a set time, on the assumption that all cell lines are derived from parental lines that have undergone similar numbers of passages and that they express approximately the same amount of telomerase activity. Every time a cell divides the telomeric structure at the end of each chromosome shortens (Harley et al. 1990). Although telomere lengths tend to stabilise below 5.5 kb, consistent with reactivation of telomerase (Wu et al. 2003), cancer cells often display short (dysfunctional) telomeres making them susceptible to DNA repair and resulting in aberrant chromosomal fusion events. This is a characteristic commonly seen in MM (Walker et al. 2014), that can potentially drive genomic instability and clonal evolution (Artandi et al. 2000; Jones et al. 2012; Jones et al. 2014; Hyatt et al. 2017). Indeed, the relative short telomere of all the cell lines is confirmation of the clonal nature of them and that they have all likely been exposed

to genomic instability, but also the similar lengths of the telomeres confirm a common origin/clone shared between the cell lines.

Migratory comparison between MM.1S^{dim} and MM.1S^{bright} by transwell and dynamic migration models has shown sub-clonal variation in migration, with a positive correlation existing between migration and CD38 expression, a similar occurrence seen in another B-cell derived malignancy, CLL (Walsby et al. 2014c). What is unclear (especially for MM.1S^{dim}) is whether up regulation of CD38 expression occurs as a result of migration, or rather cells are more likely to migrate if have higher expression of CD38. Furthermore, what role CD38 plays in migration or is CD38 simply a by-product/surrogate marker of the process of migration/cell activity. My data shows that migrated cells compared to non-migrated cells have higher Ki-67 expression and have undergone an additional cell division, both factors suggestive that migrated cells are more metabolically active. Indeed, my data shows the small but brightly expressing Ki-67 population for both cell lines (section 5.2), also has increased CXCR4, CD49d and CD38 expression. Thus, suggestive even within a sub-clone, cell marker expression can be regulated, depending on how metabolically active the cell is. However, to date I have not been able to stimulate an increase in CD38 expression for MM.1S^{dim}, either through adhesion to stromal/endothelial, shear force in dynamic circulation or B-cell stimulation signals such as anti-IgM antibodies. Successful cell stimulation using anti-IgM has been shown to be related to CD38 expression in CLL cells (Zupo et al. 1996), but no such effects were observed in the MM.1S^{dim} sub-clone. CD38 weakly expressing sub-clones have been identified in myeloma patients treated with the CD38 monoclonal antibody daratumumab (Nijhof et al. 2016b). In such patients, upregulation of CD38 expression with Vitamin A derivatives such as ATRA has been seen (Nijhof et al. 2015). Treatment of the MM.1S^{dim} cell line with ATRA or vitamin A, would be an additional method not attempted (due to lack of time) in proving that expression can be altered. Regulation of CD38 expression does vary in the course of B-cell maturation to a plasma cell and in 80% of cases (Manzanera et al. 2005) is downregulated upon transformation to a MM cell. Thus MM.1S^{dim}, could be a sub-clone derived from a different stage of plasma cell maturation to that of MM.1S^{bright}. Measuring key CD38 downstream non-receptor tyrosine kinases such as BTK/phospho-BTK (Moreno-Garcia et al. 2005) as well as BTK regulated substrates such as Protein-Kinase-C (PKC), Phosphatidylcholine-Phospholipase C (PC-PLC) and Phospholipase-D (PLD), would confirm if CD38 related cell-signalling cascades are affected by reduced CD38 expression.

Indeed, the concept of immunophenotypically distinct clones with differing drug sensitivities within MM.1S is not new (Bjorklund et al. 2011; Bjorklund et al. 2013). Bjorklund et al. separated distinct CD44 expressing sub-clones of MM.1S, through exposure of Lenalidomide. The Lenalidomide resistant clone had increased CD44 expression and mRNA, with the antigen believed to be instrumental in resistance through enhanced adhesion to stromal cell, resulting in activation of Wnt/β-catenin axis and possibly activation of Akt. ATRA was shown to blockade the Wnt/β-catenin signalling pathway, thus reducing the protective actions of CD44 against lenalidomide. Measurement of CD44 antigen as well Wnt/β-catenin signalling cascade of MM.1S^{dim} and MM.1S^{bright} would confirm whether Bjorklund's CD44/lenalidomide resistant clones correspond to the CD38 clones. Whether CD38 expression has a similar direct impact on drug resistance remains unclear, but to my knowledge no direct link between CD38 and dexamethasone sensitivity exists, nor was I able to comprehensively establish one in this thesis.

Although I was unable to causally link the difference in dexamethasone sensitivity between the MM.1S CD38 sub-clones, I was able to confirm that a number of known drug resistant mechanisms did not contribute to the altered dexamethasone sensitivity. These included GR gene (*NR3C1*) mutations, the efflux pump P-gp expression (although in MM.1R, expression statistically increased upon exposure to dexamethasone, not observed in MM.1S, thus suggestive P-gp can contribute to dexamethasone resistance in other MM cell lines) and variation in the CAM-DR expression of CD49d/L-selectin. Although I was unable to show any evidence of difference in CAM-DR between MM.1S^{dim} and MM.1S^{bright}, it has been shown by others that MM cell lines exhibit multiple drug resistant clones, predominantly attributed to CAM-DR. RPMI 8226 exhibits resistant doxorubicin and melphalan sub-clones, partly due to increase expression of integrins (VLA-4, CD49d) when adhered to fibronectin (Damiano et al. 1999).

Although MM.1S expresses the integrins VLA-4 and LFA-1, required for adhesion to stromal cells (Sanz-Rodriguez and Teixido 2001; Azab et al. 2009a; Azab et al. 2012), MM.1S does not strongly adhere to immobilised ICAM, thus inferring the reduced importance of LFA-1 in MM.1S adhesion, whereas VLA-4 and its ligand receptor does adhere to immobilised VCAM, thus having a potential greater role in MM.1S CAM-DR (Azab et al. 2009a). Data included in the supplementary figures, showed that MM.1S^{bright} has a greater adhesive propensity to HS-5 than MM.1S^{dim} (71% vs. 44% of total co-cultured cells, see appendix). It is therefore plausible that CAM-DR plays a role in MM.1S^{bright}

dexamethasone resistance compared to MM.1S^{dim}. Given greater time, other adhesion markers such as L-selectin and P-selectin on MM cells as well as HUVEC/HS-5 selectins could have been measured in co-culture as well as its ligand PSGL-1, as to alternative CAM-DR mechanisms.

The other possible explanation of the differing dexamethasone sensitivities, may lie within IL-6. Hideshima et al. has shown the dexamethasone apoptotic effect on MM.1S can be reversed by IL-6 through the activation of the PI3-K/Akt pathway, in addition to activation of Ras/Raf/MEK/MAPK and JAK/STAT3 promoting MM cell survival/proliferation (Hideshima et al. 2001). Although not statistical, my data did show that MM.1S^{bright} has a higher baseline cytoplasmic expression of IL-6 than MM.1S^{dim}. Given additional time, the impact and role of IL-6 on the two CD38 populations could have been explored, including dexamethasone cytotoxic assays with increasing concentrations of IL-6, in addition to expression levels of phospho-proteins of the fore mention pathways related to IL-6 expression.

5.8.2 Genetic analysis

The confirmation of the clonal origin of GC resistance through either key genetic mutations or phylogenetic analysis has been difficult. My limited bioinformatics knowledge, time and resources has potentially restrained the depth of genetic analysis. Regardless, I feel I have identified a number of key findings. Firstly, with over 95% of mutations common to all 3 cell lines, the common ancestor or original driving clone are likely to remain intact for all 3 cell lines. This gives reassurances that no contamination with other cell lines occurred and the functional and phenotypic differences observed are from sub-clone mutations or alteration in their gene expression. The variation in the four different mutation calling strategies, raises the possibilities of false positive/negative called mutations, for example *RANBP9* mutations called by Edwards V data but not my own, could represent such an occurrence. The comparison of different exome sequence data therefore must be interpreted with caution for such reasons as well as the potential variation in the samples and post analytical analysis. Such variation includes different exclusion criteria, use of older dbSNP and 1KGP databases, age of cell line, read coverage and acquisition of new mutations through successive passages. Duplicate exome sequencing at different time points with greater read depths, although expensive and time consuming would be able to remove uncertainties and confirm true mutations. Bolli et al. have shown (by serial sampling) diverse patterns of clonal evolution, including linear evolution, differential clonal response and branching evolution (Bolli et al. 2014). For

example, the acquired driver mutations seen in my cell lines e.g. ROBO2 and TTN cannot be fully assumed they occurred in-vivo (i.e. in the patient) and not post cell line immortalisation. Bolli et al, describes the diverse processes that contribute to the mutational repertoire, to include kataegis, somatic hypermutation and their relative contribution changes over time. This all contributes to the huge heterogeneity of the disease and difficulty in analysing it.

Identifying high frequency mutations in an attempt to prove clonality has it flaws. By its own definition, these genes are more likely to develop further mutations amongst it clones, leading to gradual genetic drift/distinction. And such mutations are not guaranteed to result in a functional change, or selection advantage. Regardless of this matter, high frequency SNV are useful to follow as they will be passed on to subsequent generations, whereupon distinct sub-clones with functional differences occur. It also remains a crude filtering mechanism for mutation gene analysis.

Such analysis, highlighted only 2 high frequency mutation genes shared between MM.1S^{dim} and MM.1S^{bright} (KCNJ12 and KRRT83), whereas MM.1R shares an equal number of high frequency mutations for MM.1S^{dim} and MM.1S^{bright} (8 each including COL6A3 and *SSPO*). This would suggest that MM.1R contains sub-clones that represent both MM.1S^{dim} and MM.1S^{bright}, and not solely derived from MM.1S^{bright}. But also, the greatest genetic variation and most distinct sub-clones observed, was between MM.1S^{bright} and MM.1S^{dim}. Ultimately to prove if MM.1S^{dim} sub-clone remains active within MM.1R, both MM.1S CD38 sub-clones could be grown in low dose dexamethasone as outlined by Greenstein et al. to see whether dexamethasone resistance could be established (Greenstein et al. 2003).

Interrogation of gene function of the high frequency mutation analysis can provide mechanisms of clonal evolution. For example, COL6A3 mutation is present only in MM.1S^{dim}. Although mutations in this gene have not been linked with MM or EMD to date, the gene codes for a protein integral to type VI collagen, important in binding of extracellular matrix proteins (gene 2018). Collagen proteins have been shown to be of importance in binding MM cells to the extracellular matrix in bone marrow (Chauhan et al. 1996; Mahindra et al. 2010). Such mutations, could be of significance in migration/extramedullary disease and could warrant genetic sequencing of primary MM samples to establish whether a significant frequency of gene mutation occurs. Functional assays such as 3D collagen matrix migration exists that can analyse the

migration of cells and examine sub-clone potential to migrate to other sites (Wolf et al. 2009; Rommerswinkel et al. 2014).

Other high frequency genes of potential interest were *SP140* and *SP140L* (SP140 like), with 2 common missense mutations observed in the cell lines, but a unique mutation of *SP140L* in MM.1S^{dim}. Bolli et al. whole exome analysis of 67 MM patients, identified 4 truncated *SP140* mutations (2 frameshift, 1 nonsense, 1 splice site) and a missense mutation. The proteins coded by *SP140* and *SP140L* are restricted to lymphoid cells, a homologue of *SP100* and implicated in mature B cells antigen responses (Madani et al. 2002). *SP140L* is likely an evolutionarily consequence of unequal meiotic recombination of *SP140* and *SP100* genes, but maintains the same function as *SP140* (Madani et al. 2002; Saare et al. 2015). The authors concluded that the significant frequency of inactivating somatic mutations in *SP140* could implicate the gene being a novel candidate tumour suppressor in MM and a potential clonal driver mutation (Bolli et al. 2014). The high frequency and variation of *SP140* and *SP140L* within my exome sequence could thus provide a mechanism of sub-clonal formation.

Although not applied in this chapter, pathway analysis software using high frequency mutations could identify signalling pathways integral to the formation of sub-clones as oppose to single 'driver mutations'. For example, Enrichr (Kuleshov et al. 2016) software identified that the highly mutated *SSPO* gene (6 separate non-common mutations) affects the NF-κB pathway. The link with *SSPO* and NF-κB is an important one as this pathway has been linked to be a key driver in formation of sub-clones and drug resistance in myeloma (Chapman et al. 2011).

A much simpler method to identify mutations that could cause sub-clone formation, was to reference known MM driver mutations with my sequenced data. Of the 200 most common mutated genes (Corre et al. 2015) in MM, I focused on the 10 most recognised mutations of driving clonal evolution (Chapman et al. 2011; Egan et al. 2012; Bolli et al. 2014; Manier et al. 2017; Rasche et al. 2017). Expanding the number over this figure would not only be time consuming but raised the possibility of analysing mutations that only have a limited impact on disease progression. The analysis concluded the cell lines are highly mutagenic (8 of the 10 driver genes mutations were observed) and for the most part was shared between the 3 cell lines. The gene *TTN*, contained a large number (44) of different mutations, 42 of which were common to the 3 cell lines. Chapman et al, questions the validity of *TTN* as being a disease driver mutation as its function does not commonly

correlate with disease in cancer, thus regarding it as a highly mutable gene with little supported by Titin the protein that coded by *TTN*, contains the most number of exons (363) in the whole genome (Bang et al. 2001), thus increasing the likelihood of mutations simply because it contains the longest base pair sequence of any other driver gene. Of the other 10 driver gene mutations, the only other gene where mutational variation between the cell lines was observed was *ROBO2* and offers a more promising explanation as to a cause of sub-clonal formation than *TTN*. The mutation is catalogued in the COSMIC database (http://cancer.sanger.ac.uk/cosmic/gene/analysis?ln=ROBO2) and the function of this protein correlates more appropriately with plasma cell function/cancer than *TTN*. *ROBO2* is a tumour suppressor gene, a member of ROBO family which codes for a transmembrane receptor for the slit homolog 2 protein (Slit2). Binding to Slit2 regulates cell migration and axon guidance, with overexpression resulting in G0/G1 cell cycle growth arrest and cell apoptosis (Xu et al. 2015). In cancer, Slit2/Robo signalling has been shown to downregulate c-myc and cyclin D1 expression via the PI3K/Akt pathway. In cancer mutations in *ROBO1/2* has been shown to infer a poor prognosis in MDS, with low Slit2 expression in stromal fibroblasts, associated with lymph node metastasis (Chang et al. 2012; Xu et al. 2015). The same *ROBO2* mutations were observed in MM.1S^{dim} and MM.1R, but not MM.1S^{bright}. Again, this reinforces the distinct clonal separation between MM.1S^{dim} and MM.1S^{bright} and that MM.1R has evidence of key driver mutations shared both with MM.1S^{dim} and MM.1S^{bright}, suggestive MM.1R contains numerous sub-clones, including primitive forms of both MM.1S^{dim} and MM.1S^{bright}. Thus, adding weight to MM.1S^{bright} being the original clone, with *ROBO2* a potential driver mutation that parted the MM.1S CD38 sub-populations, eventually forming distinct sub-clones. Complicated bioinformatical models exist to recognise key mutational drivers in cancer (Zhao et al. 2012). GEP, SNP arrays may give additional information as to the evolution of sub clones, given more time and resources.

Phylogenetic and mutational driver analysis should complement each other as they take different approaches in establishing clonality. Whereas mutational driver analysis looks for an explanation for clonal drift by exploring gene function, phylogenetics can completely ignores gene function, in favour of pattern recognition of the inheritance of SNV that results in clonal evolution. In essence mutational driver analysis should explain the findings of phylogenetic analysis. However, while this is quite simple in bacteria, it is much less trivial in organisms that are diploid and above. In the case of cancer cell lines, it becomes even harder because there may be variable polyploidy within the cells. Ploidy is difficult to analysis phylogenetically for a number of reasons. The main one being there

are two possible bases for each position on a chromosome. For example, in the case of my three cell lines, three different genotypes may exist;

Genotype MM.1S^{dim}: A \ A

Genotype MM.1S^{bright}: A \ C

Genotype MM.1R: C \ C

In this example, it is difficult to know whether there is one mutation, followed by a recombination event or two mutations. If it is two mutations, the difficulty becomes how to interpret that there is a mutation happening on each strand of MM.1R. Notionally the 'best' approaches are ones where you do not have to infer whether there are one or two mutations as in the above example. I addressed this issue by two separate methods, by examining homozygous sites against heterozygous sites. However, the results were not totally consistent.

The homozygous analysis, fits the narrative that MM.1R sub-clone is a manifestation of MM.1S^{bright}, with MM.1S^{dim} a separate sub-clone. Arguably, examining homozygous sites is more reasonable, as each variant site should potentially only require a single mutation event to be created. However, the bootstrap value is low and furthermore the number of sites (43) is very small to make any sort of strong inference on. Thus, using heterozygous sites offers an alternative as the number of sites available for analysis increases dramatically to 1,689. This alternative approach indicates that the root for the cell lines is MM.1S.^{bright}, as MM.1S^{dim} and MM.1R show more commonality and have likely genetically diverged away from MM.1S^{bright}, subsequently forming their own sub-clones. This approach conjectures the driver mutation analysis that showed MM.1S^{dim} and MM.1R share mutations that MM.1S^{bright} does not (*ROBO2* and *TTN* mutations). Thus re-iterating the mutational divergence of MM.1S^{bright} and MM.1S^{dim}, forming distinct phenotypes that are sub-clones of each other. In terms of inferring an 'ancestral' genotype, this remains problematic because the cell lines have been cultured passaged for a significant period of time. The phylogenetic analyses suggest that the 3 cell lines are all divergent from one another, with MM.1R and MM.1S^{bright} probably both being a similar distance from a shared common ancestor. However, without the addition of periodic sampling, inferring the ancestral state in a meaningful way is very difficult. Such sampling with repeated sequencing over a time period would be hugely time and resource consuming but would be the only way to answer such ancestral questioning.

5.8.3 Summary

In summary, I have shown that CD38 sub-clones pre-exist within the MM.1S cell lines and are in fact both distinct sub-clones found in the MM.1R cell line. The three cell lines all have notable functional, cytotoxic and genetic difference. My hypothesis that dexamethasone resistance is borne out of the $CD38^{bright}$ MM.1S sub-clone was not shown to be true, but rather $MM.1S^{bright}$ is a separate sub-clone to MM.1R, that diverged from the original ancestor at roughly the same point, potentially initiated through the acquired *ROBO2* driver mutation that is seen in $MM.1S^{dim}$ and MM.1R, which highlights the greater genetic similarities between these two sub-clones. This would seemingly suggest that dexamethasone resistance could be acquired through low dose dexamethasone culture of either $MM.1S^{bright}$ or $MM.1S^{dim}$. The complexity of MM sub-clone and dexamethasone sensitivity is highlighted here, confirming the huge genetic heterogeneity of the disease and that many different clones and factors may be contributing towards dexamethasone resistance and CD38 expression.

My work has also shown that CD38 expression within sub-clones correlates with increased migratory potential. This is of increasing relevance in the era of CD38 monoclonal antibody therapy, which will inevitably result in the emergence of an increasing frequency of CD38 negative clones as a new mechanism of drug resistance. Genetic explanation of the functional differences, through pathway analysis and identification of key gene mutations differences, that are shown to provide a survival benefit, would enhance the argument of sub-clonal evolution and is explored in greater detail in the next chapter.

CHAPTER 6:

Genetic Analysis of Multiple Myeloma Sub-Clones; A Model for Targeted Pharmacological Treatment

6.1 Introduction

Increased understanding of the key pathways involved in MM survival and the mutations affecting them, has led to the development of targeted pathway therapies such as the proteasome inhibitors, bortezomib, carfilzomib and more recently ixazomib (Allegra et al. 2014), all of which inhibit the NF-κB pathway (Hideshima et al. 2002b). Comparative genetic mutational analysis between sub-clones such as MM.1R, MM.1S^{dim} and MM.1S^{bright} can be used to create bespoke sub-clonal treatment strategies predominantly based on pathway analysis, which focuses on reversal of drug resistance, such as dexamethasone.

As previously discussed in chapter 5, mutational analysis can be performed either via "top-down" approach or a "bottom-up" approach. The "bottom-up" approach, is a candidate approach, where a selected gene is looked at. The "top-down" approach, although a more time-consuming approach, it theoretically ensures all mutations are considered, with reduced selection bias. To reduce the number of gene mutations in the top-down approach, exclusion criteria can be applied to the database, aiding in further analysis. Such criteria can include low-frequency mutations (as previously discussed in chapter 5) or mutations with a dbSNP reference. The dbSNP filter aims to exclude previously referenced SNPs. There remains a subtle difference between a SNP (single nucleotide polymorphism) and SNV (single nucleotide variant). A gene containing a SNP will have a single nucleotide variation with a frequency of higher than 1% in the normal population and usually labelled with a dbSNP reference ID. Although it is wrong to presume that all variations with either a dbSNP reference or a frequency greater than 1% are non-functional, in general the more 'common' a variant is among the population, the less likely it will have a direct role in cancer pathogenesis. Indeed, not all mutations will relate to disease or process being studied, or even where the normal function of the gene has no correlation to the function

of the tissue or disease where it is derived from. Such genes can be regarded as "implausible genes" (Bolli et al. 2014) and are more commonly seen in cancer cell lines, contributing to the large number of mutations identified. Applying dbSNP exclusion filter can remove many such mutations and are usually essential when applying pathway analysis tools to a large sequence of genetic mutations. Whilst such a method is almost essential in reducing the number of candidate genes to be analysed, it does risk the possibility of excluding dbSNP that are ever increasingly being shown (mainly from GWAS) to be associated with cancer (Sud et al. 2017).

Pathway analysis software tools such as Ingenuity or Enrichr provides an alternative method to mutational analysis than simply looking at the function of individual genes and is able to link many individual mutations together. The online tool Enrichr provides access to a variety of gene libraries, each of which have databases that links gene mutations to a variety of biophysiological aspects such as cell function, gene transcripts, disease and pathway analysis. The gene mutation library NCI-Nature 2016 links vast number of gene mutations to over 200 distinct pathways involved in cancer pathogenesis (Huang da et al. 2009). The Enrichr software tool reports its enrichment results by either a Fisher's exact test p-value (provides a probability of any gene belonging to any set), a z-score (modified Fisher's exact test taking into account deviation from an expected rank) and a combined score which is a combination of the p-value and z-score (Kuleshov et al. 2016).

In this chapter I further interrogated the exome sequencing data of the MM.1 cell line sub-clonal populations, MM.1R, MM.1S^{dim} and MM.1S^{bright}. The clonality of these 3 cell lines I had proven in the previous chapter and have thus referred them as sub-clones of each other in the Chapter. I also set out to go a step further by identifying sub-clonal genetic divergence that results in altered pathway inhibition or activation. In so doing, I aimed to test a proof of concept that targeting these lesions may preferentially affect those sub-clones and prevent their clonal expansion following treatment with standard therapies - so-called clonal tiding.

6.2 Functional Genetic Analysis - the "Bottom-up" approach

6.2.1 NR3C1

The gene coding for glucocorticoid receptor, is located on chromosome 5 (5q31) and is also known as GR or GCR. MM.1S^{dim} and MM.1S^{bright} both contains a heterozygous exonic synonymous (silent) SNV that MM.1R does not. GATK calling programme infers the mutation does not affect protein coding.

6.2.2 Mutations in genes pertinent to this thesis:

Table 6.1 lists various genes that codes for proteins specific to this thesis. They include the cell markers used in the flow cytometry panel from chapter 3 and key B-cell signalling proteins (Syk and PAX5), discussed in chapter 4. Table 6.2 lists those genes that contain exonic mutations that are predicted to affect protein coding (i.e. non-synonymous and/or InDel.)

7 of the 8 genes listed in table 6.2 contained mutations that were common to all 3 sub-clones. *MKI67* was the only gene that contained a mutation (heterozygous frameshift deletion) unique to a specific sub-clone, MM.1S^{dim}. The GATK calling deemed this frameshift deletion to be of a high impact significance in protein coding and expression.

Gene	Total no. mutations	Intronic SNV	Exonic synonymous SNV	Exonic non-synonymous SNV	Indel.
SYK	2	1	1		
MKI67 **(Ki-67)**	13	2	5	5	1
IL6ST	4	2		2	
IL6 **(IL-6)**	2	1†		1	
PTPRC **(CD45)**	0				
ITGA4 **(CD49d)**	6	3	2	1	
NCAM1 **(CD56)**	5	4		1	
CD40LG	3	1	2		
CD40	4	4*			
PAX5	2	1		1	
CD19	0				
CD38	0				
SDC1 **(CD138)**	1			1	
CXCL12 **(SDF-1α)**	0				
CXCR4	0				
MMP9 **(MMP-9)**	4	2‡	1	1	

Table 0.1. Selected genes and presence of mutations and type*. * Includes UTR5 mutation; †Includes intergenic mutation; ‡includes UTR3 mutation; InDel – Insertion of deletion frameshift mutation; SNV – single nucleotide variant;*

Gene	MM.1R	MM.1S^{dim}	MM.1S^{bright}
MKI67	Missense SNV‡ (het) x5	Missense SNV‡ (het) x5 **Frameshift del† (het)**	Missense SNV‡ (het) x5
IL6ST	Missense SNV‡ (het) x2	Missense SNV‡ (het) x2	Missense SNV‡ (het) x2
IL6	Missense SNV‡ (het)	Missense SNV‡ (het)	Missense SNV‡ (het)
ITGA4	Missense SNV‡ (hom)	Missense SNV‡ (hom)	Missense SNV‡ (hom)
NCAM1	Missense SNV‡ (hom)	Missense SNV‡ (hom)	Missense SNV‡ (hom)
PAX5	Missense SNV‡ (het)	Missense SNV‡ (het)	Missense SNV‡ (het)
SDC1	Missense SNV‡ (hom)	Missense SNV‡ (hom)	Missense SNV‡ (hom)
MMP9	Missense SNV‡ (hom)	Missense SNV‡ (hom)	Missense SNV‡ (hom)

Table 0.2 Targeted identification of specific gene mutations*. Exonic gene coding effect as determined by BGI/GATK calling software: †High impact (Non-synonymous InDel); ‡Moderate impact (non-synonymous SNV); Synon. – Synonymous; SNV – single nucleotide variant; Missense – missense non-synonymous SNV; – Bold genes refer to exonic non-synonymous mutations, either single nucleotide variants or InDel.*

6.3 Functional Genetic Analysis - the "Top down" approach

Basic exclusion criteria (intronic and silent/synonymous) reduced the number of mutations to 10,573. The majority of the remaining mutations were common to all 3 sub-clones, these were excluded, leaving only 452 out the 10,573 mutations. Mutations were further filtered to exclude genes with only a single individual mutation, (see section 6.2.1) or dbSNP mutations (see section 6.2.2). These consolidated lists were then subjected to Enrichr pathway analysis, matched to the NCI-Nature 2016 database.

6.3.1 Pathway analysis of genes with more than one mutation, identifies 2 key genes affecting the NF-κB pathway

By excluding genes that only contained a single mutation, i.e. targeting genes that have a higher propensity to mutate, 48 separate genes were identified for MM.1R, 37 for MM.1S^{dim} and 28 for MM.1S^{bright}. Of these genes, only two were cross-referenced to the NCI-Nature 2016 pathway analysis database; *SSPO* and *COL6A3*. As previously discussed in chapter 5, *SSPO* was a highly mutated gene (6 separate mutations across all the 3 sub-clones identified), but not all of them were identical. For example, MM.1S^{dim} and MM.1S^{bright} did not share any of the same *SSPO* mutations, whereas MM.1R shares 3 non-synonymous with MM.1S^{dim} and 1 non-synonymous mutation with MM.1S^{bright}. The Enrichr pathway analysis highlighted the NF-κB pathway and β-catenin degradation pathways to be statistically affected by this mutation (table 6.3) for all 3 sub-clones, with the highest combined score seen in MM.1S^{bright}.

Mutations in *COL6A3*, were only observed in MM.1S^{dim}. The Enrichr programme, indicated the signalling pathways potentially affected by the mutation included Syndecan-1 (p=0.082), β1 integrin cell surface interaction (p=0.12) and integrin angiogenesis (p=0.13), though none were deemed to be statistically significant.

	MM.1R	MM.1S^{dim}	MM.1S^{bright}
SSPO related Pathways			
Non-canonical NF-κB pathway	4.96 (p=0.014)*	5.26 (p=0.011)*	5.59 (p=0.008)*
Canonical NF-κB pathway	3.70 (p=0.054)	4.02 (p=0.042)*	4.36 (p=0.032)*
Atypical NF-κB pathway	3.54 (p=0.040)*	3.82 (p=0.031)*	4.13 (p=0.024)*
Degradation of β-catenin	3.35 (p=0.040)*	3.62 (p=0.031)*	3.91 (p=0.024)*
PS-1 regulation of Notch/Wnt	2.83 (p=0.105)	3.29 (p=0.082)	3.48 (p=0.062)
PLK1 signalling events	3.03 (p=0.105)	3.20 (p=0.082)	3.73 (p=0.062)
ATR signalling pathway	2.85 (p=0.09)	3.14 (p=0.070)	3.46 (p=0.053)
COL6A3 related pathways			
Syndecan-1 mediated signalling		2.82 (p=0.082)	
Integrin related angiogenesis		2.05 (p=0.13)	
β1 integrin interactions		2.39 (p=0.12)	

Table 0.3. NCI-Nature 2016 pathway analysis of non-synonymous exonic mutations *from genes that express more than one mutation and not common to all 3 cell lines. Each pathway has an Enrichr Combined score indicating gene relevance to pathway, in addition to p value; * - indicates statistical significance; PS-1 - Presenilin-1; NF-κB - nuclear factor kappa-light-chain-enhancer of activated B cells;*

6.3.2 dbSNP filter and Indel offers alternative but larger mutation list for pathway analysis

Of the 10,573 mutations, 10,354 were non-synonymous SNV, the remaining are InDel. Of the SNVs, 2.69% (276) did not have a dbSNP reference. Table 6.4 shows the number of SNV for each cell line that did not have a dbSNP reference, in addition to the number and relative frequency of InDels, (see supplementary table in appendix for a list of the individual genes that were mutated).

	Indel	**SNV**	**TOTAL:**
MM.1S^{dim}	4 (8.16%)	42 (15.22%)	46 (14.15%)
MM.1S^{bright}	2 (4.08%)	26 (9.42%)	28 (8.62%)
MM.1R	6 (12.24%)	26 (9.42%)	32 (9.85%)
MM.1S^{dim} & MM.1R	0 (0%)	1 (0.36%)	1 (0.31%)
MM.1R & MM.1S^{bright}	0 (0%)	5 (1.81%)	5 (1.54%)
MM.1S^{dim} & MM.1S^{bright}	0 (0%)	10 (3.62%)	10 (3.08%)
Common mutations	30 (61.22%)	173 (62.68%)	203 (62.46%)
Total	49 (100%)	276 (100%)	325 (100%)

Table 0.4. Number of exonic mutations *(Indel. and non-synonymous without a dbSNP reference) that was used for Enrichr analysis for each cell line.*

Using this consolidated list of mutations, table 6.5 lists the 'likely affected' pathways as predicted by Enrichr mutational analysis (using NCI-Nature 2016 database) for each cell line. Figure 6.1 showing a clustergram of the pathways and the mutated genes related to the specific pathway.

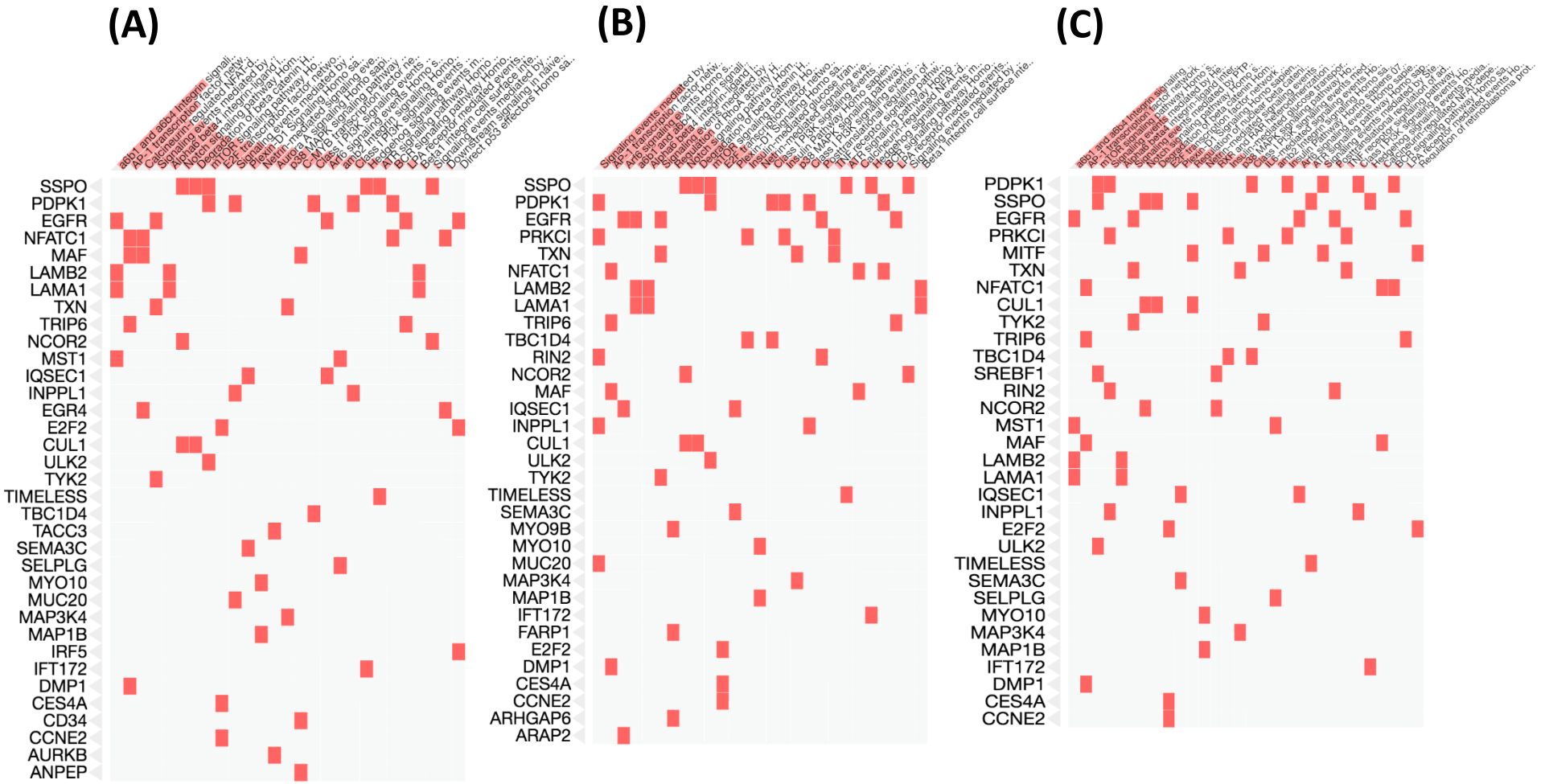

Figure 0.1. Clustergram of gene mutations from dbSNP exclusion criteria *of MM.1R (A), MM.1S^{dim} (B) and MM.1S^{bright} (C). Individual cell lines clustergram shows the 30 most likely pathways to be affected from mutational analysis by Enrichr, NCI-Nature 2016 pathway database.*

Pathway	MM.1R	MM.1S^{dim}	MM.1S^{bright}	Associated Genes
α6β1 and α6β4 integrin signalling	9.53** p=0.004	5.00* p=0.033	9.42** p=0.004	*MST1*†§*, EGFR, LAMA1, LAMB2*
α6β4 integrin-ligand interactions	4.79* p=0.011	4.64* p=0.012	4.75* p=0.011	*LAMA1, LAMB2*
AP-1 transcription factor network	7.14* p=0.018	6.55* p=0.023	7.05* p=0.019	*NFATC1, MAF, TRIP6, DMP1*
Degradation of β-catenin	3.29* p=0.025	2.62* p=0.028	2.69* p=0.025	*CUL1, SSPO*
CaN-regulated NFAT-transcription in LYM.	5.05* p=0.029	0.67 p=0.161	0.36 p=0.147	*NFATC1, MAF, EGR4*†
Signalling events mediated by PTP1B	4.96* p=0.040	4.37* p=0.047	4.73* p=0.041	*EGFE, TXN, TYK2*
Plexin-D1 Signalling	2.41* p=0.047	1.62 p=0.053	2.03* p=0.048	*SEMA3C, IQSEC1*
Notch signalling pathway	3.65 p=0.054	3.15 p=0.065	3.30 p=0.056	*CUL1, SSPO, NCOR2*
mTOR signalling pathway	3.06 p=0.079	2.55 p=0.093	6.14* p=0.019	*PDPK1, ULK2, SSPO, SREBF1*§
Arf6 signalling events	1.13 p=0.091	6.19* p=0.017	0.74 p=0.094	*IQSEC1, EGFR, ARAP2*‡
Signalling events mediated by c-Met	2.66 p=0.101	9.24* p=0.007	5.94* p=0.027	*MUC20*†‡*, PRKCI*‡§*, INPPL1, PDPK1, RIN2*‡§
Class I PI3K signalling events mediated by Akt	1.57 p=0.087	1.11 p=0.098	1.16 p=0.089	*TBC1D4, PDPK1, INPPL1*
Regulation of RhoA activity	-2.14 p=0.490	4.18* p=0.035	-2.31 p=0.496	*FARP1, MY09B*‡*, ARHGAP6*‡*,*

Table 0.5. NCI-Nature 2016 pathway analysis of non-synonymous *(no dbSNP reference) and InDel exonic mutations from the 3 cell lines. Each pathway has an Enrichr Combined score indicating gene relevance to pathway, in addition to p value; * <0.05 statistical significance; **<0.005 statistical significance. c-Met - tyrosine-protein kinase Met; CaN – Calcineurin; LYM – lymphocytes; - Gene mutations unless otherwise specified present in all 3 cell lines; †MM.1R; ‡MM.1S^{dim}; §MM.1S^{bright}*

A number of significant differences between the sub-clones were observed from the pathway analysis;

i. α6β1 and α6β4 integrin signalling pathway; all 3 sub-clones pathway was significantly affected, but MM.1R and MM.1S^{bright} had an additional mutation *MSTI,* resulting in lower p value (MM.1S^{dim} p=0.033, MM.1S^{bright} and MM.1R both p=0.004). Integrin's such as α6β1 (also known as VLA-6) and α6β4 (also known as TSP180) are known to play a role in drug resistance, with the α6 subunit being a laminin receptor (Damiano et al. 1999; Hynes 2002).

ii. Calcineurin-regulated NFAT-dependent transcription in lymphocytes pathway is affected statistically in MM.1R (p=0.029), but not in MM.1S^{dim} (p=0.161) or MM.1S^{bright} (p=0.147) due to *EGR4* mutation in MM.1R. Calcineurin targeted therapy (HDAC inhibitor Panobinostat) has been shown in part to be effective in MM patients, especially those with bortezomib resistance (Imai et al. 2016).

iii. Arf6 signalling events was affected statistically in MM.1S^{dim} (p=0.017), but not in the other 2 cell lines due to mutation in *ARAP2*. Arf6 (ADP-ribosylation factor 6) is a GTPase-protein involved in plasma cell membrane trafficking, predominately endocytosis and actin remodelling (de Beco et al. 2012). Recent studies have suggested activation of Arf6 signalling, are correlated with cancer invasion and metastasis of numerous solid tumours, although to date no discoveries linking this pathway in MM or other haematological malignancies have been made (Li et al. 2017).

iv. Signalling events mediated by c-Met pathway showed the greatest amount of variation between the 3 cell lines. MM.1R contained 3 mutations related to this pathway, but was not deemed significant (p=0.101). MM.1S^{bright} contained 4 mutations, 2 shared with MM.1R but was deemed to be significant (p=0.027). MM.1S^{dim} contained 5 mutations (2 common to all 3 cell lines, 1 shared with MM.1R and 2 shared with MM.1S^{bright}) and was highly significant (p=0.007). c-Met encoded by the proto-oncogene MET, is a receptor tyrosine kinase receptor and is involved in an array of cellular responses such as embryonic development, proliferation, wound healing, motility and invasion. It also has a role in cancers, as activation has been shown to correlate with tumour growth and angiogenesis (Ma et al. 2003). c-Met once engaged activates multiple signal transduction pathways that include PI3K, RAS, STAT, beta-catenin and Notch (Gentile et al. 2008).

v. Regulation of RhoA activity pathway was significantly affected in MM.1S^{dim} (p=0.035), but not in the other 2 cell lines (due to the additional mutations in *MY09B* and *ARHGAP6*). Rho proteins promote reorganization of the actin

cytoskeleton and regulate cell shape, attachment, and motility. Overexpression of this gene is associated with tumour cell proliferation and metastasis (Etienne-Manneville and Hall 2002; McBeath et al. 2004). It has also been shown to potentially play a role in MM SDF-1-induced adhesion, chemotaxis, and homing of MM cells to the BM (Azab et al. 2009a).

vi. mTOR signalling pathway was significantly affected in MM.1S^{bright} ($p=0.019$) but not the other 2 cell lines, due to an additional mutation in *SREBF1*. mTOR is an atypical protein kinase belonging to the PI3K-related kinase family (Laplante and Sabatini 2012) and part of the PI3K/AKT/mTOR signalling pathway important in cell cycle/proliferation. This pathway becomes activated in many cancers including MM and is regarded as a potential target for therapy (Li et al. 2014).

6.3.3 Analysis of key B-cell pathways reveals high degree of mutations within PI3K/Akt pathway

Coupled with the pathway analysis in section 6.1.2.2 (statistical difference between the sub-clones for the mTOR and c-Met signalling pathways), I felt the PI3K/Akt pathway and its related genes, specifically deserved further analysis.

Of the 341 known genes involved in the PI3K/AKT signalling pathway (Belinky et al. 2015), 109 of these genes contained either non-synonymous SNV or InDel mutations, which were common to all 3 sub-clones. These included *PIK3CD, TP53* and *PIK3R1-3.* Only 7 PI3K/AKT signalling pathway-related genes, contained mutations not shared between the sub-clones, listed in table 6.6. MM.1S^{dim} contained the highest number of mutations (5 of the 7). The MM.1S^{dim} mutations *COL4A6, LAMB1* (laminin subunit β1) and *FN1* (fibronectin) all have important roles in integrin signalling. FN1 activity has been shown to be associated with chemotherapy drug resistance such as doxorubicin, mechanism of which is believed to be the activation of the Akt/mTOR pathway (Hazlehurst et al. 2001; Xiong et al. 2012).

MM.1S^{dim} mutations	**MM.1S^{bright} mutations**	**MM.1R mutations**
THBS3	*PDGFRA*	*LAMB4*
COL6A3	*FN1*	*COL4A6*
FN1	*LAMB1*	
LAMB1		
COL4A6		

Table 0.6. Gene mutations related to the PI3K/Akt pathway *that were not common to all 3 cell lines.*

6.4 PI3Kinase p110δ expression varies between the sub-clones

The discrepancies in sub-clonal PI3K/Akt pathway mutations could potentially result in altered PI3K pathway activation or even transcriptional or expression changes, between the sub-clones. The class I PI3K catalytic subunit has 4 isoforms. They are all coded by different genes and are expressed by different cells. The delta isoform (p110δ) is primarily expressed in leukocytes and is over expressed in numerous cancers (Chantry et al. 1997) including primary MM samples and cell lines (Ikeda et al. 2010). I therefore aimed to show whether mutational differences between the sub-clones correlated to altered p110δ expression.

6.4.1 Immunoblotting shows MM.1S^{dim} upregulates expression of PI3K and AKT compared to MM.1S^{bright} and MM.1R

Analysis of the PI3K/p110δ isoform by immunoblotting showed that MM.1S^{dim} had higher p110δ and Akt expression compared to other MM.1 sub-clones. p110δ expression, expressed as a percentage of Actin in MM.1S^{dim} was 37.1%, 18.2% in MM.1S^{bright} and 9.0% in MM.1R (Figure 6.2 and table 6.7*)*. The same trend was seen for Akt expression, 66.6% in MM.1S^{dim}, 48.3% in MM.1S^{bright} and 33.5% in MM.1R.

Cell line	Actin	Akt	p110δ	Akt norm.	p110δ norm.
MM.1S^{dim}	45367	30196	16837	66.6%	37.1%
MM.1S^{bright}	49126	23721	8961	48.3%	18.2%
MM.1R	48752	16342	4373	33.5%	9.0%

Table 0.7. Differences in Akt and p110δ expression between sub-clones. *Analysis of bands using ImageJ software. Normalised (norm.) to Actin and expressed as a percentage (n=2).*

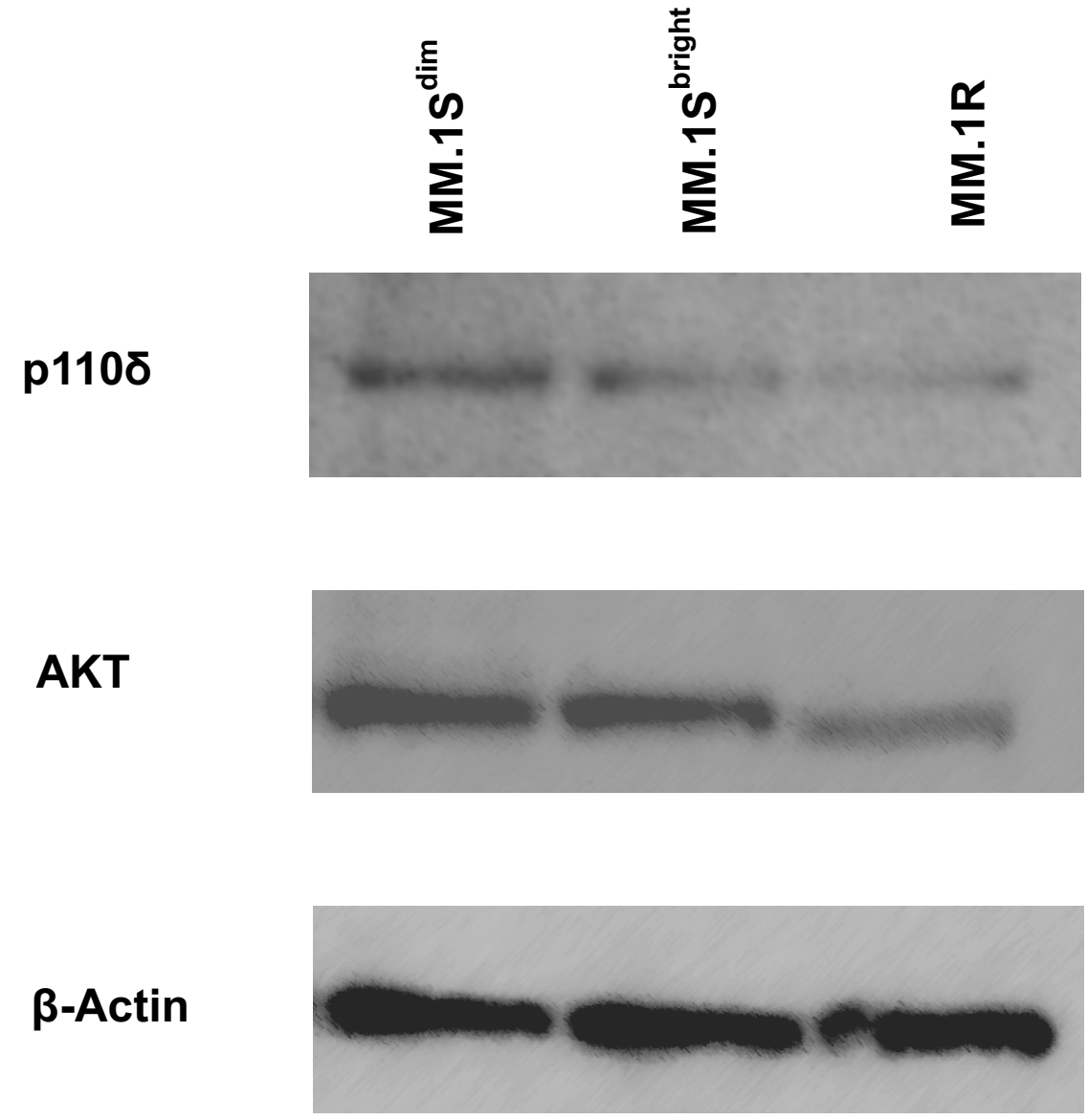

Figure 0.2. Differences in Akt and p110δ expression between sub-clones. *Total lysates from cell lines MM.1R, MM.1S^{dim} and MM.1S^{bright}. Lysates were analysed by SDS-PAGE and Immunoblotting using β-Actin, AKT and p110δ specific antibodies. Exposure to autoradiographic film for 30 minutes*

6.4.2 qPCR shows increase in PIK3CD gene transcription, providing rationale for increased PI3K/p110δ protein expression

To confirm the quantification of PI3K/p110δ of the sub-clones, Real-Time PCR (qPCR) quantification of PIK3CD transcript was undertaken. PIK3CD is the gene that codes for PI3K/p110δ. MM.1S^{dim} (RQ 1.56±0.24) showed a 1.5-fold increase in transcript compared to MM.1S^{bright} (RQ 1.06±0.10) and a 2-fold increase in gene expression compared to MM.1R (RQ 0.80±0.09). Thus, confirming the immunoblotting data. No statistical difference was observed between MM.1R and MM.1S PIK3CD transcript (p=0.27). However statistically significant difference was observed between MM.1S^{dim} and both MM.1S^{bright} (p=0.032) and MM.1R (p=0.0072). No difference was observed between MM.1S^{bright} and MM.1S (p=0.70).

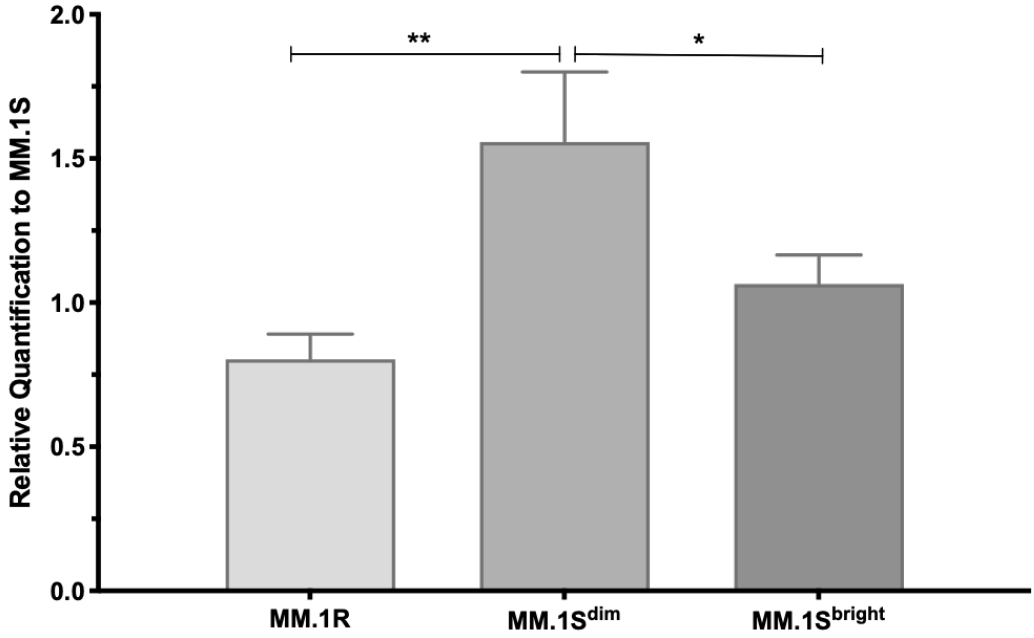

Figure 0.3. Baseline qPCR of PIK3CD transcripts of the 4 MM.1 sub-clones. *Transcript expression is quantified by ThermoFisher Relative Quantification (RQ) calculation which normalises each cell lines transcript to the cell lines housekeeping control gene, GAPDH and then relative to MM.1S. RQ results; MM.1S^{bright} 1.064 (SD±0.101), MM.1S^{dim} 1.557 (SD±0.243), MM.1R 0.803 (SD±0.087) and MM.1S 1.000 (SD±0.251). Significance calculated by unpaired T-test parametric 2 tailed and is of the product of n=3 experiments.*

6.5 Sub-clone PI3K/p110δ expression variation due to methylation of PIK3CD promoter region

Having shown that MM.1 sub-clones have differing expression of the PI3K/p110δ transcript, no unique *PIK3CD* gene mutation were observed between the sub-clones to explain expression differences. However, changes in expression or function can still occur without nuclear DNA sequence alteration, the study of which is described as epigenetics. Methylation analysis of MM.1S^{dim}, MM.1S^{bright} and MM.1R aimed to identify a reason for different levels of PIK3CD transcript. If epigenetic changes were the cause of transcript variation, then hypomethylation would be observed in MM.1S^{dim} compared to the other 2 sub-clones.

6.5.1 Methylation analysis within the same promoter region, reveals contrasting methylation status.

Two separate Qiagen PIK3CD primer assays were used in analysis. Primer-1 contained 8 CpG sites while Primer-2 contained 3 CpG sites. Overall methylation for the PIK3CD-1 primer were, MM.1S^{dim} 8.08% (SD±5.01), MM.1S^{bright} 8.61% (SD±5.01) and MM.1R 9.57% (SD±4.64). A statistical difference existed between MM.1S^{dim} and MM.1R (p=0.0026). No difference was seen between the 2 MM.1S sub-clones (p=0.44) (figure 6.4A).

Overall methylation for PIK3CD-2 were, MM.1S^{dim} 62.5% (SD±3.61), MM.1S^{bright} 65.17% (SD±5.38) and MM.1R 67.62% (SD±5.92). Again, statistically significant difference was seen between MM.1R and MM.1S^{dim} (p=0.001, figure 6.4B), but no significance between the 2 MM.1S cell sorted cell lines (p=0.083).

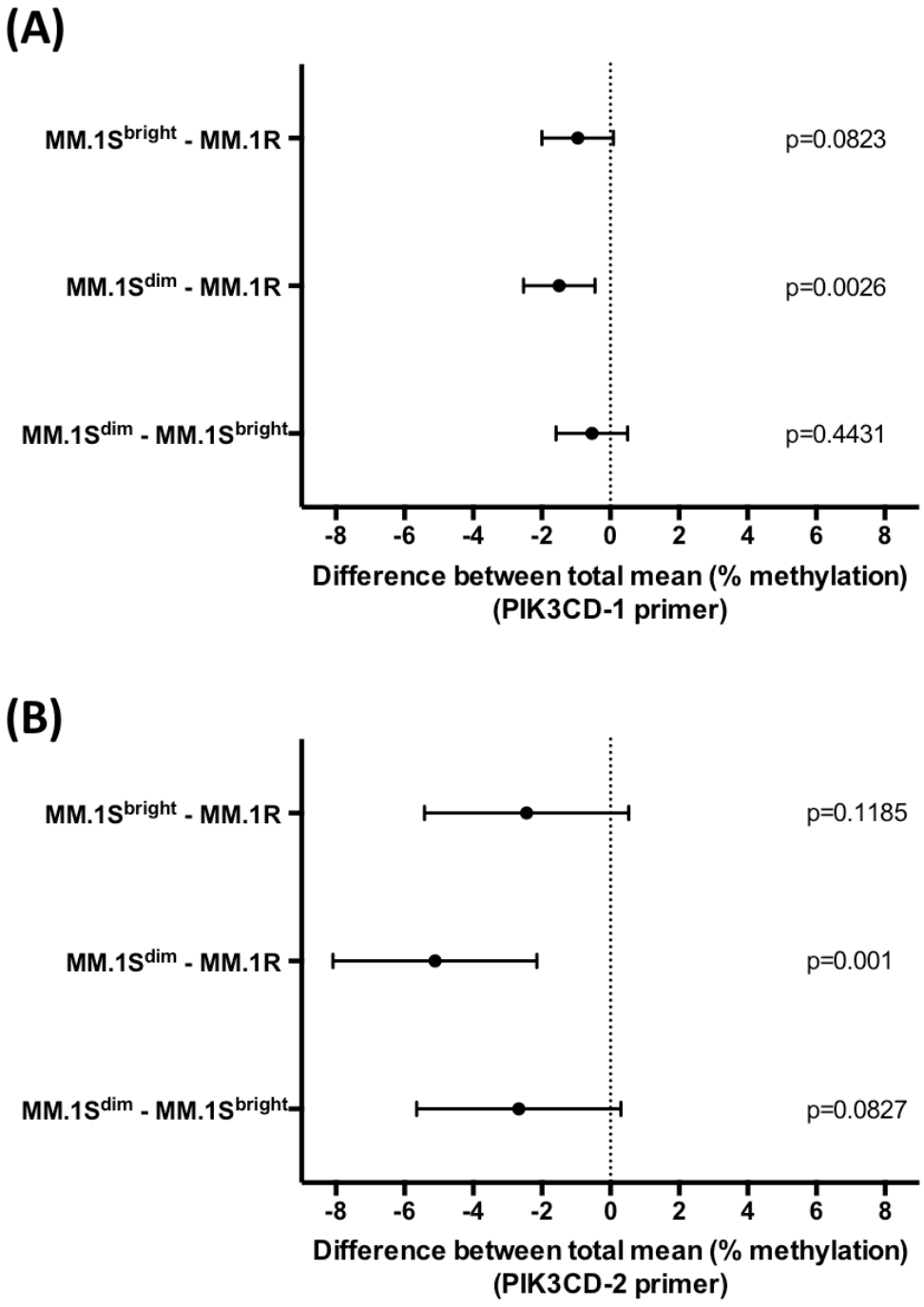

Figure 0.4. Methylation studies of MM.1 sub-clones PIK3CD promoter regions. *Box and whisker plots showing 95% Confidence Intervals (Corrected Tukey's) of overall methylation of the 2 primers (A) Primer PIK3CD-1, n=12 (B) Primer PIK3CD-2 (n=4). Experiment followed as per Qiagen methylation protocol, using DNA extraction from 2x10^6 cells and results are the product of 2 separate experiments in duplicate.*

6.5.2 Analysis of individual CpG sites identifies unique hypomethylation in MM.1S^{dim}

Table 6.8 shows the percentage methylation of individual CpG sites within the PIK3CD promoter. Statistical comparison and percentage methylation bar charts of individual CpG sites are shown in figure 6.5 (PIK3CD-1 primer) and figure 6.6 (PIK3CD-2).

CpG Site	% Methylation (SD ±)		
	MM.1S^{dim}	MM.1S^{bright}	MM.1R
PIK3CD-1			
1	4.51% (SD ± 2.17)	5.16% (SD ± 3.73)	7.08% (SD ± 4.54)
2	4.74% (SD ± 2.98)	5.09% (SD ± 2.68)	6.54% (SD ± 3.46)
3	4.64% (SD ± 3.25)	7.13% (SD ± 6.16)	7.85% (SD ± 4.51)
4	5.32% (SD ± 2.64)	5.00% (SD ± 2.24)	7.91% (SD ± 4.97)
5	13.82% (SD ± 12.02)	14.05% (SD ± 12.09)	14.09% (SD ± 9.49)
6	10.72% (SD ± 9.92)	9.64% (SD ± 8.04)	8.65% (SD ± 4.05)
7	16.80% (SD ± 15.46)	18.12% (SD ± 18.68)	19.08% (SD ± 17.48)
8	4.05% (SD ± 3.05)	4.70% (SD ± 3.47)	5.32% (SD ± 2.84)
PIK3CD-2			
1	66.08% (SD ± 2.19)	67.03% (SD ± 2.27)	67.84% (SD ± 1.63)
2	58.86% (SD ± 1.89)	59.11% (SD ± 2.11)	61.58% (SD ± 2.12)
3	62.57% (SD ± 3.97)	69.37% (SD ± 3.35)	73.42% (SD ± 1.98)

Table 0.8. Percentage of methylation *(±SD), of individual CpG sites with the 2 separate assays. PIK3CD-1 methylation (n=12 for each site). PIK3CD-2 methylation (n=4 for each site). Standard deviation and are calculated by repeated independent experiments.*

CpG site methylation comparison between the sub-clones for each revealed a statistical difference at two separate sites, one for each primer, both at CpG site 3. PIK3CD-2 primer CpG site 3 (figure 6.6B) methylation for MM.1S^{dim} was 62.57%, lower than MM.1S^{bright} (69.37%, p=0.0091) and MM.1R (73.42%, p=0.0001). PIK3CD-1 primer CpG site 3 methylation for MM.1S^{dim} was 4.74%, compared to MM.1R (6.54%, p=0.0295. figure 6B).

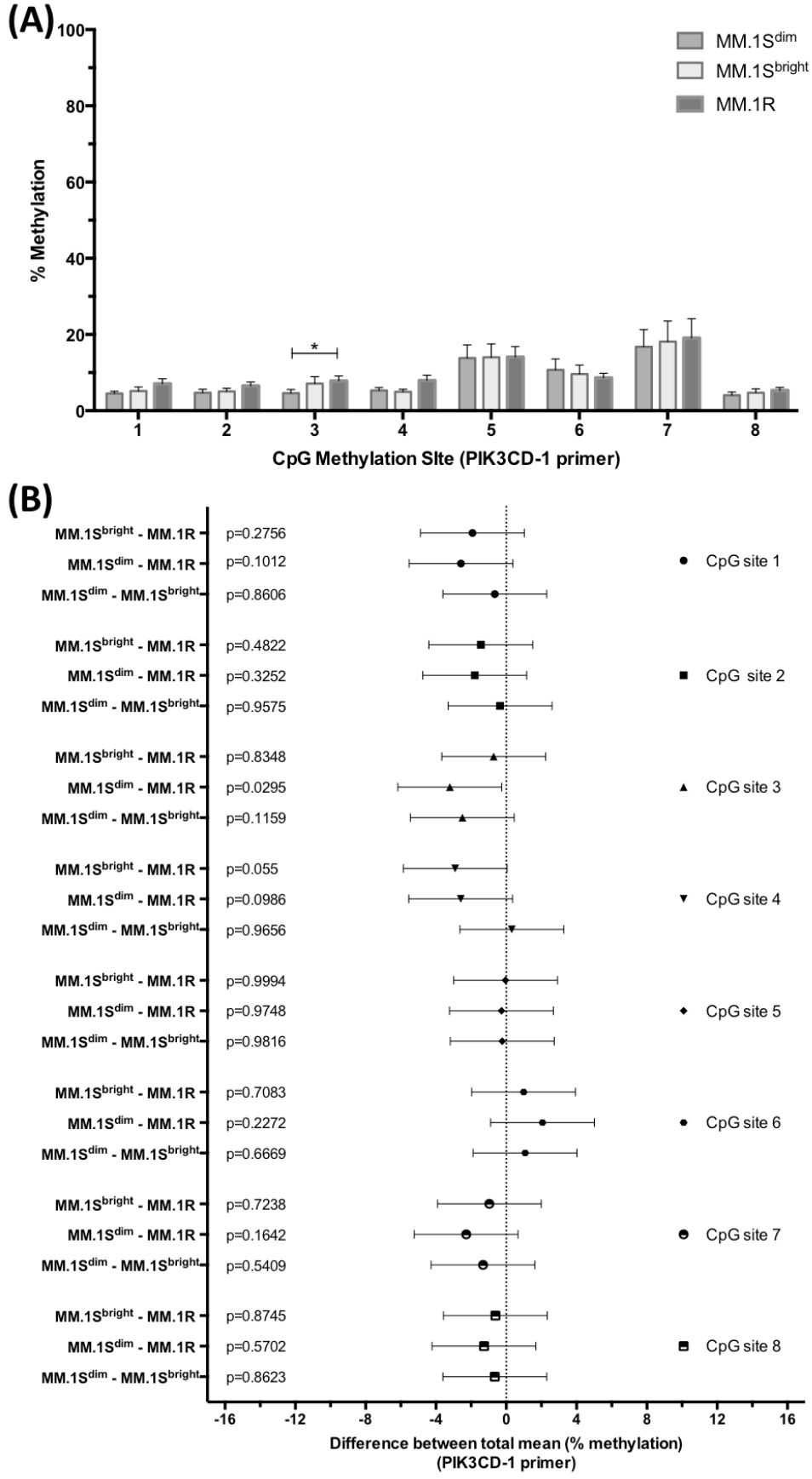

Figure 0.5 Percentage Methylation of individual CpG sites from PIK3CD-1 Primer *(A) Mean % methylation at PiK3CD-1 primer region (8 CpG sites) (B) 95% Confidence Intervals (Corrected Tukey's) of individual PiK3CD-1 methylation sites (n=12). Experiment followed as per Qiagen methylation protocol, using DNA extraction from 2x10^6 cells and results are the product of 4 separate experiments in triplicate.*

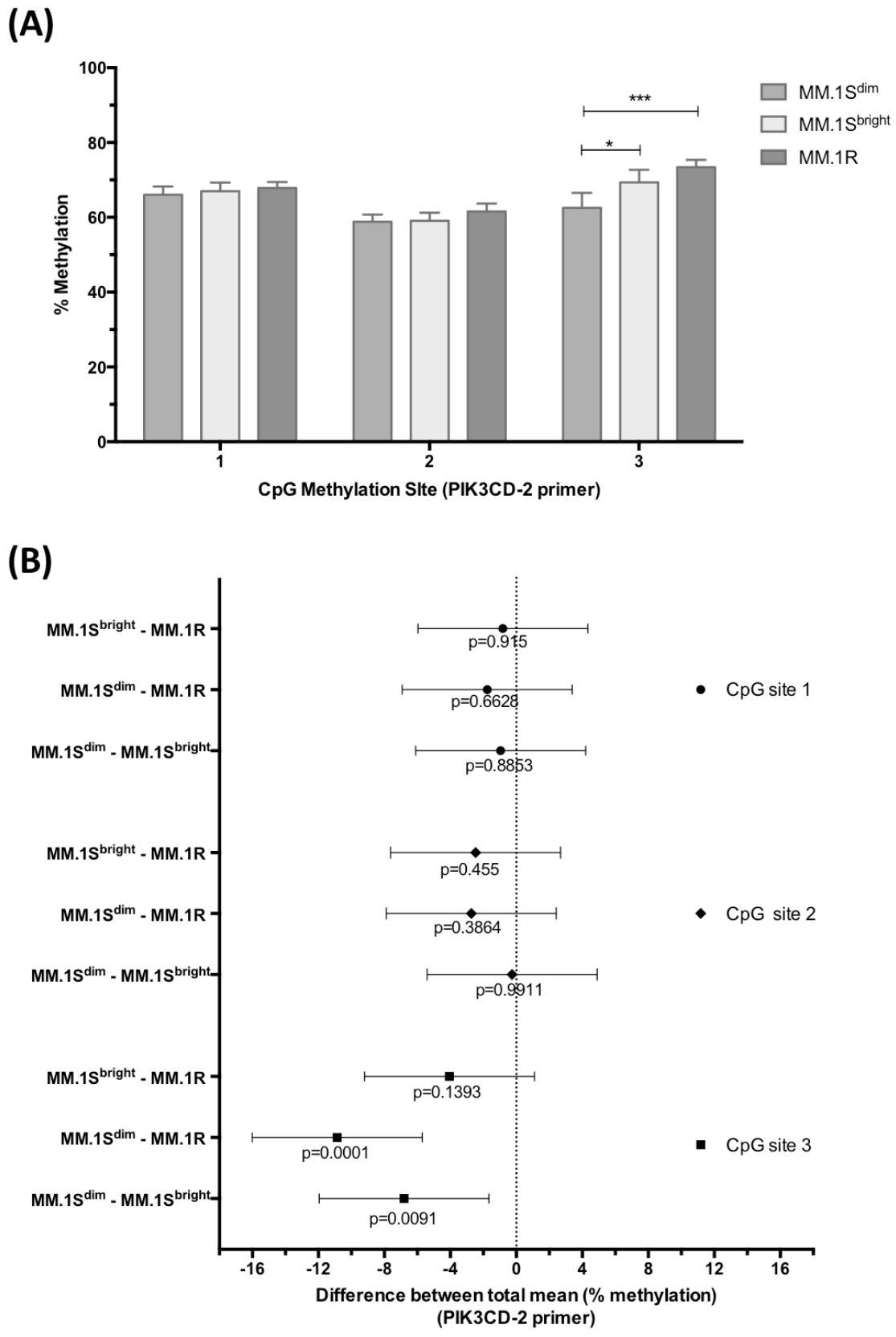

Figure 0.6. Percentage Methylation of individual CpG sites from PIK3CD-2 Primer *(A) Mean % methylation at PiK3CD-2 primer region (3 CpG sites) (B) 95% Confidence Intervals (Corrected Tukey's) of individual PiK3CD-2 methylation sites (n=4). Experiment followed as per Qiagen methylation protocol, using DNA extraction from 2x10^6 cells and results are the product of 2 separate experiments in duplicate.*

6.6 PI3K-targeted treatment of Sub-clones

Having confirmed varying expression levels of PI3K/p110δ within the sub-clones, my next aim was to see if this led to differential sensitivity to PI3K inhibition and cell cytotoxicity, thus representing a potentially promising treatment strategy for MM. The selective PI3K/p110δ inhibitor, idelalisib (CAL-101, GS-1101), has shown potency in malignant lymphoid cell lines. It has an EC50 in cell-free assays of between 2.5 nM and 8nM and a LD50 cell of around 50μM (Herman et al. 2010; Ikeda et al. 2010; Lannutti et al. 2011).

6.6.1 The selective PI3K inhibitor Idelalisib shows an increasing cytotoxic effect that correlates to increasing expression levels

The sub-clones, MM.1S^{dim}, MM.1S^{bright} and MM.1R were exposed to increasing doses of the idelalisib, with both cytotoxic and anti-proliferative effect measured (figures 6.7 and 6.8). MM.1S^{dim} (LD50=41.67μM) was more sensitive to the cytotoxic effects of idelalisib, showing greater cell death than MM.1S^{bright} (LD50=58.28μM, p=0.0077) and MM.1R (LD50=85.28μM, p<0.0001).

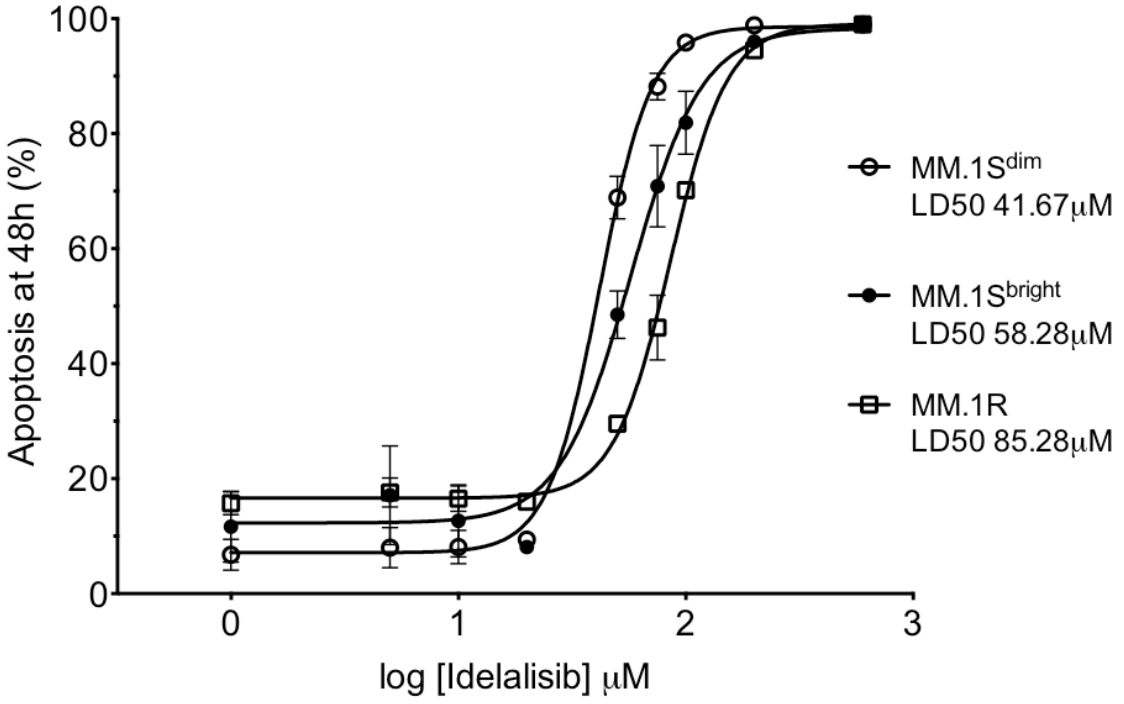

***Figure 0.7. Dose response curves of the sub-clones exposed to idelalisib over 48h period**. 0.5x10^6 cells were exposed to increasing doses of idelalisib, cell death recorded by annexin V and PI immuno-staining and analysed on BD Accuri flow cytometer. Results are the product of 3 separate independent experiments (n=3)*

6.6.2 Anti-Proliferative effects of Idelalisib

All 3 sub-clones experienced a dose-dependent anti-proliferative affect from idelalisib. Baseline doubling time (chapter 4) has already been discussed as a marker of cell proliferation. Doubling times (DT) were compared between MM.1S^{dim} and MM.1S^{bright} at different doses of idelalisib. Statistically significant anti-proliferative effects were observed at the non-cytotoxic concentration of 10μM (p=0.001) (table 6.9 and figure 6.9), indicating that MM.1S^{dim} cells was more sensitive to idelalisib anti-proliferative effects than MM.1S^{bright} cells.

Idelalisib (μM)	**Doubling Time – hours (±SD)**			**P value MM.1S^{bright} vs MM.1S^{dim}**	**Summary**
	MM.1R	**MM.1S^{bright}**	**MM.1S^{dim}**		
1μM	51.7 (±4.13)	45.0 (±3.03)	50.0 (±2.46)	0.835	ns
5μM	48.3 (±3.37)	58.6 (±4.53)	60.8 (±6.20)	0.647	ns
10μM	62.3(±5.26)	61.5 (±1.28)	76.8 (±5.42)	0.001	**
50μM	110.1 (±12.31)	92.4 (±17.05)	187.4 (±31.42)	0.014	*
75μM	100.6 (±67.52)	86.7 (±13.08)	203.6 (±57.89)	0.003	**
100μM	116.9 (±15.69)	116.4 (±25.80)	199.4 (±65.78)	0.016	*

Table 0.9. Comparison of doubling time between *the 3 sub-clones at different concentrations of idelalisib n=3 with standard deviation (±). P-values is a comparison of DT between MM.1S^{dim} and MM.1S^{bright} calculated by multiple t-test (Holm-Sidak method). S*

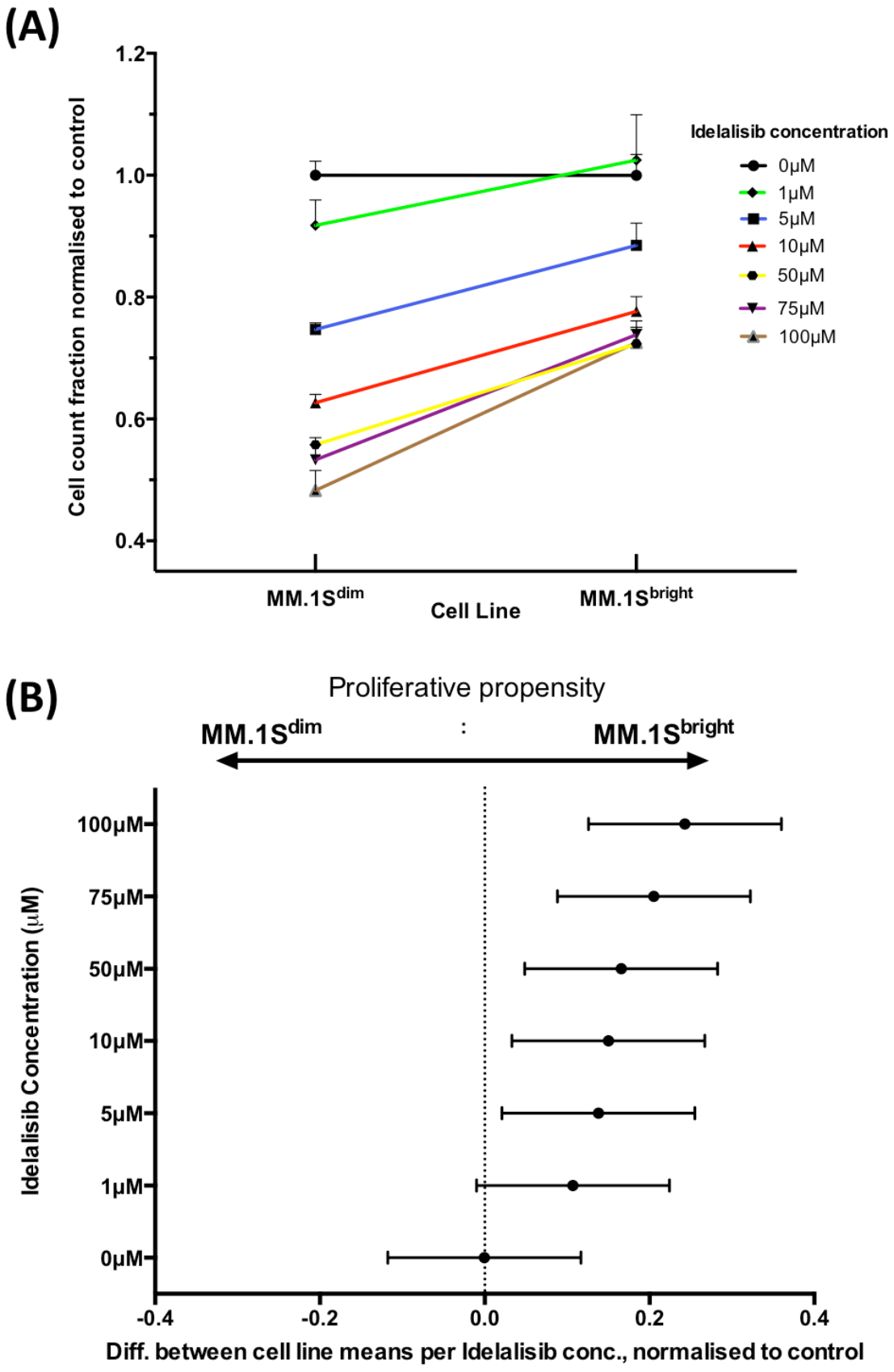

Figure 0.8. Comparison of proliferation and doubling times between MM.1S^{bright} and MM.1S^{dim} at 48 hours *at different concentrations of idelalisib, normalised to 0μM DT. (B) 95% Confidence Intervals (Sidak) comparison between MM.1S^{Dim} and MM.1S^{Bright} normalised proliferation at 48 hours at different concentrations of idelalisib.*

6.6.3 Cytotoxic differences abolished by using a pan-PI3K/mTOR inhibitor

To establish whether the differences in sub-clonal idelalisib cytotoxic effects were due to different p110δ expression and/or dependence on this isoform, the sub-clones were exposed to the pan PI3K/mTOR inhibitor, PKI-402. The results showed that PKI-402 was equipotent in both MM.1S^{bright} and MM.1S^{dim} cells (*t*-test between the data, p=0.89). MM.1S^{dim} LD50 124nM (SEM±11.7), MM.1S^{bright} LD50 126nM (SEM±15.4) and MM.1R LD50 129nM (SEM±10.1).

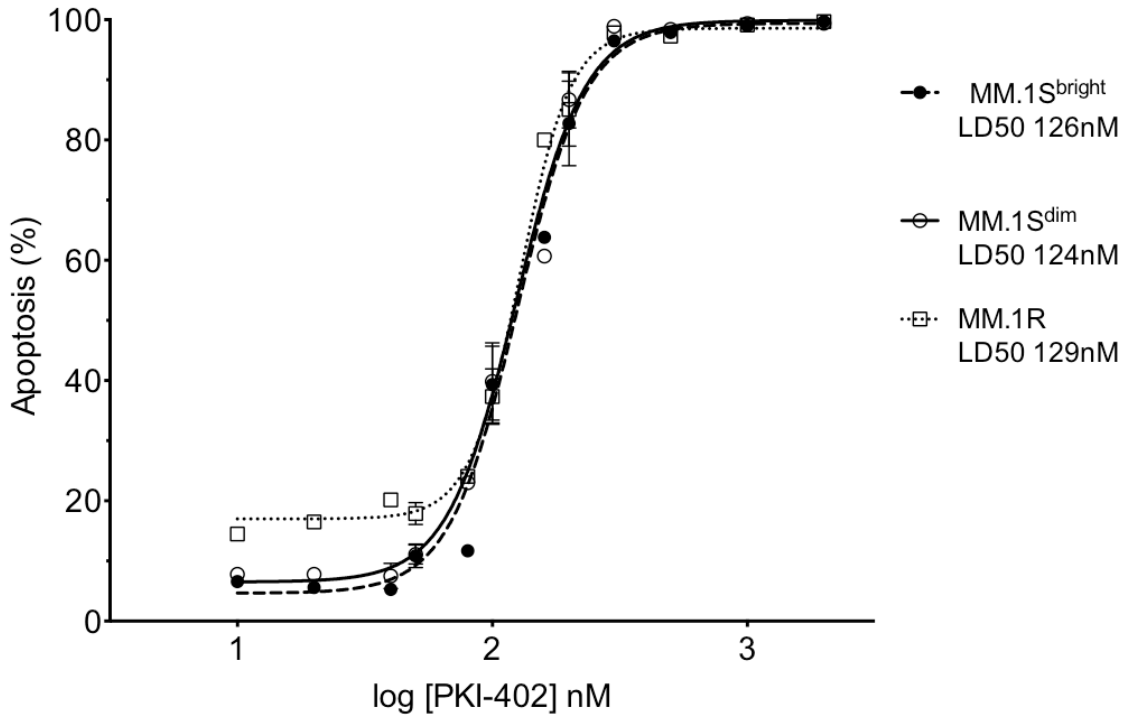

Figure 0.9. Dose response curves of the sub-clones exposed to PKI-402 over 48h period. *0.5x10^6 cells were exposed to increasing doses of PKI-402, cell death recorded by annexin V and PI immuno-staining and analysed on a BD Accuri flow cytometer. Results are the product of 3 separate experiments (n=3).*

6.6.4 Synergistic effect with Dexamethasone offers a therapeutic option.

Combination therapy is common place in the treatment of MM. Given that the anti-proliferative effects of idelalisib were apparent at sub-cytotoxic concentrations in all three sub-clones, I set out to combine idelalisib with dexamethasone. The aim of these experiments was to determine whether dexamethasone resistance could be reversed in both MM.1R and MM.1S^{bright} by co-administering idelalisib. The optimal fixed molar ratio for the two drugs was experimentally determined starting with 1:20 deamethazone:idelalisib and finishing with a fixed molar ratio of 1:200.

6.6.4.1 MM.1S sub-clones show synergistic effect that MM.1R does not

Figure 6.10 shows the individual dose response curves, including dexamethasone combined with idelalisib (ratio 1:200). To calculate whether the combined drugs equated to synergy, dose-effect-curves as well as combination-index and median-dose-plot (see supplementary figures in appendix) were calculated using CalcuSyn software. Combination-index (CI) curves were plotted the CI values at ED50, ED75 and ED90 were obtained. The results of which are outlined in table 6.10 and figure 6.12B. Table 6.10 shows that MM.1S^{dim} and MM.1S^{bright} experienced synergistic effects with combined of idelalisib and dexamethasone, whereas MM.1R did not (ED50 0.99) show a synergistic effect. At best an additive effect was possibly seen when ED50 and ED75 were measured. MM.1S^{bright} showed the greatest synergy, ED90 for MM.1S^{bright} was 0.12 compared to MM.1S^{dim} 0.38 while MM.1R showed an antagonistic effect with a CI of 1.25.

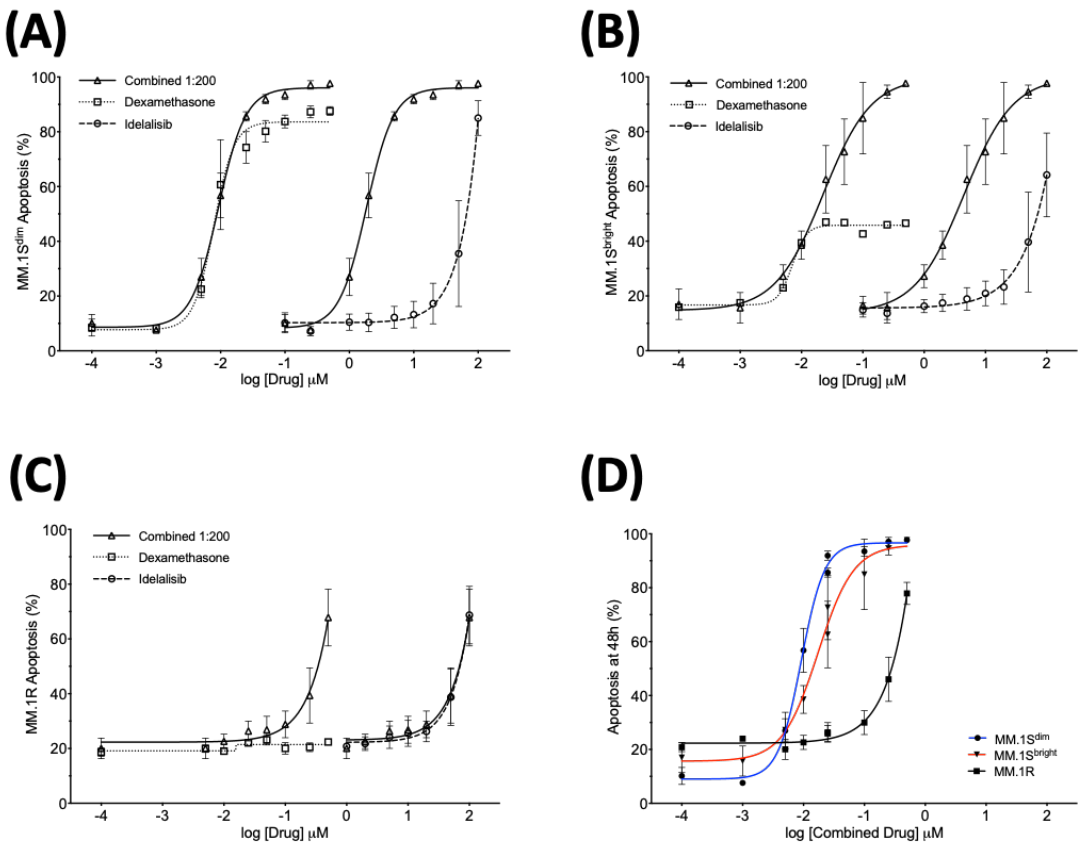

Figure 0.10. Cytotoxic dose response curves *(n=3) comparing the effects of single agent Dexamethasone and Idelalisib with the added effect of the 2 drugs combined at a fixed concentration ratio of 200:1, for combined drug responses, 2 separate curves have been for each cell line, representing the individual drug concentration when combined, but are the same data. (A) MM.1S^{dim} individual drug curves and combined (B) MM.1S^{bright} individual drug curves and combined; (C) MM.1R individual drug curves and combined; (D) Cytotoxic dose response curves comparison of the 3 cell lines combined Idelalisib and dexamethasone at fixed ratio of 200:1, dose response curves are plotted for the dexamethasone dose. 0.5x10^6 cells were exposed to increasing doses of the drugs, cell death recorded by annexin V and PI immuno-staining and analysed on a BD Accuri flow cytometer. Results are the product of 3 separate experiments (n=3)*

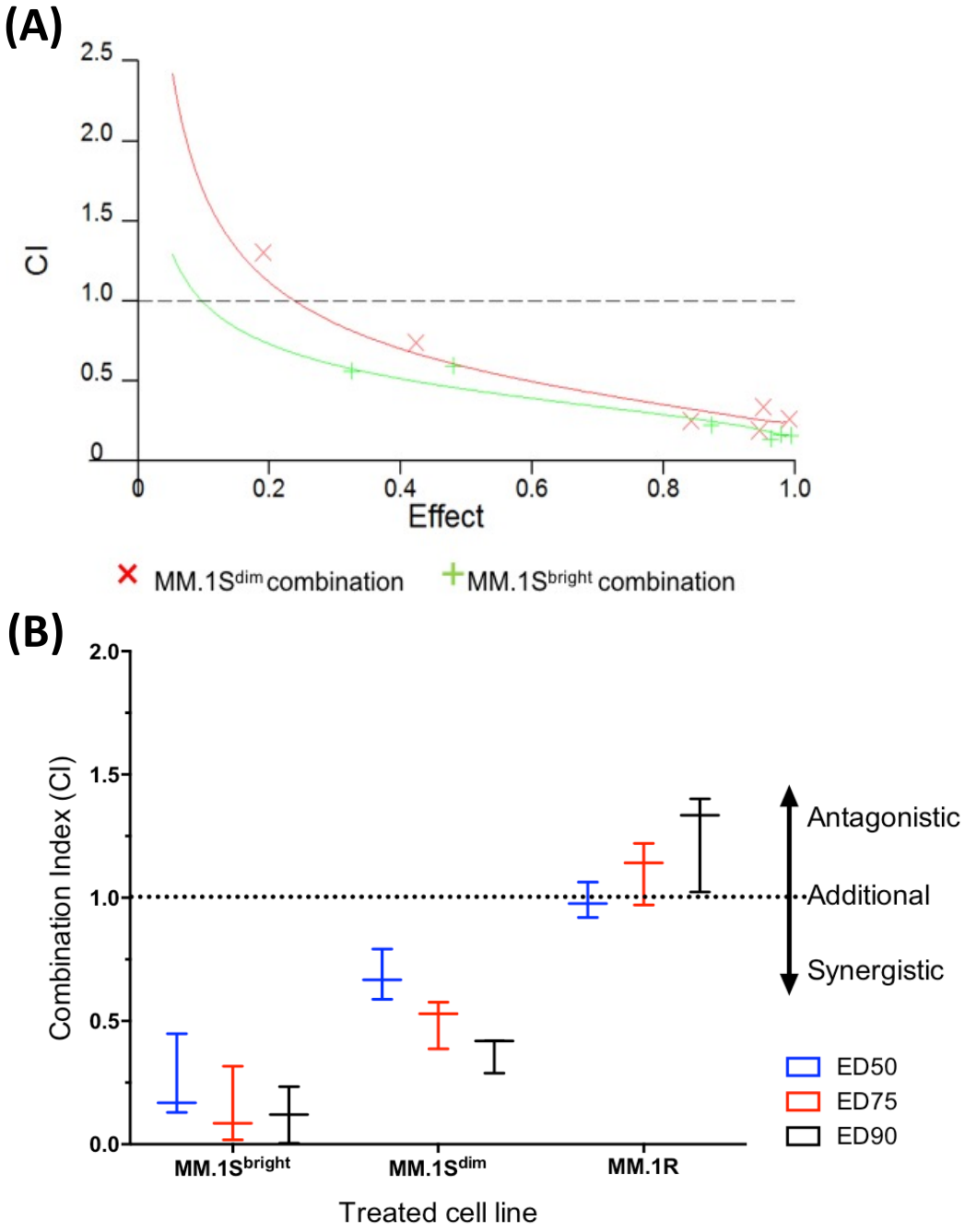

	MM.1S^{dim}	MM.1S^{bright}	MM.1R
ED50	0.68 (SD ± 0.10)	0.25 (SD ± 0.17)	0.99 (SD ± 0.07)
ED75	0.50 (SD ± 0.10)	0.14 (SD ± 0.16)	1.11 (SD ± 0.13)
ED90	0.38 (SD ± 0.08)	0.12 (SD ± 0.11)	1.25 (SD ± 0.20)

Figure 0.11. Synergistic effect of Idelalisib with dexamethasone *in MM.1S^{bright} and MM.1S^{dim,} but not MM.1R. (A) Algebraic estimate of the combination index (CI) constructed by CalcuSyn computer analysis of the data. (B) Distribution of individual CI (n=3) among the 3 different sub-clones at 50% Effective dose (ED50), 75% (ED75) and 90% (ED90). Table shows the Mean and SD of sub-clone CI between the different sub-clones at the various ED values at shown from figure 4.22 (n=3). Figures less than 1 are deemed synergistic, the lower the number, the greater the synergistic effect. Figures more than 1 are deemed antagonistic*

6.6.4.2 Idelalisib median dose effect significantly decreases with addition of Dexamethasone in dexamethasone sensitive MM.1 sub-clones

Both MM.1S^{dim} and MM.1S^{bright} experienced a 38-fold reduction in Idelalisib drug required if combined with dexamethasone (Table 6.11 and figure 6.13). The differences in Idelalisib drug concentrations achieving the same degree of toxicity were both significant (MM.1S^{dim} p=0.027 and MM.1S^{bright} p=0.017), unlike for MM.1R (p=0.7485).

	MM.1S^{dim}	MM.1S^{bright}	MM.1R
Idelalisib	69.82 (±23.69)	104.2 (±46.26)	144.7 (±72.63)
Idelalisib + Dexamethasone	1.82 (±0.27)	2.75 (±0.60)	137.70 (±64.42)
P value	0.027	0.017	0.7485
Summary	*	*	ns

Table 0.10. Idelalisib Median Effect Dose (Dm) *of the 3 cell lines comparing single agent Idelalisib treatment with Idelalisib in combination with Dexamethasone at a fixed ratio dose 1:200. P value is comparison of cell lines Dm's between single agent and combination.*

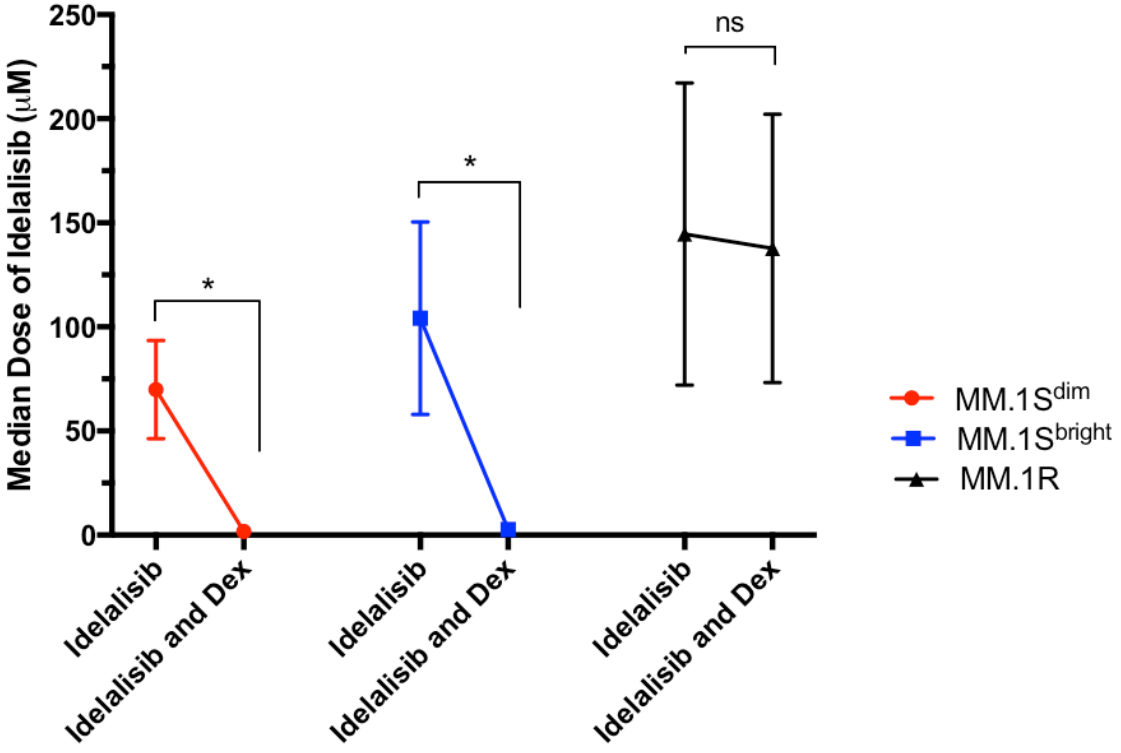

Figure 0.12. 'Median Effect Dose' (Dm) - as calculated by CalcuSyn Dose-Effect Analyzer software *(Lombardo et al. 2012) of Idelalisib with and without Dexamethasone (fixed ratio 1:200) on the sub-clones MM.1S$^{dim+bright}$ and MM.1R (n=3). paired fixed ratio T test (n=3). Difference between 2 treated groups were significant for MM.1S^{dim} and MM.1S^{bright}*

6.7 Discussion

The majority of this chapter's mutational analysis focused on how specific mutations potentially affected cell-signalling pathways. Such analysis is able to highlight the most frequently mutated pathways involved in disease pathologies, leading to new targets for therapy. Such strategies are already in existence in MM research, with early phase trials of RAS inhibitors, the most commonly mutated gene/pathway in MM, having already occurred (Walker et al. 2015; Ostrem and Shokat 2016). My pathway analysis was done through Enrichr, the free online enrichment tool. Mutation pathway analysis was compared to the NCI-Nature 2016 Pathway Interaction Database (PID), a collaborative between the NCI and Nature Publishing Group (from 2006 until 2012). It contains 212 separate recognised cancer pathways, with numerous genes associated to each pathway. Although the database is no longer contributed to by the NCI, the running of the database is now undertaken by the Network database exchange Project (NDEx), who describes it as a "highly-structured, curated collection of information about known bio-molecular interactions and key cellular processes assembled into signalling pathways" (Pratt et al. 2015). Although the database is not as frequently updated compared to other pathway analysis tools such as Ingenuity Pathway Analysis (IPA), the simplicity of user interface, with cancer focus pathways makes it attractive as a comparable database. Provided with more time and expertise, IPA could have provided more in-depth information regarding the effect on specific pathways such as PI3K/Akt and explanations as to the reasons of difference in drug sensitivity. A pathway of particular interest not fully explored in this thesis would have been the CD38 signal transduction pathway and whether mutations affecting this pathway leads to the emergence of CD38 weak/negative sub-clones as well as determining if CD38 expression can be altered through pathway related mutations. Such understanding may also offer new therapy targets of CD38 negative drug resistant clones, which will become more predominate in the era of CD38 monoclonal antibody therapy.

The other functional genetic analysis method I employed was searching for isolated gene mutations, by far the most applicable and easiest way to analyse specific differences between sub-clones. Despite limited analysis resources, I felt I made a number of significant findings by this simplistic but systematic approach. Functional genetic analysis has provided some plausible explanations to some of the differences observed between the cell lines. The frameshift InDel mutation (of high significance) of *MKI67* observed only within MM.1S^{dim} and can be assumed to be an inactivating mutation, because MM.1S^{dim} cells grow more slowly Ki-67 (the protein encoded by *MKI67)* is immunophenotypically

reduced in the MM.1S^{dim} population, both in static culture, but also upon migration compared to MM.1S^{bright} and MM.1R. It also explains why MM.1S^{dim} has longer telomere lengths compared to the other sub-clones, but also has particular significance as over time, the CD38 higher expressing sub-clone would outgrow the weakly expressing CD38 sub-clone in cell tissue culture and may partly explain why other research groups have not reported my findings. The difference in Ki-67 expression between the sub-clones could also have implication in aggressiveness of the sub-clones. Ki-67 is a key marker of proliferative activity in many cancers including MM and is also associated with bone marrow angiogenesis (increased microvessel density of the bone marrow), tumour burden and poor prognosis (Alexandrakis et al. 2004a; Alexandrakis et al. 2004b; Himani et al. 2016). Increase expression has also been shown to have clinical importance in therapy choice. A 3.7-fold upregulation of *MKI67* expression, was associated with early-onset vincristine-induced peripheral neuropathy (Broyl et al. 2010).

The decision to focus on the PI3K/Akt pathway as a model for drug therapy between sub-clones and potential dexamethasone resistance reversal was multi-fold. For one, it is an attractive pathway for drug induced inhibition as involved in cell proliferation, apoptosis, cell cycle, autophagy and dexamethasone resistance and unsurprisingly has become a target for novel therapy (Ikeda et al. 2010; Munugalavadla et al. 2014). In addition, the presence of PIK3CD synonymous mutations in all 3 sub-clones as well as mutations in over 1/3 of all PI3K/Akt pathway related genes, highlighted the high frequency of mutations in this key cell-signalling pathway. Although Enrichr pathway analysis showed PI3K regulation to be affected but not quite significantly (p=0.089), 2 other pathways with direct links to PI3K/Akt were statistically affected, these were mTOR (MM.1S^{bright}) and c-Met (MM.1S^{dim}>MM.1S^{bright}).

Indeed, Ikeda et al in 2010 proclaimed PI3K to be an interesting therapeutic target in MM, showing the p110δ isoform (1 of 8 distinct mammalian isoforms of Class IA PI3K) is expressed (by immunoblotting) in both primary MM cells and MM cell lines (Ikeda et al. 2010). Although PI3K inhibition has been undertaken on MM cell lines before, none have compared the effects between sub-clones from the same patient, cell line or pre-existing drug resistance (Munugalavadla et al. 2014; Zhang et al. 2014). The selective PI3K/p110δ inhibitor Idelalisib (CAL-101, GS-1101) has up to a 300-fold greater selectivity for p110δ than the other isoforms and has shown promising results in a number of B-cell malignancies such as CLL and follicular lymphoma and therefore seemed an obvious choice to study the effects of PI3K inhibition of MM sub-clones. Indeed, the effects of

Idelalisib on myeloma cell lines has also been previously investigated, the cell line U266 showed 76% inhibition of proliferation at 40μmol/L (96nM) (Ikeda et al. 2010; Zhang et al. 2014). Cytotoxic effects on the 3 sub-clones were seen at higher concentrations (3 log difference) than this, with LD50 40-80μM.

My data not only confirmed p110δ isoform expression in the sub-clones as previously shown by Ikeda et al., but that expression levels varied between the sub-clones and with my results confirmed by Real-Time PCR (PIK3CD expression). Ikeda et al. showed varying expression of PI3K isoforms between the MM.1S and MM.1R, both expressing P110γ, but only MM.1S expressed p110α and p110δ very weakly (shown by immunofluorescence slide fixation), while only MM.1R expresses p110β. My results similarly showed MM.1S expressed p110δ more than MM.1R, but my work in addition showed than MM.1S p110δ expression predominantly arises from the MM.1S^{dim} sub-clone. It is therefore highly possible that differences seen in the expression of the alpha and beta isoform between MM.1S and MM.1R also arise from sub-clones not present in one or the other sub-clones.

The cause of expression variation could not be attributed to *PIK3CD* mutations as all cell lines expressed the same synonymous SNV. An alternative explanation that I explored was epigenetic changes by methylation of cytosine residues. CpG sites are regions of DNA where a cytosine nucleotide is followed by a guanine. CpG islands are usually around 200bp (<500 bp) that contain a high frequency of CG (55% or more). They are usually in the promoter region but can also occur in enhancer regions of the gene. The methylation of CpG islands by DNA methylase (resulting in hypermethylation) can lead to gene inactivation. This silencing of gene expression is frequently seen in cancers and offers a therapeutic strategy as reversal of this process may restore normal expression of transcriptionally silenced genes (Ehrlich 2009; Qiagen 2009). And it was this method that provided a likely explanation of expression variation of PI3K between the sub-clones. The methylation analysis of the *PIK3CD* promotor region of the 3 sub-clones, showed a statistically significant hypomethylation of CpG site 3 site of the PIK3CD-2 primer assay.

Although I have not ruled out other causes of protein expression variation such as post-translational changes or degradation of the protein, epigenetic changes remains the most plausible cause and one that is well known in occur in MM cell lines (Peng et al. 2006). I found the methylation analysis an extremely technical procedure, with huge potential of methodological variation, especially within the bisulfite conversation step. This step traditionally requires harsh conditions of high temperatures and low pH, which can lead

to DNA fragmentation, reducing purification. To overcome this I used the Qiagen bisulfite conversation and methylation kit, the advantage of which reduced the degree of variability and by using a thermal cycler in the bisulfite conversion, cytosine conversion rates are claimed to be over 99% (Qiagen 2009).

Furthermore, I showed the correlation between increasing PI3K/p110δ expression and the cell's susceptibility to targeted therapy. The LD50 difference between the sub-clones were shown to be statistical, with MM1.S^{dim} having the greatest expression, but also greatest sensitivity. This observation proved to be specific to PI3K/p110δ inhibition as the pan-PI3K/mTOR inhibitor PKI-406 removed any cytotoxic differences. Although this drug was extremely potent, such a combination is unlikely to be tested clinically due to unacceptable toxic side effects from the pan-PI3K inhibition. Though beyond the scope of this thesis, mTOR inhibition (without pan-PI3K inhibition) has been targeted in MM therapy (Li et al. 2014), with the novel pan-PIM kinase inhibitor LGB321 showing mTOR signalling inhibition (Garcia et al. 2014). Additionally, inhibition of mTOR signalling pathway with rapamycin inhibits JNK signalling, which sensitises both MM primary cells and cell lines to glucocorticoid-induced apoptosis (Smith and Cidlowski 2010). Thus, raising the possibility that mTOR inhibition is just as important in reversing the effects of sub-clonal dexamethasone resistance than PI3K.

Combination therapy of dexamethasone and Idelalisib did not provide synergy in MM.1R, thus I was unable to reverse dexamethasone resistance by the addition of PI3K inhibition. However, impressive synergistic effect was seen with MM.1S^{dim} and MM.1S^{bright}, with a lower CI observed in MM.1S^{bright}. This suggests, that the dexamethasone resistance obtained in the MM.1S^{bright} compared to MM.1S^{dim}, was indeed reversed by PI3K inhibition. Activation of the PI3K/Akt signalling pathway has been shown to correlate with the expansion of glucocorticoid-resistant MM cells in the bone marrow (Hideshima et al. 2007a; Smith and Cidlowski 2010), thus inhibition of this pathway in theory should reverse such expansion. The mechanism of PI3K/Akt pathway induced glucocorticoid resistance is through the inhibitory phosphorylation of important apoptotic mediators such as Bcl-2-associated death promoter (BAD), caspase 9, Fox03A/FKHRL and CREB. In addition, AKT inhibits the transcription of the pro-apoptotic Bim through inhibitory phosphorylation of Fox03A/FKHRL which further contributes to glucocorticoid resistance (Maddika et al. 2007; Smith and Cidlowski 2010). Thus, it is possible that the increased dexamethasone resistance found in MM.1S^{bright} cells when compared to MM.1S^{dim} cells, is not due to reduced GR, but rather one of the aforementioned PI3K activation, as inhibition

of PI3K reversed its dexamethasone resistance. One of the most important activators of the PI3K/Akt pathway is MM cells is IL-6 which can also activate MEK/ERK signalling pathway, both of which are able to trigger proliferation of MM cells and protects against dexamethasone induced apoptosis (Cantley 2002; Luo et al. 2003; Steelman et al. 2004; Ikeda et al. 2010).

Finding a suitable combination ratio was difficult, with 3 other ratios attempted before 1:200 showed the most synergy for both of the MM.1S sub-clones. However, this ratio was likely not optimal in either confirming or disproving MM.1R synergy, for this reason the antagonist effects suggested by the high CI (1.25), should be interpreted with caution. Based on more accurate LD50 of single therapy toxicity for MM.1R, a ratio of at least 1:1 or lower should be attempted before certain confirmation of lack of synergy can be made. This is especially pertinent in view of data not shown (see appendix), where a possible MM.1R additive effects exists at a fixed ratio of 1:20 of 100μM idelalisib (single agent 38% cell death) and 5μM dexamethasone (combined 67%). Of note, the highest dexamethasone concentration reached (5μM) in my experiments, is still lower than the standard clinical dose used (20-40mg/ 10-20μM daily) (Bird et al. 2011). Unfortunately, time constraints meant I was unable to undertake MM.1R synergy experiments at the lower fixed molar ratios. It is unclear why at 5μM dexamethasone a sudden additive effect is seen, either the dexamethasone at such high doses results in pathway activation through alternative signalling than the GR or possibly the high doses actually causes an increase in GR expression, a phenomenon that has been previously described in MM cell lines (Danel-Moore et al. 1992), thus allowing for GR induced transcriptional changes. The other possibility regarding the antagonistic effects seen at ED90 could lie with P-gp expression. I have already shown that at high doses of dexamethasone, MM.1R P-gp expression is increased (section 5.6.1), providing a potential mechanism of efflux of Idelalisib. Although Idelalisib is a known substrate of P-gp, it has been shown to inhibit P-gp expression and activity (Jin et al. 2015), further complicating the matter.

In summary, I have provided a number of possible genomic causes to the MM.1S sub-clonal difference in dexamethasone sensitivity, such as the effects of individual mutations have on key signalling pathways such as PI3K/Akt/mTOR, Arf6, α1 integrin signalling, c-Met and RhoA. Furthermore, I have shown the potential for developing bespoke treatment plans based on the identification of cell signalling pathway mutations via genomic sequencing, exemplified through PI3K/Akt pathway analysis and subsequent

successful inhibition. I have shown that the synergy between dexamethasone and the PI3K inhibitor Idelalisib requires cell surface GR expression and that the effects of dexamethasone when combined with Idelalisib are not "off target effects". The MM.1S^{bright} sub-clone mechanism of decreased dexamethasone sensitivity compared to MM.1S^{dim} cannot be due to absence of GR, as the drug combination reversed any survival benefit it may have compared to MM.1S^{dim}. This would suggest the mechanisms or pathways causing difference in dexamethasone sensitivity between the 2 sub-clones MM.1S^{dim} and MM.1S^{bright}, are different to the mechanisms between MM.1S and MM.1R. My work only enhances the necessity for multi-combination drug therapy, to prevent epigenetic, mutational, or transcriptional changes resulting in complete drug resistance. By selective targeting of confirmed genetic lesions or affected pathways, it may be possible to remove multiple sub-clones thereby diminishing the possibility of selecting drug resistant clones in future treatment. In theory, this could result in longer time to relapse and ultimately improved overall survival.

CHAPTER 7

Final Summary and Future Directions:

7.1 Summary:

This study first set out to design a complex multi-parameter flow cytometry panel, enabling clonal and sub-clonal immunophenotypic analysis of both primary MM samples and known MM cell lines. Access to quality primary samples proved more difficult than first anticipated. Nevertheless, my 10-colour panel revealed numerous immunophenotypically distinct sub-populations within both primary samples and MM cell lines. Although the concept of MM clones is not novel, I have shown that both primary samples and MM cell lines exhibit wide variation in CD38 expression and multiple, phenotypically distinct, sub-populations exhibiting variable expression of functional markers within my flow panel (CXCR4, MMP-9, CD49d, IL-6). Thus, identification of sub-clones by immunophenotyping has the advantage over other clonal identification methods, in that very small sub-clones can be accurately identified and functional differences, that can result in possible selection advantages, driving clonal evolution can be explored. One example of this is CXCR4 expression. Using a novel dynamic migratory model, I showed that CXCR4 expression was more highly expressed on migrated MM cells than non-migratory cells. Myeloma cell CXCR4 expression levels are notoriously variable, with numerous studies giving conflicting results (Hideshima et al. 2001; Moller et al. 2003). My results suggest that migrated cells, even in the presence of a high CXCL12 chemokine gradient, do not downregulate CXCR4 expression. Indeed, expression is seemingly higher on cells migrating towards higher levels of CXCL12. The pattern of CXCR4 expression appeared bimodal, rather than uniformly upregulated when migrated cells retrieved from EVS were stained for CXCR4 expression. The possibility of myeloma CXCR4 sub-clones with differing migratory potential adds weight to the spatial heterogeneity of MM sub-clones in different parts of the bone marrow (Rasche et al. 2017). Such work only confirms the heterogeneity of the disease and that multiple treatment strategies are required to treat and or even cure the disease.

Although pathway and mutational analysis may identify targets for cytotoxic therapy and were therefore investigated in this thesis, inhibiting MM migration and preventing the

interaction of early MM clones with the BM microenvironment before secondary somatic mutations (such as *KRAS* and *TP53*) occur, offers an alternative treatment strategy. Indeed heterogeneous somatic mutations in adhesion molecules, has been shown to allow for sub-clonal evolution (Leich et al. 2013). The inhibition of the CXCR4/CXCL12 axis and adhesion molecules have been shown to affect such events, which in turn results in improved efficacy of cytotoxic agents (Azab et al. 2009b; Azab et al. 2012). Transendothelial migration is a multi-step process, whereby cells circulating under shear force, initially arrest onto endothelium and then roll. Commonly, this leads to encounter with tight junctions (the interface between two endothelial cells), where the cells experience high local concentrations of cytokines resulting in migration (Johnson-Leger et al. 2000; Salanueva et al. 2007). When these processes are lost or inhibited migration is significantly affected. Therefore, developing the dynamic circulatory model, as previously used in our research group (Walsby et al. 2014a), for MM was essential to investigate the effects of shear force on MM adhesion and migration.

To my knowledge I have been the first to show that dual inhibition of CD49d and CXCR4 within a dynamic migratory model is required to induce a statistically significant reduction in CXCL12-induced MM migration. The reasons why combination therapy caused this is likely due to the complimentary roles the receptors have on migration. The two are inexorably linked; CXCR4 regulates VLA-4 adhesion, with migration only occurring if there is both an adhesion signal coupled with a homing signal prior to transendothelial migration (Parmo-Cabanas et al. 2004).

A further question remained as to when in the plasma cell dyscrasia course would CXCR4 and/or CD49d inhibition be most effective? CXCR4 expression is a recognised marker of clonal plasma cell migration potential and is highest in the pre-myelomatous phase MGUS and lowest in relapse (Moller et al. 2003). Although in my work I showed no statistical difference in CXCR4 expression between MGUS and newly diagnosed MM, there was a statistical difference between relapsed MM and newly diagnosed (higher in the later). These finding lead to the conclusion that CXCR4 inhibition in relapsed disease may be less effective due to lower expression and that targeted therapy should be aimed in the high-risk smouldering myeloma/MGUS or newly diagnosed. However, this would need to be tested both *in vitro* and in clinical trials.

The logistics of culturing primary samples, meant that further phenotypic, genetic and functional analysis of primary samples proved difficult. Although some primary samples

had distinct CXCR4 and CD49d sub-populations, the limit of my work meant that I could not test whether these sub-populations had different adhesion or migratory potential, i.e. behave in a functionally different manner. Furthermore, although immunophenotyping is often used in Myeloma to infer clonality, it does not prove it, which is usually achieved through molecular testing. A technique that is not routine in clinical practice, where time and resources are finite. Therefore, the practical ease of inferring clonality by immunophenotyping makes it more appealing, especially if it has treatment implications. It was therefore of great interest that the MM.1S cell line was shown to have bimodal CD38 sub-populations. To my knowledge, this is the first report of this phenomenon and offers the potential for differential treatment responses due to the emergence of anti-CD38 therapies, such as the monoclonal antibody Daratumumab. Combined with the existence of a dexamethasone resistant related cell line MM.1R, this allowed me to explore the origins of glucocorticoid drug resistance in relation to CD38 expression.

CD38 weak or negative expressing populations have not been described in great detail in the literature, they have an estimated incidence of two cases per 1000 examinations (Minarik et al. 2017). Even in commercial MM cell lines, I and others have shown the U266 cell line to negative express CD38 (Drent et al. 2016). Indeed, MM cell lines are known to have immunophenotypically distinct populations, for example CD138, CD56 and CD45 sub-populations have been described within MM cell lines (Wu et al. 2015), as well as the presence drug resistant sub-clones. Keith Stewart's group in Scotsdale, Arizona has described a lenalidomide resistant clone within MM.1S. Such resistance would have been borne out of pre-existing selection advantage to the drug, as the cell line originated prior to the advent of IMiD therapy (Bjorklund et al. 2011; Zhu et al. 2011). This implies multiple sub-clones pre-exist within MM.1S, each with their own unique mutations, resulting in differing pathway activation and specific target for clonal inhibition.

In chapter 5, analysis of the two phenotypically distinct CD38 expressing subsets within the MM.1S cell line revealed both functional and genetic differences thereby confirming the sub-clonal architecture within this cell line. Intriguingly, our data point to the pre-existence of CD38 expressing sub-clones, that have differing cytotoxic sensitivity to dexamethasone. The existence of the dexamethasone resistant cell line MM.1R allowed me to perform comparative genomics thereby identifying 2 possible genetic origins of dexamethasone resistance. In one scenario MM.1S^{bright} cells were selected and tracked to the subsequent clonal evolution (induction) in the MM.1R cells. However, a lack of obvious driver genes made this origin less plausible and an alternative scenario inferring

MM.1S^{bright} is a separate sub-clone to MM.1R more likely. The later scenario implied that MM.1S^{dim} and MM.1S^{bright} diverged from the original ancestor at roughly the same point, potentially initiated through the acquired *ROBO2* driver mutation seen only in MM.1S^{dim} that is then passed onto MM.1R. Mutations in *ROBO2* have been recently linked to spatial genomic heterogeneity in MM and offers the explanation of genetic drift between MM.1S^{bright} and MM.1S^{dim} (Rasche et al. 2017).

The comparative exome analysis in both Chapters 5 and 6, identified other significant mutational differences between the 3 sub-clones, such as *MKI67,* mutated only in MM.1S^{dim}. This mutation is likely to cause a downregulation in Ki-67 expression, which in part explains the difference in reduced proliferative propensity between MM.1S^{dim} and the other sub-clones. The analysis also confirmed the glucocorticoid receptor gene, *NR3C1,* was unmutated, correlating with pre-existing cell line sequence data/COSMIC database, implying the absence of GR in MM.1R and subsequent steroid resistance is likely due to epigenetic changes or bi-allelic inactivation (Greenstein et al. 2003; Sánchez-Vega et al. 2006).

In Chapter 6, pathway analysis of the exome mutation data was also used to identify genetic differences in the sub-clones that could be used as therapeutic target and one such target that was explored was the PI3K/AKT pathway. The PI3K/AKT pathway is a key pathway involved in MM disease progression, survival and activation of the signalling pathway shown to correlate with the expansion of glucocorticoid-resistant MM cells in the bone marrow (Hideshima et al. 2007a; Smith and Cidlowski 2010). To date, comprehensive genetic sequencing of MM has shown mutations involved in the PI3K/AKT pathway are relatively rare (<1%), with the most frequent mutations involved in the RAS/MAPK and NF-κB pathways (>25%) (Chapman et al. 2011; Lohr et al. 2014; Walker et al. 2015). Although my sequencing data is from cell lines, it is largely supportive of this, with a high number of mutations (e.g. *SSPO*) related to the NF-κB pathway. Even when concentrating on one particular pathway, I identified 7 unique PI3K/AKT pathway related gene mutations. PI3K inhibition of the sub-clones showed a preferential cytotoxicity to the sub-clone, MM.1S^{dim} with greatest expression of the PIK3CD p110δ isoform. This discovery, also highlighted the variability in expression of key signalling pathway proteins amongst sub-clones, thus illustrating the potential for using genetic mutations as a means of identifying differential sub-clonal responses to specific pathway inhibitors. To clarify the frequency of these 7 unique mutations in my primary sample data would take time and resources. Such complimentary work between primary material and

cell lines is essential in establishing the correlation between pathway mutations of for example PI3K/AKT, expression levels of PI3K/p110δ and effects of PI3K inhibition. In time, individually sequencing specific genes, will be replaced by more efficient methods, e.g. targeted NGS or WES, with the ultimate goal to undertake WES of individual patients at the start of treatment and subsequent lines of treatment. Outside of clinical trials this has yet to happen, but seems likely to be the next step forward in achieving individualised treatment plans.

7.2 Future Directions:

The most pressing of future directions is the role MM.1S^{dim} may play in the era of anti-CD38 therapy. Just as MM.1S and MM.1R has become a model for the study of glucocorticoid resistance in MM, MM.1S^{dim} and MM.1S^{bright} could become the model for understanding the emergence of CD38 negative clones and anti-CD38 resistance. In this thesis, I was unable to fully explain the cause of the reduction in CD38 expression in the MM.1S^{dim} sub-clone, but suffice it to say, it was not due to a genetic mutation in the *CD38* gene. The advent of daratumumab treatment, the anti-CD38 monoclonal antibody, has inevitably resulted in the existence of CD38 negative clones, (Minarik et al. 2017). The Minarik et al. case report suggests the CD38 MM cells were not distinct clones, but were genetically identical, with the likelihood that epigenetic changes downregulate the expression. These case reports will over the next few years become more apparent and should truly confirm whether, daratumumab resistance is brought upon by epigenetic changes or sub clonal selection, much like the dexamethasone resistance paradigm. The likelihood is of course a combination of the 2 factors. The clonal selection challenges brought upon by new treatment, will enforce epigenetic changes in the sub-clones more adept to form resistance. Thus, work in establishing whether MM.1S^{dim} shows resistance to daratumumab compared to the other sub-clones is of importance before fully exploring the origins of CD38 weak/negative MM sub-clones.

The dynamic migratory model that I adapted has huge potential in not only studying other inhibitory migratory agents in MM, but also in studying the interaction of bone marrow stromal cells with MM, by using the EVS as a "make shift" bone marrow microenvironment. The effects of interactions between different MM sub-clones and bone marrow stromal cells (BMSC) is not well documented. BMSCs are known to stimulat MM growth and survival, in part by the CXCL12/CXCR4 signalling pathway (Feng et al. 2010) and their own mechanical integrity can be affected by the interaction of MM cells to

varying degrees dependent on CD138 expression (Wu et al. 2015). The effect can be somewhat reversed through CXCR4 inhibition and it is another example of immunophenotypic analysis potentially determining treatment. A more detailed investigation into how sheer force affects this interaction and migration potential on immunophenotypic distinct sub-clones is certainly warranted.

Clinical trials using CXCR4 inhibitors (Ghobrial et al. 2014), show rapid mobilisation of plasma cells at 2 hours post-inhibitor, with an equally rapid return of circulating plasma cells to baseline levels at 4 hours post-inhibitor. My experimental methodology of the circulatory migratory model, is of the assumption that migration is a one-way process, i.e. from circulation into the EVS. This is certainly not the case *in vivo* where myeloma cells are in a constant flux in and out of the bone marrow microenvironment (Alsayed et al. 2007) and indeed such two-way migration has already been proven in this circulatory model for CLL cells (Walsby et al. 2014c). Thus, it is plausible that migrated MM cells could "escape" back into the circulation once the effect of Natalizumab and/or ONO-7161 start to wear off. Attempting to identifying peak migratory time points over 48 hours and whether at these points, administration of additional drugs such as the proteasome inhibitor, Bortezomib, would aid in inhibiting migration further or lead to greater cell death is an interesting concept and could be investigated further. Ultimately working with primary MM samples would help to validate the results and conclusions I have reached using MM cell lines. Culturing primary MM cells has its technical difficulties (Bam et al. 2015) and although groups have undertaken experiments without additional cells (Stühmer et al. 2010), the widely accepted method of co-culture has relied on mesenchymal cells such as human stromal cells, having pre-selected CD138 positive MM plasma cells via bead columns (Pawlyn et al. 2017). More complex models, that try to create the bone marrow environment with either healthy or disease BM cells and cytokines have also been developed, that have been able to keep MM cells alive for extended periods (Kirshner et al. 2008; Bam et al. 2015). Developing such a 3D model within the dynamic circulatory EVS would be a unique experiment and an additional advantage of this novel circulatory model being its versatility to create different migratory compartments. Further research work could be attempted to more accurately reflect a functioning bone marrow environment in the EVS. This might include human stromal cells (HS-5), osteoclasts, MRC-5 fibroblasts in addition to myeloma cells. Drug therapy could then be added either to circulation or EVS (such as ONO-7161) in an attempt to cause myeloma cell escape from the EVS into the circulating compartment and assess whether this would sensitise cells to standard cytotoxic agents such as proteasome inhibitors or immunomodulatory drugs.

The complexity of this model is also its potential weakness - huge numbers of variables mean trying to accurately replicate experiments can be difficult. The expense and time required in setting it up compared to transwell experiments means only highly focussed and limited questions can be answered in a timely manner. Nevertheless, it is a unique model that allows for greater understanding of myeloma cell migration and study of potential therapeutic treatments.

The future of combining genetic analysis (be it mutational, cytogenetic or pathway signalling analysis), with immunophenotypic, biochemical and clinical features to formulate a bespoke treatment strategy is the ultimate goal in MM management. However, the introduction of such treatment strategies will be determined by the accessibility of data sharing, allowing for Artificial intelligence and machine learning to develop complex algorithms to not only treat a single myeloma clone, but the whole disease that includes all sub-clones. My pathway analysis through Enrichr, adopted a logical "top-down" approach and identified 6 separate cancer-related pathways where statistical regulation differences between the sub-clones, due to differences in gene mutations. With more time, each of the following pathways could have been further evaluated, offering alternative therapeutic targets and if successful is showing variation in pathway inhibition, again this could highlight the importance of setting up treatment regimens that are sub-clonally targeted.

i. α6β1 and α6β4 integrin signalling pathway showed a regulatory statistical difference through the gene mutations for all 3 cell lines, but greater statistical difference in MM.1R or MM.1S^{bright} ($p=0.004$) than MM.1S^{dim} ($p=0.033$). Alpha 6 is a potentially novel integrin in MM pathogenesis, but has shown to mediate leukocyte tether on laminin under physiological shear and should explain the different adhesive properties of the sub-clones (Kitayama et al. 2000).
ii. The CaN-regulated NFAT-transcription pathway was statistically affected in MM.1R, but not the other 2 pathways. In view of calcineurin targeted therapies, such as the HDAC inhibitor Panobinostat, synergy experiments with HDAC inhibitors and dexamethasone could be attempted to see if resistance could be reversed.
iii. The regulation of RhoA activity pathway was significantly affected in MM.1S^{dim} ($p=0.035$), but not in the other 2 cell lines. RhoA has been shown to be involved in MM SDF-1-induced adhesion, chemotaxis, and homing of MM cells to the BM (Azab et al. 2009a), which to some extend could explain the differences in

transwell migration between the sub-clones and offers a mechanism of sub-clonal expansion dependent on differing migratory potential.

iv. Mutation in *SSPO* and *CUL1* were seen in all 3 cell lines and predicted to statistically (p=0.03) affect degradation of β-Catenin and alter the Wnt/β-Catenin signalling pathway. This pathway is involved in cell-cell adhesion, disease progression, osteoblast activation, lytic lesions and over expression in MM has been related to lenalidomide resistance (Tian et al. 2003; Bjorklund et al. 2011; Clevers and Nusse 2012; Bjorklund et al. 2013).

Computer software programmes such as Ingenuity, can further compare disease mechanisms such as proliferation between multiple mutational sequencing data sets. Mutational analysis of my 3 cell lines, specifically looking at proliferation, identified non-synonymous homozygous SNV in 2 of the 6 IGF binding proteins (*IGF2R* and *IGFBP1*), shared between the 3 cell lines. The myeloma growth factors, IGF/IGF-1R are known to promote MM growth, survival, migration and drug resistance (Bataille et al. 2005; Sprynski et al. 2009; Kuhn et al. 2012). High peripheral blood levels are linked to poor prognosis, and levels are reduced by 6 different IGF binding proteins (Bieghs et al. 2016). Though no specific proliferation associated mutation differences were identified between the cell lines, it provides targeted genes that could be looked at in more detail, for example identifying if *IGF2R* and *IGFBP1* protein expression differs between the cell lines.

Furthermore, studying of the sub-clones in xenograft models, would provide greater understanding of the in-vitro proliferative properties as external factors e.g. bone marrow microenvironment, or other sub-clonal interactions would be considered and do not form part of my functional proliferative assays. Mice xenograft models, using retroviral transduction of the cell lines (LeBlanc et al. 2002; Mitsiades et al. 2004) have been instrumental in showing the clinical benefits of proteasome inhibitors (LeBlanc et al. 2002; Richmond and Su 2008) and would be key in the studying of the effect of novel cytotoxic agents, especially if wanting to observe the differing effects between sub-clones.

Xenograft modelling would also allow for further investigation of the sub-clone migratory potential or spread of extra medullary disease, which has been shown to be regulated by CXCR4 (Roccaro et al. 2015). Although no statistical difference in CXCR4 expression was observed between the sub-clones, MM.1S^{bright} has a greater MFI expression than MM.1S^{dim} (1,903 vs. 1,722 p=0.870) and could explain the increase in CXCL12 induced static transwell migration observed for MM.1S^{bright}. Greater CXCR4 expression can also result in increased

cellular invasion, metastasis and ultimately disease progression (Roccaro et al. 2015). Although Roccaro et al showed that by blocking CXCR4 extra-medullary disease (EMD) was less likely, the full migratory mechanisms are less understood but epithelial mesenchymal transitions is thought to play a pivotal part. The increase in MM.1S^{bright} CXCR4 expression could also result in a greater propensity for EMD to form. To date, no existing literature exists regarding CD38 expression and extra medullary disease (Kumar et al. 2010). The one immunophenotype that is recognised with EMD is the absence of CD56 (Dahl et al. 2002), similar to plasma cell leukaemia (Pellat-Deceunynck et al. 1998). I have shown than MM.1S^{bright} has lower CD56 expression than MM.1S^{dim} (1,613 vs. 2,164 p=0.517), although non-statistical it could infer again that MM.1S^{bright} has a greater propensity for EMD, which could be confirmed through xenograft modelling.

The emergence of widely available NGS in additional to other informative genetic techniques such as CHIPseq (Thomas et al. 2015), has opened up the possibility of identifying key mutations and affected pathways for individual patient's disease. This may lead to the advent of NGS based screening tools designed to predict cytotoxic susceptibility and aid in treatment decision for patients with cancer. Targeted NGS at present is a more feasible approach than WES (Ikeda et al. 2015), but the key issues with NGS is the difficulty in knowing what mutations to look for and what the clinical significance are, but could allow for the prediction of drug resistance and facilitate improvements in the treatment of MM patients. What makes this task especially difficult, is that MM in keeping with many other cancers, demonstrates significant sub-clonal heterogeneity. Consequently, what treatment may be good for the eradication of one clone, may cause rapid clonal expansion in another clone (Keats et al. 2012). A perfect example of this has resulted in the early suspension of the BELLINI trial, the use of the BCL2 inhibitor Venetoclax, where a decrease in overall survival in non t(11:14) MM was observed. This makes clinicians' treatment decisions more difficult, especially in the later stages of disease where large difference in sub-clonal drug sensitivities are more likely. To overcome the possibility of treatment causing worsening disease progression and/or evolution, analyse of the mutation variation between the many different sub-clones must occur and will pave the way for the development of sophisticated models for designing bespoke therapies. By selective targeting of these genetic lesions it may be possible to remove multiple sub-clones thereby diminishing the potential for clonal tiding and the development of drug resistance. In theory, this approach could be used to optimise the depth of remissions and improve overall survival by targeting sub-clonal architecture.

APPENDIX:

8.1 MM adherence to the CXCL12 secreting fibroblasts MRC-5

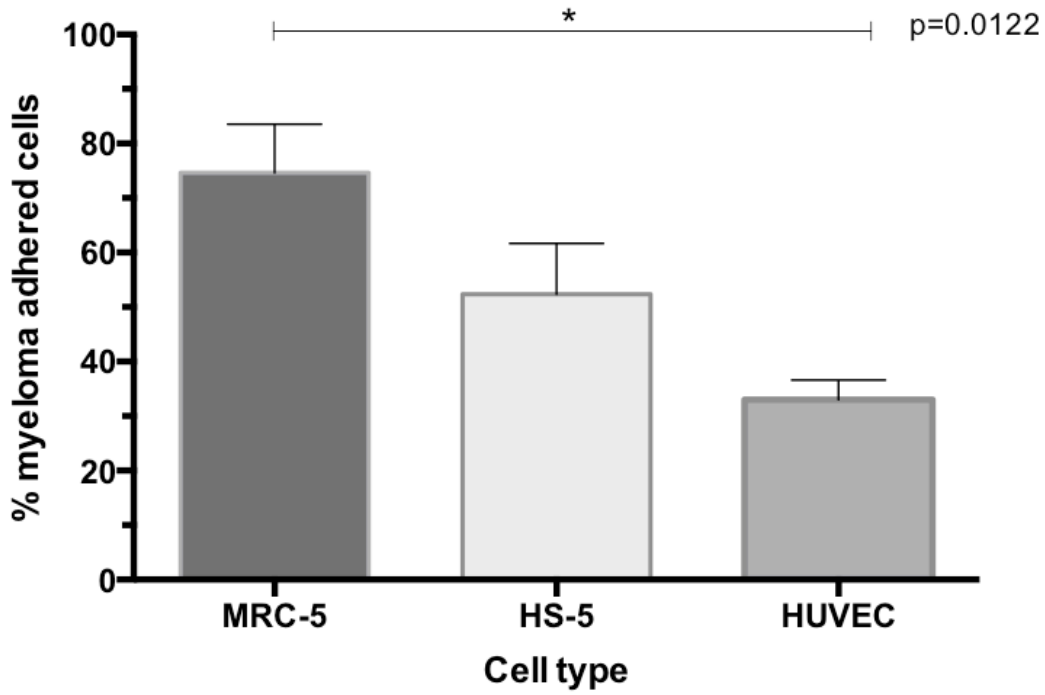

Supplementary Figure 1; Percentage of myeloma cells (cell lines MM.1S) adhered to the CXCL12 secreting fibroblasts MRC-5*, Human fibroblast stromal cells HS-5 and the endothelial cell HUVEC. Myeloma cells were co-cultured with the corresponding fibroblast/endothelial cell for 4 hours (n=3). Non-adhered myeloma cells were removed by media replacement with cell numbers counted by Vi-cell. Percentage adherence measure by retrieved myeloma cells deducted by total myeloma cells used, divided by total.*

8.2 Co-culture between MM and fibroblasts/endothelial cells

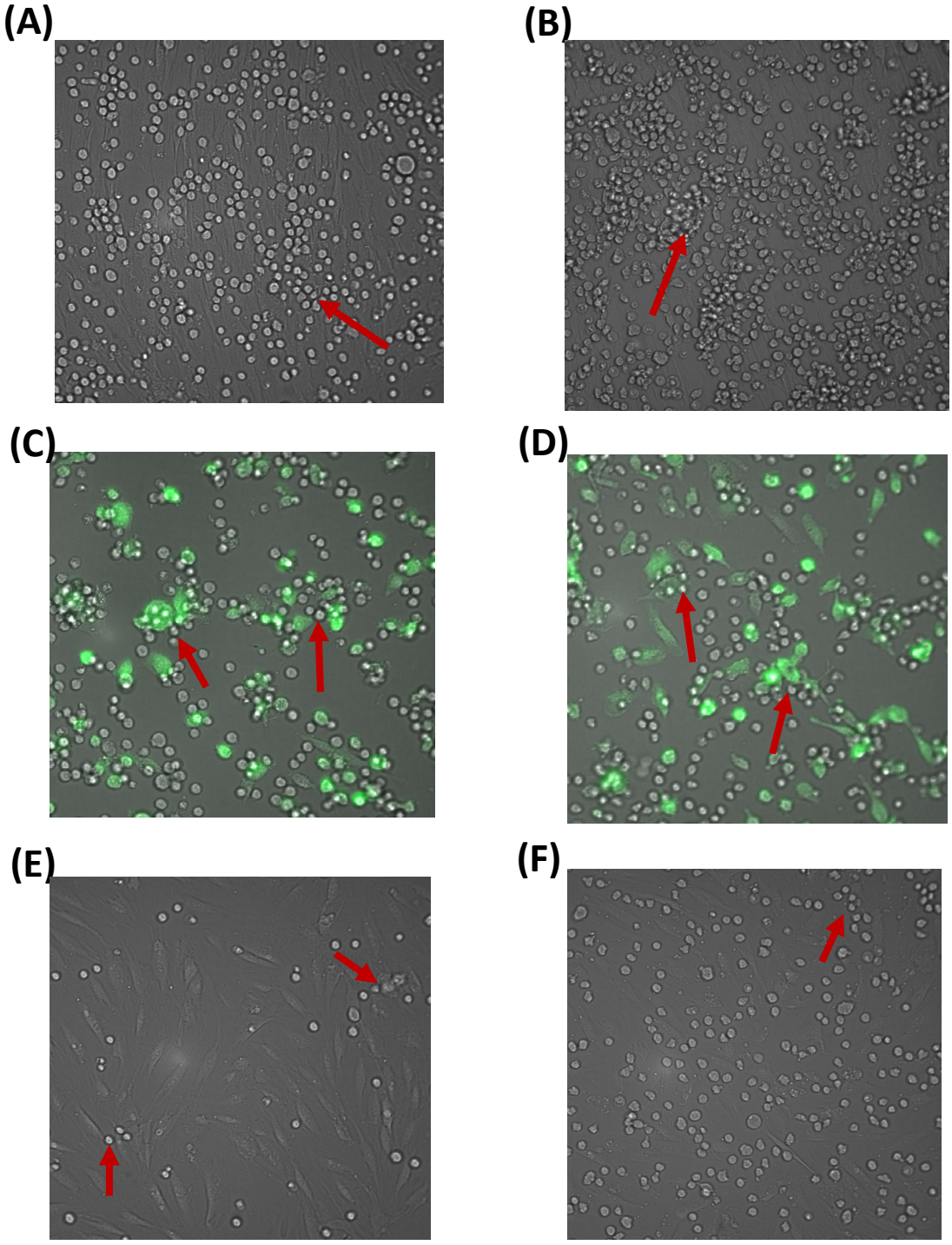

Supplementary Figure 2. Light microscope 40X magnification photographs of co-culture between MM.1S CD38 sorted cell populations and fibroblasts/endothelial cells. *Roughly 0.5x10^6 Fibroblasts/endothelial cells were plated on 6-well plates and left for 24h, non-adhered cells were removed and 5x10^6 MM.1S^{bright} or MM.1S^{dim} cells added to culture. After 4 hours, non-adhered cells were removed, counted and photographs taken of co-cultures. Red arrows indicate group of MM cells adhered to fibroblast/endothelial cells. Co-cultures were as follow (A) MM.1S^{bright} and fibroblast MRC-5; (B) MM.1S^{dim} and fibroblast MRC-5; (C) MM.1S^{bright} and human stromal fibroblast HS-5, GFE tagged (appearing fluorescence green); (D) MM.1S^{dim} and human stromal fibroblast HS-5, GFE tagged (appearing fluorescence green); (E) MM.1S^{bright} and endothelial HUVEC; (F) MM.1S^{dim} and endothelial HUVEC.*

8.3 Comparison of P-gp expression within different MM cell lines

(A)

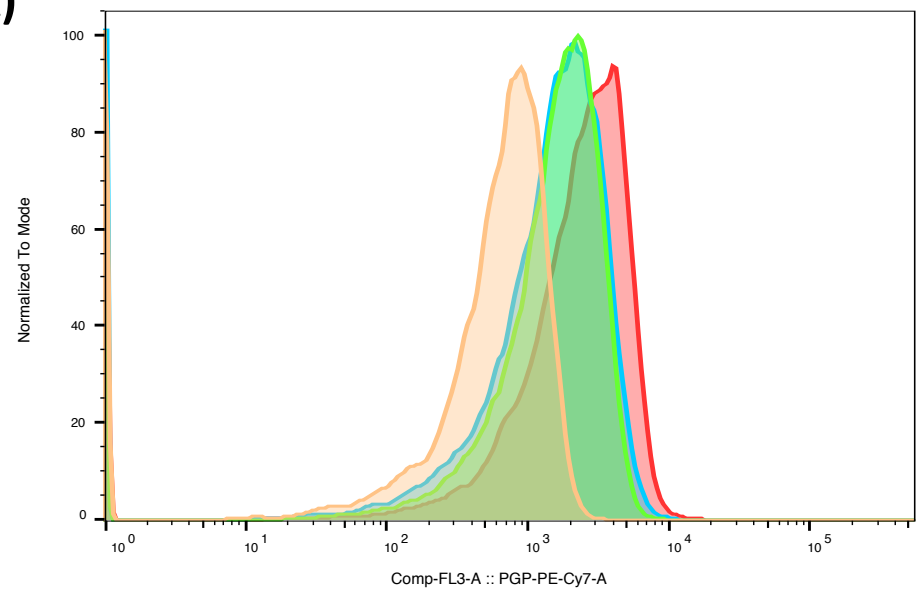

	Subset Name with Gating Path	Count	Mean : Comp-FL3-A	Median : Comp-FL3-A	PGP-PE-Cy7-A+ :: Freq. of Parent
	C01 MM1S unstained.fcs/Alive/Single Cells	8915.0	694.0	657.1	0.3
	C02 MM1S stained.fcs/Alive/Single Cells	44271.0	1734.0	1597.3	28.5
	B02 MM1R stained.fcs/Alive/Single Cells	36020.0	1625.0	1399.8	26.8
	A02 RPMI stained.fcs/Alive/Single Cells	9391.0	2657.8	2388.3	36.1

(B)

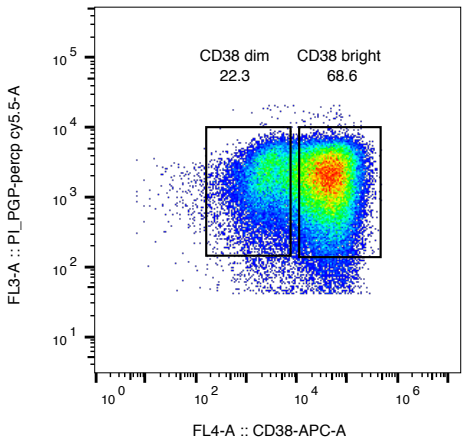

(C)

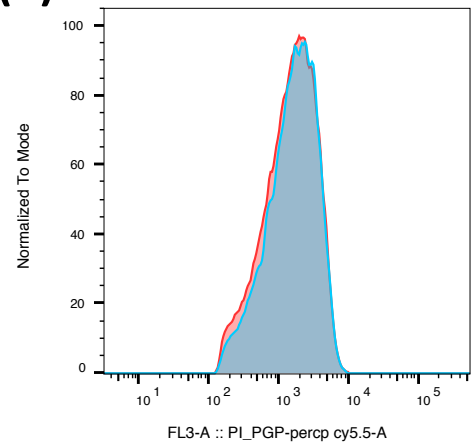

	Subset Name with Gating Path	Count	Mean : FL3-A	Mean : FL4-A	Freq. of Parent
	F01 MM1S-2(pgp) 48hr vel 0.fcs/Alive/Single Cells/CD38_Pgp/CD38 dim	15188.0	2008.5	3124.8	22.3
	F01 MM1S-2(pgp) 48hr vel 0.fcs/Alive/Single Cells/CD38_Pgp/CD38 bright	46772.0	1924.9	52445.9	68.6

***Supplementary Figure 3. Comparison of P-gp expression within different MM cell lines**, measured on BD Accuri. (A) Overlay histograms of static cultic P-gp expression (stained with PE-Cy7-CD243) of MM.1S, MM.1R and RPMI-8226. MM.1S and MM.1R overlay histograms were comparable (MM.1S; MFI-1,736, 28.6% positivity vs. MM.1R; MFI-1,628, 26.7% positivity). As a comparison, the cell line RMPI-8226 has greater P-gp expression (MFI-2,652, 36.1% positivity) (B) Flow cytometry dot plot of MM.1S comparing P-gp expression with CD38 expression. CD38 gating shown in boxes. (C) Overlay histograms comparing P-gp expression of the two CD38 gated subsets as shown in figure 4B. All measurements done on BD Accuri. Tables state corresponding overlay histograms events counted (Count), mean and median fluorescence intensity (Mean and median) and P-gp percentage positivity relative to unstained sample of same cell line (Freq. of Parent).*

8.4 Overlay histograms of P-gp expression

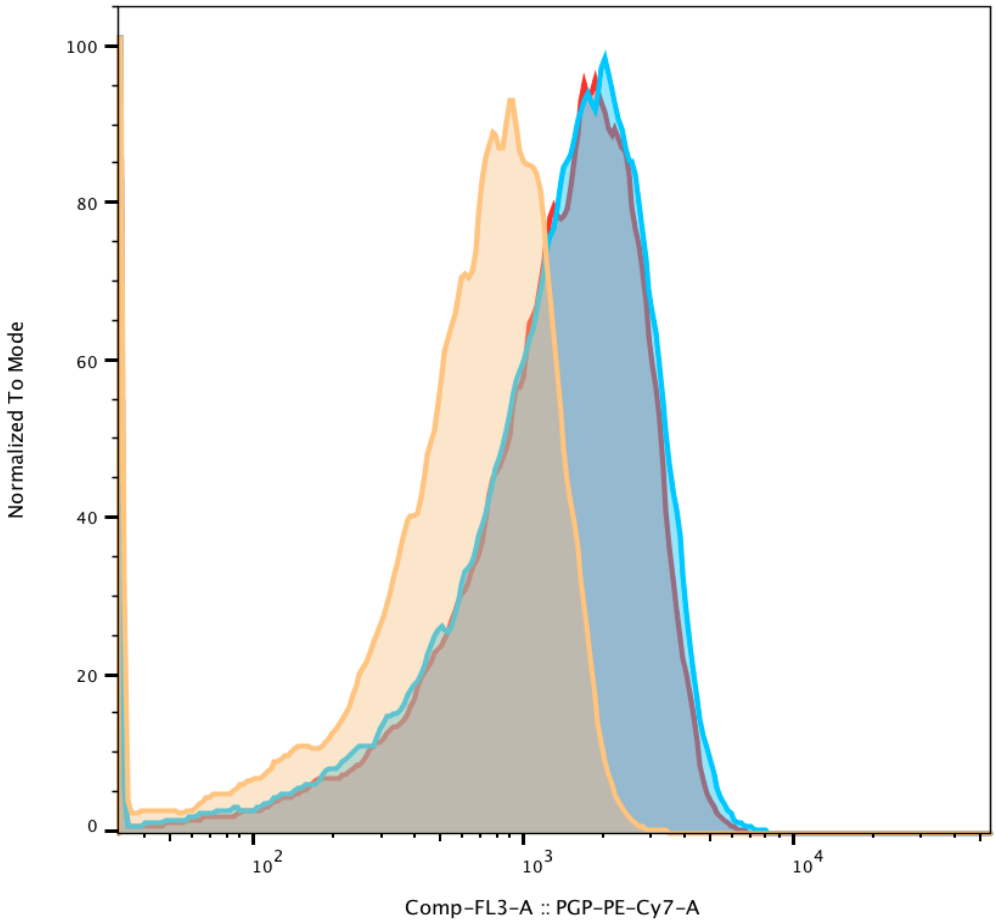

	Subset Name with Gating Path	Count	Mean : Comp-FL3-A	PGP-PE-Cy7-A+ :: Freq. of Parent
	C01 MM1S unstained.fcs/Alive/Single Cells	8918.0	696.9	0.3
	F02 Bright stained.fcs/Alive/Single Cells	36441.0	1498.7	26.5
	E02 dim stained.fcs/Alive/Single Cells	38304.0	1482.1	25.2

Supplementary Figure 4. Overlay histograms of P-gp expression *measured by BD Accuri. Cells stained with PE-Cy7-CD243. Comparison between the unstained MM.1S and the sorted cell lines MM.1S^{bright} and MM.1S^{dim}. Histograms show almost identical MFI and percentage positivity (MM.1S^{brigth} MFI 1,498, 26.5% positivity vs. MM.1S^{dim} MFI 1,482 25.2% positivity).*

8.5 Overlay histograms of CD38 expression between MM.1S^{dim} and MM.1S^{bright}

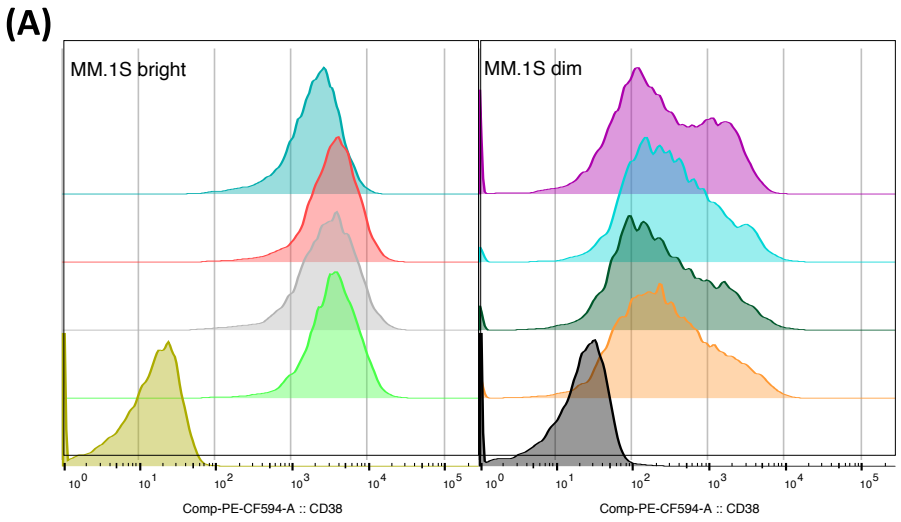

	Subset Name with Gating Path	Median : Comp-PE-CF594-A	Mean : Comp-PE-CF594-A
	MM1S Bright_stained_002.fcs/Alive cells/Single Cells/CD138, CD56 subset	2072.4	2420.0
	MM1S-Bright_HS-5 stained - susp_008.fcs/Alive cells/Single Cells/CD138, CD56 subset	3488.9	4151.3
	MM1S-Bright_MRC-5 stained - susp_010.fcs/Alive cells/Single Cells/CD138, CD56 subset	2996.0	3826.0
	MM1S-Bright_HUVEC stained - susp_012.fcs/Alive cells/Single Cells/CD138, CD56 subset	3467.7	4231.5
	MM1S Bright_unstained_001.fcs/Alive cells/Single Cells	8.6	12.6
	MM1S Dim_stained_004.fcs/Alive cells/Single Cells/CD138, CD56 subset	207.8	637.1
	MM1S-Dim_HS-5 stained - susp_014.fcs/Alive cells/Single Cells/CD138, CD56 subset	272.5	740.6
	MM1S-Dim_MRC-5 stained - susp_016.fcs/Alive cells/Single Cells/CD138, CD56 subset	196.1	667.0
	MM1S-Dim_HUVEC stained - susp_018.fcs/Alive cells/Single Cells/CD138, CD56 subset	231.9	736.0
	MM1S Dim_unstained_003.fcs/Alive cells/Single Cells	19.1	21.9

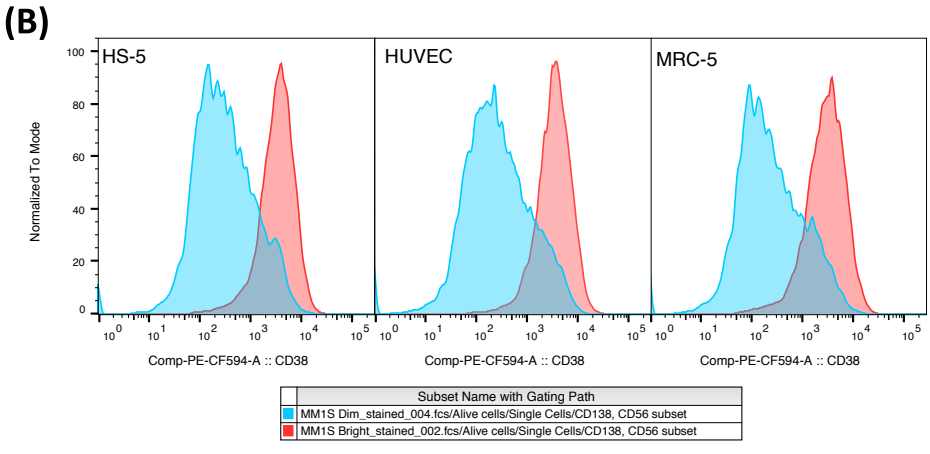

Subset Name with Gating Path
MM1S Dim_stained_004.fcs/Alive cells/Single Cells/CD138, CD56 subset
MM1S Bright_stained_002.fcs/Alive cells/Single Cells/CD138, CD56 subset

Supplementary Figure 5. Overlay histograms of CD38 expression between MM.1S^{dim} and MM.1S^{bright} *in fibroblast/endothelial co-culture (same experiment as figure 17). Non-adhered cells were washed away with media, leaving adhered cells which were removed with Trypsin 0.05% and subsequently immunostained for flow cytometry measured on BD Fortessa. MM cell lines were identified from fibroblast/endothelial by CD138/CD56 gating. (A) Comparison of CD38 expression between separate co-culture experiments of either MM.1S^{dim} or MM.1S^{bright} adhered to MRC-5, HS-5 or HUVEC. Legend contains MFI value for each histogram. (B) Overlay histogram comparing CD38 expression of MM.1S^{dim} and MM.1S^{bright} within the different co-culture experiments (HS-5, HUVEC or MRC-5)*

8.6 Overlay histograms of CD56 expression between MM.1S^{dim} and MM.1S^{bright}

(A)

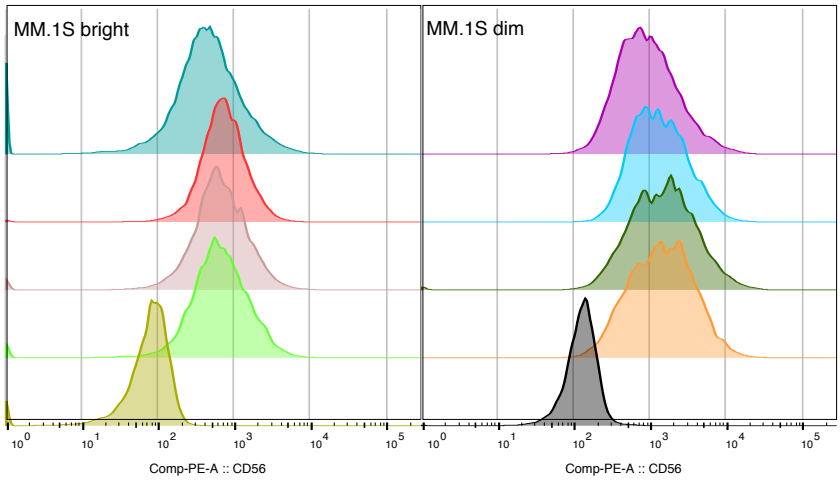

Subset Name with Gating Path	Median : Comp-PE-A	Mean : Comp-PE-A
MM1S Bright_stained_002.fcs/Alive cells/Single Cells/CD138, CD38 subset	425.2	743.3
MM1S-Bright_HS-5 stained - susp_008.fcs/Alive cells/Single Cells/CD138, CD38 subset	694.3	867.3
MM1S-Bright_MRC-5 stained - susp_010.fcs/Alive cells/Single Cells/CD138, CD38 subset	618.4	869.0
MM1S-Bright_HUVEC stained - susp_012.fcs/Alive cells/Single Cells/CD138, CD38 subset	616.5	888.3
MM1S Bright_unstained_001.fcs/Alive cells/Single Cells	79.9	83.8
MM1S Dim_stained_004.fcs/Alive cells/Single Cells/CD138, CD38 subset	833.6	1402.1
MM1S-Dim_HS-5 stained - susp_014.fcs/Alive cells/Single Cells/CD138, CD38 subset	1208.7	1807.0
MM1S-Dim_MRC-5 stained - susp_016.fcs/Alive cells/Single Cells/CD138, CD38 subset	1446.7	2263.5
MM1S-Dim_HUVEC stained - susp_018.fcs/Alive cells/Single Cells/CD138, CD38 subset	1377.9	2104.0
MM1S Dim_unstained_003.fcs/Alive cells/Single Cells	125.3	134.6

(B)

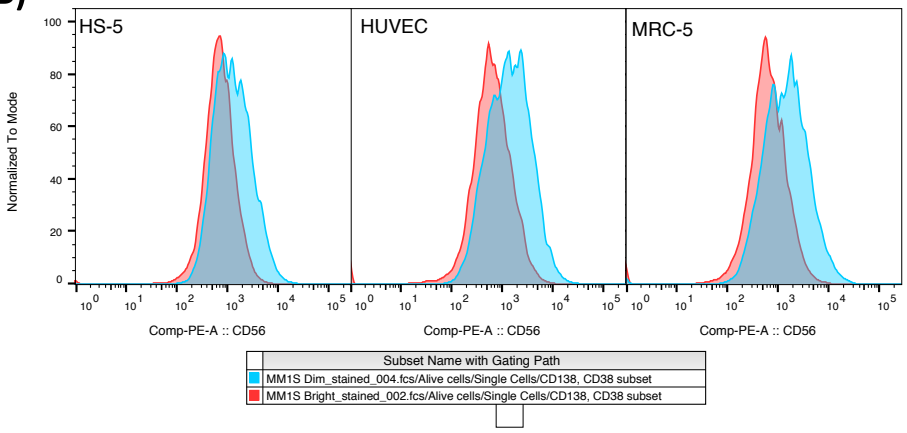

Supplementary Figure 6. Overlay histograms of CD56 expression between MM.1S^{dim} and MM.1S^{bright} *in fibroblast/endothelial co-culture (same experiment as figure 17). Non-adhered cells were washed away with media, leaving adhered cells which were removed with Trypsin 0.05% and subsequently immunostained for flow cytometry measured on BD Fortessa. MM cell lines were identified from fibroblast/endothelial by CD138/CD38 gating. (A) Comparison of CD56 expression between separate co-culture experiments of either MM.1S^{dim} or MM.1S^{bright} adhered to MRC-5, HS-5 or HUVEC. Legend contains MFI value for each histogram. MM.1S^{bright} CD56 expression did not vary upon adherence to fibroblasts or endothelial cells. This is in contrast to MM.1S^{dim}, where increase in CD56 expression was observed, with greatest increase seen with MRC-5 adherence (MFI (mean) 2,264 vs baseline 1,402). (B) Overlay histogram comparing CD56 expression of MM.1S^{dim} and MM.1S^{bright} within the different co-culture experiments (HS-5, HUVEC or MRC-5). Overlay histograms between the two CD38 sub-populations confirmed the expression difference between the two sub-populations, with approximately 0.5 log increase in MM.1S^{dim} CD56 expression.*

8.7 Overlay histograms of IL-6 expression between MM.1S^{dim} and MM.1S^{bright}

(A)

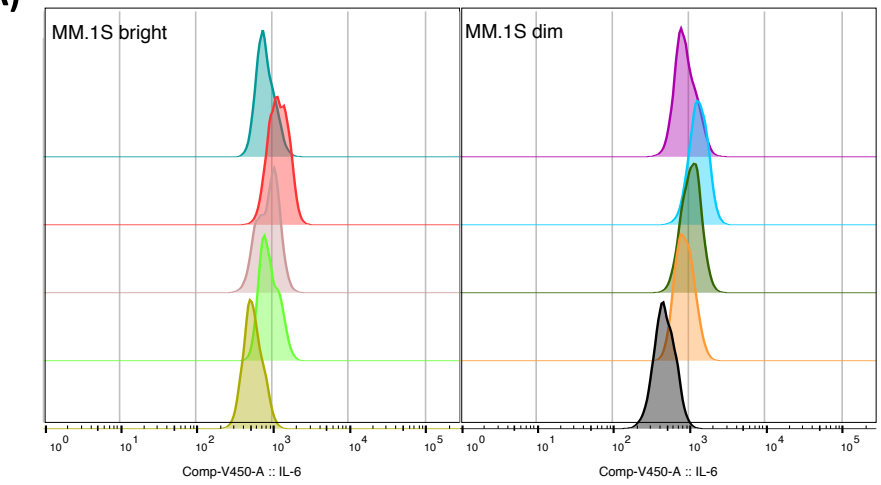

Subset Name with Gating Path	Median : Comp-V450-A	Mean : Comp-V450-A
MM1S Bright_stained_002.fcs/Alive cells/Single Cells/CD138, CD38 subset	751.5	809.2
MM1S-Bright_HS-5 stained - susp_008.fcs/Alive cells/Single Cells/CD138, CD38 subset	1147.7	1201.9
MM1S-Bright_MRC-5 stained - susp_010.fcs/Alive cells/Single Cells/CD138, CD38 subset	877.9	887.9
MM1S-Bright_HUVEC stained - susp_012.fcs/Alive cells/Single Cells/CD138, CD38 subset	843.8	913.1
MM1S Bright_unstained_001.fcs/Alive cells/Single Cells	526.2	559.4
MM1S Dim_stained_004.fcs/Alive cells/Single Cells/CD138, CD38 subset	833.6	909.8
MM1S-Dim_HS-5 stained - susp_014.fcs/Alive cells/Single Cells/CD138, CD38 subset	1280.7	1325.0
MM1S-Dim_MRC-5 stained - susp_016.fcs/Alive cells/Single Cells/CD138, CD38 subset	1034.8	1066.6
MM1S-Dim_HUVEC stained - susp_018.fcs/Alive cells/Single Cells/CD138, CD38 subset	831.0	877.8
MM1S Dim_unstained_003.fcs/Alive cells/Single Cells	454.7	486.3

(B)

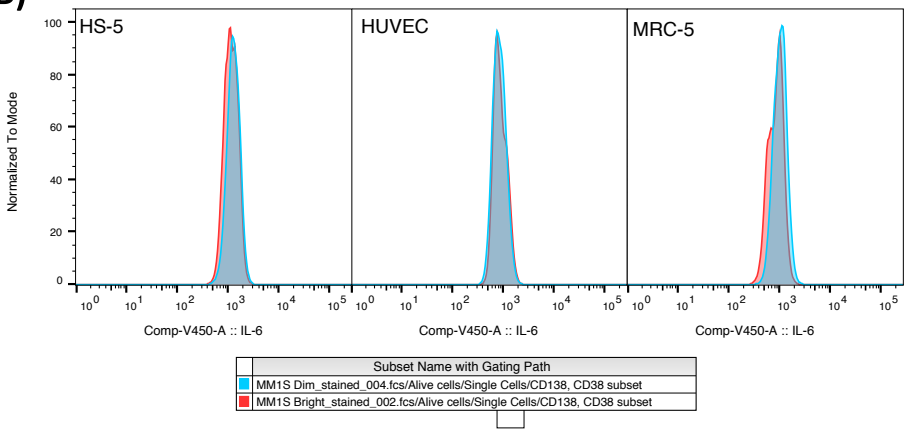

Supplementary Figure 7. Overlay histograms of IL-6 expression between MM.1S^{dim} and MM.1S^{bright} *in fibroblast/endothelial co-culture (same experiment as figure 17). Non-adhered cells were washed away with media, leaving adhered cells which were removed with Trypsin 0.05% and subsequently immunostained for flow cytometry measured on BD Fortessa. MM cell lines were identified from fibroblast/endothelial by CD138/CD38 gating. (A) Comparison of IL-6 expression between separate co-culture experiments of either MM.1S^{dim} or MM.1S^{bright} adhered to MRC-5, HS-5 or HUVEC. Legend contains MFI value for each histogram. MM.1S^{bright} and MM.1S^{dim} adhesion to the stromal fibroblast HS-5 upregulated expression of the intracellular markers IL-6 by roughly 0.5 log difference compared to static culture. (B) Overlay histogram comparing IL-6 expression of MM.1S^{dim} and MM.1S^{bright} within the different co-culture experiments (HS-5, HUVEC or MRC-5) No difference was observed in HS-5 adhesion related upregulated expression of IL-6 between the two cell lines.*

8.8 Overlay histograms of MMP-9 expression between MM.1S^{dim} and MM.1S^{bright}

(A)

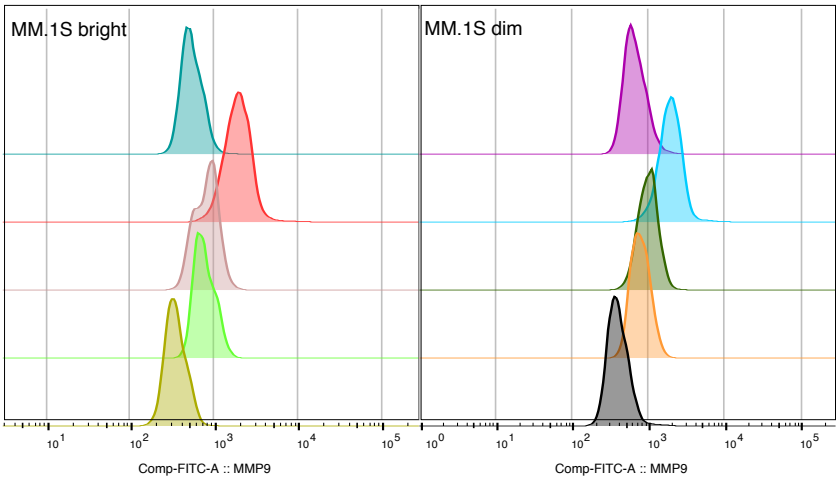

	Subset Name with Gating Path	Median : Comp-FITC-A	Mean : Comp-FITC-A
	MM1S Bright_stained_002.fcs/Alive cells/Single Cells/CD138, CD38 subset	510.2	549.6
	MM1S-Bright_HS-5 stained - susp_008.fcs/Alive cells/Single Cells/CD138, CD38 subset	1856.7	2034.8
	MM1S-Bright_MRC-5 stained - susp_010.fcs/Alive cells/Single Cells/CD138, CD38 subset	802.4	815.7
	MM1S-Bright_HUVEC stained - susp_012.fcs/Alive cells/Single Cells/CD138, CD38 subset	718.0	776.2
	MM1S Bright_unstained_001.fcs/Alive cells/Single Cells	328.0	352.4
	MM1S Dim_stained_004.fcs/Alive cells/Single Cells/CD138, CD38 subset	620.3	687.8
	MM1S-Dim_HS-5 stained - susp_014.fcs/Alive cells/Single Cells/CD138, CD38 subset	1872.2	2034.6
	MM1S-Dim_MRC-5 stained - susp_016.fcs/Alive cells/Single Cells/CD138, CD38 subset	953.2	987.5
	MM1S-Dim_HUVEC stained - susp_018.fcs/Alive cells/Single Cells/CD138, CD38 subset	746.5	789.9
	MM1S Dim_unstained_003.fcs/Alive cells/Single Cells	374.1	415.2

(B)

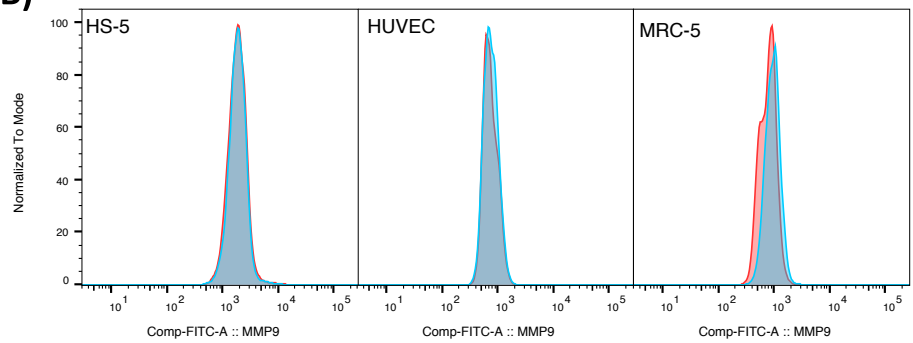

	Subset Name with Gating Path
	MM1S Dim_stained_004.fcs/Alive cells/Single Cells/CD138, CD38 subset
	MM1S Bright_stained_002.fcs/Alive cells/Single Cells/CD138, CD38 subset

Supplementary Figure 8. Overlay histograms of MMP-9 expression between MM.1S^{dim} and MM.1S^{bright} *in fibroblast/endothelial co-culture (same experiment as figure 17). Non-adhered cells were washed away with media, leaving adhered cells which were removed with Trypsin 0.05% and subsequently immunostained for flow cytometry measured on BD Fortessa. MM cell lines were identified from fibroblast/endothelial by CD138/CD38 gating. (A) Comparison of MMP-9 expression between separate co-culture experiments of either MM.1S^{dim} or MM.1S^{bright} adhered to MRC-5, HS-5 or HUVEC. Legend contains MFI value for each histogram. MM.1S^{bright} and MM.1S^{dim} adhesion to the stromal fibroblast HS-5 upregulated expression of the intracellular markers MMP-9 and IL-6 by roughly 0.5 log difference compared to static culture. (B) Overlay histogram comparing MMP-9 expression of MM.1S^{dim} and MM.1S^{bright} within the different co-culture experiments (HS-5, HUVEC or MRC-5). No difference was observed in HS-5 adhesion related upregulated expression of MMP-9 between the two cell lines*

8.9 Overlay histograms of CXCR4 expression between MM.1S^{dim} and MM.1S^{bright}

(A)

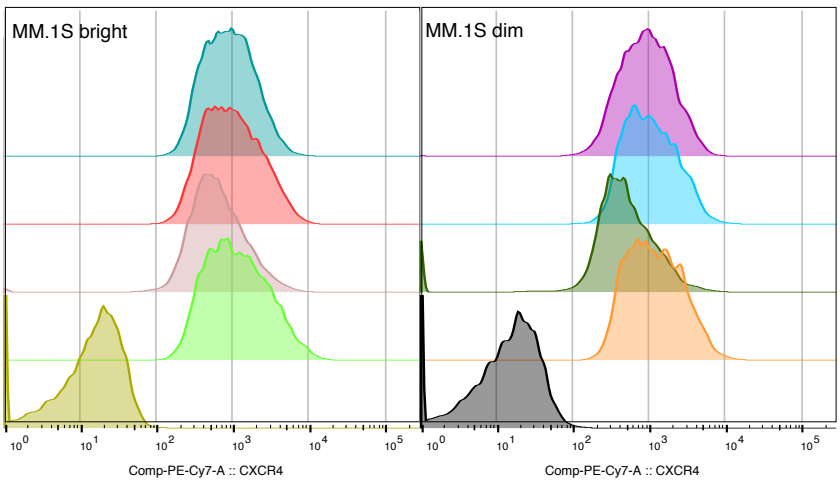

Subset Name with Gating Path	Median : Comp-PE-Cy7-A	Mean : Comp-PE-Cy7-A
MM1S Bright_stained_002.fcs/Alive cells/Single Cells/CD138, CD38 subset	843.8	1151.5
MM1S-Bright_HS-5 stained - susp_008.fcs/Alive cells/Single Cells/CD138, CD38 subset	883.2	1355.7
MM1S-Bright_MRC-5 stained - susp_010.fcs/Alive cells/Single Cells/CD138, CD38 subset	569.6	875.5
MM1S-Bright_HUVEC stained - susp_012.fcs/Alive cells/Single Cells/CD138, CD38 subset	1009.9	1680.3
MM1S Bright_unstained_001.fcs/Alive cells/Single Cells	8.9	13.2
MM1S Dim_stained_004.fcs/Alive cells/Single Cells/CD138, CD38 subset	872.5	1175.9
MM1S-Dim_HS-5 stained - susp_014.fcs/Alive cells/Single Cells/CD138, CD38 subset	941.6	1381.5
MM1S-Dim_MRC-5 stained - susp_016.fcs/Alive cells/Single Cells/CD138, CD38 subset	435.7	680.7
MM1S-Dim_HUVEC stained - susp_018.fcs/Alive cells/Single Cells/CD138, CD38 subset	1066.8	1590.9
MM1S Dim_unstained_003.fcs/Alive cells/Single Cells	4.3	11.7

(B)

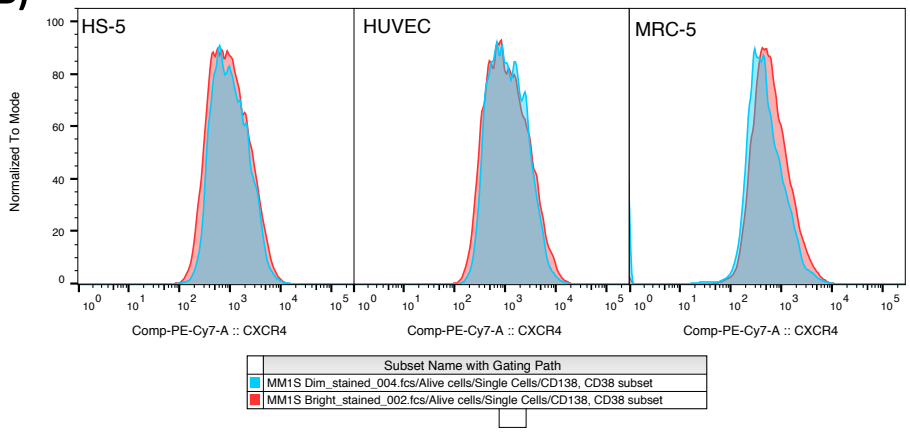

Subset Name with Gating Path
MM1S Dim_stained_004.fcs/Alive cells/Single Cells/CD138, CD38 subset
MM1S Bright_stained_002.fcs/Alive cells/Single Cells/CD138, CD38 subset

Supplementary Figure 9. Overlay histograms of CXCR4 expression between MM.1S^{dim} and MM.1S^{bright} *in fibroblast/endothelial co-culture (same experiment as figure 17). Non-adhered cells were washed away with media, leaving adhered cells which were removed with Trypsin 0.05% and subsequently immunostained for flow cytometry measured on BD Fortessa. MM cell lines were identified from fibroblast/endothelial by CD138/CD38 gating. (A) Comparison of CXCR4 expression between separate co-culture experiments of either MM.1S^{dim} or MM.1S^{bright} adhered to MRC-5, HS-5 or HUVEC. Legend contains MFI value for each histogram. CXCR4 expression was reduced for both for cell lines, but to a greater degree for MM.1S^{dim} (MFI (mean) MM.1S^{bright} 1,152 (static) vs 875 (co-culture) and MM.1S^{dim} 1,176 (static) vs 680 (co-culture)) (B) Overlay histogram comparing CXCR4 expression of MM.1S^{dim} and MM.1S^{bright} within the different co-culture experiments (HS-5, HUVEC or MRC-5). Adhesion to HS-5, CXCR4 MFI for MM.1S^{bright} was 1,355 and MM.1S^{dim} 1,381, with no difference in overlay histograms. Adhesion with HUVEC saw upregulation of CXCR4 expression, with no differences between the cell lines (MFI MM.1S^{bright} 1,680 and MM.1S^{dim} 1,591).*

8.10 Overlay histograms of CD49d expression between MM.1S^{dim} and MM.1S^{bright}

(A)

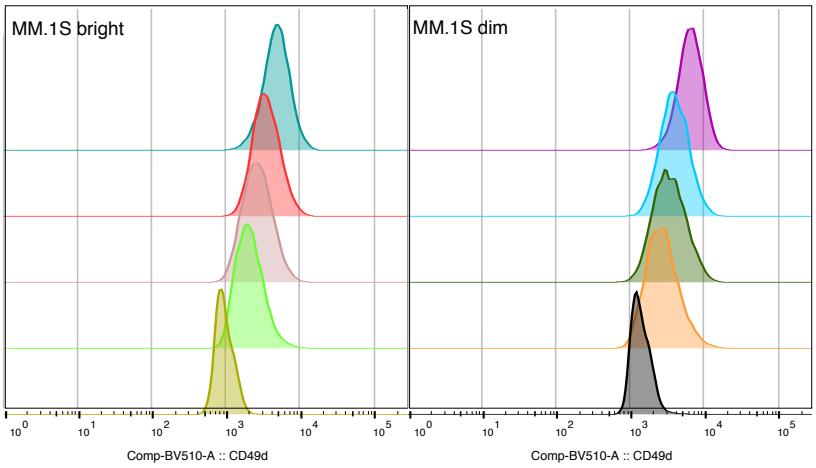

	Subset Name with Gating Path	Mean : Comp-BV510-A	Median : Comp-BV510-A
	MM1S Bright_stained_002.fcs/Alive cells/Single Cells/CD138, CD38 subset	4997.6	4645.6
	MM1S-Bright_HS-5 stained - susp_008.fcs/Alive cells/Single Cells/CD138, CD38 subset	3712.2	3322.9
	MM1S-Bright_MRC-5 stained - susp_010.fcs/Alive cells/Single Cells/CD138, CD38 subset	2857.2	2526.2
	MM1S-Bright_HUVEC stained - susp_012.fcs/Alive cells/Single Cells/CD138, CD38 subset	2307.4	1949.9
	MM1S Bright_unstained_001.fcs/Alive cells/Single Cells	955.3	885.9
	MM1S Dim_stained_004.fcs/Alive cells/Single Cells/CD138, CD38 subset	6677.6	6261.6
	MM1S-Dim_HS-5 stained - susp_014.fcs/Alive cells/Single Cells/CD138, CD38 subset	4183.0	3753.5
	MM1S-Dim_MRC-5 stained - susp_016.fcs/Alive cells/Single Cells/CD138, CD38 subset	3690.8	3193.9
	MM1S-Dim_HUVEC stained - susp_018.fcs/Alive cells/Single Cells/CD138, CD38 subset	3009.1	2541.6
	MM1S Dim_unstained_003.fcs/Alive cells/Single Cells	1425.0	1284.6

(A

(B)

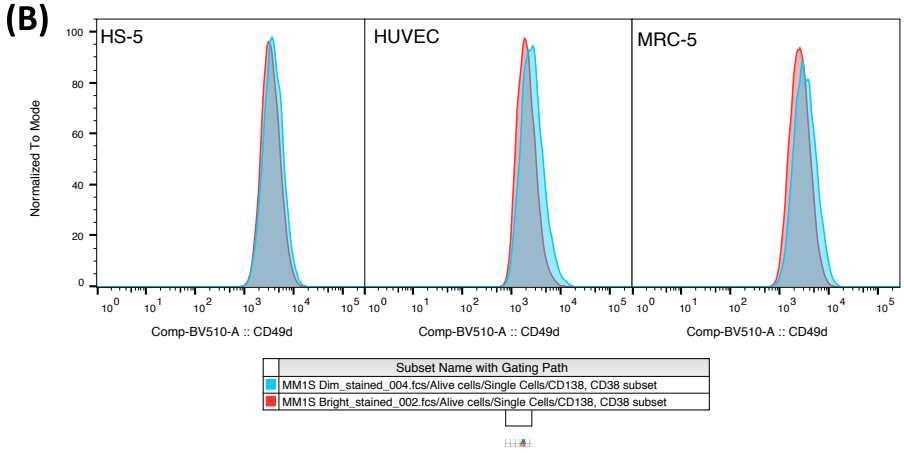

Subset Name with Gating Path
MM1S Dim_stained_004.fcs/Alive cells/Single Cells/CD138, CD38 subset
MM1S Bright_stained_002.fcs/Alive cells/Single Cells/CD138, CD38 subset

Supplementary Figure 10. Overlay histograms of CD49d expression between MM.1S^{dim} and MM.1S^{bright} *in fibroblast/endothelial co-culture (same experiment as figure 17). Non-adhered cells were washed away with media, leaving adhered cells which were removed with Trypsin 0.05% and subsequently immunostained for flow cytometry measured on a BD Fortessa flow cytometer. MM cell lines were identified from fibroblast/endothelial by CD138/CD38 gating. (A) Comparison of CD49d expression between separate co-culture experiments of either MM.1S^{dim} or MM.1S^{bright} adhered to MRC-5, HS-5 or HUVEC. Legend contains MFI value for each histogram. CD49d expression was reduced from static baseline (i.e. not in co-culture). The greatest reduction in CD49d expression was observed in HUVEC co-culture, followed by MRC-5 and then HS-5. (B) Overlay histogram comparing CD49d expression of MM.1S^{dim} and MM.1S^{bright} within the different co-culture experiments (HS-5, HUVEC or MRC-5). MM.1S^{dim} reduction in expression (relative to static baseline) was marginally less than for MM.1S^{bright} for each fibroblast/endothelial adhesion. The greatest difference was seen in HUVEC co-culture, where MM.1S^{bright} MFI (mean) was 1,95011 compared to MM.1S^{dim} MFI 2,542, with increase expression non-overlapping occurring for MM.1S^{dim}*

8.11 Number of Non-synonymous (SNP) or coding frameshift (InDel) Exonic Mutations

Cell line mutations	No. of Indel	No. of SNV	Total No.
Non-filtered mutations (no exclusion criteria)			
Total Number	2,741 (100%)	39,812 (100%)	42,553 (100%)
Common mutations	2,122 (77.42%)	37,044 (93.05%)	39,166 (92.04%)
MM.1S^{dim}	87 (3.17%)	348 (0.87%)	435 (1.02%)
MM.1S^{bright}	96 (3.50%)	251 (0.63%)	347 (0.82%)
MM.1R	117 (4.27%)	376 (0.94%)	493 (1.16%)
MM.1S^{dim} & MM.1R	93 (3.39%)	633 (1.59%)	726 (1.71%)
MM.1R & MM.1S^{bright}	129 (4.71%)	630 (1.58%)	759 (1.78%)
MM.1S^{dim} & MM.1S^{bright}	97 (3.54%)	530 (1.33%)	627 (1.47%)
Filtered mutations – (Inclusion criteria exonic Indel. or SNV)			
Total Number	219 (100%)	10,354 (100%)	10,573 (100%)
Common mutations	194 (88.58%)	9,856 (95.19%)	10,050 (95.05%)
MM.1S^{dim}	4 (1.83%)	88 (0.85%)	92 (0.87%)
MM.1S^{bright}	6 (2.74%)	47 (0.45%)	53 (0.50%)
MM.1R	11 (5.02%)	80 (0.77%)	91 (0.86%)
MM.1S^{dim} & MM.1R	1 (0.46%)	126 (1.22%)	127 (1.20%)
MM.1R & MM.1S^{bright}	1 (0.46%)	88 (0.85%)	89 (0.84%)
MM.1S^{dim} & MM.1S^{bright}	2 (0.91%)	69 (0.67%)	71 (0.67%)

Supplementary Table 1. Number of Non-synonymous (SNP) or coding frameshift (InDel) Exonic Mutations *in the 3 cell lines as outlined in Venn diagram, figure 5.21.*

8.12 Location of VCF files of whole exome sequence

https://www.dropbox.com/sh/kdrde9xex7zotul/AAB3umWDQOQ-m4YWXLpOTKMTa?dl=0

8.13 Comparison of WES genetic mutations

	Samples	MM.1R	MM.1S bright	MM.1S dim	Total	Com-mon
Coding	Frameshift	240	236	226	259	211
InDel	Non-frameshift insertion	111	102	106	113	96
	Non-frameshift deletion	120	109	114	130	97
	Stoploss	5	6	5	6	5
	Startloss	4	3	3	4	3
	Splicing	42	41	43	44	39
InDel	Total InDels	3,671	3,641	3,579	4,164	2,979
	% of InDels in dbSNP	86.62	87.06	87.18	84.05	90.37
	% of InDels in 1000g	72.41	72.56	73.01	68.32	78.58
	Novel	356	342	330	515	183
	Homozygous	1,576	1,558	1,523	NA	1,364
	Heterozygous	2,095	2,083	2,056	NA	1,615
	Intron	2,367	2,387	2,316	2,717	1,912
	5' UTRs	71	61	72	82	55
	3' UTRs	114	121	113	129	102
	Upstream	72	73	70	84	54
	Downstream	74	74	76	87	60
	Intergenic	180	174	167	202	142
Coding	Synonymous	11,611	11,478	11,542	11,923	10,965
SNP	Missense	10,333	10,187	10,231	10,687	9,661
	Stopgain	82	81	85	95	73
	Stoploss	34	34	33	34	33
	Startloss	21	21	21	21	20
	Splicing	64	68	65	74	58
SNP	Total SNPs	46,889	46,527	46,630	48,752	43,711
	% of SNPs in dbSNP	97.84	97.85	97.73	97.1	98.37
	% of SNPs in 1000g	94.53	94.56	94.41	93.44	95.58
	Novel	794	800	844	1176	537
	Homozygous	17,593	17,779	17,624	NA	17,099
	Heterozygous	29,296	28,748	29,006	NA	26,612

	Intron	17,897	17,844	17,849	18,663	16,692
	5' UTRs	767	743	759	825	662
	3' UTRs	907	897	905	945	844
	Upstream	676	659	662	705	609
	Downstream	532	529	530	559	495
	Intergenic	1,787	1,846	1,804	1,949	1,603
	Ti/Tv	2.58	2.58	2.58	2.54	2.62

Supplementary Table 2 Comparison of genetic mutations *through exome sequence between the cell lines, MM1.R, MM1.S^{Bright} and MM1.S^{dim}*

8.14 Comparison between my exome sequence and the COSMIC cell line database

Mutation Type	COSMIC database MM.1S	Present in all 3 cell lines	Present in at least 1 cell line	Not present in any cell line
Complex deletion In frame	1	1	-	-
Complex Frameshift	3	1	2	-
Deletion Frameshift	7	3	-	4
Deletion In frame	4	3	-	1
Insertion Frameshift	7	4	1	2
Substitution Coding silent	225	169	23	33
Substitution Missense	363	171	80	112
Substitution Nonsense	16	9	3	4
Unknown	50	16	4	30
Total	676	377	113	186

Supplementary Table 3. Comparison between my exome sequence and the COSMIC cell line database *for MM.1S mutations.*

8.15 List of exonic gene mutations detected from WES

List of exonic mutations (without dbSNP reference)
Common ABCA7, ABCC5, ADAM33, ADO, AGPHD1, ALCAM, ALDH18A1, ANKEF1, ANLN, ANXA10, APOL4, APPL2, ARHGAP18, ARHGAP32, ATRN, BC128043, BICC1, C19orf60, C19orf73, C4orf47, C6orf163, C7orf13, CACNB4, CAPN11, CCDC110, CCDC80, CCNE2, CD1D, CD34, CES4A, CHD9, CIRH1A, COL10A1, CUL1, CYB561, CYP11A1, DGCR2, DISP1, DLX3, DMP1, DNAH10, DNAH12, DNAH17, DNAH3, DNAJB12, DOCK7, DPP10, DYRK1A, EEF1D, EGFR, ELP6, ENTPD6, ESYT1, FAM46C, FARP1, FEM1A, GALNT8, GPR98, GPRIN1, GUCY1A2, HHIPL2, HRNR, IFT172, IGLL5, INPPL1, IQSEC1, ITIH1, ITPA, KANSL2, KANSL3, KCNH3, KCNJ2, KIAA1024, KIAA1109, KIAA1704, KIF26A, KIR2DS5, KIR3DS1, KRT39, KRTAP10-1, KRTAP19-6, KRTAP4-4, LAMB2, LARGE, LECT1, LMAN1L, LONRF3, LRFN3, LRRC32, LRRC37BP1, LY75, LY75-CD302, LYST, MAF, MAP1B, MCFD2, METTL8, MGA, MMP26, MRTO4, MYO10, NAIF1, NAPRT1, NBPF7, NCOR2, NFATC1, NOG, NPC1, NSUN3, NUDT11, OFCC1, OPLAH, OR2A1, OR52M1, OR5T3, OR8B4, OTUD7A, PAPPA2, PAXBP1, PBX1, PDIA6, PDPK1, PIGR, PLEC, PLLP, PLXNB2, POLR3A, POP1, PPP1R32, PPP1R35, PRICKLE3, PTCHD2, RAB11FIP1, RALGAPA2, RAP2C, RBM38, RIMS1, RMND5A, RNF180, RSBN1, SARM1, SASH1, SEMA3C, SGK2, SH3PXD2A, SLC12A2, SLC12A4, SLC16A5, SLC17A9, SLC25A19, SLC35G3, SLC9C1, SLCO3A1, SPOCD1, SREBF2, SSPO, SSU72, TAS2R5, TBC1D4, TBX18, TBXAS1, TCHH, TCRBV11S1A1T, TIMELESS, TLR6, TMC3, TMEM169, TMEM239, TMEM52B, TNKS1BP1, TOPAZ1, TRIM41, TRIP6, TTLL10, TTN, TXN, TYK2, UBR7, UBXN6, ULK2, USP31, USP48, WDR96, WHSC1, XPA, YARS2, YBX2, ZER1, ZFP28, ZKSCAN7, ZNF107, ZNF382, ZNF536, ZNF581, ZNF621, ZPBP2, ZZEF1
MM.1S^{dim} ABCC8, ADAMTS20, ARAP2, ARHGAP6, ATG9B, BSN, BTN2A3P, C1orf68, C6orf141, CASC4, CCDC27, CCDC84, DNAH14, DNMBP, FHAD1, GRID2IP, GRM5, GUCA1B, HTR3E, IRF2BP2, KXD1, LHFPL1, LRRC15, MAML3, MKI67, MYBPC1, MYH14, MYO9B, OR52R1, PEA15, POLR1E, PRDM16, PSMD14, RAI14, RSRC1, RUNX1T1, SASH1, SLC13A2, THBS3, TM4SF19, TM4SF19-TCTEX1D2, TOM1L2, USP33, VPS16, ZNF354C, ZPLD1
MM.1S^{bright} ADGB, ADRB1, ATE1, DENND4B, DENND5B, DPM1, ERN1, FCGBP, FIP1L1-PDGFRA, GANC, GCFC2, GLIS3, INSM1, ISYNA1, KANK2, KMT2E, LRRC7, MITF, OR4A5, PLCH1, SLC35D2, SLC4A9, SREBF1, TRDC, UGT1A1, USP34, VWA3B, WBP2
MM.1R ANPEP, DLG3, EGR4, ERCC6, ERN1, FAM120C, FMO1, GALNT5, GPCPD1, GPR126, GSPT2, HOXC13, KIAA0319, LAMB4, LRFN1, MCTP2, NR2F6, OR10AG1, PDCD6IP, PDIA5, PRICKLE1, PRKG1, PUS1, RFX6, RNF24, SLCO1C1, ZBTB47, ZFP112, ZNF729, ZP2
MM.1R and MM.1S^{bright} CD24, CHD1L, CIRBP-AS1, TMC3, UNC13D
MM.1S^{dim} and MM.1S^{bright} AFM, AGBL2, GTF2I, ICAM5, MYT1L, OR4S2, PRKCI, RIN2, ZNF366
MM.1R and MM.1S^{dim} UPF3

***Supplementary Table 4. List of all exonic gene mutations**, that did not have a dbSNP reference. Mutated gene list is divided into cell lines for which the mutation is present i*

8.16 Dose-effect curves and median-effect plots of individual cell lines calculated by CalcuSyn

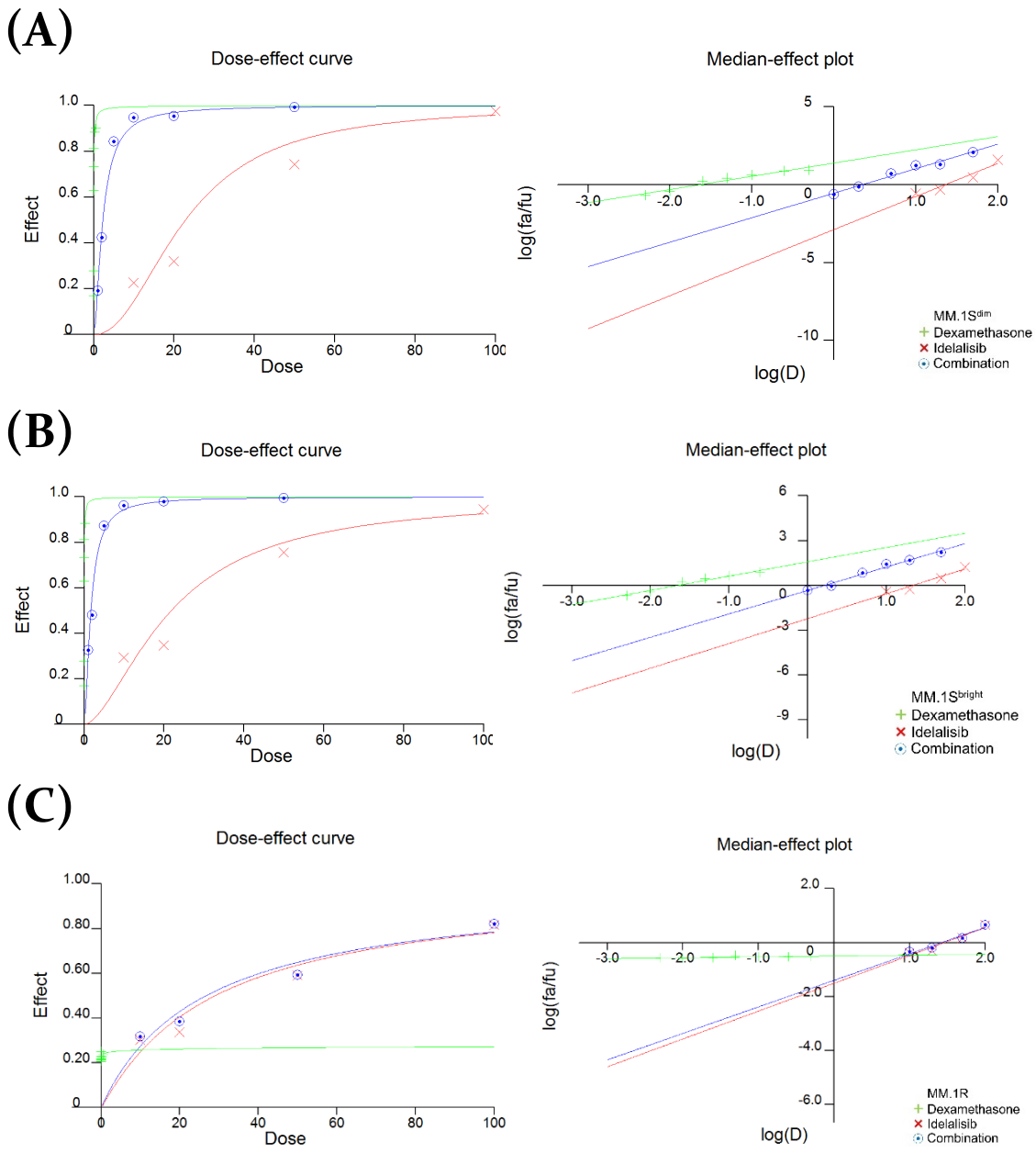

Supplementary figure 11; Dose-effect curves and median-effect plots of individual cell lines calculated by CalcuSyn*; (A) MM.1S^{dim}; (B) MM.1S^{bright}; (C) MM.1R;*

8.17 MM.1R apoptosis exposed to 100μM of Idelalisib for 48h, with varying doses of dexamethasone

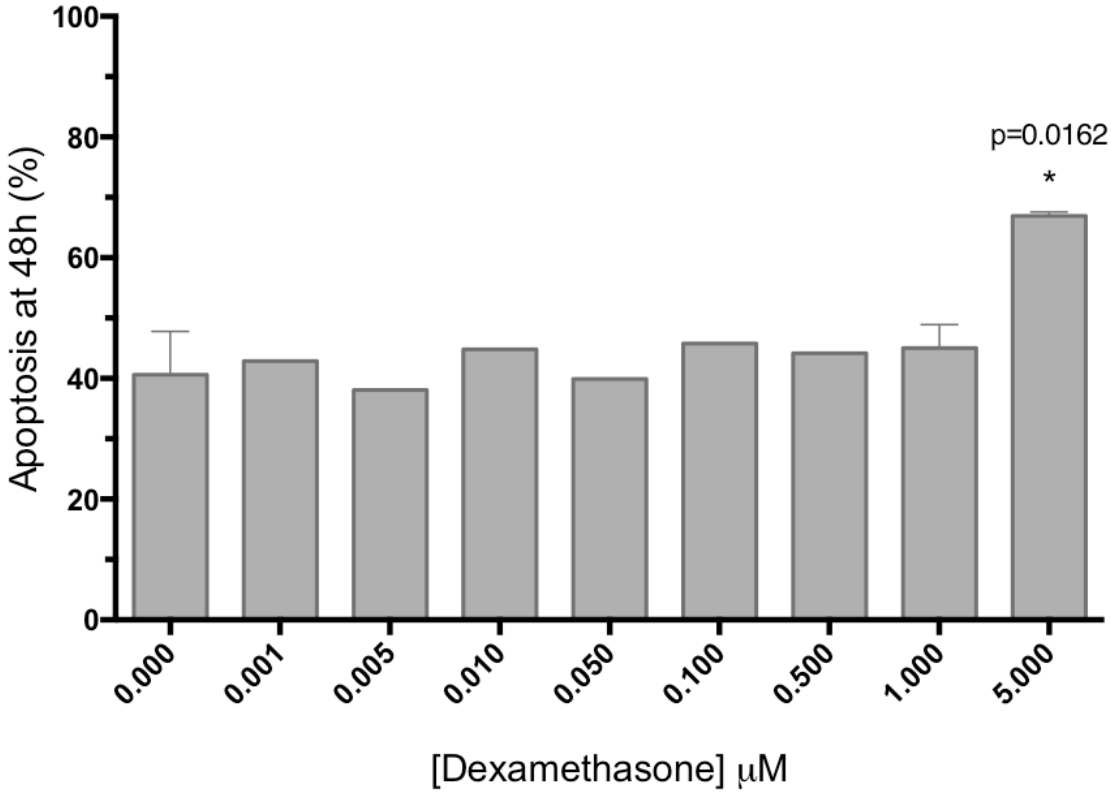

Supplementary figure 12. MM.1R cell line exposed to 100μM of Idelalisib for 48h, with varying doses of dexamethasone*. Statistical difference seen between 5μM of dexamethasone and control Idelalisib with no addition of dexamethasone (p=0.0162 n=3). Cell death was not affected by the addition of dexamethasone (between 40%-50%) up to a dose of 1μM. However, with the addition of 5μM dexamethasone (highest dose added), cell death statistically increased (p=0.0162) from the control (40.63% to 66.95%).*

8.18 Consent forms used for MM bone marrow sample collection

Developing novel targeted agents in Multiple Myeloma

Patient Information Sheet for Adults

Sponsored by Cardiff University

Chief Investigator: Professor Chris Pepper,
Principal Investigator: Professor Chris Fegan
University Hospital of Wales, Heath Park Cardiff

As you know you are undergoing a bone marrow test to ascertain if you have a condition called multiple myeloma or not. Although there are many treatments available should you have myeloma more treatments are needed and the research group at Cardiff University/Cardiff and Vale University Health Board are aiming to develop new treatments. We therefore need to be able to test our new treatments against real multiple myeloma cells from patients to see if they are able to kill the multiple myeloma cells in the laboratory before attempting to treat actual patients.

Before you decide whether to take part, it is important for you to understand why this research is being done and what it will involve. Please take time to read the following information carefully and if there is anything that is not clear or if you would like more information please feel free to ask us. Take as much time as you need to decide whether you wish to take part.

Why have I been chosen?
You are being invited to take part in the study simply because the doctors looking after you feel that you may have a condition called multiple myeloma based on blood, urine and possibly x rays which you have already had performed. You require a bone marrow test to see if this is the case or not.

What is Multiple Myeloma and why are more treatments needed?
Multiple Myeloma is a form of cancer of the bone marrow. There are many treatments available for multiple myeloma but more are needed. At present treatment is aimed at controlling the disease as no present treatment is curative. From our laboratory tests we now know a lot about what keeps multiple myeloma cells alive and have developed several treatments aimed at stopping the cells from living.

Developing novel targeted agents in Multiple Myeloma

CONSENT FORM

Name of Researchers: **Professor Chris Pepper and Professor Chris Fegan**

Please initial boxes

1. I confirm that I have read and understand the information sheet dated (Version 2, Date 30th December 2013) for the above study and have had the opportunity to ask questions. ☐
2. I understand that my participation is voluntary and that I am free to withdraw at any time, without giving any reason, without my medical care or legal rights being affected. ☐
3. I consent to the collection of an extra 1ml (1/5 of a tea spoon) of my bone marrow as part of the diagnostic bone marrow to determine if I have multiple myeloma. This extra sample will be taken to the Research Laboratory and anonymised for potential use in various laboratory tests to assess new treatments for multiple myeloma. ☐
4. I understand that should my bone marrow test show that I do not have multiple myeloma that the extra sample of bone marrow I have donated will be removed from the Research Laboratory before any tests have taken place on it and destroyed. ☐

Name of person taking consent	Date	Signature
_____	_____	_____

Name of Patient	Date	Signature
_____	_____	_____

5. I consent that the extra bone marrow sample that has been stored in the Research Laboratory and anonymised will now be used for use in various laboratory tests with the aim of using whole multiple myeloma cells to see if new treatments under development in Cardiff can kill the myeloma cells or not. ☐

REFERENCES:

Abraham, M. et al. 2017. The CXCR4 inhibitor BL-8040 induces the apoptosis of AML blasts by downregulating ERK, BCL-2, MCL-1 and cyclin-D1 via altered miR-15a/16-1 expression. *Leukemia*, doi: 10.1038/leu.2017.82

Adams, J. 2003. The proteasome: structure, function, and role in the cell. *Cancer Treat Rev* 29 Suppl 1, pp. 3-9.

Alexandrakis, M. G. et al. 2004a. The relation between bone marrow angiogenesis and the proliferation index Ki-67 in multiple myeloma.*J Clin Pathol*. Vol. 57. pp. 856-860.

Alexandrakis, M. G. et al. 2004b. Ki-67 proliferation index: correlation with prognostic parameters and outcome in multiple myeloma. *Am J Clin Oncol* 27(1), pp. 8-13.

Alexanian, R. et al. 1992. Primary dexamethasone treatment of multiple myeloma. *Blood* 80(4), pp. 887-890.

Allegra, A. et al. 2014. New orally active proteasome inhibitors in multiple myeloma. *Leukemia research* 38(1), pp. 1-9.

Allen, C. D. et al. 2007. Germinal-center organization and cellular dynamics. *Immunity* 27(2), pp. 190-202. doi: 10.1016/j.immuni.2007.07.009

Alsayed, Y. et al. 2007. Mechanisms of regulation of CXCR4/SDF-1 (CXCL12)–dependent migration and homing in multiple myeloma. *Blood* 109(7), pp. 2708-2717.

Altekruse, S. et al. 2010. *SEER Cancer Statistics Review, 1975-2007, National Cancer Institute. Bethesda, MD, http://seer.cancer.gov/csr/1975_2007/, based on November 2009 SEER data submission, posted to the SEER web site, 2010*. Available at: [Accessed.

Altieri, A. et al. 2006. Familial risks and temporal incidence trends of multiple myeloma. *Eur J Cancer* 42(11), pp. 1661-1670. doi: 10.1016/j.ejca.2005.11.033

Aparicio, A. et al. 1998. In vitro cytoreductive effects on multiple myeloma cells induced by bisphosphonates. *Leukemia* 12(2), pp. 220-229.

Aplin, A. E. et al. 1999. Cell adhesion molecules, signal transduction and cell growth. *Curr Opin Cell Biol* 11(6), pp. 737-744. doi: 10.1016/s0955-0674(99)00045-9

Argyriou, A. A. et al. 2008. Bortezomib-induced peripheral neuropathy in multiple myeloma: a comprehensive review of the literature. *Blood* 112(5), pp. 1593-1599. doi: 10.1182/blood-2008-04-149385

Artandi, S. E. et al. 2000. Telomere dysfunction promotes non-reciprocal translocations and epithelial cancers in mice. *Nature* 406(6796), pp. 641-645. doi: 10.1038/35020592

Attal, M. et al. 2017. Lenalidomide, Bortezomib, and Dexamethasone with Transplantation for Myeloma. *N Engl J Med* 376(14), pp. 1311-1320. doi: 10.1056/NEJMoa1611750

Attal, M. et al. 2012. Lenalidomide maintenance after stem-cell transplantation for multiple myeloma. *N Engl J Med* 366(19), pp. 1782-1791. doi: 10.1056/NEJMoa1114138

Avet-Loiseau, H. et al. 2007. Genetic abnormalities and survival in multiple myeloma: the experience of the Intergroupe Francophone du Myelome. *Blood* 109(8), pp. 3489-3495. doi: 10.1182/blood-2006-08-040410

Avet-Loiseau, H. et al. 2001. Rearrangements of the c-myc oncogene are present in 15% of primary human multiple myeloma tumors. *Blood* 98(10), pp. 3082-3086.

Azab, A. K. et al. 2009a. RhoA and Rac1 GTPases play major and differential roles in stromal cell-derived factor-1-induced cell adhesion and chemotaxis in multiple myeloma. *Blood* 114(3), pp. 619-629. doi: 10.1182/blood-2009-01-199281

Azab, A. K. et al. 2012. P-selectin glycoprotein ligand regulates the interaction of multiple myeloma cells with the bone marrow microenvironment. *Blood* 119(6), pp. 1468-1478. doi: 10.1182/blood-2011-07-368050

Azab, A. K. et al. 2009b. CXCR4 inhibitor AMD3100 disrupts the interaction of multiple myeloma cells with the bone marrow microenvironment and enhances their sensitivity to therapy. *Blood* 113(18), pp. 4341-4351. doi: 10.1182/blood-2008-10-186668

Azab, A. K. et al. 2014. CXCR7-dependent angiogenic mononuclear cell trafficking regulates tumor progression in multiple myeloma. *Blood* 124(12), pp. 1905-1914. doi: 10.1182/blood-2014-02-558742

Bailey, S. et al. 2001. The role of AP-1 in glucocorticoid resistance in leukaemia. *Leukemia* 15(3), pp. 391-397.

Baird, D. M. et al. 2003. Extensive allelic variation and ultrashort telomeres in senescent human cells. *Nat Genet* 33(2), pp. 203-207. doi: 10.1038/ng1084

Bam, R. et al. 2015. Primary myeloma interaction and growth in coculture with healthy donor hematopoietic bone marrow.*BMC Cancer*. Vol. 15.

Bang, M. L. et al. 2001. The complete gene sequence of titin, expression of an unusual approximately 700-kDa titin isoform, and its interaction with obscurin identify a novel Z-line to I-band linking system. *Circ Res* 89(11), pp. 1065-1072.

Bao, L. et al. 2013. CXCR4 is a good survival prognostic indicator in multiple myeloma patients. *Leuk Res* 37(9), pp. 1083-1088. doi: 10.1016/j.leukres.2013.06.002

Barillé, S. et al. 1997. Metalloproteinases in multiple myeloma: production of matrix metalloproteinase-9 (MMP-9), activation of proMMP-2, and induction of MMP-1 by myeloma cells. *Blood* 90(4), pp. 1649-1655.

Barlogie, B. et al. 2006. Thalidomide and hematopoietic-cell transplantation for multiple myeloma. *N Engl J Med* 354(10), pp. 1021-1030. doi: 10.1056/NEJMoa053583

Barlogie, B. et al. 2008. Seven-year median time to progression with thalidomide for smoldering myeloma: partial response identifies subset requiring earlier salvage therapy for symptomatic disease. *Blood* 112(8), pp. 3122-3125. doi: 10.1182/blood-2008-06-164228

Bataille, R. et al. 2006. The phenotype of normal, reactive and malignant plasma cells. Identification of "many and multiple myelomas" and of new targets for myeloma therapy. *Haematologica* 91(9), pp. 1234-1240.

Bataille, R. et al. 1989. Serum levels of interleukin 6, a potent myeloma cell growth factor, as a reflect of disease severity in plasma cell dyscrasias. *J Clin Invest* 84(6), pp. 2008-2011. doi: 10.1172/jci114392

Bataille, R. et al. 2005. CD221 (IGF-1R) is aberrantly expressed in multiple myeloma, in relation to disease severity. *Haematologica* 90(5), pp. 706-707.

Bayer-Garner, I. B. et al. 2001. Syndecan-1 (CD138) immunoreactivity in bone marrow biopsies of multiple myeloma: shed syndecan-1 accumulates in fibrotic regions. *Modern Pathology* 14(10), pp. 1052-1058.

Beider, K. et al. 2011. CXCR4 antagonist 4F-benzoyl-TN14003 inhibits leukemia and multiple myeloma tumor growth. *Exp Hematol* 39(3), pp. 282-292. doi: 10.1016/j.exphem.2010.11.010

Belinky, F. et al. 2015. PathCards: multi-source consolidation of human biological pathways. *Database (Oxford)* 2015, doi: 10.1093/database/bav006

Bellamy, W. T. 1996. P-glycoproteins and multidrug resistance. *Annu Rev Pharmacol Toxicol* 36, pp. 161-183. doi: 10.1146/annurev.pa.36.040196.001113

Berdeja, J. et al. 2017. Durable Clinical Responses in Heavily Pretreated Patients with Relapsed/Refractory Multiple Myeloma: Updated Results from a Multicenter Study of bb2121 Anti-Bcma CAR T Cell Therapy.

Bergsagel, P. L. and Kuehl, W. M. 2001. Chromosome translocations in multiple myeloma. *Oncogene* 20(40), pp. 5611-5622. doi: 10.1038/sj.onc.1204641

Bhatnagar, V. et al. 2017. FDA Approval Summary: Daratumumab for Treatment of Multiple Myeloma After One Prior Therapy. *Oncologist* 22(11), pp. 1347-1353. doi: 10.1634/theoncologist.2017-0229

Bieghs, L. et al. 2016. Abnormal IGF-Binding Protein Profile in the Bone Marrow of Multiple Myeloma Patients. *PLoS One* 11(4), p. e0154256. doi: 10.1371/journal.pone.0154256

Billadeau, D. et al. 1996. Clonal circulating cells are common in plasma cell proliferative disorders: a comparison of monoclonal gammopathy of undetermined significance, smoldering multiple myeloma, and active myeloma. *Blood* 88(1), pp. 289-296.

Bird, J. M. et al. 2011. Guidelines for the diagnosis and management of multiple myeloma 2011. *Br J Haematol* 154(1), pp. 32-75. doi: 10.1111/j.1365-2141.2011.08573.x

Birney, E. and Soranzo, N. 2015. Human genomics: The end of the start for population sequencing. *Nature* 526(7571), pp. 52-53. doi: 10.1038/526052a

Bjorklund, C. C. et al. 2013. Evidence of a role for CD44 and cell adhesion in mediating resistance to lenalidomide in multiple myeloma: therapeutic implications. *Leukemia*, doi: 10.1038/leu.2013.174

Bjorklund, C. C. et al. 2011. Evidence of a role for activation of Wnt/beta-catenin signaling in the resistance of plasma cells to lenalidomide. *J Biol Chem* 286(13), pp. 11009-11020. doi: 10.1074/jbc.M110.180208

Bloch, D. B. et al. 2000. Sp110 localizes to the PML-Sp100 nuclear body and may function as a nuclear hormone receptor transcriptional coactivator. *Mol Cell Biol* 20(16), pp. 6138-6146.

Boise, L. H. et al. 1993. bcl-x, a bcl-2-related gene that functions as a dominant regulator of apoptotic cell death. *Cell* 74(4), pp. 597-608.

Bolli, N. et al. 2014. Heterogeneity of genomic evolution and mutational profiles in multiple myeloma. *Nat Commun* 5, p. 2997. doi: 10.1038/ncomms3997

Breier, A. et al. 2013. New insight into p-glycoprotein as a drug target. *Anti-Cancer Agents in Medicinal Chemistry (Formerly Current Medicinal Chemistry-Anti-Cancer Agents)* 13(1), pp. 159-170.

Brenner, H. et al. 2008. Recent major improvement in long-term survival of younger patients with multiple myeloma. *Blood* 111(5), pp. 2521-2526. doi: 10.1182/blood-2007-08-104984

Britton, M. et al. 2009. Selective inhibitor of proteasome's caspase-like sites sensitizes cells to specific inhibition of chymotrypsin-like sites. *Chemistry & biology* 16(12), pp. 1278-1289.

Broyl, A. et al. 2010. Mechanisms of peripheral neuropathy associated with bortezomib and vincristine in patients with newly diagnosed multiple myeloma: a prospective analysis of data from the HOVON-65/GMMG-HD4 trial. *Lancet Oncol* 11(11), pp. 1057-1065. doi: 10.1016/s1470-2045(10)70206-0

Bulian, P. et al. 2014. CD49d is the strongest flow cytometry-based predictor of overall survival in chronic lymphocytic leukemia. *J Clin Oncol* 32(9), pp. 897-904. doi: 10.1200/jco.2013.50.8515

Cancer Research UK. 2014. *Cancer survival for common cancers*. Cancer Research UK. Available at: http://www.cancerresearchuk.org/cancer-info/cancerstats/survival/common-cancers/#One- [Accessed.

Cancer Research UK. 2015. *Myeloma incidence statistics*. Available at: http://www.cancerresearchuk.org/health-professional/cancer-statistics/statistics-by-cancer-type/myeloma/incidence [Accessed.

Cantley, L. C. 2002. The phosphoinositide 3-kinase pathway. *Science* 296(5573), pp. 1655-1657. doi: 10.1126/science.296.5573.1655

Cesano, A. et al. 1998. Role of CD38 and its ligand in the regulation of MHC-nonrestricted cytotoxic T cells. *J Immunol* 160(3), pp. 1106-1115.

Chang, P. H. et al. 2012. Activation of Robo1 signaling of breast cancer cells by Slit2 from stromal fibroblast restrains tumorigenesis via blocking PI3K/Akt/beta-catenin pathway. *Cancer Res* 72(18), pp. 4652-4661. doi: 10.1158/0008-5472.can-12-0877

Chantry, D. et al. 1997. p110delta, a novel phosphatidylinositol 3-kinase catalytic subunit that associates with p85 and is expressed predominantly in leukocytes. *J Biol Chem* 272(31), pp. 19236-19241.

Chapman, M. A. et al. 2011. Initial genome sequencing and analysis of multiple myeloma. *Nature* 471(7339), pp. 467-472. doi: 10.1038/nature09837

Chatterjee, M. et al. 2013. The PI3K/Akt signaling pathway regulates the expression of Hsp70, which critically contributes to Hsp90-chaperone function and tumor cell survival in multiple myeloma. *Haematologica* 98(7), pp. 1132-1141. doi: 10.3324/haematol.2012.066175

Chauhan, D. et al. 2002. Identification of genes regulated by dexamethasone in multiple myeloma cells using oligonucleotide arrays. *Oncogene* 21(9), pp. 1346-1358.

Chauhan, D. et al. 1996. Multiple myeloma cell adhesion-induced interleukin-6 expression in bone marrow stromal cells involves activation of NF-kappa B. *Blood* 87(3), pp. 1104-1112.

Cheah, C. Y. and Fowler, N. H. 2016. Idelalisib in the management of lymphoma.*Blood*. Vol. 128. pp. 331-336.

Chen, D. et al. 2011. Bortezomib as the First Proteasome Inhibitor Anticancer Drug: Current Status and Future Perspectives. *Curr Cancer Drug Targets* 11(3), pp. 239-253.

Chen, E. Y. et al. 2013. Enrichr: interactive and collaborative HTML5 gene list enrichment analysis tool. *BMC Bioinformatics* 14, p. 128. doi: 10.1186/1471-2105-14-128

Chen, P. and Hochstrasser, M. 1996. Autocatalytic subunit processing couples active site formation in the 20S proteasome to completion of assembly. *Cell* 86(6), pp. 961-972.

Chen, R. et al. 2016. The role of SH3GL3 in myeloma cell migration/invasion, stemness and chemo-resistance.*Oncotarget*. Vol. 7. pp. 73101-73113.

Cherry, B. M. et al. 2013. Modeling progression risk for smoldering multiple myeloma: results from a prospective clinical study. *Leuk Lymphoma* 54(10), pp. 2215-2218. doi: 10.3109/10428194.2013.764419

Chiecchio, L. et al. 2006. Deletion of chromosome 13 detected by conventional cytogenetics is a critical prognostic factor in myeloma. *Leukemia* 20(9), pp. 1610-1617. doi: 10.1038/sj.leu.2404304

Chng, W. J. et al. 2008. Clinical and biological significance of RAS mutations in multiple myeloma.*Leukemia*. Vol. 22. England, pp. 2280-2284.

Chretien, M. L. et al. 2015. Understanding the role of hyperdiploidy in myeloma prognosis: which trisomies really matter? *Blood* 126(25), pp. 2713-2719. doi: 10.1182/blood-2015-06-650242

Clevers, H. and Nusse, R. 2012. Wnt/beta-catenin signaling and disease. *Cell* 149(6), pp. 1192-1205. doi: 10.1016/j.cell.2012.05.012

Corral, L. G. et al. 1999. Differential cytokine modulation and T cell activation by two distinct classes of thalidomide analogues that are potent inhibitors of TNF-alpha. *J Immunol* 163(1), pp. 380-386.

Corre, J. et al. 2015. Genetics of multiple myeloma: another heterogeneity level?*Blood*. Vol. 125. pp. 1870-1876.

Dahl, I. M. et al. 2002. Differential expression of CD56 and CD44 in the evolution of extramedullary myeloma. *Br J Haematol* 116(2), pp. 273-277.

Damiano, J. S. et al. 1999. Cell adhesion mediated drug resistance (CAM-DR): role of integrins and resistance to apoptosis in human myeloma cell lines. *Blood* 93(5), pp. 1658-1667.

Danel-Moore, L. et al. 1992. Dexamethasone reverses glucocorticoid receptor RNA depression in multi-drug resistant (MDR) myeloma cell lines. *Med Oncol Tumor Pharmacother* 9(4), pp. 199-204.

de Beco, S. et al. 2012. New insights into the regulation of E-cadherin distribution by endocytosis. *Int Rev Cell Mol Biol* 295, pp. 63-108. doi: 10.1016/b978-0-12-394306-4.00008-3

de Weers, M. et al. 2011. Daratumumab, a novel therapeutic human CD38 monoclonal antibody, induces killing of multiple myeloma and other hematological tumors. *The Journal of Immunology* 186(3), pp. 1840-1848.

Deaglio, S. et al. 2010. CD38/CD31 interactions activate genetic pathways leading to proliferation and migration in chronic lymphocytic leukemia cells. *Mol Med* 16(3-4), pp. 87-91. doi: 10.2119/molmed.2009.00146

Defer, G. et al. 2012. CD49d expression as a promising biomarker to monitor natalizumab efficacy. *J Neurol Sci* 314(1-2), pp. 138-142. doi: 10.1016/j.jns.2011.10.005

Dianzani, U. et al. 1994. Interaction between endothelium and CD4+CD45RA+ lymphocytes. Role of the human CD38 molecule. *J Immunol* 153(3), pp. 952-959.

Dimopoulos, M. et al. 2013. Vorinostat or placebo in combination with bortezomib in patients with multiple myeloma (VANTAGE 088): a multicentre, randomised, double-blind study. *Lancet Oncol* 14(11), pp. 1129-1140. doi: 10.1016/s1470-2045(13)70398-x

Dimopoulos, M. A. et al. 2016. Daratumumab, Lenalidomide, and Dexamethasone for Multiple Myeloma. *N Engl J Med* 375(14), pp. 1319-1331. doi: 10.1056/NEJMoa1607751

Dispenzieri, A. et al. 2008. Immunoglobulin free light chain ratio is an independent risk factor for progression of smoldering (asymptomatic) multiple myeloma. *ASH Annual Meeting Abstracts* 111(2), pp. 785-789. doi: 10.1182/blood-2007-08-108357

Drach, J. et al. 1992. The biological and clinical significance of the KI-67 growth fraction in multiple myeloma. *Hematol Oncol* 10(2), pp. 125-134.

Drayson, M. T. et al. 2019. Levofloxacin prophylaxis in patients with newly diagnosed myeloma (TEAMM): a multicentre, double-blind, placebo-controlled, randomised, phase 3 trial. *Lancet Oncol* 20(12), pp. 1760-1772. doi: 10.1016/s1470-2045(19)30506-6

Drent, E. et al. 2016. Pre-clinical evaluation of CD38 chimeric antigen receptor engineered T cells for the treatment of multiple myeloma.*Haematologica*. Vol. 101. pp. 616-625.

Dunleavy, E. M. et al. 2009. HJURP is a cell-cycle-dependent maintenance and deposition factor of CENP-A at centromeres. *Cell* 137(3), pp. 485-497. doi: 10.1016/j.cell.2009.02.040

Durie, B. G. and Salmon, S. E. 1975. A clinical staging system for multiple myeloma. Correlation of measured myeloma cell mass with presenting clinical features, response to treatment, and survival. *Cancer* 36(3), pp. 842-854.

Dutta, A. K. et al. 2017. Cutting edge genomics reveal new insights into tumour development, disease progression and therapeutic impacts in multiple myeloma. *Br J Haematol* 178(2), pp. 196-208. doi: 10.1111/bjh.14649

Edwards V, D. et al. 2012. Extensive Genetic Characterization of MM.1R and MM.1S Identifies Several Events Contributing to Dexamethasone Resistance. *ASH Annual Meeting*.

Egan, J. B. et al. 2012. Whole-genome sequencing of multiple myeloma from diagnosis to plasma cell leukemia reveals genomic initiating events, evolution, and clonal tides. *Blood* 120(5), pp. 1060-1066.

Ehrlich, M. 2009. DNA hypomethylation in cancer cells. *Epigenomics* 1(2), pp. 239-259. doi: 10.2217/epi.09.33

El-Amm, J. and Tabbara, I. A. 2013. Emerging Therapies in Multiple Myeloma. *Am J Clin Oncol*, doi: 10.1097/COC.0b013e3182a4676b

Elstak, E. D. et al. 2012. A novel Dutch mutation in UNC13D reveals an essential role of the C2B domain in munc13-4 function. *Pediatr Blood Cancer* 58(4), pp. 598-605. doi: 10.1002/pbc.23253

Engvall, E. et al. 1986. Molecular assembly, secretion, and matrix deposition of type VI collagen. *J Cell Biol* 102(3), pp. 703-710.

Etienne-Manneville, S. and Hall, A. 2002. Rho GTPases in cell biology. *Nature* 420(6916), pp. 629-635. doi: 10.1038/nature01148

European Medicines Agency, E. 2007. *Tysabri: EPAR - Scientific Discussion*. Available at: http://www.ema.europa.eu/docs/en_GB/document_library/EPAR_-_Scientific_Discussion/human/000603/WC500044690.pdf

Facon, T. et al. 2019. Daratumumab plus Lenalidomide and Dexamethasone for Untreated Myeloma. *N Engl J Med* 380(22), pp. 2104-2115. doi: 10.1056/NEJMoa1817249

Fang, X. et al. 2010. CD24: from A to Z. *Cell Mol Immunol* 7(2), pp. 100-103. doi: 10.1038/cmi.2009.119

FDA. 2019. *FDA Warns about the risks associated with the investigational use of Venclexta in Multiple Myeloma*. Available at: https://www.fda.gov/Drugs/DrugSafety/ucm634120.htm [Accessed.

Fedyk, E. R. et al. 1999. Maturation decreases responsiveness of human bone marrow B lineage cells to stromal-derived factor 1 (SDF-1). *J Leukoc Biol* 66(4), pp. 667-673.

Feng, Y. et al. 2010. Bone marrow stromal cells from myeloma patients support the growth of myeloma stem cells. *Stem Cells Dev* 19(9), pp. 1289-1296. doi: 10.1089/scd.2010.0010

Fernandez, A. et al. 1995. Oxygen radical production and thiol depletion are required for Ca(2+)-mediated endogenous endonuclease activation in apoptotic thymocytes. *J Immunol* 155(11), pp. 5133-5139.

Flores-Montero, J. et al. 2016. Immunophenotype of normal vs. myeloma plasma cells: Toward antibody panel specifications for MRD detection in multiple myeloma. *Cytometry B Clin Cytom* 90(1), pp. 61-72. doi: 10.1002/cyto.b.21265

Forbes, S. A. et al. 2017. COSMIC: somatic cancer genetics at high-resolution. *Nucleic Acids Res* 45(D1), pp. D777-d783. doi: 10.1093/nar/gkw1121

French, J. D. et al. 2002. Analysis of IL-6-mediated growth control of myeloma cells using a gp130 chimeric receptor approach. *Leukemia* 16(6), pp. 1189-1196. doi: 10.1038/sj.leu.2402516

Ganju, R. K. et al. 1998. The alpha-chemokine, stromal cell-derived factor-1alpha, binds to the transmembrane G-protein-coupled CXCR-4 receptor and activates multiple signal transduction pathways. *J Biol Chem* 273(36), pp. 23169-23175.

Garcia, P. D. et al. 2014. Pan-PIM kinase inhibition provides a novel therapy for treating hematologic cancers. *Clin Cancer Res* 20(7), pp. 1834-1845. doi: 10.1158/1078-0432.ccr-13-2062

Gazdar, A. et al. 1986. Establishment and characterization of a human plasma cell myeloma. *Blood* 67(6), pp. 1542-1549.

gene, E. 2018. *COL6A3 collagen type VI alpha 3 chain [Homo sapiens (human)] - Gene - NCBI*. Pubs. Available at: https://www.ncbi.nlm.nih.gov/pubmed/ [Accessed.

Gentile, A. et al. 2008. The Met tyrosine kinase receptor in development and cancer. *Cancer Metastasis Rev* 27(1), pp. 85-94. doi: 10.1007/s10555-007-9107-6

Ghobrial, I. et al. 2014. Phase I/II Trial of Plerixafor and Bortezomib As a Chemosensitization Strategy in Relapsed or Relapsed/Refractory Multiple Myeloma. *ASH 2014*. 2014-12-06. American Society of Hematology.

Glauer, J. et al. 2013. A novel selective small-molecule PI3K inhibitor is effective against human multiple myeloma in vitro and in vivo. *Blood Cancer J* 3, p. e141. doi: 10.1038/bcj.2013.37

Godder, K. et al. 1991. Heparanase activity in cultured endothelial cells. *J Cell Physiol* 148(2), pp. 274-280. doi: 10.1002/jcp.1041480213

Goldman-Leikin, R. E. et al. 1989. Characterization of a novel myeloma cell line, MM. 1. *J Lab Clin Med* 113(3), pp. 335-345.

Gomez-Angelats, M. et al. 2000. Cell volume regulation in immune cell apoptosis. *Cell Tissue Res* 301(1), pp. 33-42.

Gonzalez, D. et al. 2007. Immunoglobulin gene rearrangements and the pathogenesis of multiple myeloma. *Blood* 110(9), pp. 3112-3121. doi: 10.1182/blood-2007-02-069625

Gotlib, J. and Cools, J. 2008. Five years since the discovery of FIP1L1-PDGFRA: what we have learned about the fusion and other molecularly defined eosinophilias. *Leukemia* 22(11), pp. 1999-2010. doi: 10.1038/leu.2008.287

Goya, L. et al. 1993. Glucocorticoids induce a G1/G0 cell cycle arrest of Con8 rat mammary tumor cells that is synchronously reversed by steroid withdrawal or addition of transforming growth factor-alpha. *Mol Endocrinol* 7(9), pp. 1121-1132. doi: 10.1210/mend.7.9.8247014

Greenstein, S. et al. 2003. Characterization of the MM. 1 human multiple myeloma (MM) cell lines: a model system to elucidate the characteristics, behavior, and signaling of steroid-sensitive and-resistant MM cells. *Experimental hematology* 31(4), pp. 271-282.

Greipp, P. R. et al. 2005. International staging system for multiple myeloma. *J Clin Oncol* 23(15), pp. 3412-3420. doi: 10.1200/jco.2005.04.242

Grogan, T. M. et al. 1993. P-glycoprotein expression in human plasma cell myeloma: correlation with prior chemotherapy. *Blood* 81(2), pp. 490-495.

Gruol, D. J. and Bourgeois, S. 1997. Chemosensitizing steroids: glucocorticoid receptor agonists capable of inhibiting P-glycoprotein function. *Cancer Res* 57(4), pp. 720-727.

Guglielmelli, T. et al. 2015. mTOR pathway activation in multiple myeloma cell lines and primary tumour cells: pomalidomide enhances cytoplasmic-nuclear shuttling of mTOR protein. *Oncoscience* 2(4), pp. 382-394.

Guse, A. H. et al. 1999. Regulation of calcium signalling in T lymphocytes by the second messenger cyclic ADP-ribose. *Nature* 398(6722), pp. 70-73. doi: 10.1038/18024

Halverson, R. et al. 2004. Receptor editing is the main mechanism of B cell tolerance toward membrane antigens. *Nat Immunol* 5(6), pp. 645-650. doi: 10.1038/ni1076

Hamblin, T. J. et al. 2002. CD38 expression and immunoglobulin variable region mutations are independent prognostic variables in chronic lymphocytic leukemia, but CD38 expression may vary during the course of the disease. *Blood* 99(3), pp. 1023-1029.

Hamidi, H. and Ivaska, J. 2018. Every step of the way: integrins in cancer progression and metastasis. *Nat Rev Cancer* 18(9), pp. 533-548. doi: 10.1038/s41568-018-0038-z

Harada, H. et al. 1993. Phenotypic difference of normal plasma cells from mature myeloma cells. *Blood* 81(10), pp. 2658-2663.

Harley, C. B. et al. 1990. Telomeres shorten during ageing of human fibroblasts. *Nature* 345(6274), pp. 458-460. doi: 10.1038/345458a0

Hartman, W. R. et al. 2010. CD38 expression, function, and gene resequencing in a human lymphoblastoid cell line-based model system. *Leuk Lymphoma* 51(7), pp. 1315-1325. doi: 10.3109/10428194.2010.483299

Hazlehurst, L. A. et al. 2001. Reduction in drug-induced DNA double-strand breaks associated with beta1 integrin-mediated adhesion correlates with drug resistance in U937 cells. *Blood* 98(6), pp. 1897-1903.

Heinemeyer, W. et al. 1997. The active sites of the eukaryotic 20 S proteasome and their involvement in subunit precursor processing. *J Biol Chem* 272(40), pp. 25200-25209.

Herman, S. E. et al. 2010. Phosphatidylinositol 3-kinase-delta inhibitor CAL-101 shows promising preclinical activity in chronic lymphocytic leukemia by antagonizing intrinsic and extrinsic cellular survival signals. *Blood* 116(12), pp. 2078-2088. doi: 10.1182/blood-2010-02-271171

Hicks, L. K. et al. 2008. A meta-analysis and systematic review of thalidomide for patients with previously untreated multiple myeloma. *Cancer Treat Rev* 34(5), pp. 442-452. doi: 10.1016/j.ctrv.2008.02.003

Hideshima, T. et al. 2007a. Inhibition of Akt induces significant downregulation of survivin and cytotoxicity in human multiple myeloma cells. *Br J Haematol* 138(6), pp. 783-791. doi: 10.1111/j.1365-2141.2007.06714.x

Hideshima, T. et al. 2002a. The biological sequelae of stromal cell-derived factor-1alpha in multiple myeloma. *Mol Cancer Ther* 1(7), pp. 539-544.

Hideshima, T. et al. 2002b. NF-kappa B as a therapeutic target in multiple myeloma. *The Journal of biological chemistry* 277(19), pp. 16639-16647. doi: 10.1074/jbc.M200360200

Hideshima, T. et al. 2007b. Understanding multiple myeloma pathogenesis in the bone marrow to identify new therapeutic targets. *Nat Rev Cancer* 7(8), pp. 585-598. doi: 10.1038/nrc2189

Hideshima, T. et al. 2001. Biologic sequelae of interleukin-6 induced PI3-K/Akt signaling in multiple myeloma. *Oncogene* 20(42), pp. 5991-6000.

Hideshima, T. et al. 2011. Mechanism of action of proteasome inhibitors and deacetylase inhibitors and the biological basis of synergy in multiple myeloma. *Molecular cancer therapeutics* 10(11), pp. 2034-2042.

Hillengass, J. et al. 2019. International myeloma working group consensus recommendations on imaging in monoclonal plasma cell disorders. *Lancet Oncol* 20(6), pp. e302-e312. doi: 10.1016/s1470-2045(19)30309-2

Himani, B. et al. 2016. Ki-67 Immunostaining and its Correlation with Microvessel Density in Patients with Mutiple Myeloma. *Asian Pac J Cancer Prev* 17(5), pp. 2559-2564.

Hofmeister, C. et al. 2017. Daratumumab Monotherapy for Patients with Intermediate or High-Risk Smoldering Multiple Myeloma (SMM): Centaurus, a Randomized, Open-Label, Multicenter Phase 2 Study. 2017-12-07. American Society of Hematology.

Holohan, C. et al. 2013. Cancer drug resistance: an evolving paradigm. *Nat Rev Cancer* 13(10), pp. 714-726. doi: 10.1038/nrc3599

Huang da, W. et al. 2009. Bioinformatics enrichment tools: paths toward the comprehensive functional analysis of large gene lists. *Nucleic Acids Res* 37(1), pp. 1-13. doi: 10.1093/nar/gkn923

Hyatt, S. et al. 2017. Telomere length is a critical determinant for survival in multiple myeloma. *Br J Haematol* 178(1), pp. 94-98. doi: 10.1111/bjh.14643

Hynes, R. O. 2002. Integrins: bidirectional, allosteric signaling machines. *Cell* 110(6), pp. 673-687.

Ikeda, H. et al. 2010. PI3K/p110{delta} is a novel therapeutic target in multiple myeloma. *Blood* 116(9), pp. 1460-1468. doi: 10.1182/blood-2009-06-222943

Ikeda, H. et al. 2015. Molecular diagnostics of a single drug-resistant multiple myeloma case using targeted next-generation sequencing.*Onco Targets Ther*. Vol. 8. pp. 2805-2815.

Imai, Y. et al. 2016. Histone deacetylase inhibitor panobinostat induces calcineurin degradation in multiple myeloma. *JCI Insight* 1(5), p. e85061. doi: 10.1172/jci.insight.85061

Ito, T. et al. 2010. Identification of a primary target of thalidomide teratogenicity. *Science* 327(5971), pp. 1345-1350. doi: 10.1126/science.1177319

Jabbour, E. et al. 2014. Targeting the phosphoinositide 3-kinase pathway in hematologic malignancies. *Haematologica* 99(1), pp. 7-18. doi: 10.3324/haematol.2013.087171

Jackson, G. H. et al. 2017. Lenalidomide induction and maintenance therapy for transplant eligible myeloma patients: Results of the Myeloma XI study. *Journal of Clinical Oncology* 35(15_suppl), pp. 8009-8009. doi: 10.1200/JCO.2017.35.15_suppl.8009

Jackson, N. et al. 1989. Two new IgA1-kappa plasma cell leukaemia cell lines (JJN-1 & JJN-2) which proliferate in response to B cell stimulatory factor 2. *Clinical and experimental immunology* 75(1), p. 93.

Jacob, J. et al. 1991. Intraclonal generation of antibody mutants in germinal centres. *Nature* 354(6352), pp. 389-392. doi: 10.1038/354389a0

Jacobs, J. P. et al. 1970. Characteristics of a human diploid cell designated MRC-5. *Nature* 227(5254), pp. 168-170. doi: 10.1038/227168a0

Jain, S. et al. 2011. Emerging role of carfilzomib in treatment of relapsed and refractory lymphoid neoplasms and multiple myeloma. *Core Evid* 6, pp. 43-57. doi: 10.2147/ce.s13838

Jakubowiak, A. J. et al. 2012. A phase 1/2 study of carfilzomib in combination with lenalidomide and low-dose dexamethasone as a frontline treatment for multiple myeloma. *Blood* 120(9), pp. 1801-1809. doi: 10.1182/blood-2012-04-422683

Jean, S. and Kiger, A. A. 2014. Classes of phosphoinositide 3-kinases at a glance. *J Cell Sci* 127(5), pp. 923-928. doi: 10.1242/jcs.093773

Jin, F. et al. 2015. Clinical drug interaction profile of idelalisib in healthy subjects. *J Clin Pharmacol* 55(8), pp. 909-919. doi: 10.1002/jcph.495

Johnson-Leger, C. et al. 2000. The parting of the endothelium: miracle, or simply a junctional affair? *J Cell Sci* 113 (Pt 6), pp. 921-933.

Johnston, J. A. et al. 1998. Aggresomes: A Cellular Response to Misfolded Proteins. *J Cell Biol* 143(7), pp. 1883-1898.

Jones, C. H. et al. 2012. Telomere dysfunction and its role in haematological cancer. *Br J Haematol* 156(5), pp. 573-587. doi: 10.1111/j.1365-2141.2011.09022.x

Jones, R. E. et al. 2014. Escape from telomere-driven crisis is DNA ligase III dependent. *Cell Rep* 8(4), pp. 1063-1076. doi: 10.1016/j.celrep.2014.07.007

Jourdan, M. et al. 1998. The myeloma cell antigen syndecan-1 is lost by apoptotic myeloma cells. *Br J Haematol* 100(4), pp. 637-646. doi: 10.1046/j.1365-2141.1998.00623.x

Jourdan, M. et al. 2007. Targeting NF-kappaB pathway with an IKK2 inhibitor induces inhibition of multiple myeloma cell growth. *British journal of haematology* 138(2), pp. 160-168. doi: 10.1111/j.1365-2141.2007.06629.x

Kang, H. et al. 2005. Stromal cell derived factor-1: its influence on invasiveness and migration of breast cancer cells in vitro, and its association with prognosis and survival in human breast cancer. *Breast Cancer Res* 7(4), pp. R402-410. doi: 10.1186/bcr1022

Kappos, L. et al. 2007. Natalizumab treatment for multiple sclerosis: recommendations for patient selection and monitoring. *Lancet Neurol* 6(5), pp. 431-441. doi: 10.1016/s1474-4422(07)70078-9

Karssen, A. M. et al. 2001. Multidrug resistance P-glycoprotein hampers the access of cortisol but not of corticosterone to mouse and human brain. *Endocrinology* 142(6), pp. 2686-2694. doi: 10.1210/endo.142.6.8213

Kashyap, M. K. et al. 2016. Ulocuplumab (BMS-936564 / MDX1338): a fully human anti-CXCR4 antibody induces cell death in chronic lymphocytic leukemia mediated through a reactive oxygen species-dependent pathway. *Oncotarget* 7(3), pp. 2809-2822. doi: 10.18632/oncotarget.6465

Katagiri, S. et al. 1985. Two distinct human myeloma cell lines originating from one patient with myeloma. *International journal of cancer* 36(2), pp. 241-246.

Kato, T. et al. 2007. Activation of Holliday junction recognizing protein involved in the chromosomal stability and immortality of cancer cells. *Cancer Res* 67(18), pp. 8544-8553. doi: 10.1158/0008-5472.can-07-1307

Katz, B. Z. 2010. Adhesion molecules--The lifelines of multiple myeloma cells. *Semin Cancer Biol* 20(3), pp. 186-195. doi: 10.1016/j.semcancer.2010.04.003

Katz, B. Z. and Tavor, S. 2009. The stromal derived factor-1\CXCR4 axis--a legitimate therapeutic target in multiple myeloma? *Leukemia & lymphoma* 50(7), pp. 1067-1068. doi: 10.1080/10428190902991837

Katz, F. et al. 1983. Chromosome assignment of monoclonal antibody-defined determinants on human leukemic cells. *Eur J Immunol* 13(12), pp. 1008-1013. doi: 10.1002/eji.1830131211

Kaufman, J. L. et al. 2012. Lenalidomide, Bortezomib, and Dexamethasone (RVD) in Combination with Vorinostat As Front-Line Therapy for Patients with Multiple Myeloma (MM): Results of a Phase 1 Study. *ASH Annual Meeting Abstracts* 120(21), pp. 336-.

Kawano, Y. et al. 2012. Multiple myeloma cells expressing low levels of CD138 have an immature phenotype and reduced sensitivity to lenalidomide. *Int J Oncol* 41(3), pp. 876-884. doi: 10.3892/ijo.2012.1545

Keats, J. J. et al. 2012. Clonal competition with alternating dominance in multiple myeloma. *Blood* 120(5), pp. 1067-1076.

Kirshner, J. et al. 2008. A unique three-dimensional model for evaluating the impact of therapy on multiple myeloma. *Blood* 112(7), pp. 2935-2945. doi: 10.1182/blood-2008-02-142430

Kishimoto, H. et al. 1998. Molecular mechanism of human CD38 gene expression by retinoic acid. Identification of retinoic acid response element in the first intron. *J Biol Chem* 273(25), pp. 15429-15434.

Kisselbach, L. et al. 2009. CD90 Expression on human primary cells and elimination of contaminating fibroblasts from cell cultures. *Cytotechnology* 59(1), pp. 31-44. doi: 10.1007/s10616-009-9190-3

Kitajiri, S. et al. 2010. Actin-bundling protein TRIOBP forms resilient rootlets of hair cell stereocilia essential for hearing. *Cell* 141(5), pp. 786-798. doi: 10.1016/j.cell.2010.03.049

Kitayama, J. et al. 2000. Alpha 6 beta 1 integrin (VLA-6) mediates leukocyte tether and arrest on laminin under physiological shear flow. *Cell Immunol* 199(2), pp. 97-103. doi: 10.1006/cimm.1999.1596

Klampfl, T. et al. 2013. Somatic mutations of calreticulin in myeloproliferative neoplasms. *N Engl J Med* 369(25), pp. 2379-2390. doi: 10.1056/NEJMoa1311347

Kuhn, D. J. et al. 2012. Targeting the insulin-like growth factor-1 receptor to overcome bortezomib resistance in preclinical models of multiple myeloma. *Blood* 120(16), pp. 3260-3270. doi: 10.1182/blood-2011-10-386789

Kuleshov, M. V. et al. 2016. Enrichr: a comprehensive gene set enrichment analysis web server 2016 update. *Nucleic Acids Res* 44(W1), pp. W90-97. doi: 10.1093/nar/gkw377

Kumar, C. C. 1998. Signaling by integrin receptors. *Oncogene* 17(11 Reviews), pp. 1365-1373. doi: 10.1038/sj.onc.1202172

Kumar, S. 2017. Emerging options in multiple myeloma: targeted, immune, and epigenetic therapies. *Hematology Am Soc Hematol Educ Program* 2017(1), pp. 518-524. doi: 10.1182/asheducation-2017.1.518

Kumar, S. et al. 2017. Efficacy of venetoclax as targeted therapy for relapsed/refractory t(11;14) multiple myeloma. doi: 10.1182/blood-2017-06-788786

Kumar, S. et al. 2010. Immunophenotyping in multiple myeloma and related plasma cell disorders. *Best Practice & Research Clinical Haematology* 23(3), pp. 433-451.

Kumar, S. et al. 2005. CD45 expression by bone marrow plasma cells in multiple myeloma: clinical and biological correlations. *Leukemia* 19(8), pp. 1466-1470.

Kumar, S. K. et al. 2012. A Phase 1/2 Study of Weekly MLN9708, an Investigational Oral Proteasome Inhibitor, in Combination with Lenalidomide and Dexamethasone in Patients with Previously Untreated Multiple Myeloma (MM). *ASH Annual Meeting Abstracts* 120(21), pp. 332-.

Kumar, S. K. et al. 2011. Lenalidomide, cyclophosphamide and dexamethasone (CRd) for newly diagnosed multiple myeloma: results from a phase 2 trial. *Am J Hematol* 86(8), pp. 640-645. doi: 10.1002/ajh.22053

Kyle, R. A. et al. 2007. Clinical course and prognosis of smoldering (asymptomatic) multiple myeloma. *N Engl J Med* 356(25), pp. 2582-2590. doi: 10.1056/NEJMoa070389

Kyle, R. A. et al. 2002. A long-term study of prognosis in monoclonal gammopathy of undetermined significance. *N Engl J Med* 346(8), pp. 564-569. doi: 10.1056/NEJMoa01133202

Lakshman, A. et al. 2018. Risk stratification of smoldering multiple myeloma incorporating revised IMWG diagnostic criteria. *Blood Cancer J* 8(6), p. 59. doi: 10.1038/s41408-018-0077-4

Landgren, O. et al. 2009. Monoclonal gammopathy of undetermined significance (MGUS) consistently precedes multiple myeloma: a prospective study. *Blood* 113(22), pp. 5412-5417. doi: 10.1182/blood-2008-12-194241

Landgren, O. et al. 2013. Clinical and Correlative Pilot Study Of Carfilzomib, Lenalidomide, and Dexamethasone Followed By Lenalidomide Extended Dosing (CRd – R) In High Risk Smoldering Multiple Myeloma Patients. *ASH Annual Meeting Abstracts* 122(21), pp. 1939-1939.

Lannutti, B. J. et al. 2011. CAL-101, a p110delta selective phosphatidylinositol-3-kinase inhibitor for the treatment of B-cell malignancies, inhibits PI3K signaling and cellular viability. *Blood* 117(2), pp. 591-594. doi: 10.1182/blood-2010-03-275305

Laplante, M. and Sabatini, D. M. 2012. mTOR signaling in growth control and disease. *Cell* 149(2), pp. 274-293. doi: 10.1016/j.cell.2012.03.017

Law, P. J. et al. 2017. Genome-wide association analysis of chronic lymphocytic leukaemia, Hodgkin lymphoma and multiple myeloma identifies pleiotropic risk loci. *Sci Rep* 7, p. 41071. doi: 10.1038/srep41071

LeBlanc, R. et al. 2002. Proteasome inhibitor PS-341 inhibits human myeloma cell growth in vivo and prolongs survival in a murine model. *Cancer Res* 62(17), pp. 4996-5000.

Lee, C. et al. 2017. The lysosomal potassium channel TMEM175 adopts a novel tetrameric architecture. *Nature* 547(7664), pp. 472-475. doi: 10.1038/nature23269

Lee, H. C. and Weber, D. M. 2016. Advances and practical use of monoclonal antibodies in multiple myeloma therapy. *Hematology Am Soc Hematol Educ Program* 2016(1), pp. 512-520. doi: 10.1182/asheducation-2016.1.512

Leger, O. J. et al. 1997. Humanization of a mouse antibody against human alpha-4 integrin: a potential therapeutic for the treatment of multiple sclerosis. *Hum Antibodies* 8(1), pp. 3-16.

Leich, E. et al. 2013. Multiple myeloma is affected by multiple and heterogeneous somatic mutations in adhesion- and receptor tyrosine kinase signaling molecules. *Blood Cancer J* 3, p. e102. doi: 10.1038/bcj.2012.47

Leleu, X. et al. 2013. Pomalidomide plus low-dose dexamethasone is active and well tolerated in bortezomib and lenalidomide-refractory multiple myeloma: Intergroupe Francophone du Myélome 2009-02. *Blood* 121(11), pp. 1968-1975. doi: 10.1182/blood-2012-09-452375

Li, J. et al. 2014. The mTOR signaling pathway is an emerging therapeutic target in multiple myeloma. *Curr Pharm Des* 20(1), pp. 125-135.

Li, O. et al. 2004. CD24 expression on T cells is required for optimal T cell proliferation in lymphopenic host. *J Exp Med* 200(8), pp. 1083-1089. doi: 10.1084/jem.20040779

Li, R. et al. 2017. Roles of Arf6 in cancer cell invasion, metastasis and proliferation. *Life Sci* 182, pp. 80-84. doi: 10.1016/j.lfs.2017.06.008

Lin, P. et al. 2004. Flow cytometric immunophenotypic analysis of 306 cases of multiple myeloma. *American journal of clinical pathology* 121(4), pp. 482-488.

Lohr, J. G. et al. 2014. Widespread genetic heterogeneity in multiple myeloma: implications for targeted therapy. *Cancer Cell* 25(1), pp. 91-101. doi: 10.1016/j.ccr.2013.12.015

Lokhorst, H. M. et al. 2015. Targeting CD38 with Daratumumab Monotherapy in Multiple Myeloma. *N Engl J Med* 373(13), pp. 1207-1219. doi: 10.1056/NEJMoa1506348

Lombardo, T. et al. 2012. Median effect dose and combination index analysis of cytotoxic drugs using flow cytometry.*Flow Cytometry-Recent Perspectives*. InTech.

Lonial, S. et al. 2015. Elotuzumab Therapy for Relapsed or Refractory Multiple Myeloma. *N Engl J Med* 373(7), pp. 621-631. doi: 10.1056/NEJMoa1505654

Lonial, S. et al. 2016. Monoclonal antibodies in the treatment of multiple myeloma: current status and future perspectives. *Leukemia* 30(3), pp. 526-535. doi: 10.1038/leu.2015.223

Lopes-Carvalho, T. and Kearney, J. F. 2004. Development and selection of marginal zone B cells. *Immunol Rev* 197, pp. 192-205.

Lundberg, A. S. and Weinberg, R. A. 1998. Functional Inactivation of the Retinoblastoma Protein Requires Sequential Modification by at Least Two Distinct Cyclin-cdk Complexes.*Mol Cell Biol*. Vol. 18. pp. 753-761.

Luo, J. et al. 2003. Targeting the PI3K-Akt pathway in human cancer: rationale and promise. *Cancer Cell* 4(4), pp. 257-262.

Ma, P. C. et al. 2003. c-Met: structure, functions and potential for therapeutic inhibition. *Cancer Metastasis Rev* 22(4), pp. 309-325.

Madani, N. et al. 2002. Implication of the lymphocyte-specific nuclear body protein Sp140 in an innate response to human immunodeficiency virus type 1. *J Virol* 76(21), pp. 11133-11138.

Maddika, S. et al. 2007. Cell survival, cell death and cell cycle pathways are interconnected: implications for cancer therapy. *Drug Resist Updat* 10(1-2), pp. 13-29. doi: 10.1016/j.drup.2007.01.003

Mahindra, A. et al. 2010. Multiple myeloma: biology of the disease. *Blood Rev* 24 Suppl 1, pp. S5-11. doi: 10.1016/s0268-960x(10)70003-5

Mailankody, S. et al. 2015. Minimal residual disease in multiple myeloma: bringing the bench to the bedside. *Nat Rev Clin Oncol* 12(5), pp. 286-295. doi: 10.1038/nrclinonc.2014.239

Manier, S. et al. 2017. Genomic complexity of multiple myeloma and its clinical implications. *Nat Rev Clin Oncol* 14(2), pp. 100-113. doi: 10.1038/nrclinonc.2016.122

Manzanera, G. M. et al. 2005. Immunophenotyping of plasma cells in multiple myeloma.*Multiple Myeloma*. Springer, pp. 5-24.

Martin, K. H. et al. 2002. Integrin connections map: to infinity and beyond. *Science* 296(5573), pp. 1652-1653. doi: 10.1126/science.296.5573.1652

Martin, S. K. et al. 2015. The effect of the PI3K inhibitor BKM120 on tumour growth and osteolytic bone disease in multiple myeloma. *Leuk Res* 39(3), pp. 380-387. doi: 10.1016/j.leukres.2014.12.015

Martin, T. et al. 2013. SAR650984, a CD38 Monoclonal Antibody In Patients With Selected CD38+ Hematological Malignancies- Data From a Dose-Escalation Phase I Study. *ASH Annual Meeting Abstracts* 122(21), pp. 284-284.

Martinez-Lopez, J. et al. 2014. Prognostic value of deep sequencing method for minimal residual disease detection in multiple myeloma. *Blood* 123(20), pp. 3073-3079. doi: 10.1182/blood-2014-01-550020

Mass, R. E. 1962. A comparison of the effect of prednisone and a placebo in the treatment of multiple myeloma. *Cancer Chemother Rep* 16, pp. 257-259.

Mateos, M.-V. et al. 2013. Lenalidomide plus Dexamethasone for High-Risk Smoldering Multiple Myeloma. *New England Journal of Medicine* 369(5), pp. 438-447. doi: doi:10.1056/NEJMoa1300439

Mateos, M. V. et al. 2018. Daratumumab plus Bortezomib, Melphalan, and Prednisone for Untreated Myeloma. *N Engl J Med* 378(6), pp. 518-528. doi: 10.1056/NEJMoa1714678

Matsuda, K. et al. 2006. Characterization of the delta2 glutamate receptor-binding protein delphilin: Splicing variants with differential palmitoylation and an additional PDZ domain. *J Biol Chem* 281(35), pp. 25577-25587. doi: 10.1074/jbc.M602044200

Matsuoka, Y. et al. 1967. Production of free light chains of immunoglobulin by a hematopoietic cell line derived from a patient with multiple myeloma. *Experimental Biology and Medicine* 125(4), pp. 1246-1250.

Matsuyama, S. and Reed, J. C. 2000. Mitochondria-dependent apoptosis and cellular pH regulation. *Cell Death Differ* 7(12), pp. 1155-1165. doi: 10.1038/sj.cdd.4400779

Mattern, J. et al. 2007. Cell cycle arrest by glucocorticoids may protect normal tissue and solid tumors from cancer therapy. *Cancer Biol Ther* 6(9), pp. 1345-1354.

McBeath, R. et al. 2004. Cell shape, cytoskeletal tension, and RhoA regulate stem cell lineage commitment. *Dev Cell* 6(4), pp. 483-495.

McCarthy, P. L. et al. 2012. Lenalidomide after Stem-Cell Transplantation for Multiple Myeloma. *New England Journal of Medicine* 366(19), pp. 1770-1781. doi: doi:10.1056/NEJMoa1114083

Mellado, M. et al. 2001. Chemokine signaling and functional responses: the role of receptor dimerization and TK pathway activation. *Annu Rev Immunol* 19, pp. 397-421. doi: 10.1146/annurev.immunol.19.1.397

Metzger, T. A. et al. 2015. Pressure and shear stress in trabecular bone marrow during whole bone loading. *J Biomech* 48(12), pp. 3035-3043. doi: 10.1016/j.jbiomech.2015.07.028

Minarik, J. et al. 2017. CD38-negative relapse in multiple myeloma after daratumumab-based chemotherapy. *Eur J Haematol* 99(2), pp. 186-189. doi: 10.1111/ejh.12902

Mitra, S. K. and Schlaepfer, D. D. 2006. Integrin-regulated FAK-Src signaling in normal and cancer cells. *Curr Opin Cell Biol* 18(5), pp. 516-523. doi: 10.1016/j.ceb.2006.08.011

Mitsiades, C. S. et al. 2003. Fluorescence imaging of multiple myeloma cells in a clinically relevant SCID/NOD in vivo model: biologic and clinical implications. *Cancer Res* 63(20), pp. 6689-6696.

Mitsiades, C. S. et al. 2004. Inhibition of the insulin-like growth factor receptor-1 tyrosine kinase activity as a therapeutic strategy for multiple myeloma, other hematologic malignancies, and solid tumors. *Cancer Cell* 5(3), pp. 221-230.

Mittelman, M. 2003. The implications of anemia in multiple myeloma. *Clin Lymphoma* 4 Suppl 1, pp. S23-29.

Mo, W. et al. 2013. CXCR4/CXCL12 mediate autocrine cell- cycle progression in NF1-associated malignant peripheral nerve sheath tumors. *Cell* 152(5), pp. 1077-1090. doi: 10.1016/j.cell.2013.01.053

Moalli, P. A. et al. 1992. A mechanism of resistance to glucocorticoids in multiple myeloma: transient expression of a truncated glucocorticoid receptor mRNA. *Blood* 79(1), pp. 213-222.

Moller, C. et al. 2003. Expression and function of chemokine receptors in human multiple myeloma. *Leukemia* 17(1), pp. 203-210. doi: 10.1038/sj.leu.2402717

Moreau, P. et al. 2019. Bortezomib, thalidomide, and dexamethasone with or without daratumumab before and after autologous stem-cell transplantation for newly diagnosed multiple myeloma (CASSIOPEIA): a randomised, open-label, phase 3 study. *Lancet* 394(10192), pp. 29-38. doi: 10.1016/s0140-6736(19)31240-1

Moreau, P. et al. 2016. Oral Ixazomib, Lenalidomide, and Dexamethasone for Multiple Myeloma. *N Engl J Med* 374(17), pp. 1621-1634. doi: 10.1056/NEJMoa1516282

Moreau, P. et al. 2012. Proteasome inhibitors in multiple myeloma: 10 years later. *Blood* 120(5), pp. 947-959. doi: 10.1182/blood-2012-04-403733

Moreno-Garcia, M. E. et al. 2005. CD38 signaling regulates B lymphocyte activation via a phospholipase C (PLC)-gamma 2-independent, protein kinase C, phosphatidylcholine-PLC, and phospholipase D-dependent signaling cascade. *J Immunol* 174(5), pp. 2687-2695.

Morgan, G. J. et al. 2013. Long-term follow-up of MRC Myeloma IX trial: Survival outcomes with bisphosphonate and thalidomide treatment. *Clin Cancer Res* 19(21), pp. 6030-6038. doi: 10.1158/1078-0432.ccr-12-3211

Morgan, G. J. et al. 2012a. Cyclophosphamide, thalidomide, and dexamethasone as induction therapy for newly diagnosed multiple myeloma patients destined for autologous stem-cell transplantation: MRC Myeloma IX randomized trial results. *Haematologica* 97(3), pp. 442-450. doi: 10.3324/haematol.2011.043372

Morgan, G. J. et al. 2012b. The genetic architecture of multiple myeloma. *Nature Reviews Cancer* 12(5), pp. 335-348.

Munshi, N. C. et al. 2017. Association of Minimal Residual Disease With Superior Survival Outcomes in Patients With Multiple Myeloma: A Meta-analysis. *JAMA Oncol* 3(1), pp. 28-35. doi: 10.1001/jamaoncol.2016.3160

Munugalavadla, V. et al. 2014. The PI3K inhibitor GDC-0941 combines with existing clinical regimens for superior activity in multiple myeloma. *Oncogene* 33(3), pp. 316-325. doi: 10.1038/onc.2012.594

Nangalia, J. et al. 2013. Somatic CALR mutations in myeloproliferative neoplasms with nonmutated JAK2. *N Engl J Med* 369(25), pp. 2391-2405. doi: 10.1056/NEJMoa1312542

Naymagon, L. and Abdul-Hay, M. 2016. Novel agents in the treatment of multiple myeloma: a review about the future. *J Hematol Oncol* 9(1), p. 52. doi: 10.1186/s13045-016-0282-1

Nechipurenko, I. V. et al. 2016. A Conserved Role for Girdin in Basal Body Positioning and Ciliogenesis. *Dev Cell* 38(5), pp. 493-506. doi: 10.1016/j.devcel.2016.07.013

Nijhof, I. S. et al. 2016a. CD38 expression and complement inhibitors affect response and resistance to daratumumab therapy in myeloma. *Blood* 128(7), pp. 959-970. doi: 10.1182/blood-2016-03-703439

Nijhof, I. S. et al. 2016b. CD38 levels are associated with response and complement inhibitors contribute to resistance in myeloma patients treated with daratumumab. *Blood*, doi: 10.1182/blood-2016-03-703439

Nijhof, I. S. et al. 2015. Upregulation of CD38 expression on multiple myeloma cells by all-trans retinoic acid improves the efficacy of daratumumab. *Leukemia* 29(10), pp. 2039-2049. doi: 10.1038/leu.2015.123

Nilsson, K. et al. 1970. Established immunoglobulin producing myeloma (IgE) and lymphoblastoid (IgG) cell lines from an IgE myeloma patient. *Clinical and experimental immunology* 7(4), p. 477.

Noborio-Hatano, K. et al. 2009. Bortezomib overcomes cell-adhesion-mediated drug resistance through downregulation of VLA-4 expression in multiple myeloma. *Oncogene* 28(2), pp. 231-242. doi: 10.1038/onc.2008.385

O'Connor, O. A. et al. 2009. A phase 1 dose escalation study of the safety and pharmacokinetics of the novel proteasome inhibitor carfilzomib (PR-171) in patients with

hematologic malignancies. *Clin Cancer Res* 15(22), pp. 7085-7091. doi: 10.1158/1078-0432.ccr-09-0822

O'Rawe, J. et al. 2013. Low concordance of multiple variant-calling pipelines: practical implications for exome and genome sequencing. *Genome Med* 5(3), p. 28. doi: 10.1186/gm432

Oerlemans, R. et al. 2008. Molecular basis of bortezomib resistance: proteasome subunit beta5 (PSMB5) gene mutation and overexpression of PSMB5 protein. *Blood* 112(6), pp. 2489-2499. doi: 10.1182/blood-2007-08-104950

Omori, S. A. et al. 2006. Regulation of class-switch recombination and plasma cell differentiation by phosphatidylinositol 3-kinase signaling. *Immunity* 25(4), pp. 545-557. doi: 10.1016/j.immuni.2006.08.015

Ostrem, J. M. and Shokat, K. M. 2016. Direct small-molecule inhibitors of KRAS: from structural insights to mechanism-based design. *Nat Rev Drug Discov* 15(11), pp. 771-785. doi: 10.1038/nrd.2016.139

Ouyang, H. et al. 2012. Protein aggregates are recruited to aggresome by histone deacetylase 6 via unanchored ubiquitin C termini. *J Biol Chem* 287(4), pp. 2317-2327. doi: 10.1074/jbc.M111.273730

Pachlopnik Schmid, J. et al. 2010. Inherited defects in lymphocyte cytotoxic activity. *Immunol Rev* 235(1), pp. 10-23. doi: 10.1111/j.0105-2896.2010.00890.x

Paiva, B. et al. 2010. Utility of flow cytometry immunophenotyping in multiple myeloma and other clonal plasma cell-related disorders. *Cytometry B Clin Cytom* 78(4), pp. 239-252. doi: 10.1002/cyto.b.20512

Palumbo, A. and Anderson, K. 2011. Multiple myeloma. *N Engl J Med* 364(11), pp. 1046-1060. doi: 10.1056/NEJMra1011442

Palumbo, A. et al. 2015. Revised International Staging System for Multiple Myeloma: A Report From International Myeloma Working Group. *J Clin Oncol* 33(26), pp. 2863-2869. doi: 10.1200/jco.2015.61.2267

Palumbo, A. et al. 2016. Daratumumab, Bortezomib, and Dexamethasone for Multiple Myeloma. *N Engl J Med* 375(8), pp. 754-766. doi: 10.1056/NEJMoa1606038

Palumbo, A. et al. 2012. Continuous lenalidomide treatment for newly diagnosed multiple myeloma. *N Engl J Med* 366(19), pp. 1759-1769. doi: 10.1056/NEJMoa1112704

Pardanani, A. et al. 2006. FIP1L1-PDGFRA in eosinophilic disorders: prevalence in routine clinical practice, long-term experience with imatinib therapy, and a critical review of the literature. *Leuk Res* 30(8), pp. 965-970. doi: 10.1016/j.leukres.2005.11.011

Parmo-Cabanas, M. et al. 2004. Integrin alpha4beta1 involvement in stromal cell-derived factor-1alpha-promoted myeloma cell transendothelial migration and adhesion: role of cAMP and the actin cytoskeleton in adhesion. *Exp Cell Res* 294(2), pp. 571-580. doi: 10.1016/j.yexcr.2003.12.003

Parsons, J. T. et al. 2000. Focal adhesion kinase: a regulator of focal adhesion dynamics and cell movement. *Oncogene* 19(49), pp. 5606-5613. doi: 10.1038/sj.onc.1203877

Pawlyn, C. et al. 2017. Overexpression of EZH2 in multiple myeloma is associated with poor prognosis and dysregulation of cell cycle control. *Blood Cancer J* 7(3), p. e549. doi: 10.1038/bcj.2017.27

Peceliunas, V. et al. 2011. Six color flow cytometry detects plasma cells expressing aberrant immunophenotype in bone marrow of healthy donors. *Cytometry Part B: Clinical Cytometry* 80(5), pp. 318-323.

Pellat-Deceunynck, C. et al. 1998. The absence of CD56 (NCAM) on malignant plasma cells is a hallmark of plasma cell leukemia and of a special subset of multiple myeloma. *Leukemia* 12(12), pp. 1977-1982.

Peng, B. et al. 2006. DNA hypermethylation and partial gene silencing of human thymine-DNA glycosylase in multiple myeloma cell lines. *Epigenetics* 1(3), pp. 138-145.

Peng, S. B. et al. 2016. Inhibition of CXCR4 by LY2624587, a Fully Humanized Anti-CXCR4 Antibody Induces Apoptosis of Hematologic Malignancies. *PLoS One* 11(3), p. e0150585. doi: 10.1371/journal.pone.0150585

Pickart, C. M. and Eddins, M. J. 2004. Ubiquitin: structures, functions, mechanisms. *Biochim Biophys Acta* 1695(1-3), pp. 55-72. doi: 10.1016/j.bbamcr.2004.09.019

Pittner, B. T. et al. 2005. CD38 expression levels in chronic lymphocytic leukemia B cells are associated with activation marker expression and differential responses to interferon stimulation. *Leukemia* 19(12), pp. 2264-2272. doi: 10.1038/sj.leu.2403975

Place, E. 2015. *208462Orig1s000 PHARMACOLOGY REVIEW(S)*. Available at: https://www.accessdata.fda.gov/drugsatfda_docs/nda/2015/208462Orig1s000PharmR.pdf [Accessed.

Planey, S. L. et al. 2003. Role of apical caspases and glucocorticoid-regulated genes in glucocorticoid-induced apoptosis of pre-B leukemic cells. *Cancer Res* 63(1), pp. 172-178.

Plesner, T. et al. 2012. Daratumumab, a CD38 Monoclonal Antibody in Patients with Multiple Myeloma - Data From a Dose-Escalation Phase I/II Study. *ASH Annual Meeting Abstracts* 120(21), pp. 73-.

Podar, K. et al. 2001. Vascular endothelial growth factor triggers signaling cascades mediating multiple myeloma cell growth and migration. *Blood* 98(2), pp. 428-435.

Podar, K. et al. 2011. The selective adhesion molecule inhibitor Natalizumab decreases multiple myeloma cell growth in the bone marrow microenvironment: therapeutic implications. *Br J Haematol* 155(4), pp. 438-448. doi: 10.1111/j.1365-2141.2011.08864.x

Pratt, D. et al. 2015. NDEx, the Network Data Exchange. *Cell Syst* 1(4), pp. 302-305. doi: 10.1016/j.cels.2015.10.001

Pratt, G. et al. 2014. Updates to the guidelines for the diagnosis and management of multiple myeloma. *Br J Haematol*, doi: 10.1111/bjh.12926

Pérez-Persona, E. et al. 2007. *New criteria to identify risk of progression in monoclonal gammopathy of uncertain significance and smoldering multiple myeloma based on multiparameter flow cytometry analysis of bone marrow plasma cells*.

Qiagen. 2009. *EpiTect Bisulfite Handbook*. 09/2009 ed.

Quach, H. et al. 2010. Mechanism of action of immunomodulatory drugs (IMiDS) in multiple myeloma. *Leukemia* 24(1), pp. 22-32. doi: 10.1038/leu.2009.236

Quesada, V. et al. 2011. Exome sequencing identifies recurrent mutations of the splicing factor SF3B1 gene in chronic lymphocytic leukemia. *Nat Genet* 44(1), pp. 47-52. doi: 10.1038/ng.1032

Rack, K. et al. 2016. Genomic profiling of myeloma: the best approach, a comparison of cytogenetics, FISH and array-CGH of 112 myeloma cases. *J Clin Pathol* 69(1), pp. 82-86. doi: 10.1136/jclinpath-2015-203054

Rajan, A. M. and Kumar, S. 2016. New investigational drugs with single-agent activity in multiple myeloma. *Blood Cancer J* 6(7), p. e451. doi: 10.1038/bcj.2016.53

Rajkumar, S. V. 2016. Updated Diagnostic Criteria and Staging System for Multiple Myeloma. *Am Soc Clin Oncol Educ Book* 35, pp. e418-423. doi: 10.14694/edbk_159009

Rajkumar, S. V. et al. 2014. International Myeloma Working Group updated criteria for the diagnosis of multiple myeloma. *Lancet Oncol* 15(12), pp. e538-548. doi: 10.1016/s1470-2045(14)70442-5

Rasche, L. et al. 2017. Spatial genomic heterogeneity in multiple myeloma revealed by multi-region sequencing.*Nat Commun*. Vol. 8.

Rawstron, A. C. 2006. Immunophenotyping of plasma cells. *Current Protocols in Cytometry*, pp. 6.23. 21-26.23. 14.

Rawstron, A. C. et al. 2013. Minimal residual disease assessed by multiparameter flow cytometry in multiple myeloma: impact on outcome in the Medical Research Council Myeloma IX Study. *J Clin Oncol* 31(20), pp. 2540-2547. doi: 10.1200/jco.2012.46.2119

Rawstron, A. C. et al. 2008. Report of the European Myeloma Network on multiparametric flow cytometry in multiple myeloma and related disorders. *haematologica* 93(3), pp. 431-438.

Rawstron, A. C. et al. 1997. Circulating plasma cells in multiple myeloma: characterization and correlation with disease stage. *Br J Haematol* 97(1), pp. 46-55.

Reichardt, H. M. et al. 2000. Mice with an increased glucocorticoid receptor gene dosage show enhanced resistance to stress and endotoxic shock. *Mol Cell Biol* 20(23), pp. 9009-9017.

Reid, S. et al. 2010. Characterisation and relevance of CD138-negative plasma cells in plasma cell myeloma. *Int J Lab Hematol* 32(6 Pt 1), pp. e190-196. doi: 10.1111/j.1751-553X.2010.01222.x

Ri, M. et al. 2010. Bortezomib-resistant myeloma cell lines: a role for mutated PSMB5 in preventing the accumulation of unfolded proteins and fatal ER stress. *Leukemia* 24(8), pp. 1506-1512.

Richardson, P. G. et al. 2013a. Twice-Weekly Oral MLN9708 (Ixazomib Citrate), An Investigational Proteasome Inhibitor, In Combination With Lenalidomide (Len) and Dexamethasone (Dex) In Patients (Pts) With Newly Diagnosed Multiple Myeloma (MM): Final Phase 1 Results and Phase 2 Data. *ASH Annual Meeting Abstracts* 122(21), pp. 535-535.

Richardson, P. G. et al. 2009. High Response Rates and Encouraging Time-to-Event Data with Lenalidomide, Bortezomib, and Dexamethasone in Newly Diagnosed Multiple Myeloma: Final Results of a Phase I/II Study. *ASH Annual Meeting Abstracts* 114(22), pp. 1218-.

Richardson, P. G. et al. 2013b. PANORAMA 2: panobinostat in combination with bortezomib and dexamethasone in patients with relapsed and bortezomib-refractory myeloma. *Blood* 122(14), pp. 2331-2337. doi: 10.1182/blood-2013-01-481325

Richardson, P. G. et al. 2014. Pomalidomide alone or in combination with low-dose dexamethasone in relapsed and refractory multiple myeloma: a randomized phase 2 study. *Blood* 123(12), pp. 1826-1832. doi: 10.1182/blood-2013-11-538835

Richardson, P. G. et al. 2011. Perifosine plus bortezomib and dexamethasone in patients with relapsed/refractory multiple myeloma previously treated with bortezomib: results of a multicenter phase I/II trial. *J Clin Oncol* 29(32), pp. 4243-4249. doi: 10.1200/jco.2010.33.9788

Richmond, A. and Su, Y. 2008. Mouse xenograft models vs GEM models for human cancer therapeutics. *Dis Model Mech* 1(2-3), pp. 78-82. doi: 10.1242/dmm.000976

Ridley, R. C. et al. 1993. Expression of syndecan regulates human myeloma plasma cell adhesion to type I collagen. *Blood* 81(3), pp. 767-774.

Rivara, S. et al. 2016. Heparanase: a rainbow pharmacological target associated to multiple pathologies including rare diseases. *Future Med Chem* 8(6), pp. 647-680. doi: 10.4155/fmc-2016-0012

Roccaro, A. M. et al. 2015. CXCR4 Regulates Extra-Medullary Myeloma through Epithelial-Mesenchymal-Transition-like Transcriptional Activation. *Cell Rep* 12(4), pp. 622-635. doi: 10.1016/j.celrep.2015.06.059

Rodningen, O. K. et al. 2008. Radiation-induced gene expression in human subcutaneous fibroblasts is predictive of radiation-induced fibrosis. *Radiother Oncol* 86(3), pp. 314-320. doi: 10.1016/j.radonc.2007.09.013

Rommerswinkel, N. et al. 2014. Analysis of cell migration within a three-dimensional collagen matrix. *J Vis Exp* (92), p. e51963. doi: 10.3791/51963

Runnels, J. M. et al. 2011. Optical techniques for tracking multiple myeloma engraftment, growth, and response to therapy. *J Biomed Opt* 16(1), p. 011006. doi: 10.1117/1.3520571

Saare, M. et al. 2015. SP140L, an Evolutionarily Recent Member of the SP100 Family, Is an Autoantigen in Primary Biliary Cirrhosis. *J Immunol Res* 2015, doi: 10.1155/2015/526518

Salanueva, I. J. et al. 2007. Integrin regulation of caveolin function. *J Cell Mol Med* 11(5), pp. 969-980. doi: 10.1111/j.1582-4934.2007.00109.x

San Miguel, J. et al. 2013. Pomalidomide plus low-dose dexamethasone versus high-dose dexamethasone alone for patients with relapsed and refractory multiple myeloma (MM-003): a randomised, open-label, phase 3 trial. *Lancet Oncol* 14(11), pp. 1055-1066. doi: 10.1016/s1470-2045(13)70380-2

Sanderson, R. D. and Yang, Y. 2008. Syndecan-1: a dynamic regulator of the myeloma microenvironment. *Clin Exp Metastasis* 25(2), pp. 149-159. doi: 10.1007/s10585-007-9125-3

Sanz-Rodriguez, F. et al. 2001. Chemokine stromal cell-derived factor-1alpha modulates VLA-4 integrin-mediated multiple myeloma cell adhesion to CS-1/fibronectin and VCAM-1. *Blood* 97(2), pp. 346-351.

Sanz-Rodriguez, F. and Teixido, J. 2001. VLA-4-dependent myeloma cell adhesion. *Leuk Lymphoma* 41(3-4), pp. 239-245. doi: 10.3109/10428190109057979

Schabath, H. et al. 2006. CD24 affects CXCR4 function in pre-B lymphocytes and breast carcinoma cells. *J Cell Sci* 119(Pt 2), pp. 314-325. doi: 10.1242/jcs.02741

Schmidt, M. et al. 2011. Increased in vivo efficacy of lenalidomide and thalidomide by addition of ethacrynic acid. *In Vivo* 25(3), pp. 325-333.

Schmidt, S. et al. 2004. Glucocorticoid-induced apoptosis and glucocorticoid resistance: molecular mechanisms and clinical relevance. *Cell Death Differ* 11 Suppl 1, pp. S45-55. doi: 10.1038/sj.cdd.4401456

Scholzen, T. and Gerdes, J. 2000. The Ki-67 protein: from the known and the unknown. *J Cell Physiol* 182(3), pp. 311-322. doi: 10.1002/(sici)1097-4652(200003)182:3<311::aid-jcp1>3.0.co;2-9

Schwartz, M. A. and Assoian, R. K. 2001. Integrins and cell proliferation: regulation of cyclin-dependent kinases via cytoplasmic signaling pathways. *J Cell Sci* 114(Pt 14), pp. 2553-2560.

Shah, J. J. et al. 2012. A Multi-Center Phase I/II Trial of Carfilzomib and Pomalidomide with Dexamethasone (Car-Pom-d) in Patients with Relapsed/Refractory Multiple Myeloma. *ASH Annual Meeting Abstracts* 120(21), pp. 74-.

Shanafelt, T. D. et al. 2008. CD49d expression is an independent predictor of overall survival in patients with chronic lymphocytic leukaemia: a prognostic parameter with therapeutic potential. *Br J Haematol* 140(5), pp. 537-546. doi: 10.1111/j.1365-2141.2007.06965.x

Shapiro-Shelef, M. and Calame, K. 2005. Regulation of plasma-cell development. *Nat Rev Immunol* 5(3), pp. 230-242. doi: 10.1038/nri1572

Sharma, S. and Lichtenstein, A. 2008. Dexamethasone-induced apoptotic mechanisms in myeloma cells investigated by analysis of mutant glucocorticoid receptors. *Blood* 112(4), pp. 1338-1345.

Sherry, S. T. et al. 2001. dbSNP: the NCBI database of genetic variation. *Nucleic Acids Res* 29(1), pp. 308-311.

Shlomchik, M. J. and Weisel, F. 2012. Germinal center selection and the development of memory B and plasma cells. *Immunol Rev* 247(1), pp. 52-63. doi: 10.1111/j.1600-065X.2012.01124.x

Siegel, D. S. et al. 2012. A phase 2 study of single-agent carfilzomib (PX-171-003-A1) in patients with relapsed and refractory multiple myeloma. *Blood* 120(14), pp. 2817-2825. doi: 10.1182/blood-2012-05-425934

Silbermann, R. and Roodman, G. D. 2013. Myeloma bone disease: Pathophysiology and management. *J Bone Oncol* 2(2), pp. 59-69. doi: 10.1016/j.jbo.2013.04.001

Singh, P. P. et al. 2013. Lenalidomide Maintenance Therapy In Multiple Myeloma: A Meta-Analysis Of Randomized Trials. *ASH Annual Meeting Abstracts* 122(21), pp. 407-407.

Sison, E. A. et al. 2013. Dynamic chemotherapy-induced upregulation of CXCR4 expression: a mechanism of therapeutic resistance in pediatric AML. *Mol Cancer Res* 11(9), pp. 1004-1016. doi: 10.1158/1541-7786.mcr-13-0114

Smadja, N. V. et al. 2001. Hypodiploidy is a major prognostic factor in multiple myeloma. *Blood* 98(7), pp. 2229-2238.

Smith, L. K. and Cidlowski, J. A. 2010. Glucocorticoid-induced apoptosis of healthy and malignant lymphocytes. *Prog Brain Res* 182, pp. 1-30. doi: 10.1016/s0079-6123(10)82001-1

Snowden, J. A. et al. 2017. Guidelines for screening and management of late and long-term consequences of myeloma and its treatment. *Br J Haematol* 176(6), pp. 888-907. doi: 10.1111/bjh.14514

Song, E. K. et al. 2012. NAADP mediates insulin-stimulated glucose uptake and insulin sensitization by PPARgamma in adipocytes. *Cell Rep* 2(6), pp. 1607-1619. doi: 10.1016/j.celrep.2012.10.018

Springer, T. A. 1994. Traffic signals for lymphocyte recirculation and leukocyte emigration: the multistep paradigm. *Cell* 76(2), pp. 301-314.

Sprynski, A. C. et al. 2009. The role of IGF-1 as a major growth factor for myeloma cell lines and the prognostic relevance of the expression of its receptor. *Blood* 113(19), pp. 4614-4626. doi: 10.1182/blood-2008-07-170464

Stavnezer, J. and Amemiya, C. T. 2004. Evolution of isotype switching. *Semin Immunol* 16(4), pp. 257-275. doi: 10.1016/j.smim.2004.08.005

Steelman, L. S. et al. 2004. JAK/STAT, Raf/MEK/ERK, PI3K/Akt and BCR-ABL in cell cycle progression and leukemogenesis. *Leukemia* 18(2), pp. 189-218. doi: 10.1038/sj.leu.2403241

Steinberg, M. and Silva, M. 2010. Plerixafor: A chemokine receptor-4 antagonist for mobilization of hematopoietic stem cells for transplantation after high-dose chemotherapy for non-Hodgkin's lymphoma or multiple myeloma. *Clin Ther* 32(5), pp. 821-843. doi: 10.1016/j.clinthera.2010.05.007

Stessman, H. A. et al. 2013. Reduced CXCR4 expression is associated with extramedullary disease in a mouse model of myeloma and predicts poor survival in multiple myeloma patients treated with bortezomib. *Leukemia* 27(10), pp. 2075-2077. doi: 10.1038/leu.2013.148

Stühmer, T. et al. 2010. Preclinical anti-myeloma activity of the novel HDAC-inhibitor JNJ-26481585. *British journal of haematology* 149(4), pp. 529-536.

Sud, A. et al. 2017. Genome-wide association studies of cancer: current insights and future perspectives. *Nat Rev Cancer* 17(11), pp. 692-704. doi: 10.1038/nrc.2017.82

Suzuki, k. et al. 2013. Prognostic Value of Expression of Cd45 and Cd49d in Newly Diagnosed Multiple Myeloma. *Clinical Lymphoma, Myeloma & Leukemia* 13,

Szalat, R. et al. 2016. Gene Expression Profiles in Myeloma: Ready for the Real World?*Clin Cancer Res*. Vol. 22. United States: (c)2016 American Association for Cancer Research., pp. 5434-5442.

Sánchez-Vega, B. et al. 2006. Glucocorticoid receptor transcriptional isoforms and resistance in multiple myeloma cells. *Molecular cancer therapeutics* 5(12), pp. 3062-3070.

Tai, Y.-T. et al. 2003. CD40 induces human multiple myeloma cell migration via phosphatidylinositol 3–kinase/AKT/NF-κB signaling. *Blood* 101(7), pp. 2762-2769.

Tai, Y. T. et al. 2012. Bruton tyrosine kinase inhibition is a novel therapeutic strategy targeting tumor in the bone marrow microenvironment in multiple myeloma. *Blood* 120(9), pp. 1877-1887. doi: 10.1182/blood-2011-12-396853

Tai, Y. T. et al. 2007. Targeting MEK induces myeloma-cell cytotoxicity and inhibits osteoclastogenesis. *Blood* 110(5), pp. 1656-1663. doi: 10.1182/blood-2007-03-081240

Terpos, E. et al. 2016. Increased circulating VCAM-1 correlates with advanced disease and poor survival in patients with multiple myeloma: reduction by post-bortezomib and lenalidomide treatment. *Blood Cancer J* 6, p. e428. doi: 10.1038/bcj.2016.37

Thomas, A. L. et al. 2015. Identification of potential glucocorticoid receptor therapeutic targets in multiple myeloma.*Nucl Recept Signal*. Vol. 13.

Tian, E. et al. 2003. The role of the Wnt-signaling antagonist DKK1 in the development of osteolytic lesions in multiple myeloma. *N Engl J Med* 349(26), pp. 2483-2494. doi: 10.1056/NEJMoa030847

Tonko, M. et al. 2001. Gene expression profiles of proliferating vs. G1/G0 arrested human leukemia cells suggest a mechanism for glucocorticoid-induced apoptosis. *Faseb j* 15(3), pp. 693-699. doi: 10.1096/fj.00-0327com

Trudel, S. S., A. Sutherland, H. et al. 2016. A PHASE IB STUDY OF THE AKT INHIBITOR AFURESERTIB IN COMBINATION... by Dr. Suzanne Trudel. *Haematologica* 101(supp; 1):P273,

Tukey, R. H. and Strassburg, C. P. 2000. Human UDP-glucuronosyltransferases: metabolism, expression, and disease. *Annu Rev Pharmacol Toxicol* 40, pp. 581-616. doi: 10.1146/annurev.pharmtox.40.1.581

Ueda, K. et al. 1987. The human multidrug resistance (mdr1) gene. cDNA cloning and transcription initiation. *J Biol Chem* 262(2), pp. 505-508.

Urashima, M. et al. 1997. The development of a model for the homing of multiple myeloma cells to human bone marrow. *Blood* 90(2), pp. 754-765.

Vaisitti, T. et al. 2010. CD38 increases CXCL12-mediated signals and homing of chronic lymphocytic leukemia cells. *Leukemia* 24(5), pp. 958-969. doi: 10.1038/leu.2010.36

van de Donk, N. W. et al. 2016. Monoclonal antibodies targeting CD38 in hematological malignancies and beyond. *Immunol Rev* 270(1), pp. 95-112. doi: 10.1111/imr.12389

Verbrugge, S. E. et al. 2012. Inactivating PSMB5 mutations and P-glycoprotein (multidrug resistance-associated protein/ATP-binding cassette B1) mediate resistance to proteasome inhibitors: ex vivo efficacy of (immuno)proteasome inhibitors in mononuclear blood cells from patients with rheumatoid arthritis. *J Pharmacol Exp Ther* 341(1), pp. 174-182. doi: 10.1124/jpet.111.187542

Vij, R. et al. 2012. An open-label, single-arm, phase 2 (PX-171-004) study of single-agent carfilzomib in bortezomib-naive patients with relapsed and/or refractory multiple myeloma. *Blood* 119(24), pp. 5661-5670. doi: 10.1182/blood-2012-03-414359

Walker, B. A. et al. 2015. Mutational Spectrum, Copy Number Changes, and Outcome: Results of a Sequencing Study of Patients With Newly Diagnosed Myeloma. *J Clin Oncol* 33(33), pp. 3911-3920. doi: 10.1200/jco.2014.59.1503

Walker, B. A. et al. 2014. Intraclonal heterogeneity is a critical early event in the development of myeloma and precedes the development of clinical symptoms. *Leukemia* 28(2), pp. 384-390. doi: 10.1038/leu.2013.199

Walker, M. G. and Volkmuth, W. 2002. Cell adhesion and matrix remodeling genes identified by co-expression analysis. *Gene Function & Disease* 3(3-4), pp. 109-112. doi: 10.1002/gnfd.200290000

Wallington-Beddoe, C. T. et al. 2018. Resistance to proteasome inhibitors and other targeted therapies in myeloma. *Br J Haematol* 182(1), pp. 11-28. doi: 10.1111/bjh.15210

Walsby, E. et al. 2014a. CXCL12 Enhances CLL Cell and T-Cell Migration in a Dynamic Circulating Model of CLL That Can be Abrogated By the CXCR4 Antagonist ONO-7161. *ASH Abstract*,

Walsby, E. et al. eds. 2014b. *CXCL12 Enhances CLL Cell and T-Cell Migration in a Dynamic Circulating Model of CLL That Can be Abrogated By the CXCR4 Antagonist ONO-7161*. 2014-12-06. American Society of Hematology.

Walsby, E. et al. 2014c. Development and characterization of a physiologically relevant model of lymphocyte migration in chronic lymphocytic leukemia. *Blood* 123(23), pp. 3607-3617.

Wang, L. et al. 2011a. SF3B1 and other novel cancer genes in chronic lymphocytic leukemia. *N Engl J Med* 365(26), pp. 2497-2506. doi: 10.1056/NEJMoa1109016

Wang, X. et al. 2011b. Targeting integrin-linked kinase increases apoptosis and decreases invasion of myeloma cell lines and inhibits IL-6 and VEGF secretion from BMSCs. *Med Oncol* 28(4), pp. 1596-1600. doi: 10.1007/s12032-010-9616-y

Wang, Z. et al. 2003. Dexamethasone-induced gene 2 (dig2) is a novel pro-survival stress gene induced rapidly by diverse apoptotic signals. *J Biol Chem* 278(29), pp. 27053-27058. doi: 10.1074/jbc.M303723200

Waxman, A. J. et al. 2014. Modeling the risk of progression in smoldering multiple myeloma. *ASCO Meeting Abstracts* 32(15_suppl), p. 8607.

Webb, M. S. et al. 2003. Gene networks in glucocorticoid-evoked apoptosis of leukemic cells. *J Steroid Biochem Mol Biol* 85(2-5), pp. 183-193.

Went, M. et al. 2018. Genetic correlation between multiple myeloma and chronic lymphocytic leukaemia provides evidence for shared aetiology. *Blood Cancer J* 9(1), p. 1. doi: 10.1038/s41408-018-0162-8

Willimott, S. et al. 2007. Regulation of CD38 in proliferating chronic lymphocytic leukemia cells stimulated with CD154 and interleukin-4. *Haematologica* 92(10), pp. 1359-1366. doi: 10.3324/haematol.11340

Wolf, K. et al. 2009. Collagen-based cell migration models in vitro and in vivo. *Semin Cell Dev Biol* 20(8), pp. 931-941. doi: 10.1016/j.semcdb.2009.08.005

Wu, D. et al. 2015. CD138-negative myeloma cells regulate mechanical properties of bone marrow stromal cells through SDF-1/CXCR4/AKT signaling pathway. *Biochim Biophys Acta* 1853(2), pp. 338-347. doi: 10.1016/j.bbamcr.2014.11.019

Wu, K. D. et al. 2003. Telomerase and telomere length in multiple myeloma: correlations with disease heterogeneity, cytogenetic status, and overall survival. *Blood* 101(12), pp. 4982-4989. doi: 10.1182/blood-2002-11-3451

Xiong, D. et al. 2012. Exome sequencing identifies MXRA5 as a novel cancer gene frequently mutated in non-small cell lung carcinoma from Chinese patients. *Carcinogenesis* 33(9), pp. 1797-1805. doi: 10.1093/carcin/bgs210

Xu, F. et al. 2015. Whole-exome and targeted sequencing identify ROBO1 and ROBO2 mutations as progression-related drivers in myelodysplastic syndromes. *Nat Commun* 6, p. 8806. doi: 10.1038/ncomms9806

Yang, Y. et al. 2007. Heparanase enhances syndecan-1 shedding: a novel mechanism for stimulation of tumor growth and metastasis. *J Biol Chem* 282(18), pp. 13326-13333. doi: 10.1074/jbc.M611259200

Yates, A. et al. 2016. Ensembl 2016. *Nucleic Acids Res* 44(D1), pp. D710-716. doi: 10.1093/nar/gkv1157

Zandecki, M. et al. 1995. CD19 and immunophenotype of bone marrow plasma cells in monoclonal gammopathy of undetermined significance. *Journal of clinical pathology* 48(6), pp. 548-552.

Zeltz, C. and Gullberg, D. 2016. The integrin-collagen connection--a glue for tissue repair? *J Cell Sci* 129(4), pp. 653-664. doi: 10.1242/jcs.180992

Zhang, B. et al. 2003. IL-6-independent expression of Mcl-1 in human multiple myeloma. *Oncogene* 22(12), pp. 1848-1859. doi: 10.1038/sj.onc.1206358

Zhang, K. et al. 2015. Identification of the key genes connected with plasma cells of multiple myeloma using expression profiles.*Onco Targets Ther*. Vol. 8. pp. 1795-1803.

Zhang, Q. et al. 2014. [Effect of PI3Kdelta inhibitor CAL-101 on myeloma cell lines and preliminary study of synergistic effects with other new drugs]. *Zhonghua Xue Ye Xue Za Zhi* 35(10), pp. 926-930. doi: 10.3760/cma.j.issn.0253-2727.2014.10.012

Zhao, J. et al. 2012. Efficient methods for identifying mutated driver pathways in cancer. *Bioinformatics* 28(22), pp. 2940-2947. doi: 10.1093/bioinformatics/bts564

Zhu, J. et al. 2015. A novel PI3K inhibitor PIK-C98 displays potent preclinical activity against multiple myeloma. *Oncotarget* 6(1), pp. 185-195.

Zhu, Y. X. et al. 2011. Cereblon expression is required for the antimyeloma activity of lenalidomide and pomalidomide. *Blood* 118(18), pp. 4771-4779. doi: 10.1182/blood-2011-05-356063

Zhu, Y. X. et al. 2019. Identification of lenalidomide resistance pathways in myeloma and targeted resensitization using cereblon replacement, inhibition of STAT3 or targeting of IRF4. *Blood Cancer J* 9(2), p. 19. doi: 10.1038/s41408-019-0173-0

Zonder, J. A. et al. 2012. A phase 1, multicenter, open-label, dose escalation study of elotuzumab in patients with advanced multiple myeloma. *Blood* 120(3), pp. 552-559. doi: 10.1182/blood-2011-06-360552

Zupo, S. et al. 1996. CD38 expression distinguishes two groups of B-cell chronic lymphocytic leukemias with different responses to anti-IgM antibodies and propensity to apoptosis. *Blood* 88(4), pp. 1365-1374.